VOLUME 28 (1961) No. 3

NUCLEAR PHYSICS

JOURNAL DEVOTED TO THE EXPERIMENTAL AND THEORETICAL STUDY OF THE FUNDAMENTAL CONSTITUENTS OF MATTER AND THEIR INTERACTIONS

EDITOR: L. ROSENFELD - COPENHAGEN

E. WERNER, Density modulated ground states in a gas of interacting fermions 353
R. E. PRANGE, The moment of inertia of large systems at finite temperature . 369
R. E. PRANGE, The moment of inertia of superfluid fermion systems of finite temperature 376
J. S. GEIGER, R. L. GRAHAM and G. T. EWAN, The decay of Ce^{144} 387
J. NÉMETH, The effect of pairing energy on the temperature excitation energy of an interacting fermion system 407
P. S. DUBBELDAM and R. L. WALTER, Polarization of D-D neutrons for deuteron energies from 1.9 to 11 MeV 414
NELSON JARMIE, Concerning the existence of rare light nuclei 426
A. C. L. BARNARD and C. C. KIM, Elastic scattering and reactions of protons on argon-40 428
C. C. KIM and A. C. L. BARNARD, Elastic scattering of protons by argon-36 . . . 438
RICHARD R. CARLSON, The 9.63 MeV state of C^{12} 443
G. S. MANI, A. C. L. BARNARD, T. A. TOMBRELLO and D. A. A. S. N. RAO, Levels in A^{38} observed through the Cl^{37} (p, n)A^{37} reaction near threshold 456
A. C. L. BARNARD, G. S. MANI and P. D. FORSYTH, Gross properties of levels in A^{38} with excitation near neutron separation energies 464
SÖLVE HULTBERG, DANIEL J. HOREN and JACK M. HOLLANDER, Measurements of internal conversion coefficients 471
R. BASS, H. P. HÄENNI, T. W. BONNER and F. GABBARD, Disintegration of K^{39} by fast neutrons 478
S. TAKAYANAGI, N. H. GALE, J. B. GARG and J. M. CALVERT, Neutron threshold measurements in the reactions $^{9}Be(p, n)^{9}B$, $^{10}B(p, n)\ ^{10}C$, $^{11}B(p, n)^{11}C$ . . 494
B. N. SUBBA RAO, On the levels and transitions in Gd^{155} 503
M. A. MEYER, Multiple Coulomb scattering from finite nuclei 512
R. J. N. PHILLIPS, On the analysis of the reaction $\pi^- + p \rightarrow \Lambda^0 + K^0$ 519
B. MARGOLIS, Two-photon decay and the lifetime of giant resonance states . . 524

December 1961

NORTH-HOLLAND PUBLISHING COMPANY - AMSTERDAM

EDITORIAL BOARD

AUSTRALIA & NEW ZEALAND:	H. Messel (Sydney), M. L. Oliphant (Canberra)
AUSTRIA:	B. Karlik (Vienna), H. Thirring (Vienna)
BELGIUM:	M. de Hemptinne (Louvain), J. Verhaeghe (Ghent)
CANADA:	G. Volkoff (Vancouver)
DENMARK:	C. Møller (Copenhagen), S. Rozental (Copenhagen), G. E. Brown (Copenhagen)
EGYPT & ARAB COUNTRIES:	F. El Bedewi (Cairo), M. G. Nooh (Cairo)
FINLAND:	L. Simons (Helsinki)
FRANCE:	A. Berthelot (Saclay), S. Gorodetzky (Strasbourg)
GERMANY (DEM. REP.):	G. Hertz (Leipzig)
GERMANY (FED. REP.):	W. Gentner (Freiburg i. B.), J. H. D. Jensen (Heidelberg)
GREAT BRITAIN:	W. E. Burcham (Birmingham), R. J. Blin-Stoyle (Oxford)
HUNGARY:	L. Janossy (Budapest)
INDIA:	H. Bhabha (Bombay), R. Ramanna (Trombay)
IRISH REPUBLIC:	J. McConnell (Maynooth)
ISRAEL:	G. Racah (Jerusalem)
ITALY:	E. Amaldi (Rome)
JAPAN:	S. Kikuchi (Tokay), S. Tomonaga (Tokyo)
MEXICO:	M. Moshinsky (Mexico)
NETHERLANDS:	H. Brinkman (Groningen), S. R. de Groot (Leiden)
NORWAY:	E. Hylleraas (Oslo), A. Lundby (Oslo), H. Wergeland (Trondheim)
POLAND:	L. Infeld (Warsaw), J. Werle (Warsaw)
PORTUGAL:	J. M. Araújo (Porto), J. R. de Almeida Santos (Coimbra)
SOUTH AMERICA:	G. Beck (Rio de Janeiro), J. Leite Lopes (Rio de Janeiro)
SOUTH-EAST ASIA:	T. H. R. Skyrme (Kuala Lumpur)
SPAIN:	J. M. Otero (Madrid), C. Sanchez del Rio (Madrid)
SWEDEN:	O. Klein (Stockholm), K. Siegbahn (Uppsala), I. Waller (Uppsala)
SWITZERLAND:	P. Huber (Basel), P. Scherrer (Zürich)
U.S.A.:	H. H. Barschall (Madison, Wisconsin), S. Devons (New York), G. C. Wick (Brookhaven), D. Inglis (Argonne)
U.S.S.R.:	M. A. Markov (Moscow), I. S. Shapiro (Moscow), D. V. Skobeltzyn (Moscow)
YUGOSLAVIA:	I. Supek (Zagreb)

Contributors are requested to prepare the manuscripts of their papers according to the rules and conventions described in the *Instructions to Contributors* (see Nuclear Physics 26 (1961) 697). Special copies are available on request from the publisher or the Editor.

CONTRIBUTIONS may be sent to the Editor, Professor L. Rosenfeld, NORDITA, Blegdamsvej 17, Copenhagen Ø, either directly, or preferably through the intermediary of one of the members of the Editorial Board of the country or region in which the author is working. They may be written in English, French or German.

NUCLEAR PHYSICS is published in fortnightly issues. The subscription price per volume of 700 pages is fl 57.00; 114s; $ 15.00. Post-free.

SUBSCRIPTIONS should be sent to the publishers, NORTH-HOLLAND PUBLISHING COMPANY P.O. Box 103, Amsterdam or to any subscription-agent.

BOOKS FOR REVIEW should be sent to Professor Rosenfeld.

No part of this issue may be reproduced in any form, by print, photoprint, microfilm or any other means without permission from the publisher.

Printed in the Netherlands

NUCLEAR PHYSICS 1962

Personal subscription scheme

Only to be used for new personal subscriptions, not for renewals

When Nuclear Physics was started at the end of 1955, the intention was to publish one or two volumes a year of 700 pages each. Neither the publisher nor the editor could envisage that the influx of papers would make it necessary to publish eight such volumes a year, as were in 1961.

Although since 1955 the guilder has been revaluated with 4 %, the production costs of mathematical composition have risen by approximately 25% and the number of words per page has been increased by 20% since the first volume, the subscription price per volume has been maintained at $ 15.00 (108s.).

Moreover Nuclear Physics does not impose any page charge, in order to make it easier for scientists from countries with a weak currency to contribute to the journal.

It is difficult to compare subscription prices, but per page Nuclear Physics is undoubtedly one of the less expensive journals in the field of physics.

However, we realize that a total subscription price per year of $ 120.00 for eight volumes is prohibitive for a private subscriber and the suggestion has been made that Nuclear Physics could fix a special price for personal subscriptions.

Indeed, there are a number of scientific journals which give a certain discount to private subscribers. In the case of Nuclear Physics a discount of 30% or even 50% would not be sufficient to attract private subscriptions.

Now it is known that for technical publications the composition of the type is the most expensive part of the production and that as soon as the break-even point is reached, the run-on costs are comparatively low.

Accordingly, we decided early 1961 to make Nuclear Physics available to personal subscribers at the run-on costs. This meant that starting with 1961 individual physicists could subscribe for their own use to the eight volumes (approx. 5600 pages) of Nuclear Physics scheduled for 1961 at a total price of $ 20.00 or the equivalent in other currency (postage included).

Should you want to join this personal subscription scheme for 1962, please return the order-form.

It has to be understood that the publisher has the right to refuse a personal subscription or its renewal. In case of refusal, the publisher will return the cheque.

We were glad to see that this new arrangement appealed to many nuclear physicists and that it did not lead to any misunderstanding about the extremely complicated way of fixing subscription prices for learned journals.

THE EDITOR
L. Rosenfeld

THE PUBLISHER
M. D. Frank

How to act:

Write a letter to the Subscription Department of North-Holland Publishing Company, P.O. Box 103, Amsterdam, Netherlands, asking for a personal subscription.

This letter should contain:

- **a cheque or banknotes for $ 20.00**
  (£ 7.4.0-; DM 80; N.Frs. 100)
- **a statement running as follows:**

"This subscription is for personal use only and will not replace an existing library subscription, nor will it be put at the disposal of any library now or in the future.

My position is: _____"

(Mention should be made of the institution to which you are attached.)

Any enquiry or communication concerning the personal subscription scheme should be addressed to the publisher, North-Holland Publishing Company, P.O. Box 103, Amsterdam, Netherlands.

Only to be used for NEW personal subscriptions, not for renewals

SUBSCRIPTION FORM

NORTH-HOLLAND PUBLISHING COMPANY
P.O. BOX 103
AMSTERDAM - NETHERLANDS

Date _____

Please enter my personal subscription to

NUCLEAR PHYSICS 1962

(VOLUMES 29—36)

at the **total** subscription price of $ 20.00

(£ 7.4.0.; DM. 80; N. Frs. 100)

I declare that this subscription is for my personal use only and that it will not replace an existing library subscription, nor will it be put at the disposal of any library now or in the future.

I enclose ☐ banknotes

☐ cheque

My position is _____

(mention should be made of the institution to which you are attached)

Name (please print) _____

_____

Address _____

_____

City, Zone, State _____

Signature

_____

(tear off here)

1.C *Nuclear Physics* **28** (1961) 353—368; © *North-Holland Publishing Co., Amsterdam*

Not to be reproduced by photoprint or microfilm without written permission from the publisher

DENSITY MODULATED GROUND STATES IN A GAS OF INTERACTING FERMIONS

E. WERNER

Institut für theoretische Physik der Universität des Saarlandes, Saarbrücken

Received 20 April 1961

Abstract: For an infinite system of fermions interacting through a non-local separable potential the question of the existence of density-modulated ground states is investigated in the framework of the independent pair model. It is found that for suffficiently strong interactions or alternatively sufficiently high densities there exist states exhibiting a periodic density variation whose energy is lower than the energy of the states with a homogeneous density distribution. The discussion of the dependence of the effect on the potential strength and the density shows that for nuclear matter the ground state has a uniform density distribution.

1. Introduction

The question of the existence of periodic density variations in the ground state of a system of interacting particles has been discussed recently by various authors. Gross [1]) has given a detailed investigation of the Bose-system with the result that for suitably strong two-body interactions a periodic density variation leads to a lower energy than a homogeneous density distribution. He also discussed some general aspects of periodic states for the theory of many-body systems [2]). Trainor, Bhatia and Sood [3]) have calculated the ground state energy and mean density of nuclear matter for a quasi-lattice model using the Wigner-Seitz cellular method. Overhauser [4]) using a point-interaction has shown for fermions that in a linear model there exist density-modulated solutions of the Hartree-Fock equations whose energy is lower than the energy of the solutions that have a uniform density distribution, this being true no matter how weak the interaction is. However, this last fact is a pecularity of the linear model, as was shown by Kohn and Nettel [5]). Besides Overhauser has not taken into account correlations between the particles. In the 3-dimensional case it will surely be necessary to have an interaction of finite strength in order to bring the energy of periodic-density solutions below the energy of the homogeneous solution. That for sufficiently strong interactions states with a periodic density variation are energetically more favourable was already shown long ago by Wigner [6]) for the low density electron gas.

In this paper we want to investigate the conditions for the existence of density modulated ground states of a system of fermions interacting through a separable potential. As to the correlations between the particles we use the independent pair model of Brueckner. In the general case of density fluctuations of arbitrarily large amplitudes the difficulties in carrying through the necessary calculations are rather prohibitive because of the complicated shape of the Fermi-surface. Therefore we

perform a variational calculation for the energy of the system using the amplitude of the density waves as a free parameter. This enables us to state whether under given physical conditions (mean density, strength and range of the interaction potential), the homogeneous density distribution gives the lowest energy or not. The restriction to two-body correlations means of course a restricton to the low density case or rather to the case in which roughly the mean distance of the particles is greater than the range of the interaction.

In section 2 we develop the theory, the results and their discussion are presented in section 3.

2. Variational Calculation

We consider a Fermi-gas of particles interacting through a non-local separable potential. If we assume validity of the independent-pair-approximation the ground state of the system can be calculated if one knows the solutions of the Bethe-Goldstone-equation for all relevant pair states.

In order to obtain a criterion for the existence of periodic density variations we want to carry out a variational calculation using the amplitude and the wavelength of the density variations as free parameters. The energy of a state $\psi(\boldsymbol{k}_1, \boldsymbol{k}_2)$ of two interacting particles is given by the following expectation value:

$$E_{\boldsymbol{k}_1, \boldsymbol{k}_2} = \frac{\langle \psi(\boldsymbol{k}_1, \boldsymbol{k}_2) | H_{12} | \psi(\boldsymbol{k}_1, \boldsymbol{k}_2) \rangle}{\langle \psi(\boldsymbol{k}_1, \boldsymbol{k}_2) | \psi(\boldsymbol{k}_1, \boldsymbol{k}_2) \rangle} . \tag{1}$$

In the case of a uniform density distribution one obtains

$$E_{\boldsymbol{k}_1, \boldsymbol{k}_2} = \frac{\hbar^2}{2m} (k_1^2 + k_2^2) + \langle \boldsymbol{k}_1, \boldsymbol{k}_2 | G | \boldsymbol{k}_1, \boldsymbol{k}_2 \rangle \tag{2}$$

if the solution of the Bethe-Goldstone-equation is substituted into eq. (1) Here $\langle \boldsymbol{k}_1 \boldsymbol{k}_2 | G | \boldsymbol{k}_1 \boldsymbol{k}_2 \rangle$ is the diagonal element of Brueckner's G-matrix.

In our problem we must substitute for $\psi(\boldsymbol{k}_1, \boldsymbol{k}_2)$ a wave function that exhibits a periodic density fluctuation. Instead of using plane waves as independent particle wave functions we use (box-normalisation)

$$\varphi_{\boldsymbol{k}}(\boldsymbol{r}) = \frac{1}{\sqrt{\Omega}} [e^{i\boldsymbol{k} \cdot \boldsymbol{r}} + \alpha (e^{i(\boldsymbol{k}+\boldsymbol{q}) \cdot \boldsymbol{r}} + e^{i(\boldsymbol{k}-\boldsymbol{q}) \cdot \boldsymbol{r}})], \tag{3}$$

where

$$\boldsymbol{q} = \frac{q}{\sqrt{3}} (\boldsymbol{e}_x + \boldsymbol{e}_y + \boldsymbol{e}_z), \qquad |\boldsymbol{q}|^2 = q^2.$$

Here Ω is the volume in which the system is enclosed, and α is a parameter which is related to the amplitude of the density variation. In the following we always assume that α is small compared to unity. The wave function (3) describes a state with a periodic density variation of wave vector $\boldsymbol{q}$, as is seen if one computes the absolute square of the wave function

$$|\varphi_{\boldsymbol{k}}(\boldsymbol{r})|^2 = \frac{1}{\Omega} [1 + 2\alpha \cos \boldsymbol{q} \cdot \boldsymbol{r} + O(\alpha^2)]. \tag{4}$$

Terms of the order α^2 are neglected. This restriction to $\alpha \ll 1$ means that we can only state a possible instability against build up of periodic density variations but we shall not be able to evaluate the equilibrium value of α. In eq. (1) we substitute now a modified wave function:

$$\begin{aligned}\psi(k_1, k_2) = \frac{(2\pi)^6}{\Omega^2}\Big[&\delta(k_1-k_{1_0})\delta(k_2-k_{2_0})+\chi_{k_{1_0},k_{2_0}}(k_1, k_2)\delta(k_1+k_2-k_{1_0}-k_{2_0})\\
&+\alpha\{\delta(k_1-k_{1_0})[\delta(k_2-k_{2_0}-q)+\delta(k_2-k_{2_0}+q)]+\delta(k_2-k_{2_0})[\delta(k_1-k_{1_0}-q)\\
&\qquad+\delta(k_1-k_{1_0}+q)]\\
&+[\chi_{k_{1_0},k_{2_0}+q}(k_1, k_2)+\chi_{k_{1_0}+q,k_{2_0}}(k_1, k_2)]\delta(k_1+k_2-k_{1_0}-k_{2_0}-q)\\
&+[\chi_{k_{1_0},k_{2_0}-q}(k_1, k_2)+\chi_{k_{1_0}-q,k_{2_0}}(k_1, k_2)]\delta(k_1+k_2-k_{1_0}-k_{2_0}+q)] \qquad (5)\\
&+\alpha^2[\delta(k_1-k_{1_0}-q)[\delta(k_2-k_{2_0}-q)+\delta(k_2-k_{2_0}+q)]+\delta(k_1-k_{1_0}+q)[\delta(k_2-k_{2_0}-q)\\
&\qquad+\delta(k_2-k_{2_0}+q)]\\
&+\chi_{k_{1_0}+q,k_{2_0}+q}(k_1, k_2)\delta(k_1+k_2-k_{1_0}-k_{2_0}-2q)+\chi_{k_{1_0}-q,k_{2_0}-q}(k_1, k_2)\delta(k_1+k_2-\\
&\qquad k_{1_0}-k_{2_0}+2q)\\
&+[\chi_{k_{1_0}+q,k_{2_0}-q}(k_1, k_2)+\chi_{k_{1_0}-q,k_{2_0}+q}(k_1, k_2)]\delta(k_1+k_2-k_{1_0}-k_{2_0})\}\Big].\end{aligned}$$

Here $\chi_{k_{1_0},k_{2_0}}(k_1, k_2)$ is the correlation amplitude that belongs to the unperturbed part $\delta(k_1-k_{1_0})\delta(k_2-k_{2_0})$, $\chi_{k_{1_0},k_{2_0}+q}(k_1, k_2)$ belongs to $\delta(k_1-k_{1_0})\delta(k_2-k_{2_0}-q)$, etc. The delta-function-factors are included for convenience. They originate from the conservation of total momentum of two colliding particles in each individual impact.

In the following calculations we keep only terms proportional to α^2 (terms proportional to α vanish identically). At first we compute the denominator $\langle\psi|\psi\rangle$ of eq. (1):

$$\begin{aligned}\langle\psi|\psi\rangle = 1+4\alpha^2+\frac{(2\pi)^3}{\Omega}\int|\chi_{k_{1_0},k_{2_0}}(k_{1_0}+k, k_{2_0}-k)|^2\mathrm{d}k^3\\
+\alpha^2\frac{(2\pi)^3}{\Omega}\Big\{2\chi_{k_{1_0},k_{2_0}}(k_{1_0}+q, k_{2_0}-q)+2\chi_{k_{1_0},k_{2_0}}(k_{1_0}-q, k_{2_0}+q)\\
+\int[\chi^*_{k_{1_0},k_{2_0}}(k_{1_0}+k, k_{2_0}-k)\chi_{k_{1_0}+q,k_{2_0}-q}(k_{1_0}+k, k_{2_0}-k)+\text{c. c.}]\mathrm{d}k^3 \qquad (6)\\
+\int[\chi^*_{k_{1_0},k_{2_0}}(k_{1_0}+k, k_{2_0}-k)\chi_{k_{1_0}-q,k_{2_0}+q}(k_{1_0}+k, k_{2_0}-k)+\text{c. c.}]\mathrm{d}k^3\\
+\int[|\chi_{k_{1_0},k_{2_0}+q}(k_{1_0}+k, k_{2_0}-k)|^2+|\chi_{k_{1_0},k_{2_0}-q}(k_{1_0}+k, k_{2_0}-k)|^2\\
+|\chi_{k_{1_0}+q,k_{2_0}}(k_{1_0}+k, k_{2_0}-k)|^2+|\chi_{k_{1_0}-q,k_{2_0}}(k_{1_0}+k, k_{2_0}-k)|^2]\mathrm{d}k^3\Big\}.\end{aligned}$$

In writing eq. (6) we have assumed that the deformation of the Fermi-surface through the non-uniform density distribution has a negligible influence on the form

of the correlation amplitude, i.e. that also in the non-uniform case the spectral representation of the correlation amplitude contains only states outside the original undisturbed Fermi-sphere. This assumption seems plausible since the essential feature of the Bethe-Goldstone correlation amplitude — the suppression of long wavelength correlations corresponding to states inside the Fermi-sphere — will not be appreciably changed if the amplitude of the density waves is small compared to the uniform density. As an additional approximation we now want to replace the terms

$$\chi_{k_{1_0}\pm q,\,k_{2_0}\mp q}(k_{1_0}+k,\,k_{2_0}-k),\quad \chi_{k_{1_0},\,k_{2_0}\pm q}(k_{1_0}+k,\,k_{2_0}-k),\quad \chi_{k_{1_0}\pm q,\,k_{2_0}}(k_{1_0}+k,\,k_{2_0}-k)$$

by

$$\chi_{k_{1_0},\,k_{2_0}}(k_{1_0}+k,\,k_{2_0}-k),$$

which means that we neglect the state dependence of the correlation function in these integrals. We believe that this is a rather good approximation for two reasons:

a) the essential features of the correlation function as described above are not changed by this replacement,

b) later on, in summing over all pairs of the medium an angular averaging referring to the fixed direction of the vector q is performed, whose effect is surely in the direction of an improvement of the approximation just described.

In evaluating the numerator we begin with the kinetic energy. The result is

$$\begin{aligned}
&\frac{2m}{\hbar^2}\langle\psi|T|\psi\rangle = \\
&= k_{1_0}^2+k_{2_0}^2+\frac{(2\pi)^3}{\Omega}\int[(k_{1_0}+k)^2+(k_{2_0}-k)^2]|\chi_{k_{1_0},\,k_{2_0}}(k_{1_0}+k,\,k_{2_0}-k)|^2\mathrm{d}k^3 \\
&\qquad +4\alpha^2(k_{1_0}^2+k_{2_0}^2+q^2) \\
&+\alpha^2\frac{(2\pi)^3}{\Omega}\Big\{2[(k_{1_0}+q)^2+(k_{2_0}-q)^2]\chi_{k_{1_0},\,k_{2_0}}(k_{1_0}+q,\,k_{2_0}-q) \\
&\qquad +2[(k_{1_0}-q)^2+(k_{2_0}+q)^2]\chi_{k_{1_0},\,k_{2_0}}(k_{1_0}-q,\,k_{2_0}+q) \\
&+\int[(k_{1_0}+k)^2+(k_{2_0}-k)^2][\chi^*_{k_{1_0},\,k_{2_0}}(k_{1_0}+k,\,k_{2_0}-k)\chi_{k_{1_0}+q,\,k_{2_0}-q}(k_{1_0}+k,\,k_{2_0}-k)+\text{c.c.}]\mathrm{d}k^3 \\
&+\int[(k_{1_0}+k)^2+(k_{2_0}-k)^2][\chi^*_{k_{1_0},\,k_{2_0}}(k_{1_0}+k,\,k_{2_0}-k)\chi_{k_{1_0}-q,\,k_{2_0}+q}(k_{1_0}+k,\,k_{2_0}-k)+\text{c.c.}]\mathrm{d}k^3 \\
&+\int[(k_{1_0}+k)^2+(k_{2_0}-k)^2][|\chi_{k_{1_0},\,k_{2_0}+q}(k_{1_0}+k,\,k_{2_0}-k)|^2 \\
&+|\chi_{k_{1_0},\,k_{2_0}-q}(k_{1_0}+k,\,k_{2_0}-k)|^2+|\chi_{k_{1_0}+q,\,k_{2_0}}(k_{1_0}+k,\,k_{2_0}-k)|^2 \\
&\qquad +|\chi_{k_{1_0}-q,\,k_{2_0}}(k_{1_0}+k,\,k_{2_0}-k)|^2]\mathrm{d}k^3\Big\}.
\end{aligned}\tag{7}$$

If we make the same approximation as before we obtain

$$\langle\psi|T|\psi\rangle = \frac{\hbar^2}{2m}[k_{1_0}^2+k_{2_0}^2+4\alpha^2(k_{1_0}^2+k_{2_0}^2+q^2)]$$

$$+\frac{\hbar^2}{2m}\frac{(2\pi)^3}{\Omega}\int[k_{1_0}^2+k_{2_0}^2+2k^2]|\chi_{k_{1_0},k_{2_0}}(k_{1_0}+k, k_{2_0}-k)|^2\mathrm{d}k^3$$

$$+\frac{\hbar^2}{2m}\alpha^2\frac{(2\pi)^3}{\Omega}\Big\{2[(k_{1_0}+q)^2+(k_{2_0}-q)^2]\chi_{k_{1_0},k_{2_0}}(k_{1_0}+q, k_{2_0}-q) \tag{8}$$

$$+2[(k_{1_0}-q)^2+(k_{2_0}+q)^2]\chi_{k_{1_0},k_{2_0}}(k_{1_0}-q, k_{2_0}+q)$$

$$+8\int[k_{1_0}^2+k_{2_0}^2+2k^2]|\chi_{k_{1_0},k_{2_0}}(k_{1_0}+k, k_{2_0}-k)|^2\mathrm{d}k^3\Big\}.$$

In going from (7) to (8) we have dropped the term $16k(k_{1_0}-k_{2_0})|\chi(k_{1_0}+k, k_{2_0}-k)|^2$ in the last integral since from now on we want to consider the correlation functions as spherically symmetric in k-space; then the term in question vanishes upon performing the k-integration. The assumption of spherical symmetry of the correlation functions is equivalent to neglecting the influence of the centre-of-mass momentum on the form of the correlation function.

Now, dividing $\langle\psi|T|\psi\rangle$ by $\langle\psi|\psi\rangle$ we obtain

$$\frac{\langle\psi|T|\psi\rangle}{\langle\psi|\psi\rangle} = \frac{\hbar^2}{2m}(k_{1_0}^2+k_{2_0}^2)+\frac{\hbar^2}{m}\frac{(2\pi)^3}{\Omega}\int k^2|\chi_{k_{1_0},k_{2_0}}(k_{1_0}+k, k_{2_0}-k)|^2\mathrm{d}k^3+2\alpha^2\frac{\hbar^2q^2}{m}$$

$$+2\frac{\hbar^2}{m}\alpha^2\frac{(2\pi)^3}{\Omega}\Big\{q^2[\chi_{k_{1_0},k_{2_0}}(k_{1_0}+q, k_{2_0}-q)+\chi_{k_{1_0},k_{2_0}}(k_{1_0}-q, k_{2_0}+q)] \tag{9}$$

$$+2\int k^2|\chi_{k_{1_0},k_{2_0}}(k_{1_0}+k, k_{2_0}-k)|^2\mathrm{d}k^3-q^2\int|\chi_{k_{1_0},k_{2_0}}(k_{1_0}+k, k_{2_0}-k)|^2\mathrm{d}k^3\Big\}.$$

We now drop the term $\chi_{k_{1_0},k_{2_0}}(k_{1_0}+q, k_{2_0}-q)+\chi_{k_{1_0},k_{2_0}}(k_{1_0}-q, k_{2_0}+q)$ because for the majority of the states it is small for the following reason: If $q \ll k_F$ except for states in a thin shell under the Fermi surface the state vectors lie inside the Fermi sphere so that the correlation vanishes identically. For $q \gg k_F$ (later on we shall see that the effect we are looking for occurs favourably for $q \approx 2\pi k_F$) the state vectors lie already far away from the Fermi surface; thus the correlation amplitude becomes again small.

If now we abbreviate the integrals

$$\int|\chi_{k_{1_0},k_{2_0}}(k_{1_0}+k, k_{2_0}-k)|^2\mathrm{d}k^3 \quad\text{and}\quad \int k^2|\chi_{k_{1_0},k_{2_0}}(k_{1_0}+k, k_{2_0}-k)|^2\mathrm{d}k^3$$

by $\langle\chi^2\rangle$ and $\langle k^2\chi^2\rangle$, respectively, we finally obtain

$$\frac{\langle\psi|T|\psi\rangle}{\langle\psi|\psi\rangle} = T_0+\frac{2\hbar^2}{m}\alpha^2\left[q^2+2\frac{(2\pi)^3}{\Omega}\langle k^2\chi^2\rangle-\frac{(2\pi)^3}{\Omega}q^2\langle\chi^2\rangle\right], \tag{10}$$

where we have used T_0 for the kinetic energy of the system whose density is distributed homogeneously.

We now evaluate the expectation value of the potential energy. We assume a separable potential for which we write

$$\langle k_1 k_2|v|k_1' k_2'\rangle = \Lambda \frac{\hbar^2}{2m}\frac{(2\pi)^6}{\Omega^2} g^*(k_1-k_2)g(k_1'-k_2')\delta(k_1'+k_2'-k_1-k_2). \tag{11}$$

Substituting (5) and (11) into (1) one obtains essentially three types of integrals:

1) integrals that contain only plane-wave states:

$$\Lambda \frac{\hbar^2}{2m}\frac{(2\pi)^6}{\Omega^2}\int\int\int\int \delta(k_1-a)\delta(k_2-b)\delta(k_1'-c)\delta(k_2'-d)g^*(k_1-k_2)g(k_1'-k_2') \times \delta(k_1'+k_2'-k_1-k_2)\mathrm{d}k_1^3\mathrm{d}k_2^3\mathrm{d}k_1'^3\mathrm{d}k_2'^3 \tag{12}$$
$$= \Lambda \frac{\hbar^2}{2m}\frac{(2\pi)^6}{\Omega^2}\delta(a+b-c-d)g^*(a-b)g(c-d);$$

2) integrals that contain one plane-wave state and one correlation function:

$$\Lambda \frac{\hbar^2}{2m}\frac{(2\pi)^6}{\Omega^2}\int\int\int\int \delta(k_1-a)\delta(k_2-b)\chi(k_1', k_2')\delta(k_1'+k_2'-k_{1_0}-k_{2_0}) \times g^*(k_1-k_2)g(k_1'-k_2')\delta(k_1+k_2-k_1'-k_2')\mathrm{d}k_1^3\mathrm{d}k_2^3\mathrm{d}k_1'^3\mathrm{d}k_2'^3 \tag{13}$$
$$= \Lambda \frac{\hbar^2}{2m}\frac{(2\pi)^6}{\Omega^2}\delta(k_{1_0}+k_{2_0}-a-b)g^*(a-b)\int \chi(k_{1_0}+k_{2_0}-k, k)g(k_{1_0}+k_{2_0}-2k)\mathrm{d}k^3;$$

3) integrals that contain twice a correlation function:

$$\Lambda \frac{\hbar^2}{2m}\frac{(2\pi)^6}{\Omega^2}\int\int\int\int g^*(k_1-k_2)g(k_1'-k_2')\delta(k_1+k_2-k_1'-k_2')\delta(k_1+k_2-k_{1_0}-k_{2_0}) \times \delta(k_1'+k_2'-k_{1_0}'-k_{2_0}')\chi^*(k_1, k_2)\chi(k_1', k_2')\mathrm{d}k_1^3\mathrm{d}k_2^3\mathrm{d}k_1'^3\mathrm{d}k_2'^3 \tag{14}$$
$$= \Lambda \frac{\hbar^2}{2m}\frac{(2\pi)^6}{\Omega^2}\left|\left\{\int g(k_{1_0}+k_{2_0}-2k)\chi(k_{1_0}+k_{2_0}-k, k)\mathrm{d}k^3\right\}\right|^2 \delta(k_{1_0}+k_{2_0}-k_{1_0}'-k_{2_0}').$$

Using (12), (13) and (14) one obtains

$$\langle\psi|v|\psi\rangle =$$
$$\Lambda \frac{\hbar^2}{2m}\frac{(2\pi)^3}{\Omega}\{|g(k_{1_0}-k_{2_0})|^2+|I(k_{1_0}, k_{2_0})|^2+[g^*(k_{1_0}-k_{2_0})I(k_{1_0}, k_{2_0})+\text{c.c.}]\}$$
$$+\alpha^2\Lambda \frac{\hbar^2}{2m}\frac{(2\pi)^3}{\Omega}\{g^*(k_{1_0}-k_{2_0})[g(k_{1_0}-k_{2_0}+2q)+g(k_{1_0}-k_{2_0}-2q)]+\text{c.c.}$$
$$+g^*(k_{1_0}-k_{2_0})[I(k_{1_0}+q, k_{2_0}-q)+I(k_{1_0}-q, k_{2_0}+q)]+\text{c.c.}$$
$$+I(k_{1_0}, k_{2_0})[g^*(k_{1_0}-k_{2_0}+2q)+g^*(k_{1_0}-k_{2_0}-2q)]+\text{c.c.}+2|g(k_{1_0}-k_{2_0}-q)|^2+$$

$$+2|g(k_{1_0}-k_{2_0}+q)|^2+[2g^*(k_{1_0}-k_{2_0}-q)g(k_{1_0}-k_{2_0}+q)+\text{c.c.}]$$
$$+[g^*(k_{1_0}-k_{2_0}-q)(I(k_{1_0},k_{2_0}+q)+I(k_{1_0},k_{2_0}-q)+I(k_{1_0}+q,k_{2_0})+I(k_{1_0}-q,k_{2_0}))$$
$$+\text{c.c.}]+[g^*(k_{1_0}-k_{2_0}+q)(I(k_{1_0},k_{2_0}+q)+I(k_{1_0},k_{2_0}-q)+I(k_{1_0}+q,k_{2_0}) \quad (15)$$
$$+I(k_{1_0}-q,k_{2_0})+\text{c.c.}]+[I^*(k_{1_0},k_{2_0}+q)I(k_{1_0}+q,k_{2_0})$$
$$+I^*(k_{1_0},k_{2_0}-q)I(k_{1_0}-q,k_{2_0})+\text{c.c.}]+|I(k_{1_0},k_{2_0}+q)|^2+|I(k_{1_0},k_{2_0}-q)|^2$$
$$+|I(k_{1_0}+q,k_{2_0})|^2+|I(k_{1_0}-q,k_{2_0})|^2\},$$

where $I(k_1, k_2)$ means

$$I(k_1, k_2) = \int \chi_{k_1, k_2}(k_1+k_2-k, k)g(k_1+k_2-2k)\mathrm{d}k^3.$$

Making once more the approximation of neglecting the state dependence of the correlation function we get for the expectation value

$$\frac{\langle\psi|v|\psi\rangle}{\langle\psi|\psi\rangle} = \langle\psi_0|v|\psi_0\rangle+\alpha^2\Lambda\frac{\hbar^2}{m}\frac{(2\pi)^3}{\Omega}\{4I(k_{1_0},k_{2_0})[g(k_{1_0}-k_{2_0}+q)+g(k_{1_0}-k_{2_0}-q)]$$
$$+g(k_{1_0}-k_{2_0})[g(k_{1_0}-k_{2_0}+2q)+g(k_{1_0}-k_{2_0}-2q)] \quad (16)$$
$$+[g(k_{1_0}-k_{2_0}+q)+g(k_{1_0}-k_{2_0}-q)]^2-2g^2(k_{1_0}-k_{2_0})+2I^2(k_{1_0},k_{2_0})$$
$$+I(k_{1_0},k_{2_0})[g(k_{1_0}-k_{2_0}+2q)+g(k_{1_0}-k_{2_0}-2q)-2g(k_{1_0}-k_{2_0})]\}.$$

Here $\langle\psi_0|v|\psi_0\rangle$ is the potential energy of the interacting pair if the density distribution is homogeneous.

Using eqs. (10) and (16) we can now write down the energy of the pair state $\psi(k_{1_0}, k_{2_0})$. In order to obtain the total energy of the system we have to sum the one-particle term $2\alpha^2\hbar^2q^2/m$ over all states of the Fermi-sphere; the remaining two-particle-terms have to be summed over all pairs. This gives for the total energy

$$E(\alpha,\Lambda,q) = E(\alpha=0)+\alpha^2\frac{\hbar^2}{m}\left\{2q^2N+\tfrac{1}{2}\frac{(2\pi)^3}{\Omega}\sum_{k_{1_0},k_{2_0}}[4\langle k^2\chi^2\rangle-2q^2\langle\chi^2\rangle]\right.$$
$$+\tfrac{1}{2}\Lambda\frac{(2\pi)^3}{\Omega}\sum_{k_{1_0},k_{2_0}}\Big[4I(k_{1_0},k_{2_0})[g(k_{1_0}-k_{2_0}+q)+g(k_{1_0}-k_{2_0}-q)] \quad (17)$$
$$+g(k_{1_0}-k_{2_0})[g(k_{1_0}-k_{2_0}+2q)+g(k_{1_0}-k_{2_0}-2q)]$$
$$+[g(k_{1_0}-k_{2_0}+q)+g(k_{1_0}-k_{2_0}-q)]^2-2g^2(k_{1_0}-k_{2_0})+2I^2(k_{1_0},k_{2_0})$$
$$\left.+I(k_{1_0},k_{2_0})[g(k_{1_0}-k_{2_0}+2q)+g(k_{1_0}-k_{2_0}-2q)-2g(k_{1_0}-k_{2_0})]\Big]\right\}.$$

The task is now to evaluate the sums in (17) and to compute the energy of the system as a function of the average density, the potential strength λ and the magnitude of the wave vector q.

In order to be able to perform explicit calculations we must now specialise to a

definite form of the interaction potential. For this purpose we choose the separable potential used by Yamaguchi [7]) in his calculations on the two-nucleon system. The form of this potential is

$$g(\boldsymbol{k}_1-\boldsymbol{k}_2)=\frac{1}{(\boldsymbol{k}_1-\boldsymbol{k}_2)^2+\beta^2}, \tag{18}$$

where β is a constant. In configuration space there corresponds to (18) a non-local potential that acts on a wave function in the following way:

$$v_{12}\psi(\boldsymbol{r}_1,\boldsymbol{r}_2)=\int \mathrm{e}^{-\beta|\boldsymbol{r}_1-\boldsymbol{r}'_1|}\mathrm{e}^{-\beta|\boldsymbol{r}_2-\boldsymbol{r}'_2|}\psi(\boldsymbol{r}'_1\boldsymbol{r}'_2)\mathrm{d}\tau'_1\,\mathrm{d}\tau'_2. \tag{19}$$

As one sees from this last equation $1/\beta$ is the "range" of the potential †. The advantage of the Yamaguchi potential lies in the fact that it is rational which allows us to perform most of the necessary integrations exactly. Its non-locality is probably not very important in our problem since the effect we want to investigate is likely to depend primarily on the depth and the range of the potential.

With the form (18) for the interaction potential we can now determine the correlation amplitudes that enter into eq. (17). To this end we now consider the Bethe-Goldstone equation which reads in momentum space

$$\psi_{\boldsymbol{k}_{1_0},\boldsymbol{k}_{2_0}}(\boldsymbol{k}_1\boldsymbol{k}_2)=\frac{(2\pi)^6}{\Omega}\left\{\delta(\boldsymbol{k}_1-\boldsymbol{k}_{1_0})\delta(\boldsymbol{k}_2-\boldsymbol{k}_{2_0})\right.$$
$$\left.-\Lambda\iint\frac{\theta\langle\boldsymbol{k}_1\boldsymbol{k}_2|v|\boldsymbol{k}'_1\boldsymbol{k}'_2\rangle\psi_{\boldsymbol{k}_{1_0}\boldsymbol{k}_{2_0}}(\boldsymbol{k}'_1\boldsymbol{k}'_2)}{k_1^2+k_2^2-k_{1_0}^2-k_{2_0}^2}\mathrm{d}k_1'^3\mathrm{d}k_2'^3\right\}, \tag{20}$$

and gives, with the potential (18),

$$\psi_{\boldsymbol{k}_{1_0},\boldsymbol{k}_{2_0}}(\boldsymbol{k}_1,\boldsymbol{k}_2)=\frac{(2\pi)^6}{\Omega^2}\delta(\boldsymbol{k}_1-\boldsymbol{k}_{1_0})\delta(\boldsymbol{k}_2-\boldsymbol{k}_{2_0})$$
$$-\frac{\Lambda}{[k_1^2+k_2^2-k_{1_0}^2-k_{2_0}^2][(\boldsymbol{k}'_1-\boldsymbol{k}'_2)^2+\beta^2]}\int\frac{\theta\psi(\boldsymbol{k}'_1,\boldsymbol{k}_1+\boldsymbol{k}_2-\boldsymbol{k}'_1)}{(\boldsymbol{k}_1+\boldsymbol{k}_2-2\boldsymbol{k}'_1)^2+\beta^2}\mathrm{d}k_1'^3. \tag{21}$$

Here θ is a projection operator on the outside of the Fermi-sphere. Abbreviating

$$\int\theta\psi(\boldsymbol{k}'_1,\boldsymbol{k}_1+\boldsymbol{k}_2-\boldsymbol{k}'_1)[(\boldsymbol{k}_1+\boldsymbol{k}_2-2\boldsymbol{k}'_1)^2+\beta^2]^{-1}\mathrm{d}k_1'^3=\xi$$

we obtain

$$\xi=\frac{(2\pi)^3}{\Omega}\frac{\dfrac{1}{(\boldsymbol{k}_{1_0}-\boldsymbol{k}_{2_0})^2+\beta^2}}{1+\Lambda\displaystyle\int\frac{\theta\dfrac{1}{[(\boldsymbol{k}_{1_0}+\boldsymbol{k}_{2_0}-2\boldsymbol{k}'_1)^2+\beta^2]^2}}{(\boldsymbol{k}_{1_0}+\boldsymbol{k}_{2_0}-\boldsymbol{k}'_1)^2+k_1'^2-k_{1_0}^2-k_{2_0}^2}\mathrm{d}k_1'^3}, \tag{22}$$

† The physical meaning of the notion of "range" of our potential will be discussed in more detail in sect. 3.

which gives

$$\psi_{k_{1_0},k_{2_0}}(k_1,k_2)=\frac{(2\pi)^6}{\Omega^2}\left\{\delta(k_1-k_{1_0})\delta(k_2-k_{2_0})\right.$$
$$\left.-\frac{\Lambda}{1+\Lambda F(k_{1_0},k_{2_0})}\frac{[(k_{1_0}-k_{2_0})^2+\beta^2]^{-1}[(k_1-k_2)^2+\beta^2]^{-1}}{k_1^2+k_2^2-k_{1_0}^2-k_{2_0}^2}\right\}. \quad (23)$$

Therefore we obtain for the correlation amplitude

$$\chi_{k_{1_0}k_{2_0}}(k_1k_2)=-\frac{\Lambda}{1+\Lambda F(k_{1_0},k_{2_0})}\frac{[(k_{1_0}-k_{2_0})^2+\beta^2]^{-1}[(k_1-k_2)^2+\beta^2]^{-1}}{k_1^2+k_2^2-k_{1_0}^2-k_{2_0}^2}, \quad (24)$$

$$F(k_{1_0},k_{2_0})=\int\theta\frac{[(k_{1_0}+k_{2_0}-2k_1')^2+\beta^2]^{-2}}{(k_{1_0}+k_{2_0}-k_1')^2+k_1'^2-k_{1_0}^2-k_{2_0}^2}\,\mathrm{d}k_1'^3. \quad (24a)$$

Having found the correlation amplitude $\chi(k_1,k_2)$ we can now compute the following quantities which enter into the expression for the energy:

a) $$\langle\chi^2\rangle=\int|\chi_{k_{1_0},k_{2_0}}(k_{1_0}+k,k_{2_0}-k)|^2\mathrm{d}k^3,$$

b) $$\langle k^2\chi^2\rangle=\int k^2|\chi_{k_{1_0},k_{2_0}}(k_{1_0}+k,k_{2_0}-k)|^2\mathrm{d}k^3,$$

c) $$I(k_{1_0},k_{2_0})=\int\chi_{k_{1_0},k_{2_0}}(k_{1_0}+k_{2_0}-k,k)g(k_{1_0}+k_{2_0}-2k)\mathrm{d}k^3.$$

In order to carry out the integrations in a), b) and c) it is most convenient to introduce relative momenta. With $k_{1_0}-k_{2_0}=k_0$ we then get

$$\langle\chi^2\rangle=\frac{4\pi\Lambda^2}{[1+\Lambda F(k_0)]^2}\frac{1}{(k_0^2+\beta^2)^2}\int_{k_F}^{\infty}\frac{k^2\mathrm{d}k}{(k^2+\beta^2)^2(k^2-k_0^2)^2}.$$

As is seen from the lower limit of integration we disregard the dependence of the correlation amplitude on the centre-of-mass momentum of the two colliding particles. With this approximation $\langle\chi^2\rangle$ depends only on the relative momentum k_0. The integrand in the last equation is a rapidly decreasing function of k for large values of k. Therefore the main contribution to the integral comes from the vicinity of k_F. For this reason one can split off one factor k in the numerator and replace it by k_F. Introducing $k^2=x$ as a new variable the integral becomes

$$\langle\chi^2\rangle=\frac{2\pi\Lambda^2}{[1+\Lambda F(k_0)]^2}\frac{k_F}{(k_0^2+\beta^2)^2}\int_{k_F^2}^{\infty}\frac{\mathrm{d}x}{(x+\beta^2)^2(x-k_0^2)^2}.$$

Now it can be evaluated and one gets for $\langle\chi^2\rangle$

$$\langle\chi^2\rangle=\frac{4\pi\Lambda^2}{[1+\Lambda F(k_0)]^2}\frac{k_F}{(k_0^2+\beta^2)^4}\left\{\frac{1}{k_0^2+\beta^2}\lg\frac{k_F^2-k_0^2}{k_F^2+\beta^2}+\tfrac{1}{2}\frac{2k_F^2+\beta^2-k_0^2}{(k_F^2+\beta^2)(k_F^2-k_0^2)}\right\}. \quad (25a)$$

In the integrals in the expressions for $\langle k^2\chi^2\rangle$ and $I(\boldsymbol{k}_{1_0}, \boldsymbol{k}_{2_0})$ the situation as to the k-dependence of the integrand is analogous to case a); making therefore the same approximations as before we can immediately evaluate the integrals. The result is

$$\langle k^2\chi^2\rangle = \frac{2\pi\Lambda^2}{[1+\Lambda F(k_0)]^2}\frac{k_F}{(k_0^2+\beta^2)^2}\left\{\frac{1}{2(k_F^2+\beta^2)(k_F^2-k_0^2)}\right.$$
$$\left. + \frac{\beta^2-k_0^2}{2(k_0^2+\beta^2)^2}\left[\frac{1}{(k_0^2+\beta^2)}\lg\frac{k_F^2-k_0^2}{k_F^2+\beta^2}+\tfrac{1}{2}\frac{2k_F^2+\beta^2-k_0^2}{(k_F^2+\beta^2)(k_F^2-k_0^2)}\right]\right\}, \quad (25b)$$

$$I(k_0) = -\frac{2\pi\Lambda}{1+\Lambda F(k_0)}\frac{k_F}{(k_0^2+\beta^2)^2}\left[\frac{1}{k_0^2+\beta^2}\lg\frac{k_F^2+\beta^2}{k_F^2-k_0^2}-\frac{1}{k_F^2+\beta^2}\right]. \quad (25c)$$

Putting $\langle\chi^2\rangle$, $\langle k^2\chi^2\rangle$ and $I(k_0)$ into the energy expression (17), we still have to perform the sums over the states of the Fermi-sphere. In carrying out these sums we have to distinguish essentially between two types of terms:

1) terms, like $\langle\chi^2\rangle$, $\langle k^2\chi^2\rangle$, $I^2(\boldsymbol{k}_0)$ which are rotationally symmetric in k-space;

2) terms, like $I(\boldsymbol{k}_0)[g(\boldsymbol{k}_0+\boldsymbol{q})+g(\boldsymbol{k}_0-\boldsymbol{q})]$ which depend on the fixed vector $\boldsymbol{q}$.

We first treat the terms independent of $\boldsymbol{q}$. The summations to be carried out are of the following type:

$$\sum = \frac{(2\pi)^3}{\Omega}\sum_{\boldsymbol{k}_1,\boldsymbol{k}_2} \to \frac{\Omega}{(2\pi)^3}\iint \mathrm{d}k_1^3\,\mathrm{d}k_2^3. \quad (26)$$

We introduce relative and total momenta by

$$\boldsymbol{k}_1+\boldsymbol{k}_2 = \boldsymbol{K}, \qquad \tfrac{1}{2}(\boldsymbol{k}_1-\boldsymbol{k}_2) = \boldsymbol{k},$$

and obtain

$$\sum = \frac{\Omega}{(2\pi)^3}\iint \mathrm{d}K^3\,\mathrm{d}k^3,$$

with the conditions on the range of integrations

$$k_1 = |\boldsymbol{k}+\tfrac{1}{2}\boldsymbol{K}| \leqq k_F, \qquad k_2 = |-\boldsymbol{k}+\tfrac{1}{2}\boldsymbol{K}| \leqq k_F.$$

This is equivalent to the following condition on the angular integration of $\boldsymbol{K}$:

$$\int \mathrm{d}\Omega_K = \begin{cases} 4\pi & \text{for } \tfrac{1}{2}K \leqq k_F-k, \\ 4\pi\left[\dfrac{k_F^2-k^2-\frac{1}{4}K^2}{k^2}\right] & \text{for } k_F-k \leqq \tfrac{1}{2}K \leqq \sqrt{(k_F^2-k^2)}, \\ 0 & \text{for } \tfrac{1}{2}K \geqq \sqrt{(k_F^2-k^2)}. \end{cases} \quad (27)$$

Then one obtains

$$\int \mathrm{d}K^3 = 4\pi\int_0^{2(k_F-k)} K^2\,\mathrm{d}K + 4\pi\int_{2(k_F-k)}^{2\sqrt{k_F^2-k^2}} K^2\,\frac{k_F^2-k^2-\frac{1}{4}K^2}{k^2}\,\mathrm{d}K \quad (28)$$
$$= \tfrac{32}{3}\pi k_F^3\left(1-\tfrac{3}{2}\frac{k}{k_F}+\tfrac{1}{2}\frac{k^3}{k_F^3}\right),$$

and the final result is

$$\sum = 2\frac{\Omega}{(2\pi)^3}\cdot\tfrac{4}{3}\pi k_F^3\cdot 16\pi\int_0^{k_F} k^2\left(1-\tfrac{3}{2}\frac{k}{k_F}+\tfrac{1}{2}\frac{k^3}{k_F^3}\right)\mathrm{d}k$$

$$= 16\pi N\int_0^{k_F} P(k)\mathrm{d}k, \tag{29}$$

where we introduced

$$P(k) = k^2\left(1-\tfrac{3}{2}\frac{k}{k_F}+\tfrac{1}{2}\frac{k^3}{k_F^3}\right), \qquad 2\frac{\Omega}{(2\pi)^3}\cdot\tfrac{4}{3}\pi k_F^3 = N.$$

In performing the summations of the second type one can carry out all operations from (26) to (28). In the angular integrations over relative momenta we can just as before perform the ϕ_k-integration, which gives a factor 2π. The integration over the polar angle θ_k can also be carried out. Here we have the following two types of integrals:

1) $$\int\frac{\mathrm{d}\Omega_k}{(k_0+p)^2+\beta^2} = 2\pi\int_0^{\pi}\frac{\sin\theta\,\mathrm{d}\theta}{k_0^2+p^2+\beta^2+2k_0p\cos\theta}$$

$$= 2\pi\int_{-1}^{+1}\frac{\mathrm{d}x}{k_0^2+p^2+\beta^2+2k_0px} = \frac{\pi}{pk_0}\lg\frac{\beta^2+(k_0+p)^2}{\beta^2+(k_0-p)^2},$$

where the vector $\boldsymbol{p}$ is $\boldsymbol{q}$ or $2\boldsymbol{q}$;

2) $$\int\left[\frac{1}{(k_0+q)^2+\beta^2}+\frac{1}{(k_0-q)^2+\beta^2}\right]^2\mathrm{d}\Omega_k$$

$$= 2\pi\int_0^{\pi}\left[\frac{1}{k_0^2+q^2+\beta^2+2k_0p\cos\theta}+\frac{1}{k_0^2+q^2+\beta^2-2k_0p\cos\theta}\right]^2\sin\theta\,\mathrm{d}\theta$$

$$= 2\pi\int_{-1}^{+1}\left[\frac{1}{(k_0^2+q^2+\beta^2+2qk_0x)^2}+\frac{1}{(k_0^2+q^2+\beta^2-2qk_0x)^2}\right.$$

$$\left.+\frac{2}{(k_0^2+q^2+\beta^2)^2-4k_0^2q^2x^2}\right]\mathrm{d}x$$

$$= \frac{2\pi}{qk_0}\left\{\frac{1}{\beta^2+(k_0-q)^2}+\frac{1}{\beta^2+(k_0+q)^2}+\frac{1}{\beta^2+k_0^2+q^2}\lg\frac{\beta^2+(k_0+q)^2}{\beta^2+(k_0-q)^2}\right\}.$$

The remaining integrations over k have to be evaluated numerically.

3. Discussion of Results

The k-integrations were carried out on the electronic computer Z 22 of the Institut für angewandte Mathematik der Universität des Saarlandes. One obtains the energy

correction ΔE as a function of the quantities k_F, β, q and Λ; is it important to note that actually ΔE can be written in the form

$$\Delta E = q^2 \bar{H}\left(\Lambda, \frac{k_F}{\beta}, \frac{q}{\beta}\right),$$

where $\bar{H}$ is a function of Λ, k_F/β and q/β.

Instead of k_F/β and q/β we want to introduce the quantities r/d and r/λ; here $r = 1/\beta$ is the "range" of the potential, $\lambda = 2\pi\sqrt{3}/q$ is the wavelength of the periodic density variation and d is the mean distance of the particles; since $k_F d = 3.84$ one

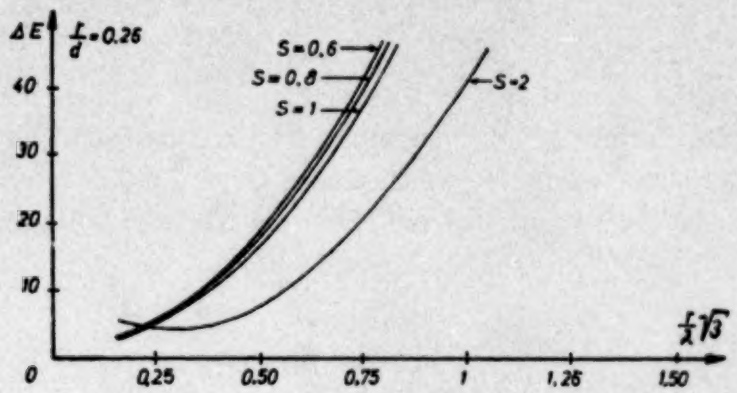

Fig. 1. Energy correction ΔE in arbitrary units as a function of r/λ with potential strength s and r/d as parameters.

gets $k_F/\beta = 3.84\, r/d$ and $q/\beta = 2\pi\sqrt{3}\, r/\lambda$. Instead of the potential strength Λ we introduce, following the notation of Yamaguchi [7]), the dimensionless quantity s defined by $\Lambda = s\beta^3/\pi^2$.

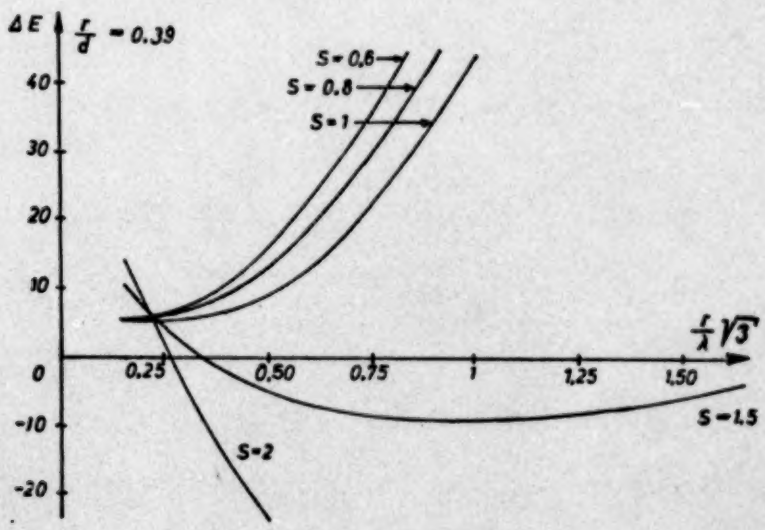

Fig. 2. See caption of fig. 1.

For the question of the existence of density-modulated ground states only the sign of the function $H(s, r/d, r/\lambda)$ is relevant. In figs. 1 to 4 we have plotted ΔE in arbitrary

units as a function of r/λ for the values of $r/d = 0.269, 0.39, 0.52, 0.76$ respectively. That we have plotted ΔE as a function of r/λ means that for a given curve the range r has to be kept fixed while λ is varied. For different values of r we would obtain curves

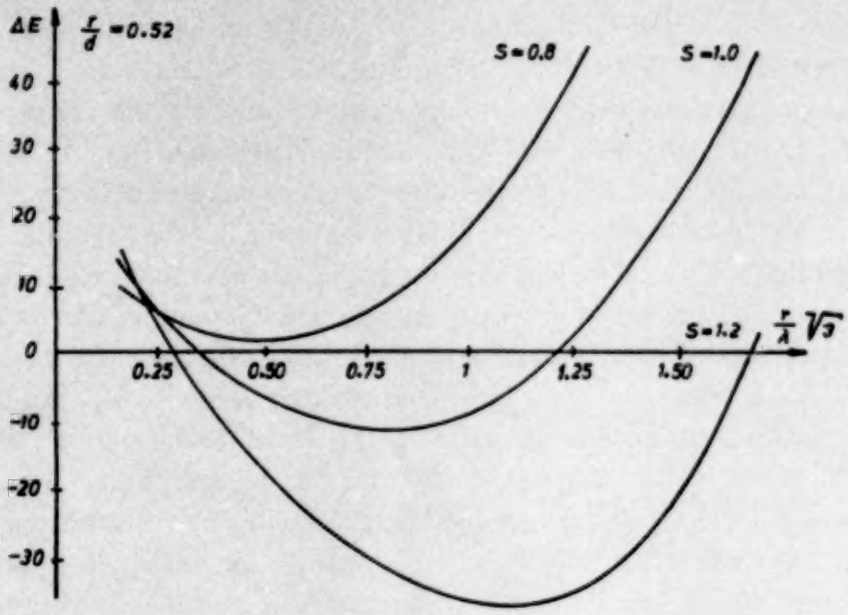

Fig. 3. See caption of fig. 1.

that follow from the original one by a similarity transformation along the ordinate. Since thereby the points where the curves intersect the abscissa are not changed the criterion for the existence of density variations is also not changed. Therefore it is

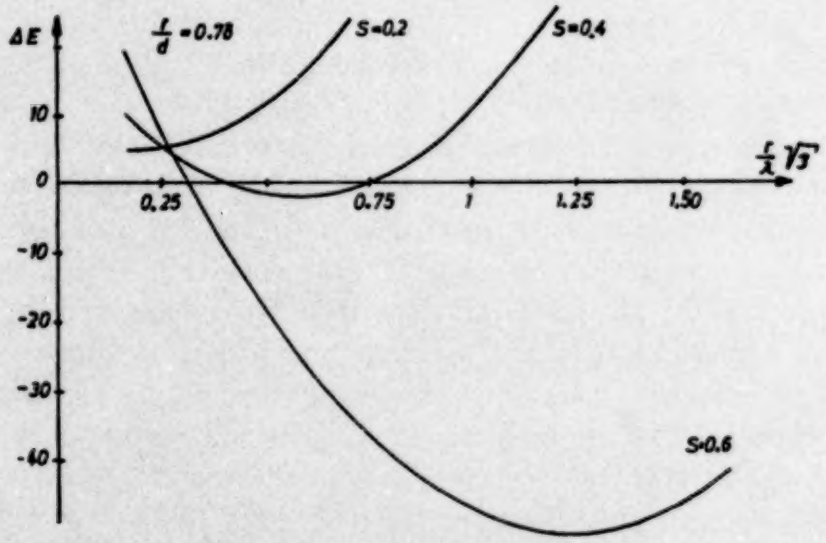

Fig. 4. See caption of fig. 1.

sufficient to draw just one curve for each value of r/d. The values of the strength parameter s are given at each curve. For $r/d = 0.26$ the quantity ΔE is always positive

since in that case values of s larger than 2 could not be used. This is due to the fact that for the potential used there exists a singularity in the solutions of the Bethe-Goldstone equation near the Fermi-surface †. The singularity arises if in the equation defining the correlation amplitude (eq. (24)) the denominator $1+\Lambda F(\boldsymbol{k}_{1_0}, \boldsymbol{k}_{2_0})$ becomes zero. Now the integral defining $F(\boldsymbol{k}_{1_0}, \boldsymbol{k}_{2_0})$ is the larger the smaller the density, since θ being a projection operator on the outside of the Fermi sphere the integration volume increases with decreasing density. Therefore the distance at which the singularity is located from the Fermi surface increases with decreasing density. If we could have performed the k-integrations exactly there would be no problem at all about the singularities, since the singularity being of the logarithmic type all integrals are finite. Because we had to evaluate the k-integrations numerically we had to adopt a special procedure to treat the singularities. This procedure was as follows: In all integrals that had to be evaluated the integrand approaches zero as k approaches k_F. For a value $\bar{k} = k_F - \delta$ there is a very narrow singularity. In all cases the integral over this singularity is very small compared to the rest of the integral. We have divided the interval from $k = 0$ to $k = k_F$ into 20 intervals so that the abscissa closest to $k = k_F$ was $k = 0.95\, k_F$. In performing the integration we then restricted the potential strength to such values that the critical quantity $1+\Lambda F(\boldsymbol{k}_{1_0}, \boldsymbol{k}_{2_0})$ which enters into all integrals is not smaller than 0.5. Thus we have a well-behaved integrand between $k = 0$ and $k = 0.95\, k_F$ and a narrow singularity between $k = 0.95\, k_F$ and $k = k_F$. At $k = k_F$ all integrands are zero. Since the integral over the singularity gives a very small contribution compared to the integral from $k = 0$ to $k = 0.95\, k_F$ we have neglected the influence of the singularity. Nevertheless we have to keep the restrictions on because otherwise the singularity could be located too far away from $k = k_F$, thus spoiling the approximation. For $r/d = 0.26$ the upper permissible value for s was $s = 2.2$.

For the other values of r/d the critical value of s was so large that long before the energy correction became negative. The result that for $r/d = 0.26$ we obtain only positive values of ΔE is not a physical one; it is rather induced by the nature of the approximation used in treating the singularities of the Bethe-Goldstone equation. If the singularities had been treated exactly there would have been of course values of s for which a negative ΔE had resulted. For weak potentials and low densities one obtains practically the parabolic variation $\Delta E \approx 1/\lambda^2$ which corresponds to the kinetic energy correction $\Delta E \approx \hbar^2 q^2/m$ of the non-interacting system. As one sees from figs. 1 to 4 the tendency to build up density modulated states increases with increasing density and increasing potential strength. The position of the minimum value of the curves shows that the energetically most favourable density distribution corresponds to wavelengths that are approximately equal to the range r of the force. It is seen that as $\lambda \to \infty$ or $r/\lambda \to 0$ the quantity ΔE does not tend to zero as one would expect. The reason for this is the following: In our derivation of the energy correction

† See, for example, ref. [8]), where also other references are given.

ΔE we have assumed that states like $\delta(k-k_0)$ and $\delta(k-k_0\pm q)$ are orthogonal to each other, which means that we cannot go to the limit $q = 0$ in the final result.

Figs. 1 to 4 were obtained for density fluctuations that are distributed in the form of a three-dimensional cubic lattice, i.e. the vector q is given by $q = \frac{1}{3}q\sqrt{3}(e_x+e_y+e_z)$. There arise other instabilities for one or two-dimensional distributions. We have evaluated the energy corrections for a one-dimensional and a square two-dimensional distribution. The energy curves are very similar to those already given. The essential difference is that instability requires less interaction strength and less density for the one and two-dimensional cases than for the three-dimensional case. In fig. 5 we have

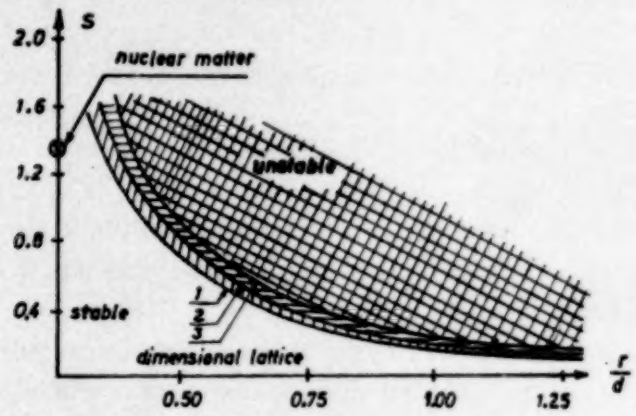

Fig. 5. Regions where the homogeneous density distribution is stable or unstable for a one-dimensional periodic distribution, a two-dimensional square lattice distribution and a three-dimensional cubic lattice distribution.

drawn in the $s-r/d$ plane the curves for the one, two and three-dimensional cases that separate the regions were the homogeneous density distribution is stable or unstable, respectively, against periodic density variations. In the nuclear case the value for β in the triplet state is $\beta = 1.45$ fm^{-1} (see Yamaguchi loc. cit.). The corresponding value of s is $s = 1.34$. Assuming a value of 1.4 fm^{-1} for k_F one gets $r/d = 0.25$. The corresponding point lies well outside the instability region.

We still have to discuss the meaning of the notion "range" for our separable potential. Eq. (19) seems to indicate that the range has a quite different meaning here since is does not refer to the distance $|r_1-r_2|$ between the particles but rather to the distances $|r_1-r_1'|$ and $|r_2-r_2'|$ respectively. Nevertheless one can demonstrate that in its effect on a wave function the Yamaguchi potential acts very much like a normal local potential of the same range. This is most easily seen if one considers the bound-state and scattering wave functions of the two-nucleon problem. It was shown by Yamaguchi that the deuteron wave function for the potential (18) is given by

$$\psi(r) = \text{const.}\,\frac{e^{-\alpha r}}{r}\,[1-e^{-(\beta-\alpha)r}],$$

where r is the distance between the particles and α is given by the binding energy of

the deuteron

$$\frac{\hbar^2\alpha^2}{m} = 2.226 \text{ MeV}.$$

This wave function is identical to the wave function that follows from the local Hulthén potential,

$$V_H(r) = V_0 \frac{e^{-(\beta-\alpha)r}}{1-e^{-(\beta-\alpha)r}}.$$

Now in our case $\beta \gg \alpha$; therefore one can say that to a good approximation the effect of the Yamaguchi potential in the bound state of the two-body system is the same as the effect of the local Hulthén potential of the same range.

Now we turn to the scattering wave function. It is of the form

$$\psi(r) = e^{ik\cdot r} + f(k)\frac{e^{ikr}-e^{-\beta r}}{r}.$$

One sees that the correlation introduced by the action of the potential is given by the term $e^{-\beta r}/r$. The range $1/\beta$ of this correlation is the same as one would expect from a local potential of range $1/\beta$.

We still want to add a remark concerning the restriction to pair interactions. The neglect of correlations of higher order does surely bring in considerable mistakes for values of $r/d > 0.5$, which correspond to systems more than twice as dense as nuclear matter. But this will not change our conclusion that for such systems the ground state is density-modulated, because higher order correlations will always be in favour of an essentially cooperative effect like the build up of periodic density fluctuations.

Finally I want to thank Dipl.-Phys. H. Martin for performing the calculations on the electronic computer.

References

1) E. P. Gross, Ann. of Phys. **4** (1958) 57, **9** (1960) 262
2) E. P. Gross, Phys. Rev. Letters **4** (1960) 599
3) L. E. Trainor, A. B. Bhatia and P. C. Sood, Nuclear Physics **9** (1958) 297
4) A. W. Overhauser, Phys. Rev. Letters **4** (1960) 415
5) W. Kohn and St. J. Kittel, Phys. Rev. Letters **5** (1960) 8
6) E. P. Wigner, Trans. Faraday Soc. **34** (1938) 678
7) Y. Yamaguchi, Phys. Rev. **95** (1954) 1628
8) V. J. Emery, Nuclear Physics **19** (1960) 154

1.C:
1.E.6

Nuclear Physics **28** (1961) 369—375; © *North-Holland Publishing Co., Amsterdam*
Not to be reproduced by photoprint or microfilm without written permission from the publisher

THE MOMENT OF INERTIA OF LARGE SYSTEMS AT FINITE TEMPERATURE

R. E. PRANGE †

Institute for Advanced Study, Princeton, New Jersey

Received 19 April 1961

Abstract: It is shown, at least for fermion systems, that the moment of inertia of a normal system tends to the classical rigid value as the volume of the system becomes large. A normal system is one for which a long wave length excitation always has low energy, in contrast to the superfluid, for which there is an energy gap. This result is true only at finite temperature.

1. Introduction

The study of the moment of inertia of large systems has a long history [1])††. Much of the motivation for the study of the problem comes from nuclear physics. On the other hand, the problem of "infinite" systems has an intrinsic interest, since the hydrodynamics of quantal fluids have been imperfectly derived from a microscopic theory.

From the latter point of view, it is important that one should consider the fluid to be at a finite temperature. There are grounds for doubting whether a calculation proceeding upon the assumption that the system is in its ground state remains valid at non-zero temperature. Indeed, at any finite temperature, the thermal energy unit kT is much greater than the characteristic energy level spacing $\delta\varepsilon = \hbar p_F/mD$ of the system. [Here p_F is the Fermi momentum (we are primarily considering fermions), m is the mass of the individual particle and D is a characteristic dimension of the system.] When the temperature tends to zero, this inequality is of course reversed.

It is apparent that some simplification must eventually occur at non-zero temperature, since at high temperatures the system can be regarded as being classical, where upon the calculation of the moment of inertia becomes rather trivial. Indeed, Blatt, Butler and Schafroth [2]) have set forth arguments which would indicate that the moment of inertia of any realistic quantal system in thermal equilibrium ought to have the classical rigid value. However, since they proved at the same time that a system having a rigid inertial moment cannot exhibit a Meissner effect, they concluded that the Meissner effect is not

† National Science Foundation Postdoctoral Fellow. Present address: University of Maryland College Park, Maryland.

†† See ref. [1]) for a more complete list of references.

an equilibrium phenomenon [3]). But there are very good experimental grounds for believing that the Meissner effect *is* an equilibrium phenomenon. Thus one must re-examine the arguments and premises presented by BBS.

One premise which has been held suspect is the following: it is postulated that for any actual system, there exists a correlation length which is independent of the size of the containing potential. This length can always be regarded as microscopic, since we consider the large volume limit. In particular, it is assumed that the momenta of particles which are separated by a distance greater than the correlation length are uncorrelated. Now, this idea of a correlation length certainly has a very strong intuitive and experimental appeal. It is tantamount to the assertion that the system exhibits extensive properties. It has been shown under fairly general conditions that systems in thermal equilibrium do have the extensive property [4]). Accordingly, it would be preferable not to give up the assumption of a correlation length.

The examination now to be presented of the arguments of BBS reveals that one step in the chain of reasoning is not sufficiently precise. The remainder of their argument appears to be sound. The result of the modified argument is that all systems can be expected to have the rigid moment of inertia at sufficiently high temperatures. For normal systems, any temperature is high enough. For superfluids, any temperature such that kT is much larger than the "energy gap" is sufficiently high. This result is not contradicted by experiment. The special case of superfluids is discussed more fully in a following paper.

2. Cranking Model Formulation

We follow previous authors by considering a system in some container of arbitrary shape. If this "bucket" is set into rotation with an angular velocity ω, the density matrix for the system becomes

$$\sigma = \mathrm{e}^{-\beta(H-\omega L_z)}/\mathrm{Tr}\,\mathrm{e}^{-\beta(H-\omega L_z)}, \tag{1}$$

where H is the Hamiltonian of the stationary system, and L_z is the component of the angular momentum operator along the axis of rotation. The angular momentum L is computed according to

$$L \equiv \langle L_z \rangle = \mathrm{Tr}\, L_z \sigma \tag{2}$$

The moment of inertia is defined by

$$\mathscr{I} = \left.\frac{\partial L}{\partial \omega}\right|_{\omega=0}. \tag{3}$$

It is not difficult to carry out this differentiation exactly, even though L_z and H do not commute. The result is conveniently expressed in terms of the eigen-

functions and energy levels of H, and is found to be

$$\begin{aligned}\mathscr{I} &= \sum_{n,\,m} \langle n|L_z|m\rangle\langle m|L_z|n\rangle \frac{e^{-\beta E_n}-e^{-\beta E_m}}{E_m-E_n} \frac{1}{\sum e^{-\beta E_k}} \\ &= 2\sum_{n,\,m} \frac{\langle n|L_z|m\rangle\langle m|L_z|n\rangle}{E_m-E_n} \frac{e^{-\beta E_n}}{\sum e^{-\beta E_k}}.\end{aligned} \tag{4}$$

This formula shows clearly how the usual zero temperature cranking model expression follows in the limit $\beta \to \infty$, keeping the volume fixed [5]).

We can also discuss the condition under which the approximation of BBS is valid. They assume $[L_z, H] \approx 0$ to obtain

$$\mathscr{I} = \beta\langle L_z^2\rangle. \tag{5}$$

The condition is simply that the important states connected by L_z shall differ by much less than $kT = 1/\beta$ in energy. One does at first form the impression that the angular momentum operator can only connect states differing very little in energy. The operator L_z is practically diagonal, since it is only because the bucket does not happen to be cylindrical that L_z does not commute with the Hamiltonian. The breakdown of the rotational symmetry involves the macroscopic dimension associated with the shape of the bucket, and does not involve the microscopic dimensions.

We feel that this geometrical argument is correct, and can in fact be extended quite generally to other operators such as the total momentum **P**, for example. However, the statement should be revised to suggest that L_z can have matrix elements between states differing but little in wave number. By "wave number" we mean the quantum number associated with the geometry of the excitation. In states of definite momentum, this would be the familiar $2\pi/\lambda$. At any rate, this is certainly the situation in the microscopic theory in which the matrix elements of L_z may be calculated.

Ordinarily, of course, states differing in wave number infinitesimally (by amounts of the order $1/D$) also differ infinitesimally in their energies. In particular, state of very long wavelength have very low excitation energies. In such a case, the energy denominators are small in comparison with kT, and the expression (4) can be replaced by that of BBS. We regarded this as the "normal" case and it is therefore of great interest. In particular, whenever the properties of the system can be calculated by perturbation theory, the system is normal, although normal systems are far more general †.

On the other hand, the theory of superfluids [7]), as presently formulated, would lead one to believe that not all of the long wavelength states have low energy, and that there are some states differing very little in wave number

† It may well be that perturbation theory never converges. See, for example, ref. [6]).

which have relatively large separations in energy. These theories †) are characterized by the appearance of an energy gap Δ. In such a case, for temperatures so low that $\beta\Delta$ can no longer be neglected in comparison with unity, the formula (5) cannot be used. The following paper will discuss this situation in more detail in the light of the microscopic theory of superconductivity.

We can now apply the rest of the arguments of BBS, which we believe to be correct. These arguments show that once we have reached expression (5) the rigid moment of inertia follows. More precisely, it follows if the system is normal, but does not follow in the particular case that eq. (5) is true because we happen to have a cylindrical bucket. For completeness, however, we briefly sketch the ideas involved in the following section.

3. Evaluation of the Trace

The central idea in the following is that one tries to compare the expectation value of one operator with the expectation value of another. In particular, we intend to show that

$$\langle L_z^2 \rangle = \langle x^2+y^2 \rangle \langle P_z^2 \rangle, \tag{6}$$

where $\langle x^2+y^2 \rangle$ is the geometrical average over the volume of the container. The way in which we proceed is to study the trace using a particular complete set of states, namely, the momentum eigenstates.

In fact, let $G = \sum G_i$ be any single particle operator which satisfies some conditions to be mentioned later. Then we have

$$\langle G \rangle = \int_V \mathrm{d}^3 x_1 \int \mathrm{d}^3 k \mathrm{e}^{-i\mathbf{k}\cdot\mathbf{x}_1} G_1 \mathrm{e}^{i\mathbf{k}\cdot\mathbf{x}_1} W(k^2), \tag{7}$$

where the function $W(k^2)$ is independent of G. A similar theorem holds for two-particle operators.

Let us take as a complete set of single particle states the functions

$$\phi_{\mathbf{k},i} = \frac{1}{\sqrt{V_1}} \mathrm{e}^{i\mathbf{k}\cdot\mathbf{x}} \theta_i(x), \qquad k_\alpha = 2\pi n_\alpha / V_1^{\frac{1}{3}}. \tag{8}$$

Here we imagine partitioning the bucket into a large number of cubes labelled by the subscript i. The projection θ_i is non-zero only in cube i where it has the value unity. The volume of a cube is denoted by V_1. This volume is supposed to be very large in comparison with the microscopic dimensions in the usual way, but small compared to V.

We suppose that: (a) the operator G is so local that the matrix elements of G connecting single particle states in different cubes i, j can be neglected;

† It must be emphasized that we do not insist upon a complete lack of low energy states. We require only that a significant fraction of those states connected by L_z be separated in energy.

(b) any effects arising in case G is not strictly defined in the states $\phi_{\mathbf{k},i}(\mathbf{x})$ can be neglected. Restriction (a) is not very serious, since we want to consider only operators whose non-locality is at most microscopic in extent. Restriction (b) is more important and may prevent the result from applying to the Bose system. An operator may be undefined because it contains differentiations. The states $\phi_{\mathbf{k},i}$ can be smoothed out a bit, so that differentiations are defined. If the single-particle states have sufficiently high momenta, the error in using eq. (11) below can be made small. Such is the case for fermions. It is more difficult to make rigorous statements in the case of bosons, because one or a few long wavelength states have to be treated accurately †.

It might be noted in passing that even though the Hamiltonian may be undefined in the states (8), the density matrix is defined. Of course, conditions on the Hamiltonian are needed to ensure that it describes an extensive system.

We complete the argument by noting that we can use as a complete set of states for the N-particle system the states

$$\Phi_{K,I}(X) = \phi_{\mathbf{k}_1 i_1}(\mathbf{x}_1) \ldots \phi_{\mathbf{k}_N, i_N}(\mathbf{x}_N) \tag{9}$$

which in addition must be properly symmetrized. This symmetrization is denoted by

$$\Phi_{K,I}(X_\mathrm{P}) = \frac{1}{N!} \sum_{\text{permutations}} \varepsilon_\mathrm{P} \phi_{\mathbf{k}_1 i_1}(\mathbf{x}_{\mathrm{P}_1}) \ldots \phi_{\mathbf{k}_N i_N}(\mathbf{x}_{\mathrm{P}_N}). \tag{10}$$

The notation is standard. The assumed properties of G allow the replacement

$$G_1 \Phi_{KI}(X) = \Phi_{KI}(X) \mathrm{e}^{-i\mathbf{k}_1 \cdot \mathbf{x}_1} G_1 \mathrm{e}^{i\mathbf{k}_1 \cdot \mathbf{x}_1}. \tag{11}$$

One obtains directly

$$\langle G \rangle = \int_\mathrm{V} \mathrm{d}^3 x_1 \int \mathrm{d}^3 k (\mathrm{e}^{-i\mathbf{k}_1 \cdot \mathbf{x}_1} G_1 \mathrm{e}^{i\mathbf{k} \cdot \mathbf{x}_1}) W(\mathbf{k}, \mathbf{x}_1), \tag{12}$$

where

$$W(\mathbf{k}, \mathbf{x}) = \sum_{\substack{i_1 \ldots i_N \\ \mathbf{k}_2 \ldots \mathbf{k}_N}} \int \mathrm{d}^3 x_2 \ldots \mathrm{d}^3 x_N \Phi^*_{KI}(X) \exp(-\beta H) \Phi_{KI}(X_\mathrm{P}). \tag{13}$$

We can restrict the structure of W by using the properties of the extensive system. If we suppose that G measures the number of particles situated near a given point and having, approximately, a given momentum, we are led to the conclusion that the function $W(\mathbf{k}, \mathbf{x})$ actually has the simpler form $W(k^2)$.

A similar argument allows us to compare the expectation value of two-particle operators. The formula to be used is

$$\langle F_{12} \rangle = \int \mathrm{d}^3 r_1 \mathrm{d}^3 r_2 \int \mathrm{d}^3 k_1 \mathrm{d}^3 k_2 \mathrm{e}^{-i(\mathbf{k}_1 \cdot \mathbf{r}_1 + \mathbf{k}_2 \cdot \mathbf{r}_2)} F_{12} \mathrm{e}^{i\mathbf{k}_1 \cdot \mathbf{r}_1 + i\mathbf{k}_2 \cdot \mathbf{r}_2} U(\mathbf{k}_1, \mathbf{k}_2, \mathbf{r}_1 - \mathbf{r}_2). \tag{14}$$

† Lebowitz and Onsager [8]), in a calculation based on the phonon model of helium, find that $\langle P^2 \rangle$ depends on the boundary conditions. This result tends to discredit our method in its application to boson systems.

Eq. (6) follows from formulas (7) and (14). The reader should refer to BBS if he is not familiar with the arguments sketched above.

Eq. (6) may be evaluated, if the system is "normal", by noticing that

$$\tfrac{1}{3}\beta\langle P^2\rangle = \frac{\partial}{\partial v}\,\mathrm{Tr}\; P_z e^{-\beta(H-vP_z)}/\mathrm{Tr}\; e^{-\beta(H-vP_z)}. \tag{15}$$

The right hand side of this equality is easily shown to be equal to the total mass of the system. In the case of the superfluid, with an energy gap, the equality (15) may not hold. In that case $\beta\langle P^2\rangle$ is reduced by the ratio of the "normal" fluid density to the total density, and a two-fluid model results.

4. Conclusions

We have here emphasized the role of the energy gap, or lack thereof, in the calculation of the moment of inertia. The ground state theory of superfluids has been criticized for making this same emphasis, since one tends to lose sight of possible changes in important matrix elements (as in eq. (4)). One sees, however, that an energy gap is essential in statistical mechanics if the theory is to account for superfluidity and a Meissner effect. Changes in the matrix elements are irrelevant in statistical mechanics if there is no energy gap.

One important case which the reasoning presented above does not completely cover is that of a charged system interacting via the long range Coulomb forces. In that case, L_z couples strongly to the high energy plasma modes. These are purely longitudinal, however, so that they should contribute exactly the correct amount to the sum (4) to give the rigid inertial moment if no other gap is present.

It should be noted that our result, if correct, demonstrates the importance of making a calculation valid at non-zero temperatures. Rockmore [9]) has asserted, in a calculation based on the ground state perturbation theory, that at zero temperature, the moment may deviate from the rigid value. It would be interesting to examine the transition to zero temperature in detail, since anomalies are already known to exist in this connection (see, e.g., ref. [10])).

The author would like to thank Professor J. Robert Oppenheimer for his hospitality at the Institute for Advanced Study. Discussions with Dr. M. Cohen and Dr. R. Amado are gratefully acknowledged.

References

1) R. E. Prange, Nuclear Physics **22** (1961) 283
2) Blatt, Butler and Schafroth, Phys. Rev. **100** (1955) 481 (this paper is called BBS in the text).
3) M. R. Schafroth, Phys. Rev. **100** (1955) 502
4) T. D. Lee and C. N. Yang, Phys. Rev. **87** (1955) 404

5) D. R. Inglis, Phys. Rev. **96** (1954) 1059
6) L. N. Cooper, Bull. Am. Phys. Soc. **6** (1961) 16
7) Bardeen, Cooper and Schrieffer, Phys. Rev. **108** (1957) 1175;
N. N. Bogoliubov, J. Phys. USSR **9** (1947) 23
8) J. Lebowitz and L. Onsager, in: Low temperature physics and chemistry, (University of Wisconsin Press, Madison, 1958) p. 119
9) R. M. Rockmore, Phys. Rev. **120** (1960) 1933
10) W. Kohn and J. M. Luttinger, Phys. Rev. **118** (1960) 41

1.C:
1.E.6

Nuclear Physics **28** (1961) 376—386; © *North-Holland Publishing Co., Amsterdam*
Not to be reproduced by photoprint or microfilm without written permission from the publisher

THE MOMENT OF INERTIA OF SUPERFLUID FERMION SYSTEMS OF FINITE TEMPERATURE

R. E. PRANGE †

The Institute for Advanced Study, Princeton, New Jersey

Received 19 April 1961

Abstract: The moment of inertia is studied as an example of the second order response of a superfluid to an external force. The theory of Bardeen, Cooper and Schrieffer is used to describe the superfluid. It is essential to use the extension of the theory which maintains gauge invariance. The result shows that the usual two-fluid model is applicable, with the superfluid component governed by the irrotational flow hydrodynamics. A correction is found to the expression for the normal fluid density which takes into account the effective mass of the excitations.

1. Introduction

In the preceding paper [1]) the importance of making hydrodynamical calculations which are valid at finite temperature was emphasized. The present paper generalizes a previous calculation [2])†† of the moment of inertia of superfluid fermion systems with that motivation in mind. It should be recognized that the computation is an example of the calculations which must be performed for the purpose of finding the response of the system to an external force. Perhaps the most important special case is the computation of the response to an external magnetic field, which is the theory of the Meissner effect.

There are a large number of contributions to the theory of the Meissner [4]) effect, which are particularly aimed at making the calculation gauge invariant. Actually, the majority of these calculations are identical except in emphasis, and in the particular form of the equations. The equations are so complicated that this fact has not always been clear.

The theory of this paper can just as easily be applied to a study of the Meissner effect. That problem has not been fully studied in its statistical mechanical form up to now. However, the moment of inertia calculation requires some generalizations not needed for the study of the magnetic response, and we have therefore restricted the discussion to the hydrodynamical theory to fix the ideas.

† National Science Foundation Postdoctoral Fellow. Present Address: University of Maryland, College Park, Maryland.

†† See also ref. [3]). The author is indebted to Prof. Oppenheimer for calling the paper of Katz and Blatt to his attention.

The result is quite as expected. It is found that a fermion superfluid behaves according to the phenomenological model of Landau [5]). Landau's theory was intended to apply to helium. Its qualitative features carry over to the fermion case, however. At least for the simplest motions, the fermion superfluid behaves as two interpenetrating fluids. The normal component has a viscosity and rotates rigidly, the superfluid component follows the hydrodynamical law of irrotational flow. The irrotational flow follows from the gauge invariance of the Hamiltonian. Some corrections are found to the expression for the normal fluid density given by the elementary theory [6]). Details of the calculation are presented in an appendix.

2. Theory of Superconductivity

We rely on the theory of Bardeen, Cooper and Schrieffer [6]), and of Bogoliubov [7]). We shall formulate it in an elementary way which at the same time contains the results of the generalizations of the theory [4]).

In this theory, one should like to take into account all interactions involving two single-particle *states* at a time. "Particle-particle", "particle-hole" and "hole-hole" interactions therefore need to be considered. The particles not explicitly under consideration are regarded as being in the thermal equilibrium state. It is convenient to identify these states, in spite of the fact that they may have different numbers of particles. If this is done, a theory results in which the number of particles apparently is not conserved, but which is much simplified.

Several ways are available to calculate the density matrix in this approximation. Here we restrict the form of the matrix, consistently with the above remarks, and use the variational principle. We choose the density matrix, consequently, to have the structure

$$\sigma_R = \mathrm{e}^{-\beta(H_R-\mu N)}/\mathrm{Tr}\,\mathrm{e}^{-\beta(H_R-\mu N}, \tag{1}$$

where

$$H_R-\mu N = \sum_{r,s} \tilde{\varepsilon}_{rs} a_r^\dagger a_s + \tfrac{1}{2}\sum \Delta_{rs}(a_r^\dagger a_s^\dagger + a_s a_r). \tag{2}$$

The operator a_r destroys a particle in the state labelled by the subscript, r. The states are not necessarily to mean momentum eigenstates, as we shall see. The unknowns $\tilde{\varepsilon}_{rs}$ and Δ_{rs} are to be determined by the variational principle. A factor $\beta = 1/kT$ has been made explicit for convenience. Clearly, this density matrix can take into account only the mentioned correlations between two single-particle states.

This assumption about the structure of the density matrix is already a very strong one. Unfortunately, the form is still too general for practical purposes. In order to make the mathematics manageable, the controversial

"pairing" hypothesis is made. According to this hypothesis, it is sufficient, as an initial approximation, to crowd the entire effect of the correlations onto the "diagonal" part of H_R, which we denote by H_{VR}. This operator has the form

$$H_{VR}-\mu N=\sum_{\nu}\tilde{\varepsilon}_{\nu}a_{\nu}^{\dagger}a_{\nu}-\tfrac{1}{2}\sum\Delta_{\nu}(a_{\nu}^{\dagger}a_{-\nu}^{\dagger}+a_{-\nu}a_{\nu}). \tag{3}$$

We have yet to specify the meaning of the states ν, and the pairing $(\nu, -\nu)$. For most purposes, the problem is relatively unimportant, since any reasonable choice leads to the same final result, if purely extensive properties are to be calculated. The moment of inertia, on the other hand, depends on the shape of the boundary. The choice of these states thus becomes important.

The choice of states and their pairing should, strictly speaking, be regarded as part of the variational problem. Since it is too difficult to carry out a direct calculation, however, a guess must be made. The states must reflect the shape of the potential, and the pairing has to be symmetric. Consequently, it is reasonable to take the states ν to be the eigenstates of a single particle contained in the bucket †. The pairing will be such that $-\nu$ is the conjugate of ν under time reversal. If time reversal is the sole symmetry, it is sufficient to define the states. When there is a further symmetry, such as rotational symmetry about some axis, the states should be chosen in such a way that the operator H_{VR} preserves the symmetry. We should like to suggest, however, that the pairing hypothesis is a relatively unimportant approximation, and that the essential approximations have already been made after the density matrix is restricted to the form characterized by the operator H_R.

It must be emphasized that it is only in the case that the container is not in rotation that the system has a time reversal symmetry. It is only for that case, therefore, that this choice of states can possibly be justified. We shall have to relax the pairing condition when the rotation is considered.

The variational equations may be obtained by maximizing the entropy, subject to the conditions that the average energy and particle number have definite values. The equations are

$$\delta\left(-\frac{1}{k}S+\beta\langle H\rangle-\beta\mu\langle N\rangle\right)=0, \tag{4}$$

where

$$S=-k\,\mathrm{Tr}\,\sigma\ln\sigma, \qquad \langle H\rangle=\mathrm{Tr}\,\sigma H, \qquad \langle N\rangle=\mathrm{Tr}\,\sigma N, \tag{5}$$

and β and $\beta\mu$ are the usual Lagrange multipliers. We of course take H to be the actual Hamiltonian of the system, which we presume to be of the form

$$H=-\sum_{i}\frac{\nabla_i^2}{2m}+U(x_i)+\sum_{j<i}v(x_i-x_j), \tag{6}$$

† If a similar approach is applied to the Bose system, the choice of states is non-trivial.

or

$$H = \sum \varepsilon_r a_r^\dagger a_r + \tfrac{1}{2} \sum v_{rsvq} a_r^\dagger a_s^\dagger a_v a_q \tag{7}$$

in the notation of second quantization. It is important that the Hamiltonian be gauge invariant. In this method, we do not ask what part of the Hamiltonian is important, but consider what kinds of correlations are important.

The above equations can be studied by diagonalizing H_{VR}. The diagonalization is carried out by means of the Bogoliubov transformation

$$a_r = U_r \alpha_r + V_r \alpha_{-r}^\dagger, \tag{8}$$

where we define

$$E_r = +\sqrt{\tilde{\varepsilon}_r^2 + \Delta_r^2}, \qquad U_r^2 = \tfrac{1}{2}\left(1 + \frac{\tilde{\varepsilon}_r}{E_r}\right), \qquad V_r^2 = \tfrac{1}{2}\left(1 - \frac{\tilde{\varepsilon}_r}{E_r}\right). \tag{9}$$

The result of the calculation is expressed by the equations

$$\Delta_r = -\sum_s v_{r-r-ss} \rho_s^0, \tag{10}$$

$$\tilde{\varepsilon}_r = \varepsilon_r - \mu + \sum_s [v_{rssr} - v_{rsrs}] \rho_s^-, \tag{11}$$

where the "filling factors" are

$$\rho_s^- = 1 - \rho_s^+ = U_s^2 f_s^- + V_s^2 f_s^+, \tag{12}$$

$$f_s^- = 1 - f_s^+ = \frac{1}{1 + e^{+\beta E_s}}, \tag{13}$$

$$\rho_s^0 = -\rho_{-s}^0 = U_s V_s \tanh\left(\tfrac{1}{2}\beta E_s\right) = \tfrac{1}{2} \frac{\Delta_s}{E_s} \tanh\left(\tfrac{1}{2}\beta E_s\right). \tag{14}$$

These are the familiar equations for the energy gap and the energy shift. The filling factor f_r^- describes the probability of finding a quasi-particle in state r. The function ρ_r^- gives the probability distribution of the particles themselves. The function ρ_r^0 is, roughly, the amplitude for finding the N particle equilibrium + two extra particle state in the $N+2$ particle equilibrium state.

It should be stressed that these quantities depend only on the energy ε_r of the single-particle state ψ_r, except for terms vanishing with $1/N$. The single particle states of interest have very short wavelengths. Consequently, groups of states with neighbouring energies can be collected into wave packets having a definite momentum and energy. It follows that the parameters characteristic of the theory, e.g. Δ_r, are independent of the set of single particle states used in their calculation. As we shall see later, however, the energy differences $\varepsilon_r - \varepsilon_s$ of neighbouring states are important. It is not possible to use wave packets in this case, hence the necessity to use single particle states appropriate to the container.

If we take this density matrix very seriously, we have the following picture. The system in thermal equilibrium is in one of a group of typical states, in which a certain fraction of the system forms a bound condensate, and the remainder exists as a cloud of more or less non-interacting quasi-particles. At a given temperature, the number of quasi-particles is a large and definite number. Because the amount of condensate is smaller, the higher the temperature, the binding energy of the condensate is correspondingly less: consequently the energy gap depends on the temperature.

The quasi-particles do interact, however, and in certain cases this interaction introduces qualitatively new effects. The interaction is believed to account for the existence of phonons, in particular. Thus the eigen-excitations are not of pure quasiparticle character, but include some excitations of collective character.

The existence of collective excitations should not affect the thermo-dynamics very seriously, for the reason that the density of states of these excitations is small. It is reasonable to regard the density operator σ_{VR} as being sufficient to describe the system, in most cases. When it becomes necessary to take into account the virtual excitations as well as the thermal ones, the quasi-particle approximations breaks down.

In order to calculate the moment of inertia, we use the formulation of the preceding paper [1]). We must evaluate the expression

$$\mathcal{I} = 2\sum_{n,\,m} \frac{\langle n|L_z|m\rangle\langle m|L_z|n\rangle}{E_m - E_n} \frac{e^{-\beta E_n}}{\sum e^{-\beta E_k}}. \tag{15}$$

It is not sufficient to make this evaluation in the quasi-particle approximation. We must also include the effect of virtual collective states.

One approximate way of carrying out the evaluation is to regard certain quasi-particle states as forming a complete set, arranging things so as to be able to make a closure approximation. This method was followed in (I). It is exactly equivalent to the method known in the literature as the random phase approximation, as well as a number of other methods. Here we prefer to use only the variational principle, although there is no significant difference in the final equations. Our method is closely related to that of Blatt [4]).

3. Slow Rotation

A slow rotation of the bucket is taken into account by the addition of the Coriolis term to the Hamiltonian. We must then perform the variation indicated in eq. (4) with the Hamiltonian H replaced by $H-\omega L_z$, where L_z is the appropriate component of the total angular momentum operator. It is no longer possible to use the original pairing hypothesis, because time reversal is not now a symmetry of the system. We are free to treat ωL_z as small, however,

and can consider density matrices of the form (1) with $H_R \to H_{VR}+\omega\delta H_R$. The perturbing operator is allowed to have the full form

$$\delta H_R = \sum_{rs} \delta\varepsilon_{rs} a_r^\dagger a_s + \tfrac{1}{2}\delta\Delta_{rs}(a_r^\dagger a_s^\dagger + a_s a_r), \tag{16}$$

but is treated in perturbation theory. We shall restrict its structure slightly, in order to make sure that it does not lead to corrections even in the absence of rotations. We may suppose that the energy conserving elements $\delta\varepsilon_{rr}$, $\delta\varepsilon_{r-r}$, $\delta\Delta_{r-r}$ vanish. Now it is possible to write the perturbed Hamiltonian in the form

$$H_{VR}+\omega\delta H_R = e^{-i\omega\mathscr{R}} H_{VR} e^{i\omega\mathscr{R}}, \tag{17}$$

where the operator $\mathscr{R}$ has the form

$$\mathscr{R} = \sum S_{rs} a_r^\dagger a_s + T_{rs}\alpha_r^\dagger \alpha_s. \tag{18}$$

This particular choice is convenient. Any arrangement of operators involving bilinear forms of creations and destructions operators would be feasible, however.

A set of equations determining $\mathscr{R}$ is particularly easy to obtain and interpret, since the operator appears in the combination

$$\mathrm{Tr}\, e^{i\omega\mathscr{R}}(H-\mu N-\omega L_z)e^{-i\omega\mathscr{R}}\sigma_{VR}. \tag{19}$$

The variational equations are

$$\mathrm{Tr}\,[a_r^\dagger a_s, [H-\mu N, \mathscr{R}]-iL_z]\sigma_{VR} = 0, \tag{20}$$

$$\mathrm{Tr}\,[\alpha_r^\dagger \alpha_s, [H-\mu N, \mathscr{R}]-iL_z]\sigma_{VR} = 0. \tag{21}$$

After some manipulation, these equations can be written

$$\begin{aligned}
&(\rho_r^- - \rho_s^-)[(\tilde{\varepsilon}_s - \tilde{\varepsilon}_r)S_{rs} - \sum_{pq}(v_{rqsp}-v_{rqps})(\rho_q^- - \rho_p^-)S_{pq}] \\
&+(\rho_r^0+\rho_s^0)[(\Delta_r+\Delta_s)S_{rs}+\sum_{pq} v_{r-s-qp}(\rho_q^0+\rho_p^0)S_{pq}] \\
&+(f_r^- - f_s^-)(U_rU_s - V_rV_s)(E_s-E_r)T_{rs} \\
&-\sum_{pq}(\rho_r^- - \rho_s^-)(v_{rqsp}-v_{rqps})(f_p^- - f_q^-)(U_pU_q+V_pV_q)T_{pq} \\
&-(\rho_r^0+\rho_s^0)\sum_{pq} v_{r-s-qp}(U_pV_q - U_qV_p)(f_p^- - f_q^-)T_{pq} \\
&= (\rho_r^- - \rho_s^-)(L_z)_{rs}
\end{aligned} \tag{22}$$

and

$$\begin{aligned}(E_s-E_r)T_{rs}&-\sum_{pq}(U_rU_s+V_rV_s)(v_{rqsp}-v_{rqps})(U_pU_q+V_pV_q)(f_p^-f_q^-)T_{pq}\\&+\sum_{pq}(U_rV_s-U_sV_r)v_{q-p-rs}(U_pV_q-U_qV_p)(f_p^-f_q^-)T_{pq}\\&+(U_rU_s+V_rV_s)[(\hat{\epsilon}_s-\epsilon_r)S_{rs}-\sum_{pq}(v_{rqsp}-v_{rqps})(\rho_q^-\rho_p^-)S_{pq}]\\&+(U_rV_s-U_sV_r)[(\Delta_r+\Delta_s)S_{rs}+\sum_{pq}v_{r-s-qp}(\rho_q^0+\rho_p^0)S_{pq}\\&=(U_rU_s+V_rV_s)(L_z)_{rs}.\end{aligned}\tag{23}$$

It is necessary to solve these equations. They are less complicated than appears at first sight. For applications to nuclear physics, an iteration solution is no doubt feasible, but iteration is out of the question here. Consider first eq. (22), in which we ignore the terms in T for the present. It is then possible to solve the equation according to the arguments given in (I).

The solution is as follows. The operator S may be separated into a longitudinal and transverse part

$$S_{rs}=\chi_{rs}+\tau_{rs},\tag{24}$$

where the longitudinal part χ is a multiplicative function of position. The matrix element of χ has the form

$$\chi_{rs}=\int\psi_r^*(\mathbf{x})\chi(\mathbf{x})\psi_s(\mathbf{x})\mathrm{d}^3x.\tag{25}$$

The longitudinal part of the solution entirely dominates the transverse, because the transverse excitations are inhibited by the energy gap, and the longitudinal ones are not. There can be no energy gap against longitudinal excitations because the interaction commutes with the generator of the excitations χ. We show in the appendix that inclusion of the terms in T affects only the transverse solution, which is negligible anyway.

Eq. (22), regarded as an equation for χ only, takes the form

$$\nabla\rho(\mathbf{x})\nabla\chi(\mathbf{x})+\left(x\frac{\partial}{\partial y}-y\frac{\partial}{\partial x}\right)\rho(\mathbf{x})=0\tag{26}$$

in coordinate space. This is the continuity equation for potential flow. From this, it will follow that χ represents the part of the response of the system which can be regarded as irrotational flow.

We next turn to the solution of the second equation, (23), with S replaced by χ. The solution of this equation represents the response of the transverse part of the normal fluid component to the Coriolis force. In the appendix, it is shown that the solution of the equation is

$$T_{rs}=\lambda_rL_{rs}^{\mathrm{T}}/(E_s-E_r),\tag{27}$$

where

$$L_{rs}^{T} = L_{rs} - (\varepsilon_s - \varepsilon_r)\chi_{rs} \tag{28}$$

is the "transverse" part of the angular momentum operator. The quantity λ_r is an effective mass correction defined by

$$\lambda_s = \left(1 + \frac{\partial V(s)}{\partial \varepsilon_s}\right) \approx \frac{M}{M^*}. \tag{29}$$

The self-consistent potential $V(s)$ is given by

$$V(s) = \sum_r (v_{srrs} - v_{srsr})\rho_r^{N}. \tag{30}$$

It is to be regarded as the Hartree interaction arising from the interaction of the quasi-particles among themselves. This self-consistent potential changes the energy-momentum dispersion relations for the quasi-particles, or, in more picturesque terms, gives rise to an effective mass. The filling factor ρ_r^{N} is that for the "normal" fluid density. It is

$$\rho_s^{N} = \int_{\epsilon_s}^{\infty} \beta f_r^{+} f_r^{-} \lambda_r \, d\varepsilon_r. \tag{31}$$

The factor λ_r corrects the customary formula.

It should be clearly recognized that the effective mass correction represented by the deviation of λ_s from unity does not correspond to a replacement of the "actual" mass of the quasi-particles by their "effective" mass. Quite the opposite situation occurs in fact. An "effective" mass is already built into the definition of the quasi-particles. We know, however, that it is the actual mass which must enter into quantities involving bulk motion [8]). The correction represented by λ_s ensures that the "actual" mass of the quasi-particles appears.

It remains to compute the moment of inertia. The formula which we must evaluate is

$$\mathscr{I} = \sum T_{rs} L_{sr} (U_r U_s + V_r V_s)(f_r^{-} - f_s^{-}) + \sum S_{rs} L_{sr} (\rho_r^{-} - \rho_s^{-}). \tag{32}$$

Using the fact that the generating operator $\mathscr{R}$ is almost diagonal (see Apendix) we can simplify the expression. It then takes the form

$$\mathscr{I} = \sum (L_z^2)_{rr} \beta f_r^{+} f_r^{-} \lambda_r + S_{rs} (iL_z)_{sr} \{\rho_r^{-} - \rho_r^{N} - \rho_s^{-} - \rho_s^{N}\}, \tag{33}$$

where the normal fluid density has been defined in eq. (31). We call $\rho_r^{S} = \rho_r^{-} - \rho_r^{N}$ the filling factor for the superfluid density.

The first term may be evaluated by summing over wave packets of definite momentum. It is found that

$$\sum (L_z^2)_{rr} \beta f_r^{+} f_r^{-} \lambda_r = \langle x^2 + y^2 \rangle \sum_r (P_z^2) \beta f_r^{+} f_r^{-} \lambda_r, \tag{34}$$

which may be completely evaluated by letting the sum tend to an integral

and integrating by parts. The second term gives the irrotational flow moment of inertia of the superfluid component. The complete result is not unexpected. It is

$$\mathcal{I} = \frac{\rho_N}{\rho}\mathcal{I}_{\text{rigid}} + \frac{\rho_S}{\rho}\mathcal{I}_{\text{irrotational}} \tag{35}$$

We have found that the theory of Bardeen, Cooper, Schrieffer and Bogoliubov, if generalized suitable, leads to the standard phenomenological model of superfluids which was originally proposed for helium. It may seem that many approximations are made in order to obtain this result. These simplifications were made primarily in order to have explicit expressions with which to work. It is probably true that the qualitative features of the phenomenological model are exact, if the microscopic theory is qualitatively true. These features depend on the existence of an energy gap which completely suppresses all transverse excitations, without enhancing the important matrix elements. The question remains completely open, however, whether many-particle correlations, not included in σ_R, lead to qualitative corrections to the theory, even if they are not numerically important.

The author wishes to thank Professor J. R. Oppenheimer for his hospitality at the Institute for Advanced Study. Valuable conversations with Dr. Michael Cohen and Dr. Ralph Amado are gratefully acknowledged.

Appendix

We present some details of the solutions to eqs. (22) and (23) of the text. We need first to state two fundamental facts which must be used throughout the calculation. The first, (A), is that the matrix elements of L_z between single-particle states are almost diagonal. The energies of states connected by L_z. or other smooth operators which we might consider, differ by quantities vanishing with $1/N$. This fact allows one to make great simplifications, which compense somewhat for the circumstance that one cannot always convert sums to integrals.

The second property which we need to use constantly is (B) momentum conservation. The momentum conserving properties of the interaction matrix elements are simple only in coordinate space or momentum space. They are not particularly simple in the space of energy eigenstates. This difficulty can be overcome by using wave-packets. The single particle energy states have very high quantum numbers. It is always possible, therefore, to group them into wave packets, which have almost no spread in energy. We label a complete set of these wave packets, by greek indices μ, and we suppress explicit labels for the spatial positions of the packets. The packets may be chosen

so that the matrix elements of the momentum and the potential satisfy

$$P_{\mu\nu} = \mu\delta_{\mu\nu} \tag{A.1}$$

and

$$v_{\mu\nu\lambda\varrho} = v(|\mu-\varrho|)\delta_{\mu+\nu,\,\lambda+\mathrm{p}}$$

respectively, except for corrections vanishing in the limit $N \to \infty$.
There exists a canonical transformation from the states r to the packets μ, given by a matrix $C_{\mu r}$. This matrix conserves energy in the sense that, when $C_{\mu r} \neq 0$,

$$\varepsilon_r - \frac{\mu^2}{2m} \to 0, \qquad N \to \infty. \tag{A.2}$$

If f_r is a smooth function of the energy, we can replace $f_r C_{\mu r}$ by $f_\mu C_{\mu r}$.

After this preliminary, we study the solution of eq. (23) of the text, with S replaced by χ. Let us study a solution of the form $\lambda_r(L_z)_{rs}/(E_s-E_r)$. We wish to evaluate

$$\sum_{pq} [(U_r U_s + V_r V_s)(v_{rqsp} - v_{rqps})(U_p U_q + V_p V_q) + (U_r V_s - U_s V_r)(v_{q-p-rs})(U_p V_q - U_q V_p)](f_p^- - f_q^-)\frac{\lambda_p (L_z)_{pq}}{E_q - E_p}. \tag{A.3}$$

Using fact (A), according to which the energy denominator practically vanishes, we may simplify (A.3) to

$$\sum_{pq} (v_{rqsp} - v_{rqps})(\beta f_p^+ f_p^- \lambda_p (L_z)_{pq}. \tag{A.4}$$

We can perform the sums over wave-packet states by using the properties (B), and obtain

$$\sum_{\sigma,\varrho,\nu,\mu} \beta f_\mu^+ f_\mu^- \lambda_\mu [v(\sigma-\mu) - v(\mu-\nu)] (\mu_2 \delta_{\mu_2\nu_2} x_{\mu\nu} - \mu_1 \delta_{\mu_1\nu_1} y_{\mu\nu})\delta_{\mu+\sigma,\,\nu+\varrho} C^*_{r\sigma} C_{s\varrho}. \tag{A.5}$$

The following simple manipulations [8]) lead to the desired result:

$$\begin{aligned}
&\sum_{\varrho\sigma} \frac{\Omega}{(2\pi)^3} \int \mathrm{d}^3\mu \lambda_\mu \beta f_\mu^+ f_\mu^- v_{(\sigma-\mu)} \frac{\mu\cdot\sigma}{\sigma^2} (\sigma_2 x_{\sigma\varrho}\delta_{\sigma_2\rho_2} - \sigma_1 y_{\sigma\varrho}\delta_{\sigma_1\rho_1}) C^*_{r\sigma} C_{s\varrho} \\
&= \sum_{\sigma\varrho} \frac{\Omega}{(2\pi)^3} \int \mathrm{d}^3\mu' \lambda_{\mu'+\sigma} \beta \overset{+}{f}_{\mu'+\sigma} \overset{-}{f}_{\mu'+\sigma} \frac{(\mu'+\sigma)\cdot\sigma}{\sigma^2} v(\mu')(L_z)_{\sigma\varrho} C^*_{r\sigma} C_{s\varrho} \\
&= -\sum_{\sigma\varrho} \frac{\Omega}{(2\pi)^3} \int \frac{\partial \rho^{\mathrm{N}}_{\mu'+\sigma}}{\partial\varepsilon_\sigma} v(\mu')(L_z)_{\sigma\varrho} C^*_{r\sigma} C_{s\varrho} \mathrm{d}^3\mu' \\
&= \sum_{\sigma\varrho} \frac{\partial}{\partial\varepsilon_\sigma} \sum_\mu \rho_\mu{}^{\mathrm{N}} (v_{\sigma\mu\mu\sigma} - v_{\sigma\mu\sigma\mu})(L_z)_{\sigma\varrho} C^*_{r\sigma} C_{s\varrho} \\
&= L_{rs} \frac{\partial V(r)}{\partial\varepsilon_r}.
\end{aligned} \tag{A.6}$$

The normal fluid density filling factor is given by eq. (31) of the text.

Similar considerations, using the commutation of χ with the potential, allow us to conclude that

$$(v_{rqsp}-v_{rqps})(f_p^- - f_q^-)\lambda_p \chi_{pq} \frac{(\varepsilon_q-\varepsilon_p)}{E_q-E_p} = +\frac{\partial V(r)}{\partial \varepsilon_r}(\varepsilon_s-\varepsilon_r)\chi_{rs}. \tag{A.7}$$

From these results, one obtains eq. (27) of the text.

We next turn to the consideration of the term

$$(E_s-E_r)T_{rs}(U_rU_s-V_rV_s)(f_r^- - f_s^-), \tag{A.8}$$

which was neglected in the study of eq. (22). We show that this term makes no contribution to the solution χ. It is enough to show that the expression is orthogonal to χ. We have

$$\sum_{rs} \lambda_r L_{rs}^{\mathrm{T}}(U_r^2-V_r^2)(f_r^- - f_s^-)\chi_{sr} = 0, \tag{A.9}$$

because the expression in (A.9) is equal to

$$\sum \chi_{rs} L_{sr}^{\mathrm{T}}(g_r-g_s) \tag{A.10}$$

by fact (A), where g_r is

$$g_r = -\int_{\varepsilon_r}^{\infty} \mathrm{d}\varepsilon_s (U_s^2-V_s^2)\lambda_s \frac{\partial f_s^-}{\partial \varepsilon_s},$$

and expression (A.10) vanishes by eq. (26) at least if $\sum |\psi_r(x)|^2 g_r$ is simply proportional to $\rho(x)$. Since the density is constant except in the neighbourhood of the boundaries, the required proportionality follows. Nothing can be said if there is a strong external force, e.g. a gravitational field, leading to a non-constant density.

The remaining terms can be discussed in a similar manner.

References

1) R. E. Prange, Nuclear Physics **28** (1961) 369
2) R. E. Prange, Nuclear Physics **22** (1961) 283 (this paper is called (I) in the text)
3) A. B. Migdal, Nuclear Physics **13** (1959) 655;
   R. M. Rockmore, Phys. Rev. **118** (1960) 1645;
   A. Katz and J. M. Blatt (preprint)
4) P. W. Anderson, Phys. Rev. **112** (1958) 1900;
   G. Rickhayzen, Phys. Rev. **115** (1959) 795;
   J. M. Blatt and T. Matsubara, Prog. Theoret. Phys. (Kyoto) **20** (1958) 781;
   K. Yosida, Prog. Theoret. Phys. (Kyoto) **21** (1959) 745;
   Y. Nambu, Phys. Rev. **117** (1960) 648
   J. M. Blatt, Prog. Theoret. Phys. (Kyoto) **24** (1960) 851;
   J. G. Valatin, preprint
5) L. D. Landau, J. Phys. (USSR) **5** (1941) 71
6) Bardeen, Cooper and Schrieffer, Phys. Rev. **108** (1957) 1175
7) N. N. Bogoliubov, Doklady Akad. Nauk. (USSR) **119** (1958) 244 (trans.: Soviet Phys. Doklady **3**(1958) 292)
8) R. Amado and K. A. Brueckner, Phys. Rev. **115** (1959) 778;
   R. Rockmore, Phys. Rev. **116** (1959) 469

1.E.1:
3.A

Nuclear Physics **28** (1961) 387—406; © *North-Holland Publishing Co., Amsterdam*
Not to be reproduced by photoprint or microfilm without written permission from the publisher

THE DECAY OF Ce^{144}

J. S. GEIGER, R. L. GRAHAM and G. T. EWAN
Atomic Energy of Canada Limited, Chalk River, Canada

Received 2 June 1961

Abstract: The results of conversion electron-gamma and gamma-gamma coincidence studies of the Ce^{144} decay are presented in this paper. The gamma-ray spectra studied include those coincident with the L_1 33.57, L_1 40.93, K 80.12, L_1 80.12, K 133.53 and L_1 133.53 keV conversion lines and with γ 80.12, γ133.53 and the Pr KX-rays. A detailed search of the conversion electron spectrum for the K line of a 66 keV transition is reported. This search gave a negative result; the intensity of such a line is <5 % of that of the L_1 33.57 conversion line. These new experiments provide both qualitative and quantitative support for the Ce^{144} disintegration scheme previously reported by us which was deduced from a high-resolution investigation of the Ce^{144} internal conversion electron spectrum. The results do not support the various modifications to this scheme which have been recently proposed by four experimental groups. The conversion electron-gamma coincidence results limit the intensity of a β feed to the 99.95 keV level in Pr^{144} to <0.3 % per disintegration.

1. Introduction

We recently published [1]) the results of a high resolution study of the Ce^{144} conversion electron spectrum and the resultant Pr^{144} level scheme. This Pr^{144} level sequence is shown in fig. 1; the level energies, spins and parities were derived uniquely from the precisely measured transition energies, their relative intensities and their multipolarities. Subsequently several further studies of the Ce^{144} decay by other workers have come to our attention [2–5]). While most of their experimental results are consistent with the decay scheme of fig. 1, there exist several points of disagreement. These are summarized below.

1.1. EXISTENCE OF LEVELS IN Pr^{144} AT 166 AND 175 keV.

The conversion line studies, β-spectrum studies, and gamma-conversion electron coincidence studies of Freeman [4]) indicate a level in Pr^{144} at 166 keV. Freeman found the L line of the 33.57 keV transition to be coincident with γ133.53. He has observed several new lines in the Ce^{144} conversion electron spectrum which are tentatively assigned to transitions of 66 and 86.5 keV. These weak transitions are assumed to occur between the proposed 166 keV level and the levels at 99.95 and 80.12 keV. His β-spectrum studies provide evidence for a β feed to this 166 keV level.

The experimental evidence for a level in Pr^{144} at 175 keV results from the gamma-conversion electron coincidence studies of Forafontov and Sorokin [3]).

These authors observed coincidences between the L conversion line of the 40.93 keV transition and γ133.53. Since a search showed no γ40.93–γ133.53 coincidences they concluded that the 40.93 keV transition goes predominantly by conversion between levels at 175 and 133. 53 keV. An earlier β-spectrum study by Parfenova, Forafontov and Shipinel [6]) provides evidence for a β feed to this proposed level.

1.2. A GAMMA TRANSITION OF ≈ 96 keV

While several experimenters have interpreted the Ce^{144} conversion line group at ≈ 53 keV as the K line of an ≈ 96 keV transition [5, 7–10]), our high-resolution

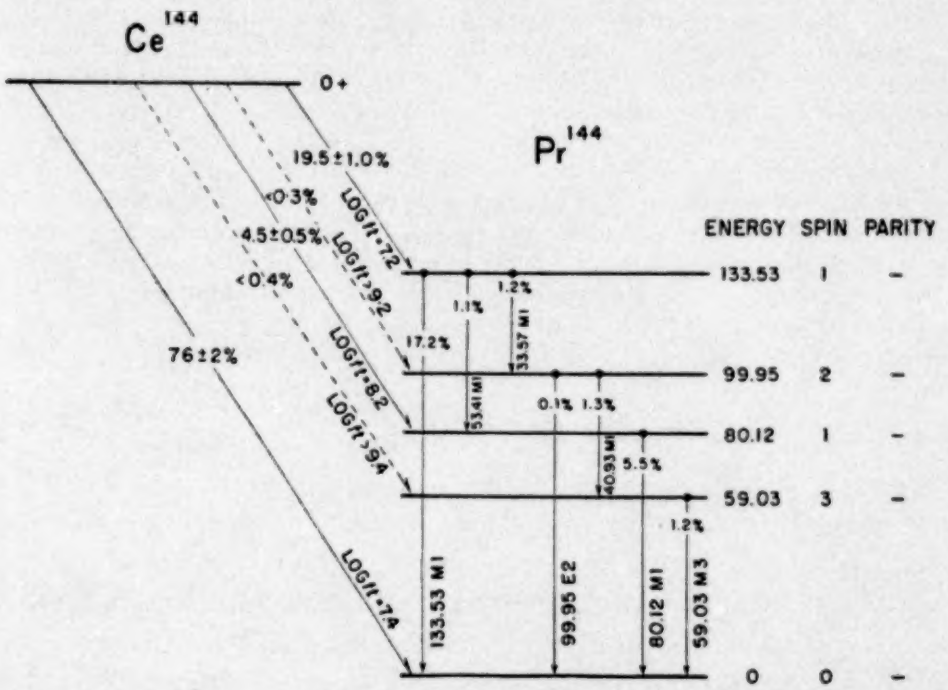

Fig. 1. This Ce^{144} disintegration scheme was deduced from the conversion electron energy and relative intensity measurements previously reported by Geiger *et al.* [1]) The conversion electron-gamma- and gamma-gamma coincidence studies and the conversion electron spectrum study reported in this paper provide additional support for this decay scheme. The intensity limit of < 0.3 % on the β feed to the 99.95 keV level has been deduced from the conversion electron-gamma coincidence results of the present investigation.

conversion line studies [1]) showed this 53 keV line group to be composed of the M_I line of the 53.41 keV transition and the L_I, L_{II} and L_{III} lines of the 59.03 keV transition (see fig. 2 of ref. [1])). Recent gamma-gamma coincidence measurements by Sengupta *et al.* [5]) however, provide evidence for quanta of ≈ 96 keV. The gamma-ray spectrum which they observed in coincidence with the Pr K X-rays (and γ33.57) has a 96 keV peak (γ99.95?) whose intensity relative to γ80.12 is some 20 times greater than can be explained on the decay scheme of fig. 1.

1.3. PRESENCE OF ADDITIONAL WEAK CONVERSION LINES IN THE Ce^{144} SPECTRUM

Freeman [4]) has observed six weak lines in the Ce^{144} conversion electron spectrum which have not previously been reported. The half-life associated with these new transitions was not established, however. Two of these lines have been tentatively assigned to a 66 keV transition and two to an 86.5 keV transition; these new transitions are assumed to feed the 99.95 and 80.12 keV levels as discussed above in sect. 1.1. The intensities of the new conversion lines are low, in the range 0.1 to 1 on the scale of ref. [1]) ($K_{133.53} = 100$), and fall in the range of the statistical counting fluctuations in the survey scans of that investigation.

1.4. THE MULTIPOLARITY OF THE 99.95 keV TRANSITION

Gnedich *et al.* [2]) have proposed an M3 multipolarity for the 99.95 keV transition on the basis of their conversion line studies. They have deduced an experimental K/L_I ratio for this transition of 3.3 ± 0.8. This must be compared with the K/L_I ratio of 8.3^{+6}_{-3} resulting from our conversion line studies [1]). Two significant differences in analysis should be noted. First, Gnedich *et al.* assumed that the 57 keV line group (M59.03 and K99.95) was composed of two components whereas our studies have shown that the line consists of three components of comparable intensity (see fig. 2 of ref. [1])). Secondly, it would appear that they attribute the entire L99.95 line intensity to conversion in the L_I shell whereas the major part of this intensity results from conversion in the L_{II} and L_{III} shells [1]). For these reasons we reject their proposed M3 assignment in favour of the E2 assignment which we deduced from K and L subshell line intensity ratios.

1.5. RESULTS OF PRESENT WORK

In this paper we present the results of some new experiments which were aimed at settling these points of dispute. The gamma-ray spectra coincident with the L_I33.57, L_I40.93, K80.12, L_I80.12, K133.53 and L_I133.53 conversion lines and with γ80.12, γ133.53 and the Pr KX-rays have been observed. A detailed search has been made for the most intense of the new conversion lines reported by Freeman, the K line of the 66 keV transition. These new results are all consistent with the decay scheme of fig. 1 and do not support any of the proposed modifications that were outlined above. The present measurements verify the gamma branching from the 99.95 keV level and provide an improved limit on the beta feeding to this level. They confirm the feeding of the 80.12 keV level as deduced in the earlier work [1]) and provide 3 experimental values for the K conversion coefficient of the 53.41 keV transition.

2. Experimental Details

The Chalk River precision beta-ray spectrometer [11]) was used for both the conversion line study and the conversion electron-gamma coincidence investiga-

tions reported in this paper. The source used for this investigation was the weaker of those prepared and used in our earlier studies [1]) and is 2 years old. The spectrometer was operated at instrumental momentum resolution settings in the range 0.1 to 0.3 % in the present work. A cylindrical, side-window proportional counter operating with a continuous flow methane filling was used as the beta detector. For the conversion line study this counter was operated at a filling pressure of 9 cm of Hg with a counter window made up of 20 layers of $5\mu g/cm^2$ VYNS film supported by an 87 % transmission metallic grid [11]). The attenuation of the film at 24 keV is $\ll 5$ %. In the conversion electron-gamma coincidence measurements a 5 cm×5 cm NaI(Tl) crystal coupled to a magnetically-shielded 5 cm photomultiplier (RCA 6342A), was used as gamma detector. This detector was isolated from the spectrometer vacuum by a 1 mm aluminium window and subtended an effective solid angle in the range 10—25 % of 4π at the source. A diagram of the experimental arrangement and the electronic circuitry is given in fig. 2. The preamplified outputs of the detectors were fed into linear amplifiers of the double delay line type [see ref. [29]) of Graham *et al.* [11])]. The integral discriminator outputs from these units operated a 6BN6 coincidence circuit which in turn gated the γ-detector pulses into a 100-channel pulse-height analyser of the Chalk River design. The resolving time of this arrangement was determined by the discriminator output pulse lengths which were $\approx$ 1 μsec. To measure the random coincidence spectrum a lumped delay line was introduced to delay one of the discriminator pulses by $\approx 4\mu$sec.

Each of the conversion electron-gamma coincidence spectra presented in this paper is the result of the following four measurements: (1) coincidences on the conversion line peak, (2) chance coincidences on the conversion line peak, (3) beta-gamma coincidences measured at a momentum setting just above the conversion line and (4) chance beta-gamma coincidences measured at this latter momentum setting. The conversion electron-gamma coincidence spectra presented here are the net true coincidences after subtracting the β and chance contributions. A cyclic procedure was used in accumulating these coincidence data. The $L_1$33.57-γ and $L_1$40.93-γ measurements were performed in two parts. The net true coincidence spectrum on the conversion line peak was first determined and in a subsequent experiment the net true β-γ contribution to this spectrum was measured. In the K80.12-γ, $L_1$80.12-γ, K133.53-γ and $L_1$133.53-γ measurements a 4-step cycle was used and all measurements made in a single experiment. Counting intervals of 2 000, 4 000 and 10 000 sec were used. The pulse-height analyser and auxiliary data [11]) appropriate to the counting interval were recorded in both typewritten and punch-tape forms.

In the gamma-gamma coincidence measurements fast-slow coincidence circuitry of resolving time $\approx 10^{-7}$ sec was used. A cyclic program sequence provided for the alternate measure of the total and random coincidence spectra

accumulated over 1-h counting intervals. The pulse-height analyser data were recorded in both typewritten and punch-tape form and a record was kept of the counting rate in the gating channel. The Chalk River Datatron computer was used in all cases to carry out the arithmetic involved in obtaining the net true coincidence spectrum from the accumulated data.

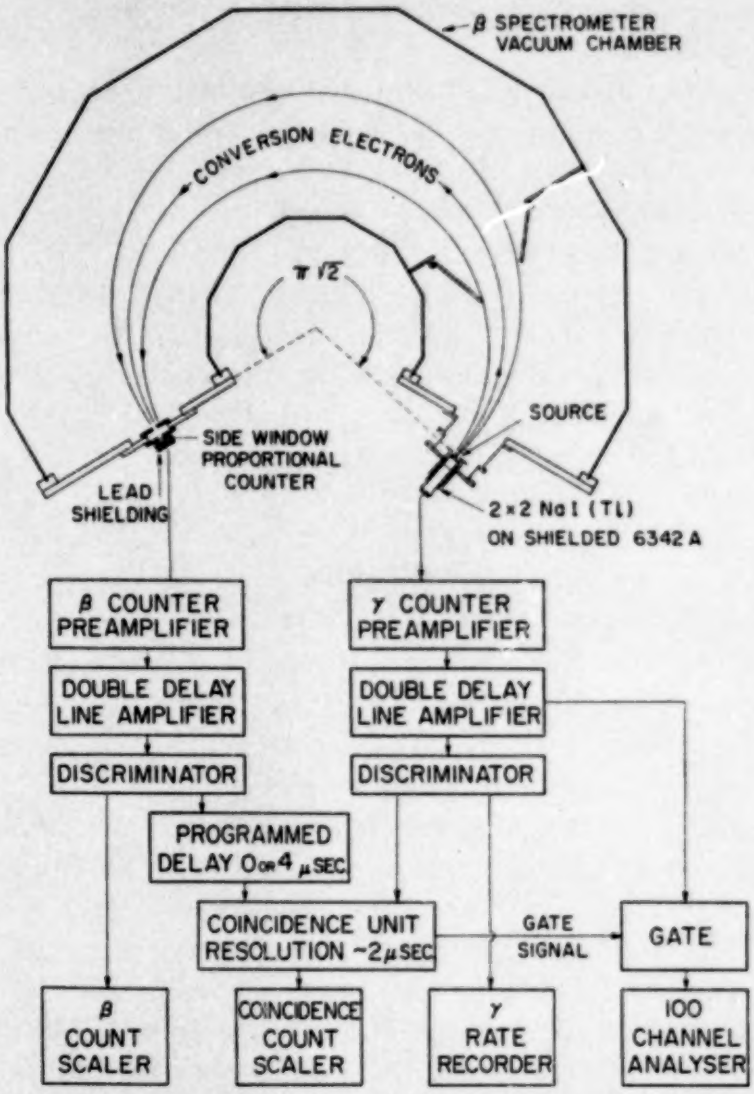

Fig. 2. This is a schematic diagram of the experimental arrangement employed in the conversion electron-gamma coincidence studies. The conversion electrons were selected by the Chalk River iron-free beta-ray spectrometer [11]) and were detected by a side-window proportional counter that was specially designed for use with this instrument by Mr. I. L. Fowler. Slow coincidence circuitry was used for these conversion electron-gamma coincidence studies. The programmed delay unit permitted the automatic sequential measurement of the total and random coincidence rates in the manner described in the text. The number of β counts, the number of coincident events and the gamma counter rate were recorded together with the coincident gamma-ray pulse-height spectrum data.

We have included in this paper all the Ce^{144} conversion electron-gamma and gamma-gamma coincidence spectra which can be measured unambiguously

and with a reasonable expenditure of effort. The conversion electron-gamma coincidence spectra, in particular, are quantitative measurements and provide upper limits on the intensity of transitions which may yet be found in the Ce^{144} decay. The following remarks are included to facilitate the interpretation of these spectra. Different experimental geometries were used for each of the following groups of coincidence experiments:

a) L_I33.57-γ (fig. 3);

b) L_I40.93-γ (fig. 3) and K133.53-γ (not shown but having a ratio of K X-ray photopeak counts to net K133.53 conversion line counts of 0.072 ± 0.002);

c) K80.12-γ, K133.53-γ and L_I80.12-γ (fig. 4);

d) L_I133.53-γ and K133.53-γ (fig. 5);

e) γ133.53-γ, γ80.12-γ and Pr K X-ray-γ spectra (figs. 6 and 7).

The effective gamma counter solid angle for the L_I33.57-γ measurements is estimated to be $\geqq 10$ %, see subsect. 3.3. The calculated correction for photon absorption and for iodine K X-ray escape from the NaI in the spectrometer experiments is 2.32, 2.03, 1.79, 1.47 and 1.17 for γ33.57, Pr K X-rays, γ40.93, γ53.47 and γ99.95 respectively.

3. Results

3.1. GAMMA SPECTRUM COINCIDENT WITH L_I33.57

The gamma spectrum coincident with the L_I33.57 conversion line is given in the upper part of fig. 3. The γ-rays of the 40.93 and 99.95 keV transitions are seen to be coincident with the 33.57 keV transition, as expected from the decay scheme of fig. 1. Failure to observe a coincident γ peak of 59.07 keV is expected because of the long lifetime (> 3 sec) predicted for the M3 transition. It should be noted in this connection that the 99.95 keV peak would not appear on the M3 assignment proposed by Gnedich *et al.* [2]) for that transition. There is no evidence in this spectrum of coincidences with the 133.53 keV γ-ray. If the 33.57 and 133.53 keV transitions were in prompt (< 1 μsec) cascade the expected 133.53 photopeak in this spectrum would run off scale. Several groups [4, 6, 12]) have measured the β component feeding the 133.53 keV level using coincidence resolving times ($< 10^{-7}$ sec) much shorter than that used in the present study and Sengupta *et al.* [5]) report the lifetime of the 133.53 keV level to be less than 10^{-9} sec. It is therefore clear that the 33.57 and 133.53 keV transitions are not in cascade. The data of ref. [1]) predict a quantum intensity ratio for γ99.95 relative to γ40.93 of 12 ± 2. The quantum intensity ratio observed in this L_I33.57-γ coincidence experiment, corrected for γ-ray absorption and iodine X-ray escape from the NaI is 12.4 ± 2.0, in good agreement with this predicted ratio. No allowance has been made in this analysis for possible angular correlation effects since the theoretical partial coefficients for L_I conversion are not available.

3.2. GAMMA SPECTRUM COINCIDENT WITH $L_1$40.93

The gamma-ray spectrum coincident with the $L_1$40.93 conversion line is

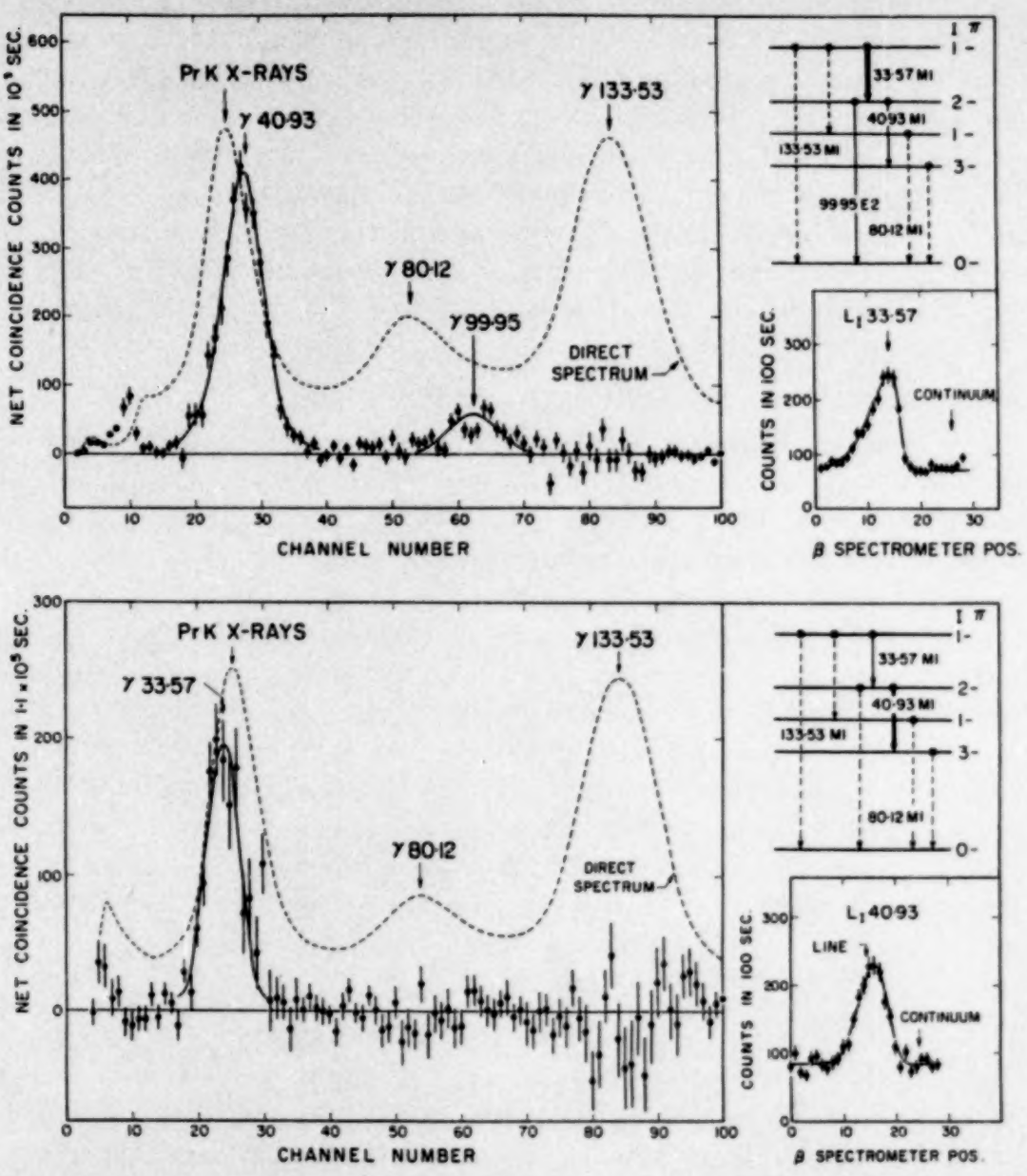

Fig. 3. The gamma-ray spectrum coincident with the L_1 conversion line of the 33.57 keV transition is shown in the upper portion of this figure. This spectrum was coincident with $(1.93 \pm 0.01) \times 10^5$ $L_1$33.57 conversion electrons and the gamma counter solid angle was $\approx$ 10 %. This spectrum shows no evidence of $L_1$33.57–γ133.53 coincidences in contradiction with the conclusions of Freeman [4]). The observed intensity ratio of the γ99.95 and γ40.93 keV peaks, corrected for absorption and iodine X-ray escape but neglecting angular correlation effects, agrees with that calculated for the decay scheme of fig. 1 and the relative line intensities of ref. [1]). The gamma-ray spectrum coincident with $(1.26 \pm 0.01) \times 10^5$ $L_1$40.93 conversion electrons is shown in the lower half of the figure. The gamma counter solid angle was 16% in this measurement. No evidence is found for $L_1$40.93 –γ133.53 coincidences in contradiction with the conclusions of Forafontov and Sorokin [3]). From these coincidence results we have deduced an intensity limit of < 0.3 % per disintegration for a β feed to the 99.95 keV level (see subsect 4.3.).

shown in the lower part of fig. 3. The 33.57 γ-ray is seen to coincide with the 40.93 keV transition as was also demonstrated by the L_I33.57-γ data. The failure to observe the 59.07 keV γ-transition in this coincidence spectrum is expected, see sect. 3.1. No evidence is found for L_I40.93–γ133.53 coincidences. If these transitions were in prompt cascade (< 1 μsec), the coincident γ133.53 photopeak would run off scale on this plot. Since the lifetime of the 133.53 keV level is $< 10^{-9}$ sec ref. [5]) we must conclude that the 40.93 and 133.53 keV transitions are not in cascade. Freeman [4]) has proposed that a 66 keV transition feeds the 99.95 keV level. There is no evidence for such a γ-ray in this coincidence spectrum and the upper limit on its quantum intensity, deduced from this spectrum and from data of ref. [1]), is $< 1.5\times10^{-4}$ γ66 quanta per disintegration.

3.3. GAMMA SPECTRA COINCIDENT WITH L_I 133.53 and K133.53

The gamma-ray spectrum coincident with the L_I conversion line of the 133.53 keV transition is shown in the lower part of fig. 4. This spectrum shows no evidence of any gamma-ray or K X-ray being coincident with the 133.53 keV transition and places an upper limit of 1 % on feeding to this level by quanta or K conversion electrons. These observations are supported by the γ133.53-γ coincidence results of sect. 3.6 and fig. 6. The γ-spectrum coincident with the K conversion line of the 133.53 keV transition observed under identical conditions, is shown in the upper part of this figure. The L_I133.53-γ result requires that the prominent K X-ray peak of this K133.53-γ spectrum be due entirely to fluorescent K X-rays associated with the K133.53 internal conversion process. This K133.53-γ measurement combined with the Pr K shell fluorescent yield of 0.90 [14]) provides a quantitative measure of the coincidence efficiency at the K X-ray energy and (when corrected for absorption and iodine X-ray escape) of the gamma counter solid angle ($\Omega = 26$ %, for the geometry of these fig. 4 measurements).

3.4. GAMMA SPECTRA COINCIDENT WITH K80.12 AND K133.53

The gamma spectrum coincident with the K conversion line of the 80.12 keV transition is shown by the solid dots in the upper part of fig. 5. This spectrum shows a single prominant peak, that of the Pr K X-rays. The 'bump' on the high energy tail (channels 34—40) of this K X-ray peak results from γ53.41 quanta. The open circles in this same plot are the gamma spectrum coincident with the K conversion line of the 133.53 keV transition observed under the same experimental conditions. The statistical errors on the two sets of coincidence data are comparable; the error bars have been omitted from the K133.53-γ points in order to reduce confusion in the diagram. It should be noted that these two spectra have been normalized to the same number of detected K conversion electrons. The K X-ray peak of the K133.53-γ data is due entirely to K133.53 fluorescent K X-rays (see subsect 3.3) and should equally

well represent the contribution of K80.12 fluorescent K X-rays to the K80.12-γ coincidence spectrum. The difference spectrum obtained by subtraction of the K133.53-γ data from the K80.12-γ data gives then the contribution of cascade transitions to the K80.12-γ spectrum. This difference spectrum, given in the central section of fig. 5, shows a resolved γ53.41 photopeak and a K X-ray

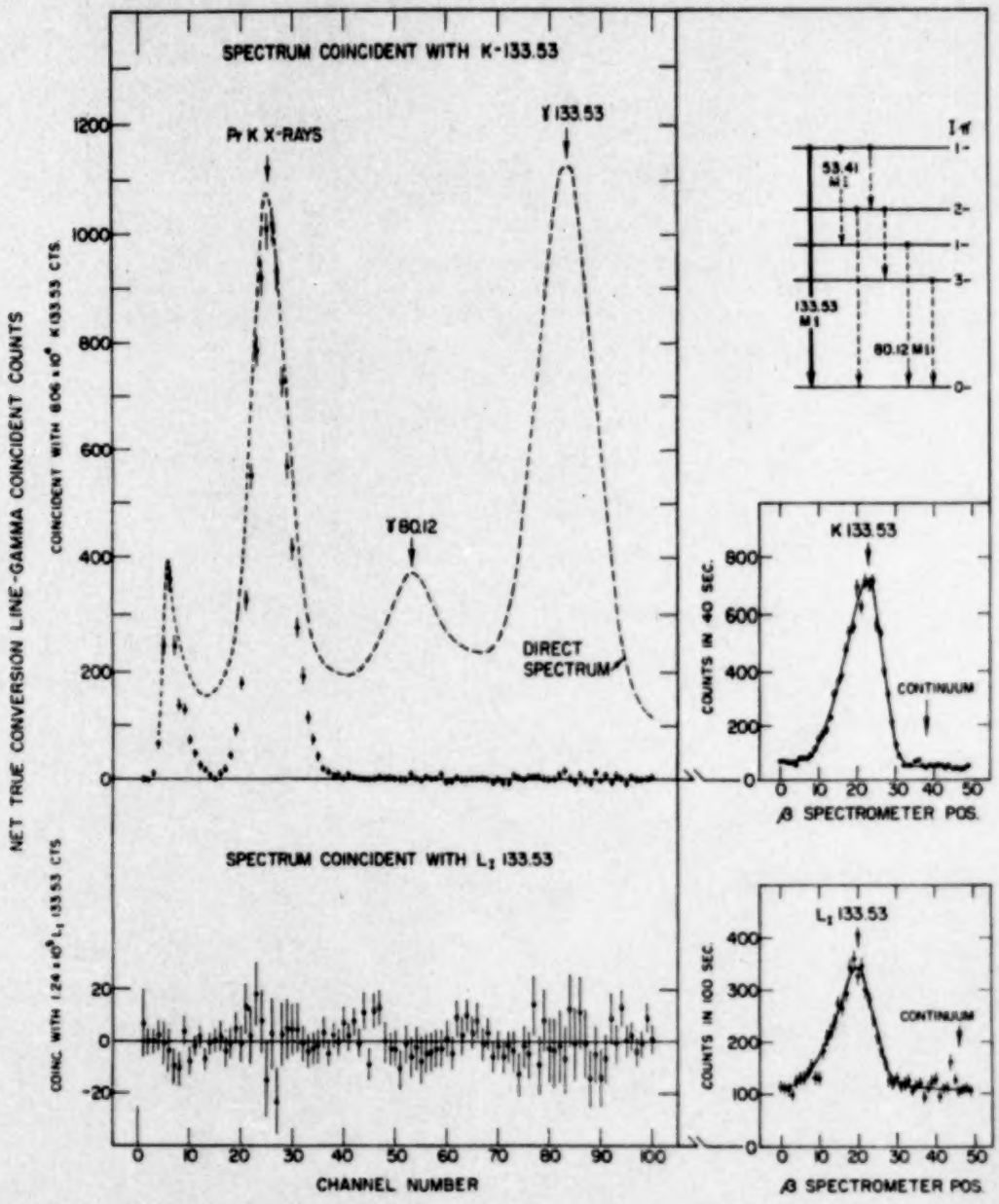

Fig. 4. The gamma-ray spectrum coincident with the L_1 conversion line of the 133.53 keV transition is shown in the lower part of this figure. There is no indication of any γ-transition being coincident with the 133.53 keV transition. The γ-ray spectrum coincident with the K-conversion line of the 133.53 keV transition is given in the upper part of the figure. The coincident Pr K X-rays observed in this spectrum are the fluorescent K X-rays resulting from the K133.53 conversion process. This coincident X-ray peak provides a measure of the coincidence detection efficiency of the apparatus.

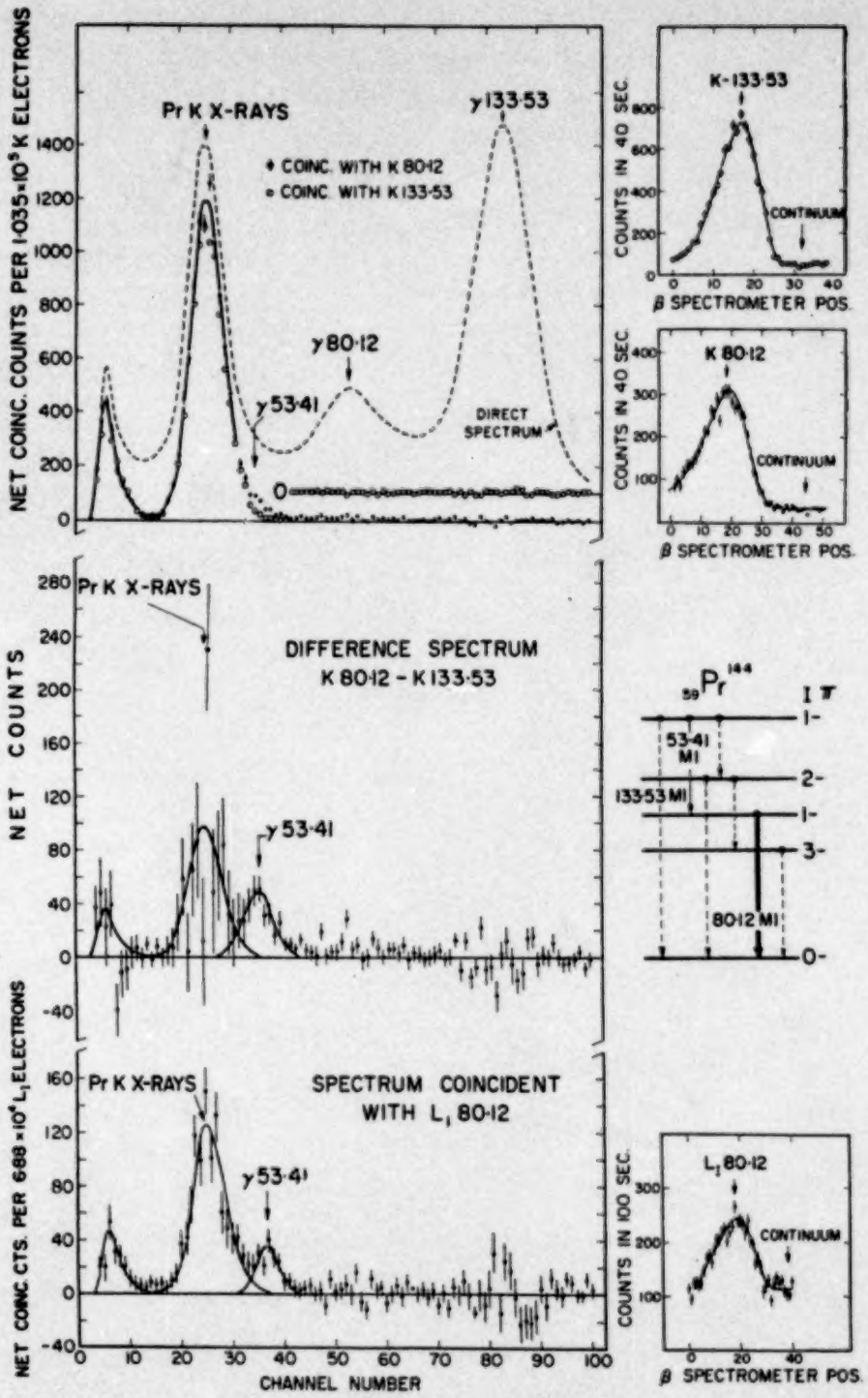

Fig. 5. The observed K80.12–γ and K133.53–γ coincidence spectra are shown in the upper section of this figure. The contribution of coincident γ-transitions to the K80.12–γ coincidence spectrum is given by the difference between the normalized K80.12–γ and K133.53–γ coincidence spectra and is shown in the central part of the figure. This difference spectrum and the $L_1$80.12–γ coincidence spectrum shown in the lower part of the figure both indicate γ53.41 coincidences and support the decay scheme given in fig. 1. The discrepancy between the relative intensities of the K X-ray and γ53.41 quantum peaks in these two spectra is discussed in subsect. 4.4.

peak that is attributed to the K conversion of this 53.41 keV transition. The K conversion coefficient for γ53.41 deduced from this spectrum, appropriately corrected for γ-ray absorption, iodine X-ray escape and fluorescent yield is $\alpha_K = 3.7 \pm 1.0$. The more direct determinations of $\alpha_{K53.41}$ permitted by the L_I80.12-γ and γ80.12-γ (fig. 6) data lead to values of α_K which are considerably higher. The discrepancy in these values is discussed in subsect. 4.4.

3.5. GAMMA SPECTRUM COINCIDENT WITH L_I80.12

The gamma-ray spectrum coincident with the L_I conversion line of the 80.12 keV transition is shown in the lower part of fig. 5. This coincidence spectrum also shows photopeaks due to γ53.41 quanta and to the Pr K X-rays associated with the K53.41 conversion electrons. The X-ray contribution in this spectrum is, however, relatively much more intense than that observed in the K80.12–K133.53 difference spectrum. The L_I80.12-γ data yield a value for $\alpha_{K53.41} = 8.6 \pm 1.8$. This result is compared with values of $\alpha_{K53.41}$ deduced from the K80.12–K133.53 difference spectrum and from the γ80.12-γ data in subsect. 4.4.

These spectra show no evidence of the 86.5 keV feed to the 80.12 keV level which Freeman [4]) has proposed. The K80.12-γ data limit the feeding of the 80.12 keV level by 86.5 keV quanta to < 2 % of the total feed; i.e., on this interpretation the upper limit on an 86.5 keV quantum intensity is < 0.12 % per disintegration.

3.6. GAMMA SPECTRA COINCIDENT WITH γ80.12 AND γ133.53

The 5.1 cm × 5.1 cm NaI(Tl) spectra coincident with γ80.12 and γ133.53 are shown in fig. 6. In obtaining these spectra, windows were set on the 10.2 cm × 10.2 cm NaI(Tl) spectrum, fig. 7, which included channels 40—48 for the γ80.12 coincidence measurement and channels 68—76 for the γ133.53 coincidence measurement. The γ133.53-γ coincidence spectrum shows no evidence for any γ or K X-ray to be coincident with the 133.53 keV transition and thus confirms the L_I133.53-γ result discussed in subsect 3.3. The counts that are observed in this γ133.53-γ spectrum (the lower half of fig. 6) are assumed to result from bremsstrahlung and from multiple scattering processes involving the high-energy Pr^{144} γ-rays.

The γ spectrum coincident with γ80.12, shown in the upper half of fig. 6, is similar to that observed in coincidence with the L_I80.12 conversion line (fig. 5), again showing the γ53.41 and K X-ray photopeaks. The γ133.53-γ and γ80.12-γ coincidence spectra of this section are consistent with those of Forafontov and Sorokin [3]) and of Sengupta *et al.* [5]). The estimated background shape and the resolution of the γ80.12-γ spectrum into its component parts is indicated by the dashed lines in the figure. The K conversion coefficient for γ53.41 deduced from this spectrum, appropriately corrected for absorption,

iodine X-ray escape, fluorescent yield and a calculated angular correlation effect is 10 ± 3. This result is in agreement with the high value deduced from the L_I80.12-γ coincidence spectrum but is greater than the theoretical value and the value deduced from the K80.12–K133.53 difference spectrum. The discrepancies are discussed in subsect. 4.4.

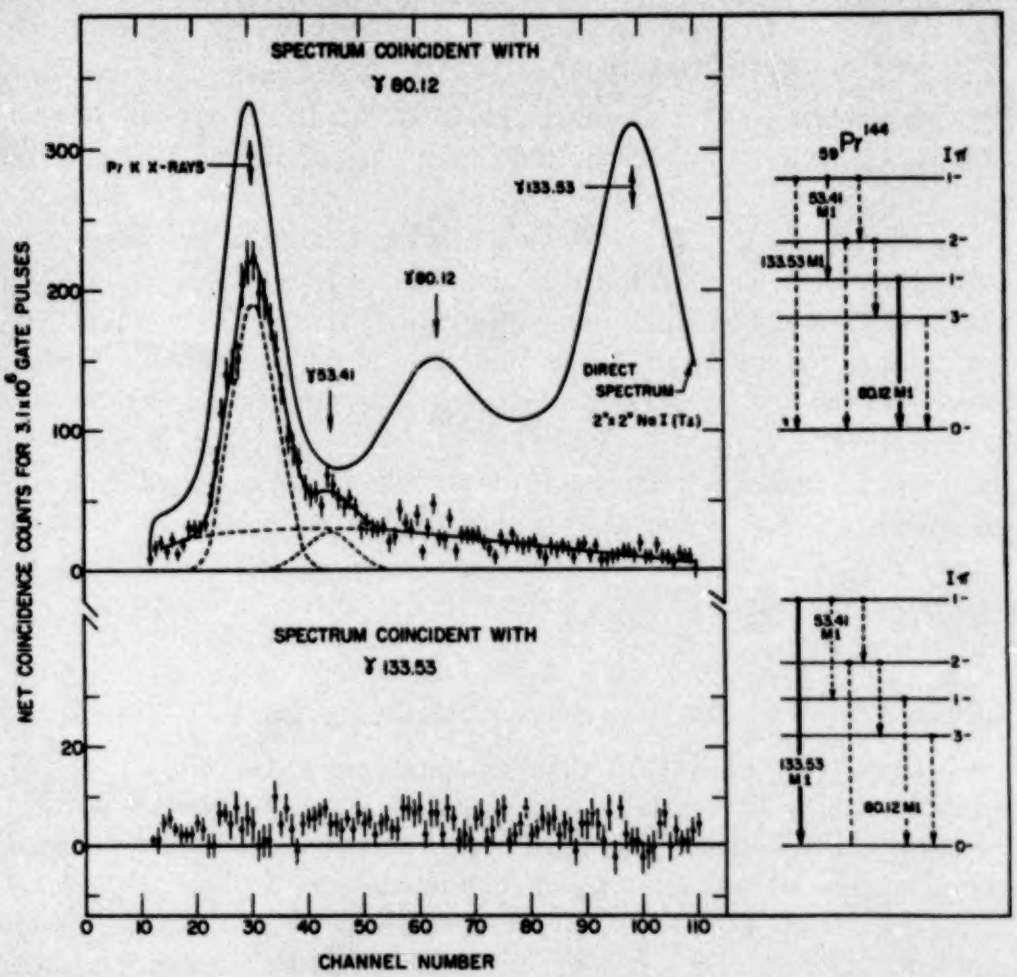

Fig. 6. This figure shows the gamma-ray spectra (5.1×5.1 cm NaI(Tl)) coincident with the 80.12 and 133.53 keV transitions. The experimental arrangement used for these gamma-gamma coincidence measurements is shown in the inset of fig. 7. The pulse-height gates used in obtaining these spectra included channels 40—48 of the direct 10.2 cm × 10.2 cm NaI pulse-height spectrum (fig. 8) in the case of γ80.12 and channels 68—76 of that spectrum in the case of γ133.53. The spectrum coincident with γ80.12 is similar to that observed in coincidence with the L_I80.12 conversion line (fig. 4) and again shows that the 80.12 and 53.41 transitions are in cascade. There is no γ-transition coincident with the 133.53 keV transition. The smoothly varying residual spectrum which is observed is attributed to bremsstrahlung processes and to multiple scattering processes involving the high-energy Pr^{144} γ-rays. These γ–γ coincidence spectra agree with the observations of Sengupta *et al.* [5]) and of Forafontov and Sorokin [3]).

3.7. GAMMA SPECTRUM COINCIDENT WITH THE Pr K X-RAYS

The 10.2 cm × 10.2 cm NaI(Tl) gamma-ray spectrum coincident with the Pr K X-rays is shown in fig. 7. In obtaining this coincidence spectrum a window

was set on the 5.1 cm × 5.1 cm NaI(Tl) pulse-height spectrum, fig. 6, which included the counts in channels 23—37. The coincidence spectrum was observed through a 0.08 cm iron filter as indicated in the inset of fig. 7 and the low-energy radiations were consequently strongly attenuated. The relative photopeak intensities expected in this coincidence spectrum, assuming (i) the decay scheme of fig. 1 and (ii) that the gate includes the Pr K X-rays, $\gamma 33.57$ and $\gamma 40.93$, are $I_{\gamma 80.12} = 1$, $I_{\gamma 99.95} = 0.04$, $I_{\gamma 53.41} = 0.2$, $I_{\gamma 40.93} = 0.04$, $I_{\text{KX-rays}} = 0.3$

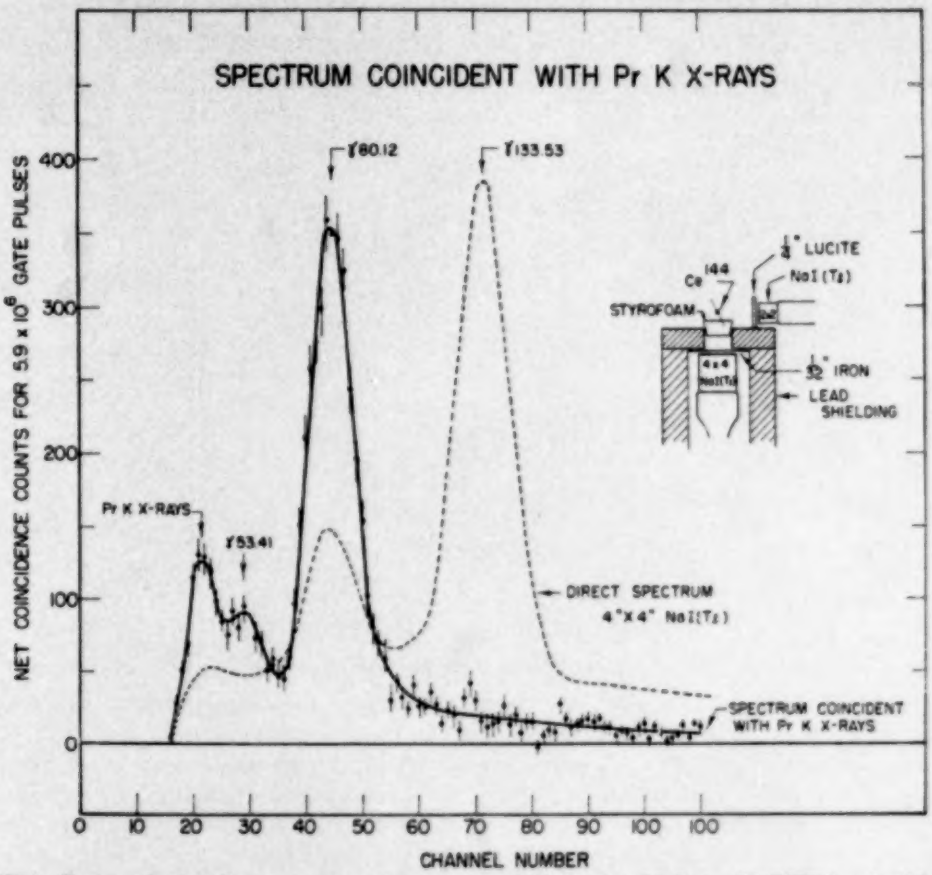

Fig. 7. This figure shows the gamma-ray spectrum (10.2 cm × 10.2 cm NaI(Tl)) coincident with the Pr K X-rays. The experimental arrangement is shown in the inset. The low-energy radiations are strongly attenuated by the 0.08 cm iron filter. The pulse-height gate used in obtaining this spectrum included channels 23—27 of the 5.1 cm × 5.1 cm NaI spectrum shown in fig. 6. The relative photopeak intensities predicted for this spectrum, assuming that the Pr K X-rays, $\gamma 33.57$ and $\gamma 40.93$ are included in the gating window and assuming the decay scheme (fig. 1) and relative transition intensities of ref. [1]) are: $I_{\gamma 80.12} = 1$, $I_{\gamma 99.95} = 0.04$, $I_{\gamma 53.41} = 0.2$, $I_{\gamma 40.93} = 0.04$, $I_{\text{Pr KX-rays}} = 0.3$ and $I_{\gamma 33.57} = 0.01$. The observed spectrum is in reasonable agreement with these predictions. The photopeak of the 99.95 keV transition is not resolved in this spectrum because of its low intensity. There is no evidence in this spectrum of the 96 keV photopeak observed by Sengupta *et al.* [5]).

and $I_{\gamma 33.57} = 0.01$. The observed spectrum is in reasonable agreement with these predicted line intensities. It will be noted that $\gamma 99.95$ is expected to be very weak and is not resolved in this spectrum. This result contradicts that of Sengupta *et al.* [5]) who observed a 96 keV peak of intensity comparable to that of $\gamma 80.12$ in their Pr K X-rays-gamma coincidence spectrum.

3.8 SEARCH FOR A K66 CONVERSION LINE

The result of a detailed search for the K66 line reported by Freeman [4]) is given in fig. 8. The plotted points represent the sum of the counts observed at each momentum setting during three successive scans. About half the observed counts in the 22—26 keV region are attributable to the background rate of the proportional counter (≈ 1 count in 2 sec). The observed full width at half-maximum of the $L_1$33.57 line, 0.24 %, is greater than the 0.2 % resolution expected at the spectrometer settings used and is attributed to energy degradation in the source. The 24 keV K66 line reported by Freeman had an intensity of $\frac{1}{10}$ that of $L_1$33.57. The expected shape for a line of this intensity

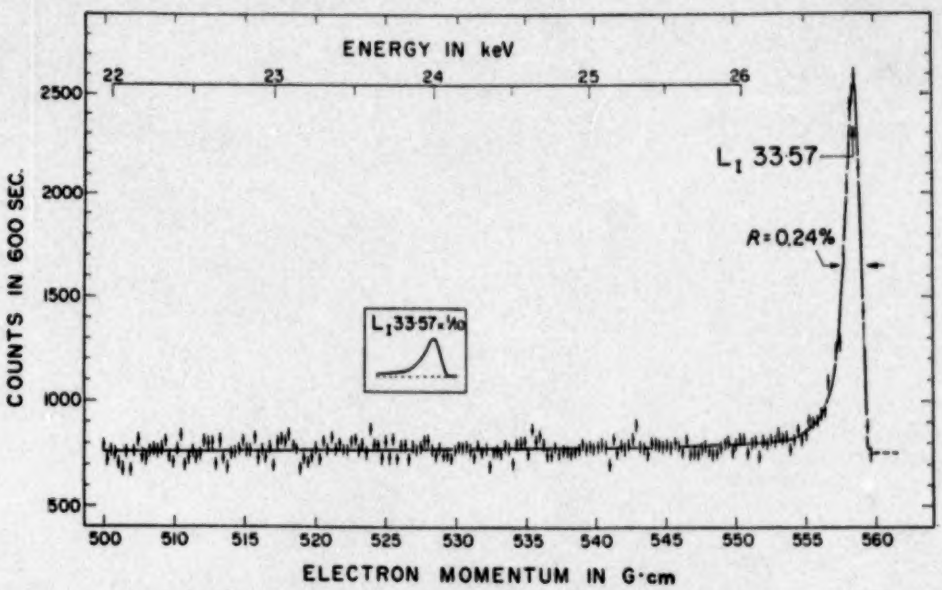

Fig. 8. The 22—26 keV region of the Ce^{144} conversion electron spectrum observed from an ≈4μCur, two-year-old Ce^{144} source is shown. An instrumental momentum resolution setting of 0.2 % was used in the study. The $L_1$33.57 line shows some additional broadening due to energy degradation in the source. The plotted points are the sum of the counts accumulated in three successive scans of this spectral region. Approximately half the counts in the 22—26 keV region are attributable to the proportional counter background. There is no evidence of the 24 keV (K66) conversion line reported by Freeman [4]). The intensity of such a line is $< \frac{1}{20}$ that of the $L_1$33.57 conversion line, i.e., smaller than one-half the intensity reported by Freeman for the line.

is given in the inset. From this spectrum we see that any Ce^{144} conversion line in the 22—26 keV region has an intensity $< \frac{1}{20} I_{L_1 33.57}$ It must be assumed therefore that the 24 keV line seen by Freeman resulted from contaminant activity in his source.

4. Discussion

4.1. CONCERNING PROPOSED Pr^{144} LEVELS AT ENERGIES > 133.53 keV

Experimental evidence supporting additional Pr^{144} levels at energies of 166 and ≈ 175 keV is provided by Ce^{144} β-spectrum studies [4, 6]) and, in particular, by the recent gamma-conversion electron coincidence results of Freeman [4]) and of Forafontov and Sorokin [3]).

Freeman's results indicated a Pr^{144} level at 166 keV. He observed γ133.53-$L_1$33.57 coincidences and found several new conversion lines which were tentatively assigned to Pr^{144} transitions of 66 and 86.5 keV. These transitions were assumed to de-excite the 166 keV level to levels at 99.95 and 80.12 keV. The $L_1$33.57-γ coincidence spectrum of the present study (fig. 3) does not indicate $L_1$33.57-γ133.53 coincidences; the intensity limit on a 133.53 keV γ photopeak in this spectrum is $< 5\,\%$ of that expected if all 33.57 keV transitions feed the 133.53 keV level. From the coincidence spectra presented by Freeman we deduce that the conversion line he observes in coincidence with γ133.53 must contribute $\approx 30\,\%$ of the intensity of the 26.6 keV conversion line peak as seen in the direct spectrum. Our $L_1$33.57-γ coincident result infers that if this 26.6 keV conversion line is due to two transitions the two conversion lines are separated by at least the momentum resolution used in our experiments, i.e. $\approx 0.3\,\%$. Any secondary line of energy $< L_1$33.57 is seen from fig. 8 to have an intensity $< \frac{1}{20} I_{L_1 33.57}$; our earlier conversion line results limit the intensity of any neighbouring conversion line to $\leqq \frac{1}{15} I_{L_1 33.57}$. Thus our search for the most intense of the new conversion lines, the K line of this 66 keV transition, was unsuccessful: if present in the conversion electron spectrum of fig. 8, it has an intensity of $< 5\,\%$ that of the $L_1$33.57 line. This upper limit is one-half the intensity reported by Freeman. The $L_1$40.93-γ coincidence results (fig. 3) give no evidence of a coincident 66 keV γ-transition; this spectrum puts a limit on a 66 keV quantum feed to the 99.95 keV level of $< 0.015\,\%$ per disintegration. The K80.12-γ, $L_1$80.12-γ and γ80.12-γ coincidence spectra show no evidence of 86.5 keV γ quanta and limit any 86.5 keV quantum feed to the 80.12 keV level to $< 0.12\,\%$ per disintegration. On the basis of these observations we conclude that the previously unreported conversion lines observed by Freeman are not associated with the Ce^{144} decay, a possibility which he does not exclude. Our results provide no support for a level at 166 keV.

Forafontov and Sorokin report coincidences between γ133.53 and the $L_1$40.93 conversion electrons and propose a level in Pr^{144} at 175 keV. The $L_1$40.93-γ coincidence spectrum of the present study (fig. 3) does not support this finding; the intensity limit on a 133.53 keV γ photopeak in this spectrum is $< 5\,\%$ of that expected if all 40.93 keV transitions feed the 133.53 keV level. Furthermore, a γ40.93-γ133.53 cascade would result in a 40.93 keV photopeak in the $L_1$133.53-γ coincidence spectrum (fig. 4) having a peak height of $\approx$ 35 counts. No such peak is observed. The report published by Forafontov and Sorokin does not permit a quantitative interpretation of their result. Our present results exclude a γ40.93-γ133.53 cascade but do not eliminate the possibility of an additional weak conversion line of energy $\approx$ 34 keV feeding the 133.53 keV level, although our earlier conversion line studies [1]) limit the intensity of such a new line to $< \frac{1}{15}$ that of the $L_1$40.93 conversion line.

4.2. CONCERNING A γ-TRANSITION OF $\approx$ 96 keV

In several of the earlier studies of the Ce^{144} conversion electron spectrum a line group at $\approx$ 53 keV was interpreted as the K line of a 96 keV transition. The re-interpretation of these lines as the L line group of the 59.03 keV transition is discussed in ref. [1]). While the Pr K X-ray-γ coincidence results of Sengupta *et al* [5]) suggest evidence for γ quanta of 96 keV we failed to confirm their observation in the results presented in this paper (fig. 7). It is possible that their observed peak at $\approx$ 96 keV resulted from Compton scattering of 133.53 keV quanta from one crystal to the other and from the escape of iodine X-rays from one crystal to the other.

4.3 THE FEEDING OF THE 99.95 AND 80.12 keV LEVELS

The L_I40.93-γ coincidence results together with the number of detected L_I40.93 conversion electrons and the coincidence efficiency of the apparatus (deduced from the K133.53-γ data) permit an estimate of the β-feed to the 99.95 keV level in Pr^{144}. The observed intensity of γ33.57 in the L_I40.93-γ coincidence spectrum fig. 4) is 11 % less than that calculated assuming no beta feed to the 99.95 keV level. This difference is evidence for a weak beta feed of 0.14 % per disintegration to this level. The log f_1t for an assumed beta component of this intensity is 8.2, a typical value for such a $0+ \rightarrow 2-$ first forbidden unique beta transition. Angular correlation effects on this L_I40.93-γ coincidence spectrum, while expected to be small (see reasoning of sect. 4.4) could conceivably influence the spectrum to this extent. With our present knowledge we can only conclude, therefore, that any β feed to the 99.95 keV level is < 0.3 % per disintegration.

The L_I80.12-γ coincidence results provide a measure of the fractional feeding of the 80.12 keV level by the quanta and K conversion electrons of the 53.41 keV transition. This fraction is 0.195 ± 0.015 of the total feed and is in satisfactory agreement with the value of 0.17 ± 0.02 deduced solely from conversion electron data and theoretical conversion coefficients [1]).

4.4. THE K CONVERSION COEFFICIENT OF THE 53.41 keV TRANSITION

The present work leads to three experimental values for the K conversion coefficient of the 53.41 keV transition. The multipolarity of this transition has been unambiguously established as M1 with < 0.2 % E2 by the L subshell conversion line intensity ratios determined in our earlier investigation [1]). The combined K80.12-γ and K133.53-γ results give a value for $\alpha_K = 3.7 \pm 1.0$, the L_I80.12-γ coincidence spectrum results give $\alpha_K = 8.6 \pm 1.8$ and the γ80.12-γ coincidence spectrum results give $\alpha_K = 10 \pm 3$. These values include corrections for photon absorption in the aluminium source holder wall and in the counter window, for iodine K X-ray escape from the NaI(Tl), for the K shell fluorescent yield [13]) and, in the case of the γ80.12-γ result, for the effect of angular correla-

tion as estimated from theory. The quoted errors, which include allowance for uncertainty in these corrections, should be regarded as standard deviations. The theoretical value for the K conversion coefficient of this M1 transition, obtained from the tables of Sliv and Band [14]) by extrapolation, is $\alpha_K = 6.5$. The α_K value deduced from the combined K80.12-γ and K133.53-γ data is inconsistent with both the L_I80.12-γ and γ80.12-γ values and with this theoretical value. The cause of the discrepancy is not known. The assumptions on which the deduction of these 3 experimental values of $\alpha_{K53.41}$ are based are the following: (1) the coincidence spectra result only from gating events attributable to the 80.12 keV and 133.53 keV transitions, (2) the 53.41 keV transition is the only one coincident with the 80.12 keV transition, (3) no gamma or conversion electron transition is coincident with the 133.53 keV transition and (4) angular correlation effects do not have a significant influence on the conversion electron-gamma coincidence spectra. Let us consider each of these assumptions in turn.

(1) The high resolution ($\approx$ 0.1 %) conversion line study of this decay [1]) provided no indication that the K80.12, L80.12 and K133.53 lines are complex. The K/L_I conversion line intensity ratios for these transitions are in agreement with those inferred from their L_I/L_{III} line intensity ratios. The β-γ contribution to the coincidence spectrum was in all cases measured at a momentum setting close to that of the conversion line (0.5 to 1.0 % higher) and so chosen as to avoid interference from neighbouring conversion lines, e.g., the L of the 99.95 keV transition in the K133.53 case. In the case of the γ80.12-γ coincidence spectrum measurements some fraction of γ99.95 was included in the coincidence gate. However, the maximum contribution which coincident γ33.57 photons could make to the K X-ray peak in this spectrum is $\approx$ 3 % and is small in comparison with other uncertainties.

(2) Within the γ-ray resolution limits of these coincidence spectra there is no evidence for transitions other than γ53.41 in coincidence with the 80.12 keV transition, nor is any such transition expected on the decay scheme of fig. 1. Studies of this decay to date do not exclude the possibility of a 19.83 keV transition but quanta of such a transition are not observed in these measurements. In any case, an additional coincident transition would lead to discrepancies in the experimental α_K values deduced from the conversion electron-gamma data only if angular correlation effects were large.

(3) A quantum ($\approx$ 35 keV) or K electron feed of 10 % to the 133.53 keV level is required to remove the discrepancy in the experimental $\alpha_{K53.41}$ values. The L_I133.53-γ and γ133.53-γ coincidence spectra limit any such quantum or K electron feed to this level to < 1 % of the total and thus exclude this possibility.

(4) While angular correlations have been neglected in treating the conversion line gamma coincidence data their effect should not significantly alter the

deduced α_K values. The fluorescent K X-rays are isotropic in distribution. The only correlation effect influencing the K80.12–K133.53 difference spectrum is that for the γ53.41–K80.12 cascade. The $P_2(\cos\theta)$ coefficient of +0.01, deduced [15, 16]) for this γ53.41–K80.12 cascade from the previously determined level spins and radiation multipolarities [1]) is too small to affect the measured $I_{\text{KX-ray}}/I_{\gamma 53.41}$ intensity ratio significantly. The effect of angular correlation on the L_I80.12-γ coincidence spectrum cannot be evaluated since the theoretical partial coefficients for L_I conversion are not available. However, since the partial coefficient for K conversion, i.e., conversion in the 1s atomic shell, is very small (< 0.1) for low-energy M1 transitions it seems probable that the analogous partial coefficient for L_I conversion, i.e., conversion in the 2s atomic shell will also be small, in any case < 1. The $P_2(\cos\theta)$ coefficient is then < 0.25 and the anisotropy correction for γ53.41 in this L_I80.12-γ coincidence spectrum is $< 15\,\%$. We are thus led to conclude that angular correlation effects are too small to account for the observed discrepancy in relative line intensities between the K80.12–K133.53 difference spectrum and the L_I80.12–γ and γ80.12–γ spectra.

A reassessment of the experimental procedure followed in these experimental studies has failed to suggest a plausible explanation for the discrepancy in these α_K values. The value deduced from the γ80.12-γ spectrum is dependent, to a large extent, on the choice of the background level and is for this reason more subjective than are the other results. The α_K value obtained from the K80.12 coincidence spectrum is dependent on a small difference between large quantities and is hence most sensitive to systematic uncertainties. The scatter of points in the X-ray region of the K80.12–K133.53 difference spectrum suggest uncertainties which exceed statistical counting errors. For these reasons we place most confidence in the α_K value of 8.6 ± 1.8 deduced from the L_I80.12-γ coincidence spectrum. This value is consistent with the theoretical value [14]) of α_K for this pure M1 transition [1]) of 6.5.

5. Conclusions

The conversion electron-gamma coincidence spectra, the gamma-gamma coincidence spectra and the conversion line search reported in this paper provide new experimental evidence that supports the Ce^{144} decay scheme proposed earlier by the present authors (fig. 1). The present results provide no support for a level in Pr^{144} at $\approx$ 166 keV. The L_I33.57-γ coincidence spectrum of the present work is in quantitative disagreement with Freeman's coincidence results. We find no evidence of a 24 keV K66 conversion line and place an upper limit on its permitted intensity of one-half the reported value [4]). Furthermore, the L_I40.93-γ coincidence spectrum provides no evidence for the 66 keV quanta, and the L_I80.12-γ, K80.12-γ and γ80.12-γ spectra show no evidence for 86.5 keV quanta expected on Freeman's proposed decay scheme.

The present work does not provide support for a level in Pr^{144} at $\approx$ 175 keV. The $L_I 40.93$-γ and $L_I 133.53$-γ and $\gamma 133.53$-γ coincidence spectra presented here show clearly that the 40.93 and 133.53 keV transitions are not in cascade, a conclusion which contradicts that of Forafontov and Sorokin [3]). The relative intensities of the 40.93 and 99.95 keV photopeaks in the $L_I 33.57$-γ coincidence spectrum are those expected on the decay scheme of fig. 1. While the gamma-conversion electron coincidence result of Forafontov and Sorokin can be explained by assuming an additional weak $\approx$ 35 keV conversion line, its intensity is limited to $\frac{1}{15}$ that of the $L_I 40.93$ conversion line by our earlier study.

The gamma-gamma coincidence spectra presented here differ from those of Sengupta *et al.* [5]) in that we fail to observe the pronounced 96 keV peak they found in coincidence with the Pr K X-rays.

Analyses of the K80.12-γ, $L_I 80.12$-γ and $\gamma 80.12$-γ coincidence spectra lead to three independent experimental values for the K conversion coefficient of the 53.41 keV transition. These are $\alpha_K = 3.7 \pm 1.0$, 8.6 ± 1.8 and 10 ± 3, respectively. The reason for the large scatter in these values, in particular for the low result deduced from the K80.12-γ data, is not understood. The value of $\alpha_K = 8.6 \pm 1.8$ deduced from the $L_I 80.12$-γ results is regarded as most reliable (see discussion, sect. 4.4) and is in agreement with the theoretical value of α_K for this pure M1 transition.

The present work limits any β feed to the 99.95 keV level of Pr^{144} to < 0.3 % per disintegration.

The present results substantiate the decay scheme shown in fig. 1.

The authors are grateful to Dr. W. T. Sharp and Dr. L. G. Elliott for helpful discussions. We wish to thank Mrs. L. Larson of the computer staff for writing the data reduction program used in this work. The technical assistance provided by Mrs. J. Fowler, Mr. R. B. Walker and Mr. W. Perry is gratefully acknowledged.

Note added in proof: Prof. D. G. E. Martin, Univ. of Liverpool, has informed us of an independent study by J. F. Burry, A. H. Cuttler and himself of the Ce^{144} conversion electron spectrum. Their results are in substantial agreement with those of our earlier publication [1]), which is summarized in fig. 1 (c.f. A. H. Cuttler, Ph. D. Thesis, University of Liverpool 1960).

References

1) J. S. Geiger, R. L. Graham and G. T. Ewan, Nuclear Physics **16** (1960) 1
2) R. V. Gnedich, L. N. Kryukova and V. V. Murav'era, JETP (U.S.S.R.) **36** (1959) 329
3) N. V. Forafontov and A. A. Sorokin, JETP (U.S.S.R.) **36** (1959) 330
4) N. J. Freeman, Proc. Phys. Soc. **74** (1959) 449
5) A. K. Sengupta, R. Bhattacharyya, J. Lahiri and P. N. Mukherjee, Ind. J. Phys. **33** (1959) 388

6) V. P. Parfenova, N. V. Forafontov and V. S. Shipinel, Izvestia Akad. Nauk S.S.S.R. Ser. Fiz. **21** (1957) 1601
7) W. S. Emmerich, G. John and J. D. Kurbatov, Phys. Rev. **82** (1951) 968
8) H. B. Keller and J. M. Cork, Phys. Rev. **84** (1951) 1079
9) W. S. Emmerich, W. J. Auth and J. D. Kurbatov, Phys. Rev. **94** (1954) 110
10) J. M. Cork, M. K. Brice and L. C. Schmid, Phys. Rev. **96** (1954) 1295
11) R. L. Graham, G. T. Ewan and J. S. Geiger, Nuclear Instr. and Methods **9** (1960) 245
12) R. L. Hickok, W. A. McKinley and S. C. Fultz, Phys. Rev. **109** (1958) 113
13) A. H. Wapstra, G. N. Nijgh and R. van Lieshout, Nuclear spectroscopy tables (North-Holland Publ. Co., Amsterdam, 1959)
14) L. A. Sliv and I. M. Band, Coefficients of internal conversion of γ-radiation (1957); Report 57 I.C.C. K1, University of Illinois
15) L. C. Biedenharn and M. E. Rose, Rev. Mod. Phys. **25** (1953) 729
16) R. C. Young, Phys. Rev. **115** (1959) 577

1.C:2.D *Nuclear Physics* **28** (1961) 407—413; © *North-Holland Publishing Co., Amsterdam*

Not to be reproduced by photoprint or microfilm without written permission from the publisher

THE EFFECT OF PAIRING ENERGY ON THE TEMPERATURE EXCITATION ENERGY OF AN INTERACTING FERMION SYSTEM

J. NÉMETH

Institute of Theoretical Physics, Eötvös University, Budapest

Received 29 May 1961

Abstract: The excitation energy of an interacting fermion system is calculated as a function of the temperature. The pairing energy gives rise to a basic change in the relation between excitation energy and temperature. This effect may change the level density of a compound nucleus and the expansion and Coulomb barrier of excited nuclei.

1. Introduction

The low excitation energies of a system consisting of free Fermi particles depend on the square of the temperature and on the number of particles as

$$E_e = cA\Theta^2. \tag{1}$$

The interaction among the particles may affect slightly the form of eq. (1), but in many cases this modification is not too important. If e.g. the particles are interacting via uncorrelated two-body forces, only the value of the constant c in eq. (1) changes. This is very important in nuclear thermodynamics, where in many cases the validity of eq. (1) is assumed and one has to determine the value of c from nuclear evaporation experiments [1]).

Recent work in the theory of superconductivity [2]) and superfluidity of nuclear matter [3]) has shown that besides the uncorrelated two-body potential, the so-called pair forces, which have a coherent character, play an important rôle. Even small correlated interactions among Fermi particles may give rise to a basic change in the properties of the system. Our purpose is to determine the relation between excitation energy and temperature for a fermion system interacting via relatively weak correlated forces, and to point out the effect of pairing forces in the nuclear evaporation theory.

2. The Energy of an Excited Fermion System

We start by considering a system of N interacting particles. The Hamiltonian is

$$H = \sum \varepsilon_k (a^\dagger_{k+} a_{k+} + a^\dagger_{k-} a_{k-}) - \tfrac{1}{2} \sum \langle k_1 \sigma_1 k_2 \sigma_2 | v | k'_2 \sigma'_2 k'_1 \sigma'_1 \rangle a^\dagger_{k_1\sigma_1} a^\dagger_{k_2\sigma_2} a_{k_2'\sigma_2'} a_{k_1'\sigma_1'}, \tag{2}$$

where k is the momentum of particles and the $\pm$ and σ refer to their spin.

To get the excitation energy one usually assumes that in first approximation, because of the Pauli principle, for not too large energies only those interactions give a contribution to the overall potential, in which the momenta of the two interacting particles either remain unchanged during the collision, or are only exchanged [4]), i.e. only the $\langle k_1\sigma_1 k_2\sigma_2|v|k_2\sigma_2 k_1\sigma_1\rangle$ and $\langle k_1\sigma_1 k_2\sigma_2|v|k_1\sigma_1 k_2\sigma_2\rangle$ matrix elements are significantly different from zero. Introducing the quantity

$$U_{kk'} = \langle k+\ k'+|v|k'+\ k+\rangle - \langle k+\ k'+|v|k+\ k'+\rangle,$$

we assume that

$$U_{kk'} = U_0 - U_1(k^2+k'^2). \tag{3a}$$

The theory of superconductivity [2]) and the superfluid properties of nuclear matter [3]) have shown that this uncorrelated interaction is not enough to describe completely the properties of a fermion system; the interaction operator has other matrix elements significantly different from zero, namely those which refer to interacting particles with opposite momentum and spin. This correlated interaction is the so-called pairing effect. Introducing the quantity

$$V_{kk'} = \langle k+\ (-k)-|v|(-k)-\ k'+\rangle - \langle k+\ (-k)-|v|k'+\ (-k')-\rangle,$$

where $V_{kk'}$ describes the transition of a pair having momenta k, $-k$ and opposite spin and directions into another $(k',\ -k')$ pair state. For the sake of simplicity we assume that

$$V_{kk'}' = \begin{cases} V & \text{for } |k-k'| < K, \\ 0 & \text{for } |k-k'| > K, \end{cases} \tag{3b}$$

where because of the energy conservation the value of K is very small. With the help of these matrix elements the Hamiltonian becomes

$$\begin{aligned} H = {} & \sum \varepsilon_k(a^\dagger_{k+}a_{k+} + a^\dagger_{k-}a_{k-}) - \tfrac{1}{2}\sum U_{kk'}(a^\dagger_{k+}a^\dagger_{k'+}a_{k'+}a_{k+} \\ & + a^\dagger_{k+}a^\dagger_{k'-}a_{k'-}a_{k+} + a^\dagger_{k-}a^\dagger_{k'+}a_{k'+}a_{k-} + a^\dagger_{k-}a^\dagger_{k'-}a_{k'-}a_{k-}) \\ & - \sum_{k'\neq k} V_{kk'}(a^\dagger_{k+}a^\dagger_{-k-}a_{-k'-}a_{k'+}) - \sum V_{kk}(a^\dagger_{k+}a^\dagger_{-k-}a_{-k-}a_{k+}). \end{aligned} \tag{4}$$

In the ground state the pairing effect has the result that the states are occupied in pairs $(k+,\ (-k)-)$. The wave function of the ground state is in this case [2])

$$\phi_0 = \prod_k [(1-h_k)^{\frac{1}{2}} + h_k^{\frac{1}{2}}a^\dagger_{k+}a^\dagger_{-k-}]\,|0\rangle,$$

where h_k is the probability that the $k+$, $(-k)$-states are occupied. In the case of excitation two particles may remain in a correlated state or the pair binding may be dissolved. The wave function of an excited pair is orthogonal to the ground state pair function, so that it may be described as $[(1-h_k)^{\frac{1}{2}}a^\dagger_{k+}a^\dagger_{-k-} - h_k^{\frac{1}{2}}]\,|0\rangle$, and the wave function of a single excited particle is simply $a^\dagger_k|0\rangle$. A typical excited state wave function can be written as

$$\psi = \prod_{G} [(1-h_k)^{\frac{1}{2}} + h_k^{\frac{1}{2}} a_{k+}^{\dagger} a_{-k-}^{\dagger}] \prod_{P} [(1-h_{k'})^{\frac{1}{2}} a_{k'+}^{\dagger} a_{-k'-}^{\dagger} - h_{k'}^{\frac{1}{2}}] \prod_{S} a_{k\pm}^{\dagger} |0\rangle, \qquad (5)$$

where G, P and S specify the states occupied by ground state pairs, excited pairs and single excited particles respectively. To take into account the conservation of the particle number, we add to E the particle number operator multiplied by a constant λ.

Let be s_k the probability that either $k+$ or $(-k)-$ is occupied by a single particle, while the probability for an excited pair in the state k is p_k and therefore the probability of a ground state pair is $1-s_k-p_k$. In this case, averaging over the different configurations, the energy becomes

$$E-\lambda N = 2\sum(\varepsilon_k-\lambda)[f_k+(1-2f_k)h_k] - 2\sum U_{kk'}[f_k+h_k(1-2f_k)][f_{k'}+h_{k'}(1-2f_{k'})]$$
$$- \sum_{kk'\neq k} V_{kk'}[h_k(1-h_k)h_{k'}(1-h_{k'})]^{\frac{1}{2}}(1-2f_k)(1-2f_{k'}) - \sum V_{kk}[h_k(1-2f_k)+p_k], \qquad (6)$$

where $2f_k = s_k+2p_k$ is the probability that a particle is in an excited state.

We have found here the energy as a function of f_k, h_k and p_k. In the first approximation we neglect the terms containing summation over k in comparison with those containing summation over k and k'. † In this case the energy does not depend on p_k, and is therefore independent of whether the excited particles are correlated or not. We determine f_k and h_k by minimizing the free energy

$$F = E - TS, \qquad (7)$$

where

$$-TS = 2\Theta \sum f_k \ln f_k + (1-f_k)\ln(1-f_k).$$

We have to differentiate eq. (7) with respect to f_k and h_k.After minimization one obtains

$$h_k = \tfrac{1}{2}\left[1 - \frac{\varepsilon_k^* - C}{\sqrt{(\varepsilon_k^*-C)^2+\Delta_k^2}}\right], \qquad (8)$$

$$f_k = \frac{1}{1+e^{\beta\sqrt{(\varepsilon_k^*-C)^2+\Delta_k^2}}}, \qquad (9)$$

where

$$C = \lambda + U_0 N - 2U_1 \sum k'^2 h_{k'}, \qquad \varepsilon_k^* = \frac{k_2}{2m^*} = \frac{k^2}{2m}(1+2mU_1 N),$$

and

$$\Delta_k = \sum_{k+K}^{k+K} V[h_{k'}(1-h_{k'})]^{\frac{1}{2}}(1-2f_{k'})$$
$$= \sum_{k-K}^{k+K} \frac{V\Delta_{k'}}{2\sqrt{\Delta_{k'}^2+(\varepsilon_k^*-C)^2}}\left(1 - \frac{2}{1+e^{\beta\sqrt{(\varepsilon_k^*-C)^2+\Delta_k^2}}}\right). \qquad 10)$$

† This approximation is good in the case of superconductivity because there the number of particles is large and the summation runs over many particles. In the case of finite nuclei this approximation seems not to be so good, therefore we wish to analyse this point in another paper.

To get the energy as a function of temperature, we have to solve first the integral equation (10). The equation always has a trivial solution $\Delta_k = 0$. If $|\varepsilon_k^* - A|$ is small, we may also find a non-trivial solution. If $2mC \gg K$, the non-trivial solution is approximately given by

$$1 = \frac{VK^2\alpha}{\sqrt{\Delta_k^2 + (\varepsilon_k^* - C)^2}} \left(1 - \frac{2}{1 + e^{\beta\sqrt{(\varepsilon_k^* - C)^2 + \Delta_k^2}}}\right), \tag{11}$$

where $\alpha = (8\pi/h^3)\Omega$. Introducing the quantity $D = KV\alpha$, we find from (11) that

$$\beta\sqrt{\Delta_k^2 + (\varepsilon_k^* - C)^2} = \beta D k^2 \left(1 - \frac{2}{1 + e^{\beta\sqrt{(\varepsilon_k^* - C)^2 + \Delta_k^2}}}\right). \tag{12}$$

Eq. (12) has a solution only if $\beta D k^2 < 2$. Thus, the critical temperature, above which the system has no superfluid state, is

$$\Theta_c = mCD.$$

If $\beta D k^2 > 3.3$, we may solve eq. (12) approximately. The solution is

$$\beta\sqrt{\Delta_k^2 + (\varepsilon_k^* - C)^2} \approx \beta D k^2 \left(1 - \frac{2}{1 + e^{\beta D k^2}}\right),$$

from which we get

$$\Delta_k = \begin{cases} \sqrt{(Dk^2)^2 \left(1 - \dfrac{2}{1 + e^{\beta D k^2}}\right)^2 - (\varepsilon_k^* - C)^2} & \text{when } k_1^2 < k^2 < k_2^2 \\ 0 & \text{when } k_1^2 > k^2,\ k_2^2 < k^2, \end{cases} \tag{13}$$

where

$$k_1^2 = \frac{2m^*C}{1 + 2m^*D'}, \qquad k_2^2 = \frac{2m^*C}{1 - 2m^*D''},$$

and

$$D' = D\left(1 - \frac{2}{1 + \exp\left[2\beta m^* DC/(1 + 2mD)\right]}\right),$$

$$D'' = D\left(1 - \frac{2}{1 + \exp\left[2\beta m^* DC/(1 - 2m^* D)\right]}\right).$$

The constant C has to be determined from the particle number conservation

$$N = \sum N_k = \sum \left[f_k + h_k(1 - 2f_k)\right]. \tag{14}$$

Substituting into (6), the average energy of a particle becomes

$$\frac{E}{N} = -\tfrac{1}{2}U_0' N + \frac{3}{10m^*}\left(\frac{3N}{2\alpha}\right)^{\frac{2}{3}} \left[1 - \tfrac{5}{3}(m^* D)^2 + \frac{5\Theta}{C}\frac{1}{1 + e^{2\beta m^* DC}}\left(\sinh 4m^{*2}D^2\beta C - m^* D \cosh 4m^{*2}D^2\beta C\right)\right]. \tag{15}$$

Here terms which are less than $\Theta/C(1+e^{2\beta m^* DC})$ were neglected.

In the case $\beta = \infty$, we obtain the ground state energy of the system as

$$\left(\frac{E}{N}\right)_G = -\tfrac{1}{2}U_0' N + \frac{3}{10m^*}\left(\frac{3N}{2\alpha}\right)^{\frac{2}{3}}[1-\tfrac{5}{3}(m^*D)^2]. \tag{16}$$

The excitation energy is

$$E_e = N\frac{3}{2m^*}\left(\frac{3N}{2\alpha}\right)^{\frac{2}{3}}\frac{\Theta}{C}\frac{1}{1+e^{2\beta m^* DC}}[\sinh 4(m^*D)^2\beta C - m^*D\cosh 4(m^*D)^2\beta C]. \tag{17}$$

If $3.3 > \beta Dk^2 > 2$, we may solve eq. (12) by expansion. The solution is

$$\Delta = \begin{cases} \sqrt{6\Theta^2\left(\dfrac{Dk^2}{\Theta}-2\right)-(\varepsilon_k^*-C)^2} & \text{when } k_1^2 < k^2 < k_2^2, \\ 0 & \text{when } k_1^2 > k^2,\ k_2^2 < k^2, \end{cases} \tag{18}$$

where

$$k_1^2 = 2m^*C\left[1+6m^*D\frac{\Theta}{C}-\frac{\Theta}{C}\sqrt{12\left(\frac{DCm^*}{\Theta}-1\right)+36D^2m^{*2}}\right],$$

$$k_2^2 = 2m^*C\left[1+6m^*D\frac{\Theta}{C}+\frac{\Theta}{C}\sqrt{12\left(\frac{DCm^*}{\Theta}-1\right)+36D^2m^{*2}}\right],$$

and C is determined from eq. (14). Taking into account terms as large as Θ^2/C^2, eq. (6) yields

$$\frac{E}{N} = -\tfrac{1}{2}U_0' N + \frac{3}{10m^*}\left(\frac{3N}{2\alpha}\right)^{\frac{2}{3}}\left[1+\frac{\Theta^2}{C^2}\left(\tfrac{5}{12}\pi^2+\sqrt{12\Gamma^3}\left\{5-\frac{10}{\Gamma+1}-3\Gamma+\tfrac{9}{7}\Gamma^2\right\}\right)\right],$$

where $\Gamma = mDC/\Theta - 1$. From this the excitation energy follows:

$$E_G = N\frac{3}{10m^*}\left(\frac{3N}{2\alpha}\right)^{\frac{2}{3}}\left[\tfrac{5}{3}(m^*D)^2+\frac{\Theta^2}{C^2}\left(\tfrac{5}{12}\pi^2+\sqrt{12\Gamma^3}\left\{5-\frac{10}{\Gamma+1}-3\Gamma+\tfrac{9}{7}\Gamma^2\right\}\right)\right]$$

$$= N\frac{3}{10m^*}\left(\frac{3N}{2\alpha}\right)^{\frac{2}{3}}\frac{\Theta^2}{C^2}\left[\tfrac{5}{3}(\Gamma+1)^2+\tfrac{5}{12}\pi^2+\sqrt{12\Gamma^3}\left(5-\frac{10}{\Gamma+1}-3\Gamma+\tfrac{9}{7}\Gamma^2\right)\right]. \tag{19}$$

3. The Relation between the Excitation Energy and the Nuclear Temperature as a Function of the Pairing Energy

From eqs. (17) and (18) we see that the excitation energy depands strongly on D, i.e. on the pairing energy. In the case of a large correlated interaction the excitation energy is very small even at large temperature. This contradicts the nuclear evaporation experiments, and we therefore conclude that the pairing energy is not very high. In the low temperature region the pairing energy stabilizes the fermion system: its

energy does not change significantly with increasing temperature. For higher temperatures the energy grows very rapidly and after a critical temperature the system behaves as a free Fermi gas.

If we wish to obtain numerical results for nuclear matter, we may determine the kinetic and potential energy for a given pairing energy, by minimizing the ground state energy of nuclear matter [6]):

$$E(\rho = \rho_0) = -15.76 \text{ MeV}, \qquad \left(\frac{dE}{d\rho}\right)_{\rho=\rho_0} = 0, \qquad \rho_0^2 \left(\frac{d^2E}{d\rho^2}\right)_{\rho=\rho_0} = 30 \text{ MeV}. \quad (20)$$

If $mD = 0$, i.e. in the case of nuclear matter without pairing energy, we have $\frac{3}{10}m^{-1}(3N/2\alpha)^{\frac{2}{3}} = 11.2$ MeV and $\frac{3}{10}m^{-1}(3N/2\alpha)^{\frac{2}{3}} = 2mU_1'\rho_0 = 29.24$ MeV, while $E_G = 3.66\, N\Theta^2 \times 10^{-2}$ MeV. For small D one obtains

$$mD = 0.141, \qquad \frac{3}{10m}\left(\frac{3N}{2\alpha}\right)^{\frac{2}{3}} = 11.73 \text{ MeV}, \qquad \frac{3}{10m}\left(\frac{3N}{2\alpha}\right)^{\frac{2}{3}} 2mU_1'\rho_0 = 29.32 \text{ MeV}.$$

In fig. 1 we represent the exitation energy as a function of nuclear temperature for $mD = 0$ and for $mD = 0.141$.

4. Conclusions

Fig. 1 shows that the pairing energy modifies in a significant way the relation (1).

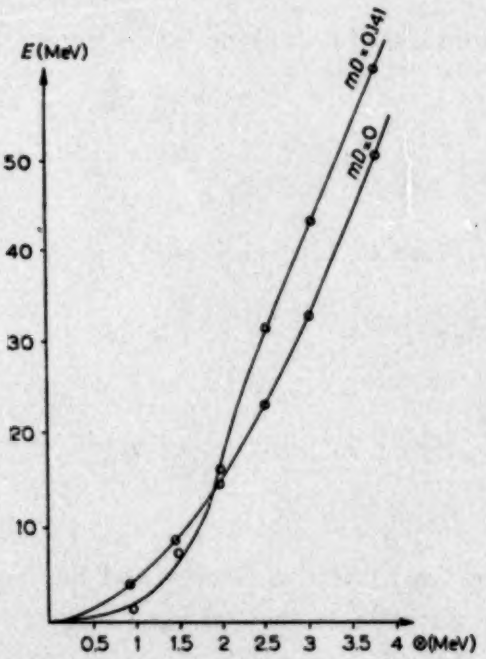

Fig. 1. The excitation energy as a function of temperature for $mD = 0$ and for $mD = 0.141$.

There is an energy range in which the energy changes very rapidly even for low temperature differences, so that the temperature is almost independent of the energy. This effect may modify the known level density of excited nuclei in such a way that the

theoretical results would be nearer to the evaporation experiments [5])†. On the other hand it is worth while to examine the effect of the pairing energy on the Coulomb barrier of excited nuclei. Because the pairing energy is not effective in excited nuclei, it may be that excited nuclei expand more than calculated [6]). This perhaps diminishes the effective Coulomb barrier of an excited nucleus, as has been shown by experiments.

The author is greatly indebted to Dr. Marx for his help and for his valuable advices and to Dr. Ericson, Dr. Györgyi and Dr. Károlyházi for their valuable remarks.

† The level density of an excited nucleus max be expressed as $\rho(E) \propto e^{S(E)}/\sqrt{T dE/dT}$, where E is the excitation energy and T is the temperature of the nucleus. The pairing energy causes, that the specific heat has a jump at the critical temperature, so the level density function has a fast increasing part at a certain energy, corresponding to the critical temperature [7]). It would be interesting to try to find this critical energy experimentally, because in this case, comparing the theoretical and experimental results, we should be able to determine the pairing energy term.

References

1) Blatt and Weisskopf, Theoretical nuclear physics (John Wiley and Sons Inc., New York, 1952) p. 371
2) J. Bardeen, L. N. Cooper and J. R. Schrieffer, Phys. Rev. **108** (1957) 1175
3) S. T. Belyaev, Mat. Fys. Medd. Dan. Vid. Selsk. **31**, no. 11 (1959)
4) K. A. Bruckner, Phys. Rev. **97** (1955) 1353, **100** (1955) 36;
H. A. Bethe, Phys. Rev. **103** (1956) 1953
5) L. Colli, U. Facchini, I. Iori, M. G. Marcazzan and A. M. Sona Nuovo Cim. **13** (1959) 730
6) J. Németh, Nuclear Physics **16** (1960) 690
7) T. Ericson, private communication

2.B

Nuclear Physics **28** (1961) 414—425; © *North-Holland Publishing Co., Amsterdam*

Not to be reproduced by photoprint or microfilm without written permission from the publisher

POLARIZATION OF D-D NEUTRONS FOR DEUTERON ENERGIES FROM 1.9 TO 11 MeV

P. S. DUBBELDAM † and R. L. WALTER

University of Wisconsin, Madison, Wisconsin ††

Received 16 June 1961

Abstract: The polarization of neutrons produced in the D(d, n)He^3 reaction was measured from 1.9 to 11 MeV by employing the technique of rotating the polarization vector with a magnetic field, the neutron detectors remaining fixed. Helium, contained under high pressure in a thin-walled cell, served as the analyzer. The background counts were reduced by observing coincidences between the helium recoils and the scattered neutrons. The polarization at 45° c.m. reaction angle was found to vary monotonically from -0.12 ± 0.02 at 1.9 MeV to $+0.30\pm0.05$ at 11 MeV, changing sign at about 4.2 MeV. At several energies angular distributions of the polarization were measured.

1. Introduction

Several investigations of the polarization of neutrons from the D(d, n)He^3 reaction have been reported for energies below 2 MeV. (For a list of references see the review article by Haeberli [1]). Above this energy few data have been obtained. Furthermore, above 0.7 MeV no angular distributions of the polarization have been reported. Because of this scarcity of data and also the possibility of the D-D reaction being useful as a source of polarized neutrons, an experiment to measure the polarization was undertaken for the energies available with a tandem electrostatic accelerator.

For this measurement, the polarization vector of the neutrons was turned with a magnetic field which was produced by a solenoid, the neutron detectors being kept fixed. This method was first employed by Hillman *et al.* [2]) for 100-MeV neutrons and applied to lower energy neutrons by Dubbeldam *et al.* [3]). Details of the method are discussed in these last two references. The advantage of this technique is that it reduces the possibility of introducing instrumental asymmetries.

As an analyzer for determining the polarization of the neutrons gaseous helium was used. The gas was contained in a thin-walled cell under high pressure. The light pulses produced by the helium recoils were viewed by a photomultiplier through a glass window. Plastic scintillators served as detectors

† Present address: R.C.A., M.T.P., Patrick Air Force Base, Florida

†† Work supported by the U.S. Atomic Energy Commission and the Wisconsin Alumni Research Foundation.

for the scattered neutrons. To reduce the background, coincidences were observed between the helium recoils in the gas cell and the pulses from the neutron detectors, in a manner similar to that employed by Pasma [4]).

2. Description of the Experiment

The right-left asymmetry R of the neutron intensity in a scattering experiment is defined as

$$R = \frac{I(\theta_2, 0°) - I(\theta_2, 180°)}{I(\theta_2, 0°) + I(\theta_2, 180°)}, \tag{1}$$

where $I(\theta_2, 0°)$ and $I(\theta_2, 180°)$ are the intensities of the scattered neutrons in the directions determined by the scattering angle θ_2 and the azimuthal angle ϕ, which has here the values 0° and 180°. In the absence of the magnetic field the azimuthal angle ϕ is defined as the angle between the normal to the reaction plane $\mathbf{n}_1$, and the normal to the scattering plane $\mathbf{n}_2$, where the directions of the normals are determined by the wave vectors $\mathbf{k}_1$ and $\mathbf{k}'_1$ of the ingoing and outgoing waves according to the equation

$$\mathbf{n}_1 = \frac{\mathbf{k}_1 \times \mathbf{k}_1'}{|\mathbf{k}_1 \times \mathbf{k}_1'|}. \tag{2}$$

This definition of the normal agrees with the convention adopted at the International Symposium on Polarization Phenomena of Nucleons in 1960 at Basle [5]). The directions defined by $\phi = 0°$ and $\phi = 180°$ may also be denoted by the words "right" and "left'. When the polarization vector is turned through 90° by a magnetic field as in the present experiment, an additional definition has to be made. The positive direction of the solenoid current will be defined in such a way that with the resulting magnetic field the position of the upper counter corresponds to the 'right' direction in the situation when no magnetic field is present.

By employing two neutron detectors and by the use of the solenoid technique (or by interchanging the neutron detectors) the efficiency of the detectors and possible time variations in the neutron-beam intensity can be eliminated, as indicated by Meier *et al.* [6]). In this case the experimental asymmetry R_{exp} corresponding to the R defined in formula (1) can be written as

$$R_{\text{exp}} = \frac{\sqrt{F} - \sqrt{F'}}{\sqrt{F} + \sqrt{F'}}, \tag{3}$$

where F and F' are the ratios of the counting rates in the upper and lower detectors, for positive and negative solenoid current, respectively.

Fig. 1 gives a schematic view of the experimental arrangement. A beam of deuterons (2 to 4 μA), accelerated by the tandem electrostatic accelerator, impinges on a deuterium gas target, 2 cm long, after passing through a thin foil. Above 3-MeV deuteron energy a 13-μm tantalum foil was used with a deuterium pressure of 6 atm in the target. The energy loss of the deuterons in the gas was 350 keV at 3.7 MeV and 175 keV at 11 MeV. Tantalum was chosen because it produces appreciably fewer neutrons and gamma rays at higher energies than the common foil materials, molybdenum and nickel †. At energies below 3 MeV a 2.5-μm nickel foil was used. With a target pressure of 3 atm the energy loss

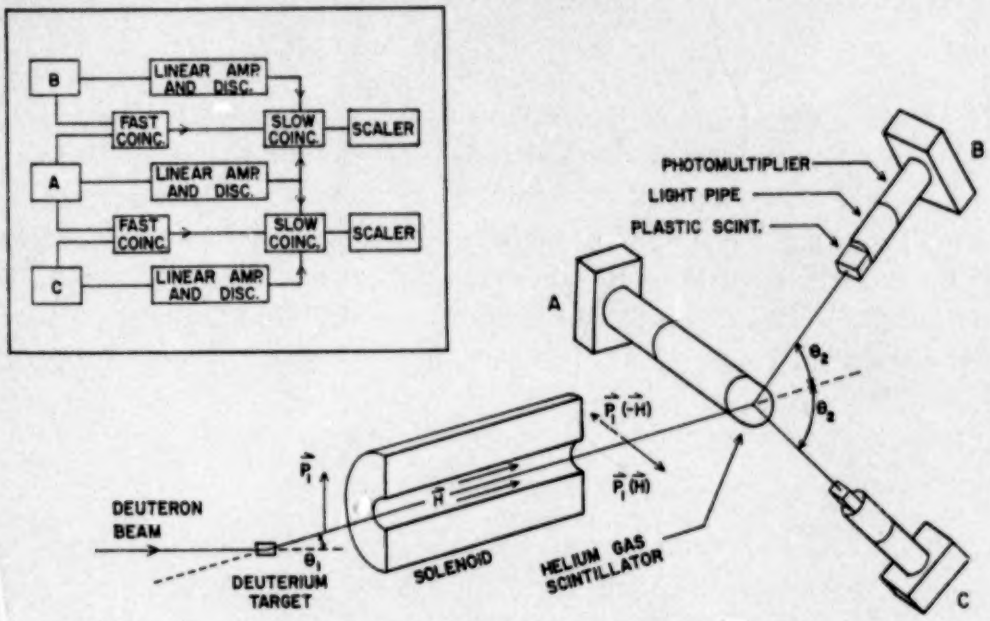

Fig. 1. Schematic view of the experimental arrangement.

in the gas varied from 320 keV at 1.9 MeV to 250 keV at 3.0 MeV. The target foils were cooled by circulating helium through a 2.5-mm thick cell which was separated from the evacuated beam tube by a 1.3 -μm nickel foil.

The solenoid consists of ten disk-shaped sections 6.9 cm thick and 26 cm in diameter with an inner diameter of 5.7 cm. The sections, averaging 142 turns, were wound from 6.4-mm square copper tubing with a 3.3-mm diameter hole. For the cooling water the coils are parallel, for the electric current, in series. The total length of the solenoid is 78 cm. At a current of 222 A the number of ampere-turns is 3.15×10^5. For this current the voltage across the solenoid is 98 V. When one takes into account the fringing field of the solenoid, the magnetic field at this current is able to turn the polarization vector of 10-MeV

† With a low discriminator setting, the number of pulses in a plastic scintillator caused by neutron and gamma-ray interactions was measured for 7-MeV deuterons incident on different foils of equal thickness when the target was evacuated. Tantalum gave one-ninth as many counts as molybdenum and one-sixteenth as many as nickel.

neutrons through 90°. With this same current the solenoid can handle higher energy neutrons without much loss in the right-left asymmetry: for 20-MeV neutrons the effect corresponding to optimum current is only diminished by about 10 %.

The helium gas scintillation counter employed in this experiment was designed by R. E. Shamu [7]). The stainless steel cell for containing the gas under high pressure had the shape of a cylinder 4.5 cm in diameter and 2.7 cm long, closed off at one end by a hemisphere of 2.3-cm radius. The wall thickness is about 1.5 mm. The interior was coated with first a layer of aluminium and then a layer of magnesium oxide to act as a reflector and lastly a layer of diphenyl stilbene to act as a wavelength shifter. A 1.9-cm thick tempered glass window, which also had a thin coating of diphenyl stilbene, covered the open end. The counter was filled with a mixture of 54 atm of helium and 5 atm of xenon. Helium recoils were viewed through the window with an EMI 6255B photomultiplier. (A quartz window photomultiplier is not essential, however, for this application.) For a polonium-alpha source inserted into the cell, the energy spread at half the maximum height of the pulse spectrum divided by the energy of the alpha particles was 8 %. Magnetic field effects on the gain of the photomultiplier were reduced by using an 18-cm lucite light pipe and several layers of soft iron shielding in addition to the Venetian blind type EMI tube. With a target-to-scatterer distance of 90 cm, the He cell subtends an angle of 3° at the target.

Neutrons were detected with two rectangular plastic scintillators 5 cm long, 5 cm wide and 2.5 cm thick, oriented as shown in fig. 1. The distance between the centres of the neutron detectors and the helium cell was 23 cm. With this geometry the angular spread of the scattered neutrons was about 18°. The spread in the azimuthal direction of the accepted neutrons does not diminish the measured effect noticeably, as it is proportional to the cosine of the azimuth. Proton recoils in the plastic scintillators were viewed by two R.C.A. 6342A photomultipliers through 13-cm lucite light pipes. Here, as well as for the helium cell, the light pipe serves to bring the photomultipliers into a region of a weaker magnetic field. To diminish further the influence of the magnetic field, these photomultipliers were also shielded with mu-metal and soft iron.

No shielding against room background neutrons or gamma rays was employed. The solenoid, together with a brass cylindrical insert with a conical hole, acted as a collimator for the neutrons from the target. The whole setup of solenoid, helium cell and neutron detectors was mounted on a table, which could rotate about a vertical axis which passed through the deuterium target.

A block diagram of the electronics is shown in the insert of fig. 1. Pulses from each neutron detector were brought into coincidence with the pulses from the helium cell in a diode circuit which had time resolution of about 12 ns. The fast coincidence pulses entered two triple coincidence circuits of 3-μs resolution

time. Pulses from two integral discriminators which determined the lower bias for linear pulses from either neutron detector served as a second input to each of the triple coincidence circuits. Pulses for the third input were provided by a window discriminator which was adjusted to select that part of the helium recoil spectrum corresponding to neutrons scattered in the direction of the neutron detectors.

In a typical run, data were recorded during ten-minute periods with the solenoid current adjusted such that the polarization vector of the neutron beam was rotated through 90°. Between periods, the direction of the current was reversed. In this way, the effects of long term drifts in amplification and in discriminator levels were minimized. As an example of the counting rate, for a deuteron energy $E_d = 7$ MeV, a reaction angle $\theta_{1\,\mathrm{c.m.}} = 45°$, an analyzing angle $\theta_{2\,\mathrm{c.m.}} = 78°$ and a beam current of 2.6 μA, about 30 counts per minute were registered in each neutron detector.

3. Results and Discussion

Table 1 shows the results of the measurements together with some relevant parameters. The quoted errors for R_{exp}, the experimental right-left asymmetry, are the standard deviations obtained from the total number of counts. This asymmetry was corrected for the influence of the magnetic field on the photomultipliers, the resulting asymmetry being given by R' in the table. As can be seen, the field influence never introduced an asymmetry greater than 0.5 %.

Chance coincidences were measured in each determination by inserting a 60-ns delay in one of the branches of the fast coincidence circuit. The background caused by neutrons other than those resulting from reactions with the deuterium gas in the target cell was determined by counting when the target cell was evacuated. A correction was applied for the background counts from these two sources. In most cases the total background was not more than 20 % and was measured with sufficient accuracy that the statistical error in the background was much smaller than the statistical error in R_{exp}. (For the measurement at $E_d = 8.9$ MeV and $\theta_{1\,\mathrm{c.m.}} = 45°$ where the D(d, n) differential cross section exhibits a minimum, the background was about 30 %. In this case, the stated error in R_{exp} was increased to account for uncertainties in the background.) The asymmetry obtained after applying the background correction is given by R'' in the table.

To check the assumption that no false asymmetries were present the right-left asymmetry was measured at 0° and 90° c.m. reaction angle for a deuteron energy of 7 and 8.9 MeV, respectively. In agreement with expectation the asymmetry was found to be zero within the limits of the statistical accuracy. A second check was made by comparing the values of R_{exp} obtained at the two positions on either side of the deuteron beam axis for which θ_1 has the same

TABLE 1

Results of the measurements

E_d (MeV)	$\theta_{1\,lab}$ (degrees)	$\theta_{1\,c.m.}$ (degrees)	E_n (MeV)	$\theta_{2\,c.m.}$ (degrees)	R_{exp} (%)	R' (%)	R'' (%)	P_2 (avg.)	P_1 (%)	$\sigma(\theta_1)$ (mb/sr)	$P_1\,\sigma$ (mb/sr)
1.9	17.5	22	5.0	78	0.7±0.7	0.7±0.7	0.9±0.9	−0.69	− 1.3±1.3	18.6	−0.24±0.24
	36	45	4.6		6.8±1.2	7.1±1.2	8.3±1.5	−0.67	−12.4±2.2	8.0	−1.00±0.18
	49	61	4.2		8.5±1.0	8.9±1.0	9.6±1.1	−0.62	−15.4±1.7	5.4	−0.83±0.09
3.0	22.5	29	6.0	78	0.8±0.8	1.0±0.8	1.1±1.0	−0.73	−1.5±1.3	14.6	−0.22±0.20
	34.5	45	5.6		4.4±0.8	4.7±0.8	5.7±1.0	−0.71	−8.0±1.4	6.5	−0.52±0.09
	53	67.5	4.9		3.3±1.4	3.6±1.4	4.2±1.6	−0.68	−6.2±2.4	5.1	−0.32±0.12
3.7	17	22.5	6.8	78	−0.4±0.5	0.1±0.5	0.1±0.5	−0.73	−0.1±0.7	21.0	−0.02±0.14
	22.5	30	6.6		−0.7±0.7	−0.3±0.7	−0.3±0.7	−0.73	0.4±1.0	14.2	0.05±0.14
	33	45	6.2		1.7±1.0	1.7±1.0	1.8±1.1	−0.73	−2.4±1.6	5.5	−0.13±0.09
	51	67	5.4		4.9±1.5	4.9±1.5	5.2±1.6	−0.71	−7.3±2.3	5.0	−0.36±0.11
	57.5	75	5.0		1.9±1.1	2.4±1.1	2.6±1.2	−0.70	−3.8±1.7	6.8	−0.26±0.12
5.5	33	45	7.7	78	−5.3±1.1	−5.3±1.1	−6.1±1.3	−0.72	8.5±1.8	4.1	0.35±0.07
7.0	0	0	10.2	78	0.2±0.7						
	16	22.5	9.8		−2.0±0.5	−2.0±0.5	−2.5±0.6	−0.66	3.8±0.9	20.2	0.77±0.18
	+32	+45	9.0		−8.7±1.9 [a]	−8.3±1.3	−11.3±1.7	−0.69	16.4±2.4	3.6	0.59±0.09
	−32	−45	9.0		−7.9±1.9 [a]						
	+32	+45	9.0	135	13.5±3.2	13.5±3.2	18. ±4	+0.93	20. ±5		
	49	67.5	7.6	78	−3.9±1.0	−3.9±1.0	−4.8±1.3	−0.72	6.6±1.8	5.0	0.33±0.09
8.9	16	22.5	11.6	78	−2.4±1.0	−2.4±1.0	−3.0±1.2	−0.62	4.8±2.0	19.4	0.9 ±0.4
	25.5	35	11.0		−8.8±1.4	−8.8±1.4	−11.6±1.9	−0.63	18. ±3	7.0	1.27±0.21
	32	45	10.4		−13.9±1.9	−13.9±1.9	−20. ±5	−0.65	31. ±8	3.3	1.0 ±0.3
	48.5	67.5	8.8		−6.2±1.1	−6.2±1.1	−8.7±1.5	−0.69	12.4±2.2	5.1	0.63±0.11
	54	75	8.2		−1.7±1.2	−1.7±1.2	−2.1±1.4	−0.71	2.9±2.0	6.0	0.18±0.12
	66	90	6.9		0.0±2.0						
11.0	32	45	12.1	78	−13.8±2.5	−13.8±2.5	−18. ±3	−0.60	30. ±5	2.9	0.86±0.15

[a]) The average of these two values is −8.3±1.3.

value. This was done at $E_d = 7$ MeV and $\theta_{c.m.} = 45°$. The two directions are indicated by the + and − signs in columns 2 and 3 of table 1. As the table shows, the measured asymmetries agreed satisfactorily.

The right-left asymmetry R is related to the initial polarization P_1 of the neutrons from the reaction by $R = P_1 P_2$, where P_2 is the polarization that would result when unpolarized neutrons are scattered by the same scatterer through the same angle. P_1 is a function of the deuteron energy E_d and the reaction angle θ_1. P_2 is a function of the neutron energy E_n and the scattering angle θ_2. For P_2 the values given by Haeberli [1]) were used. These calculations were based on phase shifts derived from the proton-helium phase shifts [8]).

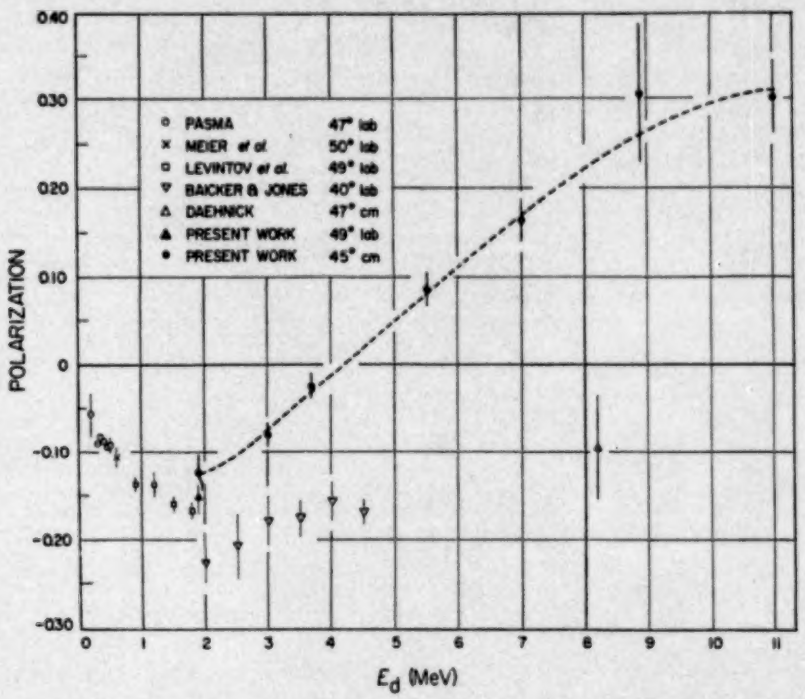

Fig. 2. Polarization of neutrons from the D(d, n)He^3 reaction as a function of deuteron energy.

Seagrave [9]) and Austin and Shamu [10]) have obtained satisfactory agreement, for neutron energies from 4.5 MeV to 14.7 MeV, between the experimental angular distributions for n-He scattering and the calculated curves based on the p-He phase shifts. It is difficult, however, to estimate the accuracy of the n-He phase shifts from these measurements. The uncertainty, ΔP_2, in the magnitude of the polarizations calculated by Haeberli for E_n less than 6 MeV has been estimated to be less than 0.1 for the analyzing angles where P_2 does not vary rapidly [1]). The latter condition is true for both values of θ_2 which were used in the present measurements. In view of the accuracy of the present results, ΔP_2 is probably less than the statistical errors stated in table 1 except perhaps for the highest energy datum. To correct for the finite size of the scatterer and detectors an average value for P_2 was calculated by weighting it with the dif-

ferential cross section for neutron-helium scattering. This average is listed in the table. The signs of P_1 and P_2 are defined relative to the directions of the normals to the reaction plane and the scattering plane, according to eq. (2).

Another test of the reliability of the present method was performed by comparing two values of P_1 obtained at a fixed reaction angle θ_1 for two

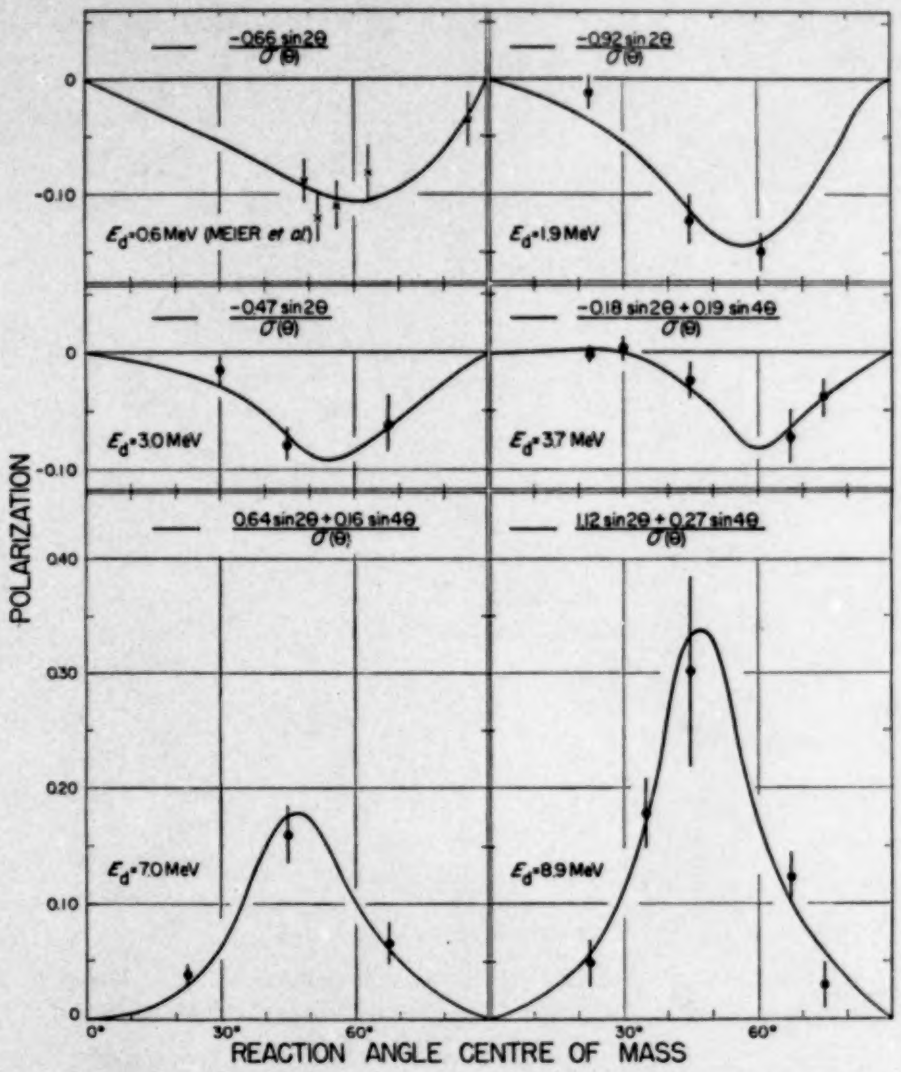

Fig. 3. Polarization of D–D neutrons as a function of the reaction angle at several deuteron energies. The curves are calculated from the solid curves in fig. 4. The crosses represent the data of Meier *et al.* [6]) and the dots represent the present data.

different analyzing angles. This comparison was made with data obtained at $E_d = 7$ MeV and $\theta_{1\,\mathrm{c.m.}} = 45°$ for the analyzing angles $\theta_{2\,\mathrm{c.m.}} = 78°$ and $\theta_{2\,\mathrm{c.m.}} = 135°$. These analyzing angles were chosen not only because the magnitude of P_2 is large at these angles, but also because the two values of P_2 have opposite signs. The resulting P_1 for both conditions are listed in table 1. These polarizations agree within the statistical accuracy of the experiment.

Fig. 2 shows the values of P_1 of the present work for $\theta_{1\,\mathrm{c.m.}} = 45°$ and of Pasma [4]), Meier *et al.* [6]), Levintov *et al.* [11]), Baicker and Jones [12]) and Daehnick [13]) for the angles reported. Appreciable disagreement exists between the present results and the measurement of Daehnick [13]) and the higher energy data of Baicker and Jones [12]). To compare the present experiment with Levintov's work, the polarization was measured at 1.9 MeV, $\theta_{1\,\mathrm{lab}} = 49°$. The measured value which is also plotted in fig. 2 was consistent with the result of Levintov at 1.8 MeV, $\theta_{1\,\mathrm{lab}} = 49°$.

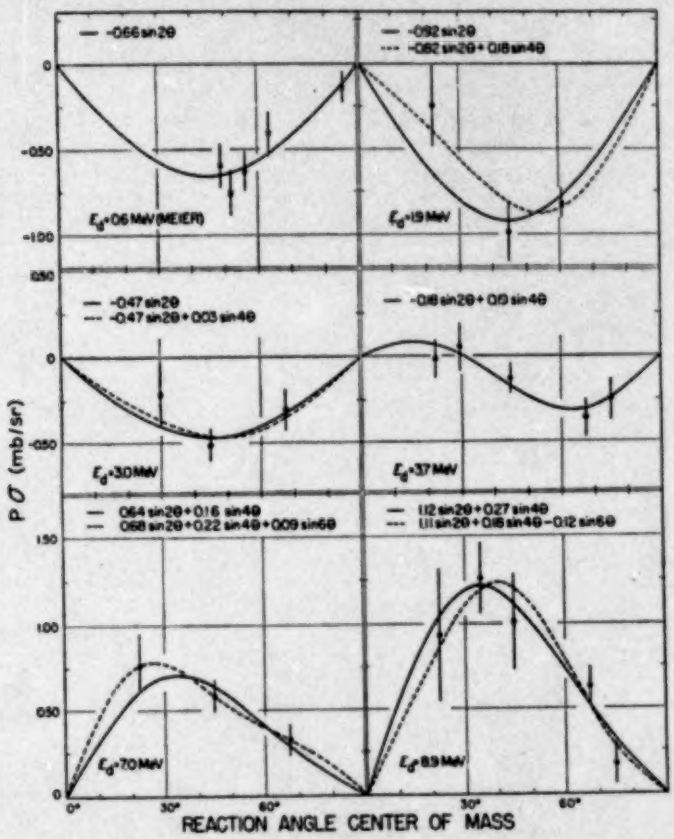

Fig. 4. $P_1\,\sigma(\theta_1)$ as a function of reaction angle at several deuteron energies. The solid and dashed curves are least square fits of eq. (4) to the data. The crosses are the data of Meier *et al.* [6]) and the dots are the present data.

The angular distributions of P_1 obtained by Meier [6]) at $E_d = 0.6$ MeV and obtained in the present experiment at higher energies are shown in fig. 3. (The curves in this figure were calculated from the solid curves of fig. 4 which are discussed below.)

Theoretically more significant than the polarization is the product of the polarization and the differential cross section $P\sigma(\theta_1)$, sometimes called the differential polarization and indicated by Π (ref. [14]). For energies up to 5 MeV the values of $\sigma(\theta_1)$ were obtained from Brolley and Fowler [15]), for higher energies from Goldberg and Le Blanc [16]). These values of σ and the calculated

values of Π are given in table 1. The values of Π as a function of angle are shown in fig. 4 along with the values derived from the experimental data of Meier.

It follows from symmetry considerations that in the D-D reaction the quantity Π can be developed in a series as follows:

$$\Pi = \sum_n a_n \sin 2n\,\theta_1, \tag{4}$$

where the order of the last term is related to the highest partial wave that contributes to the reaction.

By a least squares adjustment the angular distributions of Π were fitted with an expression of the form (4), with as few coefficients a_n as appeared to give a reasonable fit. The solid and dashed curves in fig. 4 show the results.

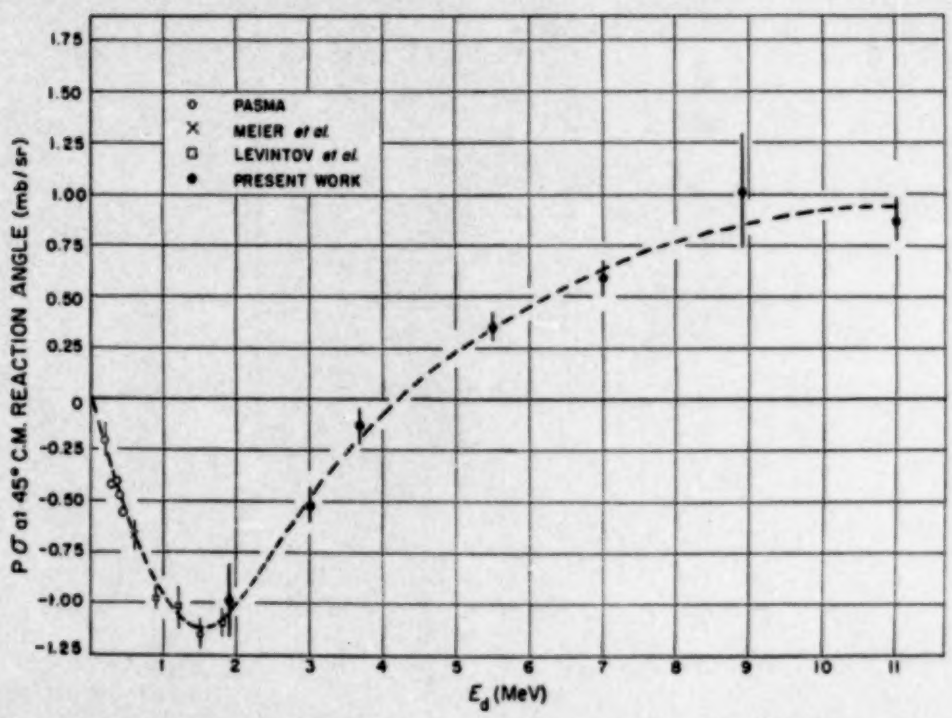

Fig. 5. $P_1\,\sigma$ as a function of deuteron energy at $\theta_{1\,\mathrm{c.m.}} = 45°$ as obtained in the present work and calculated from the data of other authors under the assumption that only a sin $2\theta_1$ dependency exists below 2 MeV.

The curve at 0.6 MeV obtained from the expression for P_1 of Meier has been included for completeness. At lower energies a development was made using first only a_1, and next a_1 and a_2. At 3.7-MeV deuteron energy there seems no doubt that a sin $4\theta_1$ term is present. At the two highest energies a fit was attempted with both two and three terms of the series. Table 2 gives the values of the coefficients with the standard deviations.

In view of the statistical uncertainty of the data it cannot be definitely concluded that a sin $6\theta_1$ term is present at the higher energies. One would expect that higher terms should occur in the development, as higher partial

TABLE 2

The coefficients in the development of the expression $P_1\sigma$ according to the equation: $P_1\sigma = \Sigma_n a_n \sin 2n\theta_1$

	E_d (MeV)	one term	two terms		three terms		
		a_1	a_1	a_2	a_1	a_2	a_3
Meier *et al.*	0.6	-0.66 ± 0.07					
Present work	1.9	-0.92 ± 0.12	-0.82 ± 0.14	0.18 ± 0.15			
	3.0	-0.47 ± 0.06	-0.47 ± 0.08	0.03 ± 0.12			
	3.7		-0.18 ± 0.04	0.19 ± 0.04			
	7.0		0.64 ± 0.09	0.16 ± 0.10	0.68 ± 0.12	0.22 ± 0.15	0.09 ± 0.12
	8.9		1.12 ± 0.12	0.27 ± 0.10	1.11 ± 0.14	0.18 ± 0.19	-0.12 ± 0.19

waves are necessary to describe the differential cross section [16]). Besides the possibility that the limits of accuracy of the present experiment fail to reveal these higher terms, it might be that the character of the nuclear forces prevents higher partial waves from contributing to the polarization, as mentioned in the analysis of Fierz [14]) for deuteron energies up to 2 MeV.

Fig. 5 shows the values of Π at $\theta_{1\,\mathrm{c.m.}} = 45°$ calculated from the present data. Under the assumption that at the lower energies only a $\sin 2\theta_1$ is present in the expansion, the values of Π for $\theta_{1\,\mathrm{c.m.}} = 45°$ were calculated from the data of Pasma [4]), Meier *et al.* [6]) and Levintov *et al.* [11]), which are presented in fig. 1. These calculated values are also plotted in fig. 5 and appear to join smoothly with the results of the present work. If over the whole energy region no terms higher than $\sin 4\theta_1$ are important, this figure represents also the coefficient a_1 as a function of energy (the $\sin 4\theta_1$ term being zero at 45°).

It appears from the present measurements that the D-D reaction has some undesirable characteristics as a source of polarized mono-energetic neutrons. At the lower bombarding energies the polarizations are less than 20 %. At bombarding energies around 10 MeV where the polarization reaches higher values, the presence of neutrons of lower energies introduces difficulties. Such neutrons are produced in the D(d, np)D breakup reaction and also in materials other than deuterium which the incident deuterons strike.

The authors wish to thank Professors H. H. Barschall and W. Haeberli for many discussions and for their comments regarding the manuscript. We are also grateful to R. E. Shamu for the loan of the gas scintillation counter which he developed and to W. Benenson, T. H. May and C. H. Poppe for their assistance in performing this experiment.

References

1) W. Haeberli, Fast neutron physics, ed. by J. B. Marion and J. L. Fowler (Interscience Publishers, to be published) part 2, chapter V.
2) P. Hillman, G. H. Stafford and C. Whitehead, Nuovo Cim. **4** (1956) 67
3) P. S. Dubbeldam, C. C. Jonker and F. J. Heemskerk, Nuclear Instruments **4** (1959) 234
4) P. J. Pasma, Nuclear Physics **6** (1958) 141
5) Sign convention for particle polarization, Nuclear Physics **21** (1960) 696
6) R. W. Meier, P. Scherrer and G. Trumpy, Helv. Phys. Acta **27** (1954) 577
7) R. E. Shamu, to be published
8) D. C. Dodder and J. L. Gammel, Phys. Rev. **88** (1952) 520
9) J. D. Seagrave, Phys. Rev. **92** (1953) 1222
10) S. M. Austin and R. E. Shamu, Bull. Am. Phys. Soc. **5** (1960) 410
11) I. I. Levintov, A. V. Miller, E. Z. Tarumov and V. N. Shamshev, Nuclear Physics **3** (1957) 237
12) J. A. Baicker and K. W. Jones, Nuclear Physics **17** (1960) 424
13) W. W. Daehnick, Phys. Rev. **115** (1959) 1008
14) M. Fierz, Helv. Phys. Acta **25** (1952) 629
15) J. E. Brolley, Jr. and J. L. Fowler, Fast neutron physics, edited by J. B. Marion and J. L. Fowler (Interscience Publishers, New York, 1960) part 1, chapt. I.C.
16) M. D. Goldberg and J. M. Le Blanc, Phys. Rev. **119** (1960) 1992

1.E.2; 4.E

Nuclear Physics **28** (1961) 426—427; © *North-Holland Publishing Co., Amsterdam*

Not to be reproduced by photoprint or microfilm without written permission from the publisher

CONCERNING THE EXISTENCE OF RARE LIGHT NUCLEI

NELSON JARMIE

Los Alamos Scientific Laboratory, University of California, Los Alamos, New Mexico †

Received 3 July 1961

Abstract: Excellent agreement is obtained in a comparison of experimental results with the predictions of A. I. Baz' concerning the masses of rare light nuclei with a large neutron or proton excess.

A. I. Baz' has recently calculated [1, 2]) the masses (in terms of maximum beta decay energies) and half lives of rare light nuclei with a large proton or neutron excess. Since his predictions have been published, a number of the nuclei involved have been discovered and studied: O^{20} (Jarmie and Silbert [3])); Ar^{42} (Jarmie and Silbert [4])); Ne^{18} (Towle and Macefield [5])); Mg^{22} (Ajzenberg-Selove *et al.* [6])); and Si^{26} (Ajzenberg-Selove and Dunning [7])).

The comparison of the experimental results to the predictions of Baz' for the maximum beta decay energies is significant and is worth reporting. This comparison is shown in table 1. Data on the half-lives are less reliable and much less significant, and will not be shown here. They agree as well as can be expected (within a factor of ten).

TABLE 1

Comparizon of predicted and experimental maximum beta decay energies

Nucleus	Isobaric spin	E_{max} (pred.) (MeV)	E_{max} (exp.) (MeV)	Difference (MeV)
O^{20}	2	4.3	3.81 ± 0.02	+0.5
Ar^{42}	3	0.5	0.58 ± 0.04	−0.1
Ne^{18}	1	3.2	3.44 ± 0.01	−0.2
Mg^{22}	1	4.2	4.08 ± 0.08	+0.1
Si^{26}	1	3.7	4.03 ± 0.08	−0.3

The experimental energies are determined from nuclear reaction Q-values.

As can be seen, the agreement is very good. In fact the standard deviation calculated from the differences is about 0.3 MeV, while Baz' only claims an accuracy "not worse than 1.5 MeV". The important conclusion is that the beta decay energies and masses predicted by Baz' can be used with some assurance and that his method is fairly well justified.

† Work performed under the auspices of the U. S. Atomic Energy Commission.

References

1) A. I. Baz', Atomnaya Energiya **6** (1959) 571
2) English translation of Atomnaya Energiya: Soviet Journal of Atomic Energy **6** (1960) 422; A. I. Baz', J. Nucl. Energy, Part A: Reactor Science **13** (1960) 74
3) N. Jarmie and M. G. Silbert, Phys. Rev. **120** (1960) 914
4) N. Jarmie and M. G. Silbert, Phys. Rev. **123** (1961) 909
5) J. H. Towle and B. E. F. Macefield, P. Phys. Soc. **77** (1961) 399
6) F. Ajzenberg-Selove, L. Cranberg and F. S. Dietrich, Bull. Am. Phys. Soc. **5** (1960) 493
7) F. Ajzenberg-Selove and K. L. Dunning, Phys. Rev. **119** (1960) 1681

2.C:2.L *Nuclear Physics* **28** (1961) 428—437; © *North-Holland Publishing Co., Amsterdam*
Not to be reproduced by photoprint or microfilm without written permission from the publisher

ELASTIC SCATTERING AND REACTIONS OF PROTONS ON ARGON-40

A. C. L. BARNARD † and C. C. KIM ††

Department of Physics and Astronomy, State University of Iowa, Iowa City, Iowa †††

Received 3 June 1961

Abstract: Thin targets of natural argon gas were bombarded with protons with energies between 0.8 and 3.5 MeV. Differential cross sections were measured at three angles for elastic scattering and for the reactions $A^{40}(p, p'\gamma)A^{40}$ and $A^{40}(p, \alpha)Cl^{37}$. Many anomalies were observed in the elastic scattering cross section, the strongest being at 1.88, 2.45 and 3.4 MeV. Spin and parity $j^{\pi} = \frac{3}{2}^-$ and $\frac{1}{2}^+$ were assigned to the levels corresponding to the first two of these. The anomalies corresponding to the previously reported $A^{40}(p, \gamma)K^{41}$ resonances were too small to be detected in this experiment. In the range of incident proton energy between 2.4 and 3.4 MeV, there were about 40 resolved or partly resolved resonances in the yield of α particles.

1. Introduction

The observation of γ-rays from proton capture in A^{40} was reported in 1948, by Bostrøm, Huus and Koch [1]), who found five separated resonances in the incident proton energy range from 900 to 1235 keV. Freier *et al* [2]) studied the elastic scattering by natural argon of protons with energies between 1.7 and 2.8 MeV. Strong anomalies were observed in the differential cross section at 155° (laboratory) at proton energies near 1.90 and 2.48 MeV. In contrast to the γ-ray work, the elastic scattering showed evidence of overlapping of compound-nucleus states. Since the K^{41} compound nucleus is formed excited to 7.84 MeV plus the kinetic energy of the system, it is unlikely that the levels corresponding to incident energies of a few MeV will be well separated from their neighbours.

In the present experiment, protons elastically scattered by natural argon (99.60 % A^{40}) were observed at centre-of-mass angles 90.0°, 123.5° and 160.0° for incident proton energies from 0.9 to 3.5 MeV. The reactions A^{40} (p, p'γ)A^{40} and A^{40} (p, α) Cl^{37} were observed through the charged reaction products. Some unpublished data taken at Duke University by Vorona, Olness and Lewis [3]) are also included here in the interests of completeness. Lewis observed protons elastically scattered from natural argon at $\theta_{CM} = 167.5°$.

† Present address: the Physics Department, Rice University, Houston, Texas

†† Present address: the Physics Department, University of Southern California, Los Angeles, California

††† Work supported in part by the U.S. Atomic Energy Commission.

Since this report was drafted, a translation of some Russian work on A^{40} (p, p)A^{40} has become available [4]). The cross section was measured at three angles in the incident energy range 1.7 to 2.7 MeV. Anomalies at 1.86 and 2.45 MeV were assigned $l = 1$ and $l = 0$, respectively, in agreement with the present work.

2. Apparatus

The gas scattering chamber used in conjunction with the State University of Iowa electrostatic generator has been described in detail by Bashkin, Carlson and Douglas [5]). It consists of a gas-filled chamber into which the proton beam passes through a 0.1μm thick nickel foil. Charged reaction products and scattered particles originating in a well-defined reaction volume may pass through a defining system into a charged-particle detector, which is a 0.010 cm thick CsI(Tl) wafer. The reaction volume, and hence the target thickness, depends on the angle of the detector relative to the incident beam. This angle may be varied between 20° and 160°. The output from the detector goes to a 256-channel pulse-height analyzer, and to scaling channels consisting of an amplifier, pulse-height discriminator and scaler. These form two independent ways of examining the detector output. In this experiment a complete pulse-height spectrum was printed out from the analyzer at each angle and each proton energy, so that the cross sections for scattering and reactions producing charged particles were measured simultaneously. Cross sections obtained in this way were checked against those obtained from scaler readings. A γ-ray detector (5.1 cm diameter by 4.4 cm deep NaI(Tl) crystal) is also mounted on the chamber to measure gamma yields at approximately 90°.

3. Results

Fig. 1 shows the charged-particle spectrum at $\theta_{CM} = 160°$ for an incident proton energy of 3.376 MeV. Three groups are observed. By considering the way in which the pulse-height of these groups changed with incident proton energy (fig. 2), the groups were identified as elastically scattered protons, inelastically scattered protons and alpha particles from the reaction to the Cl^{37} ground state. These are denoted as p, p′, and α_0, respectively, on fig. 1. The observation of A^{40}(p, p′γ)A^{40} and A^{40}(p, α)Cl^{37} has not previously been reported. In general, the yields of particles from these two reactions were small compared with the yields of elastically scattered protons. The spectrum shown in fig. 1 was one of the highest yields of reaction products.

Fig. 3 shows the elastic scattering differential cross section at $\theta_{CM} = 125.3°$ for low incident proton energies. It is clear that since the cross section shows no significant departures from the general Rutherford form, the anomalies

corresponding to the γ-ray resonances in the region (fig. 4 and ref. [1])) are small. The target thickness for this part of the experiment was about 7 keV, so that very narrow anomalies might be hidden by target thickness smearing effects. Yields of γ-rays from the reaction $A^{40}(p, \gamma)K^{41}$ were obtained by measuring yields with argon in the target chamber and subtracting the yields measured with helium in the chamber. A bias level of $E_\gamma \geqq 5$ MeV was used.

The elastic scattering differential cross sections at $\theta_{CM} = 160°$ for higher energies, together with the cross sections for the two reactions, are shown in fig. 5. In contrast to the previous figure, substantial departures from the

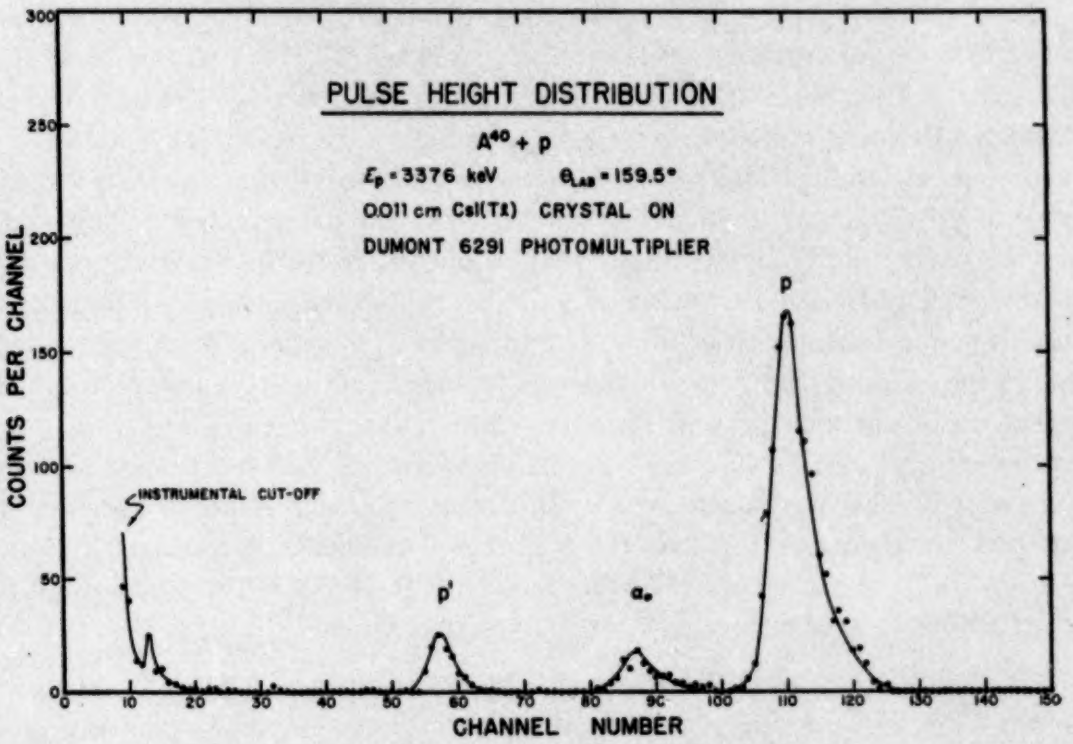

Fig. 1. Spectrum from charged-particle detector at a "high" incident proton energy.

Rutherford form are seen. The largest anomalies are at about $E_p = 1.88$, 2.45 and 3.4 MeV. Statistical errors on the elastic scattering cross section are small and the target thickness was about 10 keV here. The scattering cross sections are in general agreement with those of Freier *et al* [2]). The reaction cross sections have rather poor statistical accuracy, as only about 300 counts were taken at the peak of the largest resonance in the alpha yield. However, the reaction data were taken at three different angles of observation, and there was good agreement between the positions of the resonances at different angles. This curve suggests that in K^{41} at about 11 MeV excitation, about 40 levels per MeV have reasonable alpha partial widths.

In fig. 6 the complete elastic scattering data are shown, the cross sections

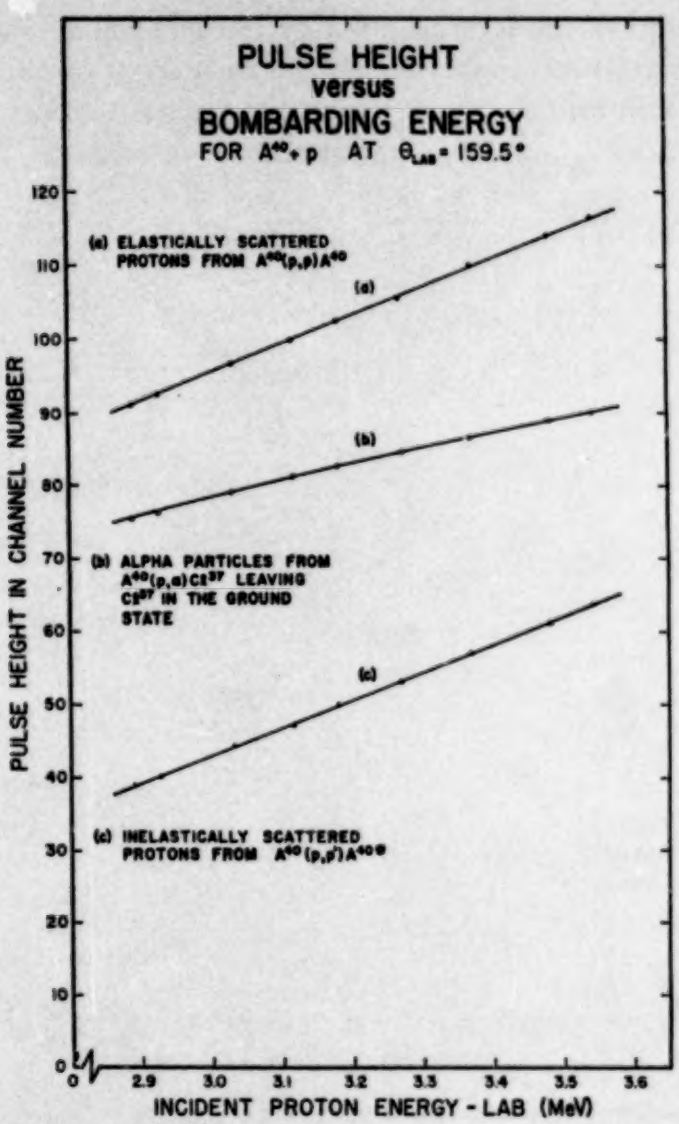
PULSE HEIGHT
versus
BOMBARDING ENERGY
FOR A40 + p AT θLAB = 159.5°
(a) ELASTICALLY SCATTERED PROTONS FROM A40(p,p)A40
(a)
(b)
(b) ALPHA PARTICLES FROM A40(p,α)Cl37 LEAVING Cl37 IN THE GROUND STATE
(c)
(c) INELASTICALLY SCATTERED PROTONS FROM A40(p,p')A40*
PULSE HEIGHT IN CHANNEL NUMBER
INCIDENT PROTON ENERGY - LAB (MeV)

Fig. 2. Variation of pulse-height of charged-particle groups with incident proton energy.

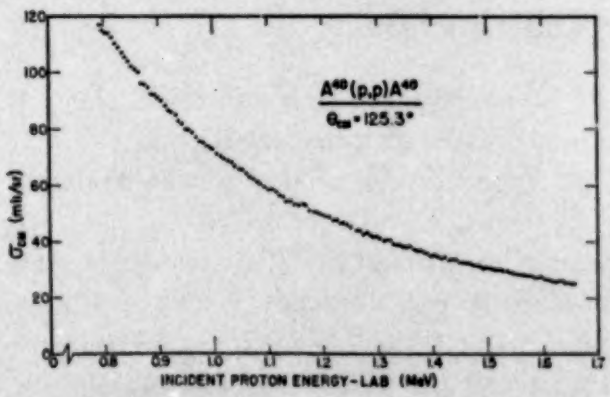

Fig. 3. Cross sections for elastic scattering of protons at $\theta_{CM} = 125.3°$ ("low" incident proton energies).

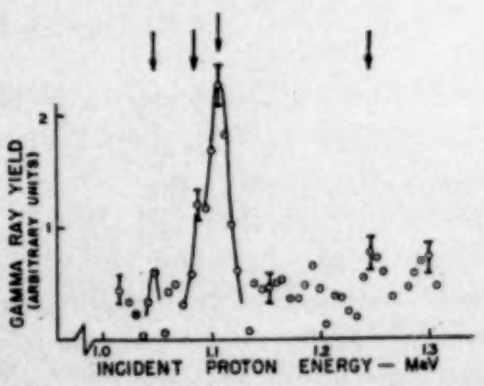

Fig. 4. Yield of γ-rays with $E_\gamma \gtrsim 5$ MeV from the reaction $A^{40}(p,\gamma)K^{41}$. Arrows indicate resonances corresponding to those in ref. [1]).

now being in units of the Rutherford cross section. The data at $\theta_{CM} = 167.5°$ were measured at Duke University [3]), and the energy calibration was taken from this curve. From the appearance of the curves it seems that the 167.5° data were taken with a thinner target than the other data.

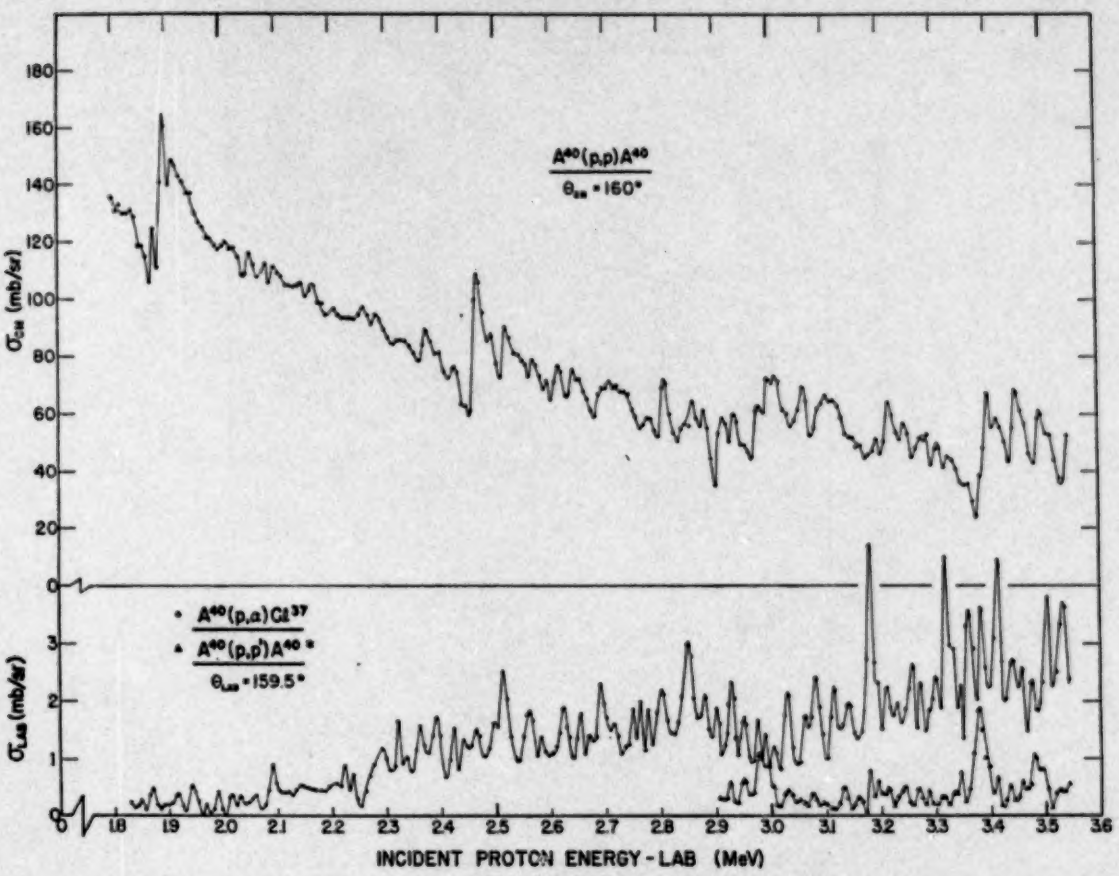

Fig. 5. Upper curve: cross sections for elastic scattering of protons at $\theta_{CM} = 160°$. Lower curve: cross-sections for (p, α) and (p, p') reactions. Both for "high" incident proton energies.

4. Discussion and Conclusions

The excitation nergies of levels in K^{41} located by resonances in the A^{40} (p, α)Cl^{37} and A^{40}(p, p'γ)A^{40} reactions are listed in the first part of table 1, whilst the second and third parts list some levels located through elastic scattering and A^{40}(p, γ)K^{41} data.

To the present authors at least, the gross behaviour of the elastic scattering cross section is surprising. Inspection of the $\theta_{CM} = 160°$ curve shows a sudden onset of anomalous behaviour at about $E_p = 1.8$ MeV. Since it is highly likely that there are levels in the lower energy region, it is concluded that their proton widths must be small. The proton penetrability is not changing rapidly with energy here; therefore the onset must correspond to a rather sudden increase in the reduced widths for proton emission. Such behaviour could

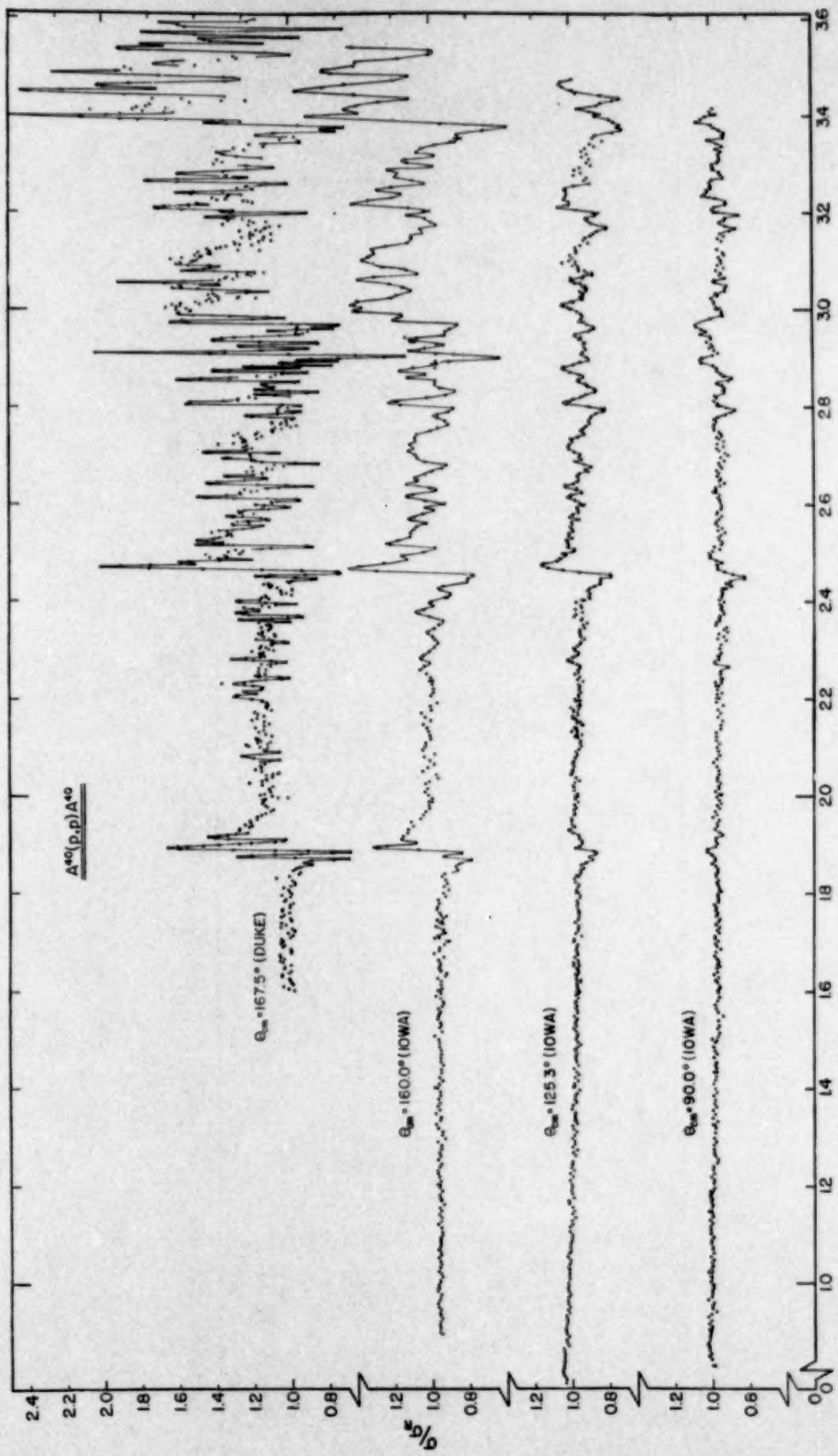

Fig. 6. Cross sections for elastic scattering of protons at four angles over the complete range of incident proton energies. Cross sections are in units of the Rutherford-scattering cross section.

TABLE 1

List of level excitation energies (E_x) in MeV with decay mode (p, α, p′, γ) through which level has been observed

E_x	Mode	E_x	Mode	E_x	Mode	E_x	Mode	E_x	Mode	E_x	Mode
9.66	α(w)	10.10	α	10.42	α	10.70	αp′(w)	10.94	α(s)p′	11.11	α(w)p′
9.71	α(w)	10.14	α	10.45	α(w)	10.72	αp′	10.95	α(w)p′	11.12	α(s)
9.74	α(w)	10.17	α	10.47	α	10.74	αp′	10.97	αp′	11.14	α(s)p′(s)
9.78	α(w)	10.19	α	10.49	α(w)	10.76	p′(s)	10.99	α(w)	11.17	α(s)p′
9.81	α(w)	10.22	α(w)	10.52	α	10.77	α(w)	11.00	p′	11.20	αp′
9.85	α(w)	10.24	α	10.53	α	10.80	αp′	11.02	α	11.22	α(w)p′(w)
9.88	α	10.28	α(w)	10.55	α	10.83	α(w)	11.03	αp′	11.23	αp′
9.93	α(w)	10.29	α(s)	10.57	α	10.85	αp′	11.05	p′	11.26	α(s)p′
9.97	α(w)	10.34	α	10.62	α(s)	10.88	α	11.06	α	11.29	α(s)p′(w)
10.04	α(w)	10.36	α(w)	10.65	α	10.91	αp′	11.08	α(s)p′(w)		
10.07	α	10.40	α	10.67	α	10.92	p′	11.09	α(w)p′(w)		
8.72	γ(a)	8.87	γ(a)	8.89	γ(a)	9.81	γ(a)	9.05	γ(a)		
9.68	p(b)	10.23	p(b)	11.16	p						

(w) comparatively weak (a) ref. [1]) (s) comparatively strong (b) refs. [2,4])

possibly be related to the "giant resonances" of Lane, Thomas and Wigner [6])

From the complex shapes of the elastic scattering curves in the higher energy region, it is clear that there is considerable overlap of neighbouring levels, so that a single level approximation of dispersion theory [7]) is not expected to be applicable. However, some information can be gleaned from fig. 6 using this approximation. The anomaly at $E_p = 1.88$ MeV has a small but definite peak ar $\theta_{CM} = 90°$ with no sign of a dip. It therefore probably

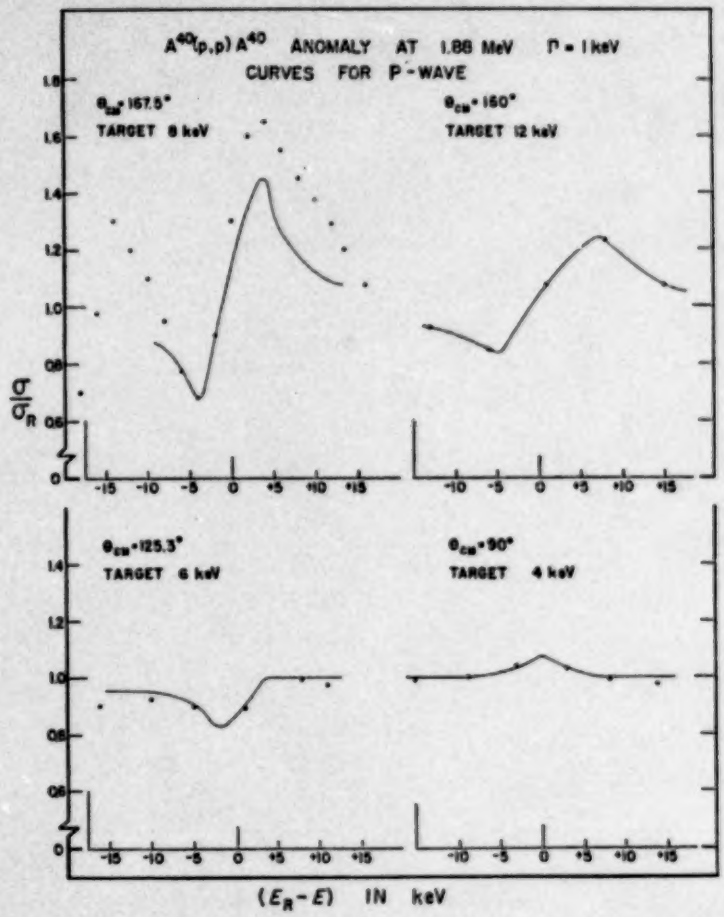

Fig. 7. Elastic-scattering anomaly at $E_p = 1.88$ MeV. Points are experimental data. Curves are computed for p-wave protons and a resonance width $\Gamma = 1$ keV. Target thickness is angle-dependent and is indicated on the figure.

corresponds to an odd value of l, the orbital angular momentum quantum number of the incoming proton. At $E_p = 2.45$ MeV there is a dip at 90°, corresponding to an even l-value. Some brief calculations were therefore made with incident p-waves at the lower anomaly and s-wave at the upper. The single level approximation was used to give curves for zero target thickness. Several identical curves were then displaced in energy and added to take into account the "smearing" effect of finite target thickness in a rough way.

At the $E_p = 1.88$ MeV anomaly, such calculations gave the curves shown in

fig. 7, the values of the parameters of the calculation being given in the caption. (The target thicknesses shown on the figure are a consistent set for the different angles). Since this incident proton energy is below the $A^{40}(p, n)K^{40}$ threshold [8]) and since the observed reaction width is very small, the proton fractional partial width $a_p = \Gamma_p/\Gamma$ was taken to be unity. It can be seen that the experimental data are well fitted with $j^\pi = \frac{3}{2}^-$, except at $\theta_{CM} = 167.5°$ where there is qualitative agreement. The fit here could be somewhat improved

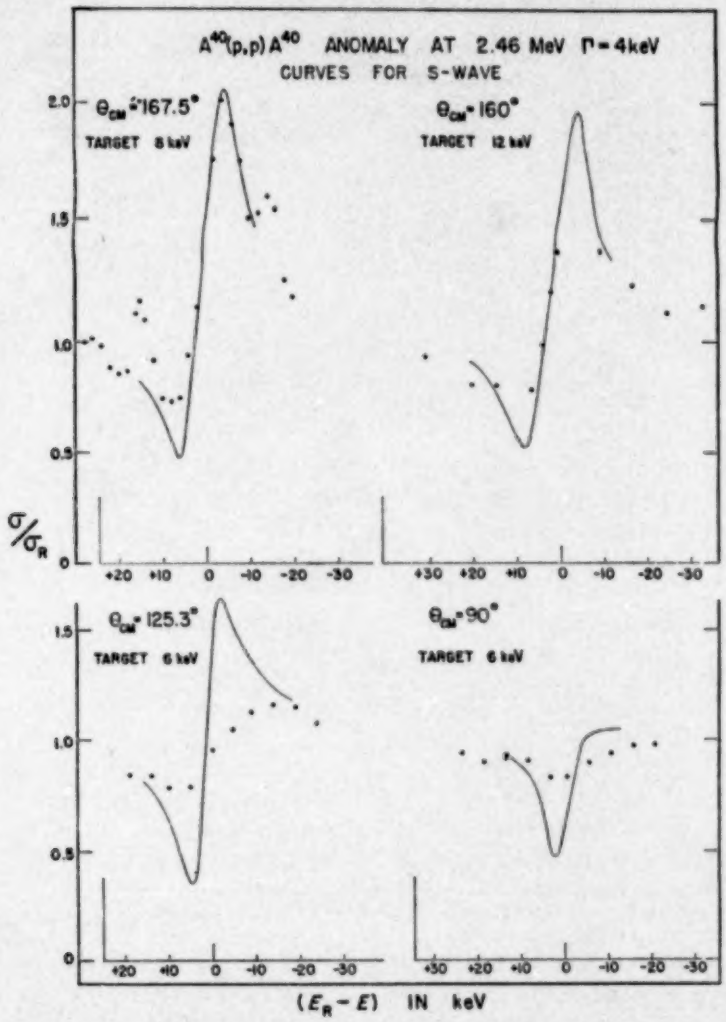

Fig. 8. Elastic-scattering anomaly at $E_p = 2.46$ MeV. Points are experimental data. Curves are computed for s-wave protons and a resonance width $\Gamma = 4$ keV.

by taking a smaller target thickness. Since there are other nearby levels, the fit deteriorates away from the resonance energy. The alternative value of j^π for $l = 1$, i.e. $j^\pi = \frac{1}{2}^-$, gives a calculated anomaly which, even with zero target thickness, has a peak value below the experimental points at the peak. as target thickness smearing will accentuate the disagreement, this value of j^π was rejected. The shapes of the anomalies are qualitatively similar for f-waves. However, both for $j^\pi = \frac{5}{2}^-$ and $\frac{7}{2}^-$ with zero target thickness the minimum

would be higher and the disagreement stronger. Further, the maximum values of the calculated anomalies are extremely high at $\theta_{CM} = 160°$, nearly four times the Rutherford value for $j^\pi = \frac{5}{2}^-$ and seven times it for $j^\pi = \frac{7}{2}^-$. The smearing effect of the target thickness (roughly 10 keV at this angle) is insufficient to reduce these calculated values to the experimental maximum value of about 1.3 times the Rutherford cross section. It is concluded that the spin and parity of the level corresponding to the $E_p = 1.88$ MeV anomaly are $\frac{3}{2}^-$. Since there obviously are interference effects from nearby levels, this assignment is not so certain as would be possible with isolated states, but the above arguments make the assignment plausible.

The results of the s-wave calculations for the upper anomaly appear in fig. 8. This anomaly is above the neutron threshold and some α particles and inelastically scattered protons are observed, so that a_p need no longer be unity. Since neutrons from a $\frac{1}{2}^+$ state to the ground state of K^{40} require $l = 3$, the neutron penetrability and hence the neutron width might be expected to be rather small near threshold. For this reason and because the observed alpha partial width was small, $a_p = 1$ was used in the calculations. It can be seen that this leads to a calculated anomaly much stronger than that observed, so that a_p must be appreciably less than unity. This suggests that at this energy, just above the reported neutron threshold [8]) ($E_p = 2.4$ MeV) the neutron width is quite large.

For d-waves at $\theta_{CM} = 125.5°$, the calculated anomaly is qualitatively different from that observed. The calculated g-wave anomalies are about six times the Rutherford value at $\theta_{CM} = 160°$ and target thickness smearing seems inadequate to reduce this to the experimental value. It is therefore likely that the level corresponding to the $E_p = 2.45$ MeV anomaly has $j^\pi = \frac{1}{2}^+$.

The authors thank Professor H. W. Lewis of Duke University for making available his unpublished data and permitting its inclusion here. Professor James A. Jacobs is thanked for many valuable discussions.

References

1) K. J. Brostrøm ,T. Huus and J. Koch, Nature **162** (1948) 695
2) G. D. Freier, K. F. Famularo, D. M. Zipoy and J. Leigh, Phys. Rev. **110** (1958) 446
3) H. W. Lewis, private communcation
4) A. K. Val'ter, I. Ya. Malakhov, P. V. Sorokin and A. Ya. Taranov, Bull. Acad. Sci. USSR (Columbia Technical Translations) **23** 839
5) S. Bashkin, R. R. Carlson and R. A. Douglas, Phys. Rev. **114** (1959) 1543
6) A. M. Lane, R. G. Thomas and E. P. Wigner, Phys. Rev. **98** (1955) 693
7) See, for example, J. W. Olness, W. Haeberli and H. W. Lewis, Phys. Rev. **112** (1958) 1702
7) H. T. Richards and R. V. Smith, Phys. Rev. **74** (1948) 1870

2.L

Nuclear Physics **28** (1961) 438—442; © *North-Holland Publishing Co., Amsterdam*

Not to be reproduced by photoprint or microfilm without written permission from the publisher

ELASTIC SCATTERING OF PROTONS BY ARGON-36

C. C. KIM †

Department of Physics and Astronomy, State University of Iowa, Iowa City, Iowa

and

A. C. L. BARNARD

Department of Physics and Astronomy, State University of Iowa, Iowa City, Iowa

and

Department of Physics, Rice University, Houston, Texas ††

Received 3 June 1961

Abstract: Absolute differential cross sections for the elastic scattering of protons by A^{36} have been measured for laboratory proton energies from 1.0 to 1.8 MeV at a centre-of-mass angle of 158.4°. The cross sections are equal to the Rutherford value except in an anomalous region near $E_p = 1.494$ MeV, corresponding to a level in K^{37} with 3.34 MeV excitation. Cross sections were measured as a function of energy at angles $\theta_{CM} = 90.0°$, 125.3° and 160.1° over the anomalous region, and an angular distribution was taken at $E_p = 1.494$ MeV. The data were analyzed in terms of dispersion theory to assign $j^\pi = \frac{1}{2}^-$ to the K^{37} state.

1. Introduction

The bombardment of A^{36} targets by protons with energies between 0.5 and 1.8 MeV was reported by Brostrøm, Huus and Koch [1]). No resonances in the γ-ray yield were seen over this energy range, which corresponds to excitation energy $2.4 < E_x < 3.7$ MeV in the compound nucleus K^{37}.

In the present experiment, argon enriched to 58 % A^{36} formed a thin gas target. Protons with energies in the range $1.0 < E_p < 1.8$ MeV were incident upon the target, and elastically-scattered protons were observed at a centre-of-mass angle of 158.4° over this energy range. Further measurements were made in an anomalous region near $E_p = 1.494$ MeV.

The remaining 42 % of the gas used consisted almost entirely of A^{40}. Since the A^{40}(p, p)A^{40} cross section follows the Rutherford form unanomalously for $E_p \lesssim 1.8$ MeV (ref. [2])), the correction for the A^{40} content was easily made in this region. However, at higher energies this cross section behaves anomalously, and correction would be difficult. For this reason A^{36}(p, p)A^{36} measurements were not continued to higher energies in the present experiment.

Attempts were made to observe a γ-ray resonance in the anomalous region, but without success. The approximate upper limit obtained for the cross section

† Present address: Physics Department, University of Southern California, Los Angeles 7, California

†† Work supported in part by the U.S. Atomic Energy Commission.

for the $A^{36}(p, \gamma)K^{37}$ reaction is, however, rather higher than the cross section corresponding to the usual magnitude of the transition probabilities observed in this mass region [3]).

2. Apparatus

The gas target chamber used for the elastic scattering measurements, made at the State University of Iowa, is exactly as described previously [2]). The γ-ray detector on the chamber was used in one attempt to observe the corresponding resonance in the γ-ray yield, but since this detector was unshielded and since there was A^{40} in the target gas, the background was high.

A second attempt at detecting this resonance was made at Rice University. The K^{37} produced by the proton-capture reaction decays by positon emission with a half-life of about 1.2 sec (ref. [4])). The proton beam entering a small gas target chamber was pulsed, 2 sec on and 10 sec off. A NaI(Tl) well-type scintillation detector was placed round the target, and pulses corresponding to the 0.511 MeV annihilation quanta were counted during two 2 sec periods. The first of these periods was almost at the beginning of, and the second almost at the end of the "beam off" time. Positon activity of comparatively long half-life is recorded during the second period, and was subtracted from the counts recorded in the first period to obtain the short-period activity. Measurements made in this way are insensitive to the A^{40} content of the target gas.

3. Results

Fig. 1 shows the elastic-scattering differential cross section at $\theta_{CM} = 158.4°$ as a function of the incident proton energy. The cross section is seen to be close to the Rutherford value except in the anomalous region near $E_p = 1.494$ MeV. In fig. 2 the cross sections in the anomalous region are shown as a function of proton energy at three angles of observation. At about the resonance energy of the anomaly, an angular distribution of elastically-scattered protons was measured, and appears in fig. 3. No resonance corresponding to this anomaly was seen in the γ-ray yield. The sensitivity of the Rice measurements was such that a peak cross section of about 30 μb would have been clearly visible.

4. Discussion and Conclusions

The single-level approximation of the dispersion theory [5]) may be used to find the spin and parity of the K^{37} level ($E_x = 3.34$ MeV) which produced the anomaly at $E_p = 1.494$ MeV. The solid curves in all figures are calculated on this basis. In figs. 1 and 2 the calculations for $j^\pi = \frac{1}{2}^-$ only are shown, but in fig. 3 both $j^\pi = \frac{1}{2}^-$ and $\frac{3}{2}^-$ appear. A level width of 3 keV was used

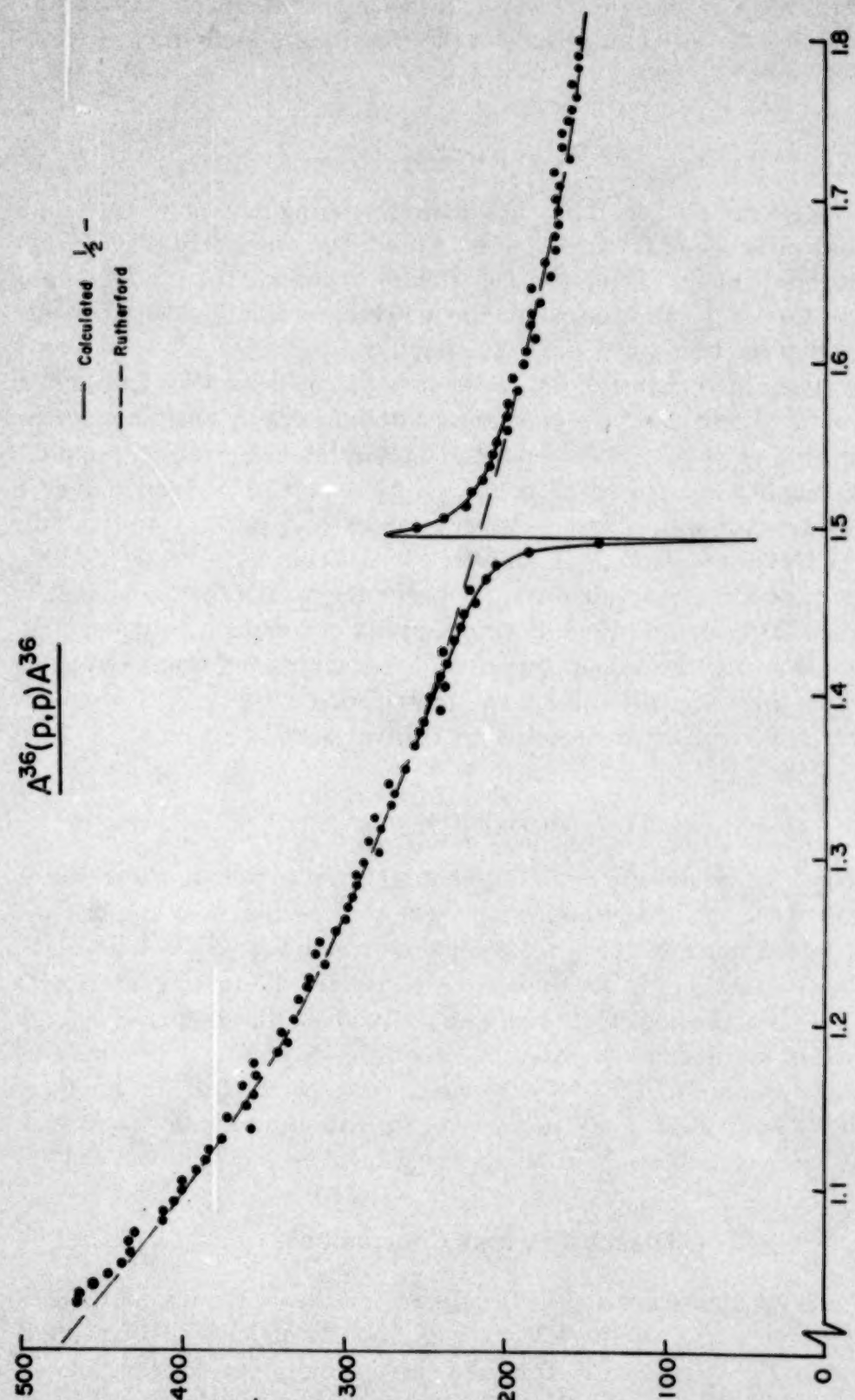

Fig. 1. Differential cross sections for the elastic scattering of protons at $\theta_{CM} = 158.4°$. The points are experimental data, the dashed curve is the Rutherford value and the solid curve is calculated from dispersion theory assuming $J^\pi = \frac{1}{2}^-$, $\Gamma = 3$ keV for the $E_x = 3.34$ MeV level in K^{37} and $\phi_1 = 0$.

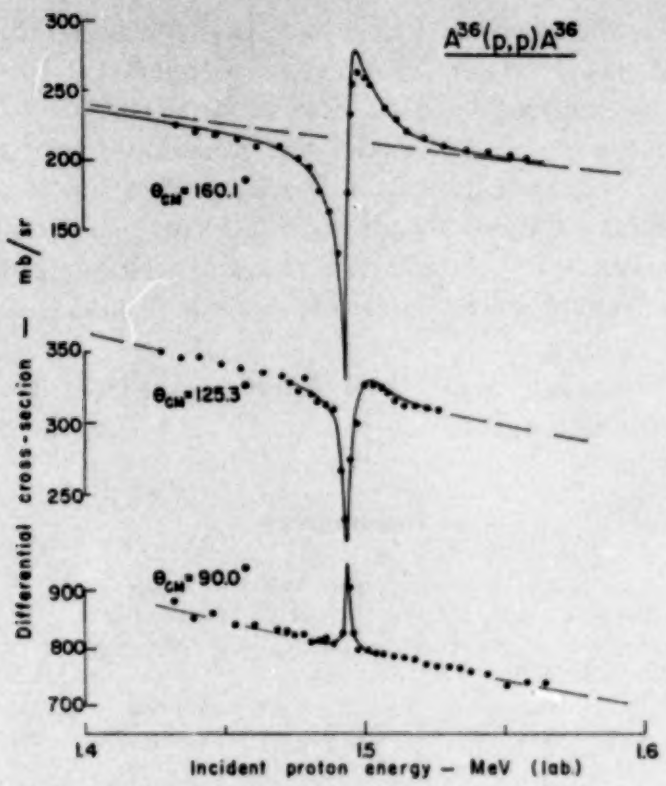

Fig. 2. Differential cross sections for the elastic scattering of protons at three angles. The points are experimental and the curves calculated from dispersion theory as for fig. 1.

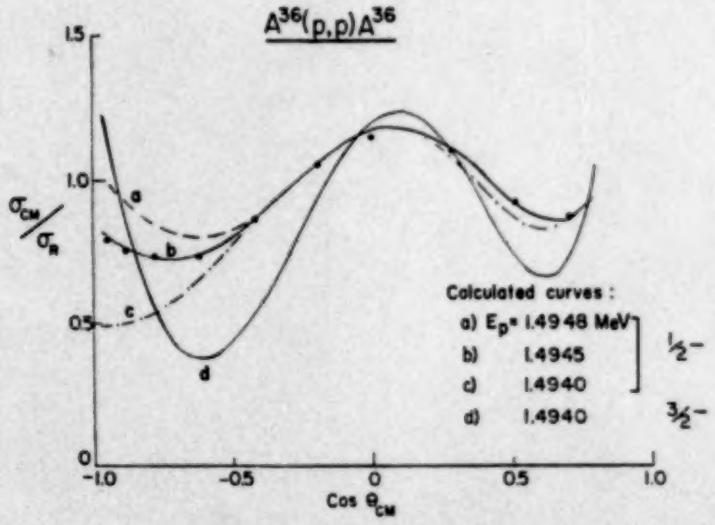

Fig. 3. Angular distributions near the resonance energy. Points are experimental data and the curves calculated from dispersion theory. Both $j^\pi = \frac{1}{2}^-$ and $\frac{3}{2}^-$ calculations are shown.

in the calculations, which are not corrected for the finite target thickness. All potential phase-shifts were put equal to zero, as suggested by their hard-sphere values. It can be seen that an assignment $j^\pi = \frac{1}{2}^-$ to the level fits the data

very well, whereas the alternative does not. It is concluded that the E_x=3.34 MeV level in K^{37} has $j^\pi = \frac{1}{2}^-$. The level reported [4]) at $E_x = 3.50$ MeV in A^{37} is probably the mirror level to that reported here.

If, in accordance with the shell model, the ground state of K^{37} is assumed to have $j^\pi = \frac{3}{2}^+$, then the transition from the $E_x = 3.34$ MeV state to ground is E1. The upper limit of about 30 μb on the A^{36}(p, γ)K^{37} cross section then corresponds to about 0.1 % of the Weisskopf transition probability. In this mass region, transition probabilities are often smaller than this.

The authors thank G. S. Mani, P. D. Forsyth and D. L. Dittmer for much help with the experimental work.

References

1) K. J. Brostrøm, T. Huus and J. Koch, Nature **162** (1948) 695
2) A. C. L. Barnard and C. C. Kim, Nuclear Physics **28** (1961) 428
3) D. H. Wilkinson, in Nuclear spectroscopy, ed. by Fay Ajzenberg-Selove (Academic Press, New York and London, 1960) p. 852
4) P. M. Endt and C. M. Braams, Revs. Mod. Phys. **29** (1957) 683
5) See, for example, J. W. Olness, W. Haeberli and H. W. Lewis, Phys. Rev. **112** (1958) 1702

1.E.1:
3.A

Nuclear Physics **28** (1961) 443—455; © *North-Holland Publishing Co., Amsterdam*
Not to be reproduced by photoprint or microfilm without written permission from the publisher

THE 9.63 MeV STATE OF C^{12}

RICHARD R. CARLSON

State University of Iowa, Iowa City, Iowa †

Received 20 May 1961

Abstract: Gamma radiation from the 16.11 MeV state to the 9.63 MeV state in C^{12} has been identified with a three-crystal pair spectrometer and with 15 cm long by 12.7 diameter NaI (Tl) crystal detectors. The 6.45±0.05 MeV line occurs with a branching ratio of 1% of the well-known 11.67 MeV—4.43 MeV cascade radiation. The 16.11 MeV state of C^{12} was obtained by bombardment of thick boron targets with protons at the 163 keV resonance for the B^{11}+p reaction. The yield of 6.45 MeV radiation showed resonance at the same energy as the cascade radiation. Coincidence spectra taken with two detectors, biased at 1.0 MeV, showed that less than 2.5% of the 6.45 MeV radiation is accompanied by gamma radiation, in agreement with the known alpha decay of the 9.63 MeV state. The angular distribution of the 6.45 MeV radiation was measured. It is only consistent with a spin and parity of 3^- for the 9.63 MeV state, when taken with the known alpha decay.

1. Introduction

The C^{12} nucleus has a bound excited state at 4.43 MeV excitation together with unbound states at 7.656 MeV and 9.63 MeV as well as higher excited states [1]). The spin and parity of the first two excited states are 2^+ and 0^+, respectively. An energy level diagram of the C^{12} nucleus is shown in fig. 1. The spin and parity of the third excited state has been presumed to be 1^-, but a recent analysis of the data from experiments involving the 9.63 MeV level suggests that this state may be 3^- instead [2]). This suggestion stimulated the present investigation.

A gamma-ray transition from the well-known 2^+ ($T = 1$) state at 16.11 MeV to the state at 9.63 MeV was sought for and found. The initial state was prepared by low-energy proton bombardment of boron. Previous attempts to observe this transition had placed an upper limit on the partial width which was considerably larger than the value found. A more recent attempt placed the upper limit immediately above the value found here [3]). A high-efficiency three-crystal pair spectrometer was used to obtain this partial width. Large 15 cm long by 12.7 cm diameter NaI (Tl) crystals were also found to show this gamma-ray line in addition to the well-known 16.11 MeV, 11.67 MeV and 4.43 MeV gamma-ray lines. This more efficient detector made possible the measurement of the angular distribution of the newly observed gamma-ray line. The measured angular distribution agrees with 3^- and not with 1^- for the spin and parity of the 9.63 MeV state.

† Work supported in part by the U.S. Atomic Energy Commission.

2. Three-Crystal Pair Spectrometer

The three-crystal pair spectrometer is an improvement over the one previously used in this laboratory [4]). Gamma rays are detected in a 5 cm long by 4.4 cm diameter NaI (Tl) crystal. The pulse output of the associated photomultiplier is analyzed in a 256-channel pulse-height analyzer when the interaction in this crystal occurs by means of pair formation and both annihilation quanta resulting from the destruction of the positon escape from the crystal. This is guaranteed by gating the analyzer for analysis only when both annihilation quanta are detected in the two NaI (Tl) crystal detectors on each side of the above crystal. These two detectors almost completely surround the above crystal. They were made from a single 15 cm long by 12.7 cm diameter crystal through which a 6.3 cm hole was drilled at right angles to the axis of the cylinder. This hole was midway along the axis between the flat faces. The crystal was then sawed in half along a plane parallel to the flat faces and packaged with transparent windows on the flat faces for viewing by photomultipliers.

The two side-crystal detectors were required to have pulses coincident within 50 ns and to have them fall within the range of the photopeak of annihilation radiation before the analyzer gate was opened. This resulted in a reduction of counting rate in the two escape peak of the centre crystal by about a factor of 20. It also resulted, of course, in the suppression of most of the complexity of the usual pulse-height spectrum from NaI (Tl). The pulse-height *versus* gamma-ray energy was linear to better than 1 % over the energy range including 2.62 MeV (The C'' natural source), 6.13 MeV ($F^{19}(p, \alpha\gamma)O^{16}$), 4.43 MeV, 11.67 MeV and 16.11 MeV ($B^{11}(p, \gamma)C^{12}$).

The three-crystal pair spectrometer was used to observe the radiation from a thick natural boron target bombarded with protons at the 163 keV resonance ($E_p = 180 \pm 3$ keV). This bombardment forms C^{12} with an excitation of 16.11 MeV. The pulse-height distribution obtained from several days bombardment with a beam current of 40 μA is shown in fig. 1. Observations were made at 55° to the beam direction and at a distance of 9.5 cm from the target to the front face of the centre crystal. Lead bricks, 5 cm thick, partially shielded the side crystals from the target but gave no collimation to the radiation incident on the centre crystal. The target chamber had been designed for angular distribution measurements and possessed cooling facilities for the target and a cold trap which completely encircled the target except for the beam entrance hole. Beam current to the target was integrated and secondary electron suppression was obtained with suitable voltages.

The pulse-height distribution in fig. 1 shows the expected peaks due to the 4.43 MeV, 11.67 MeV and 16.11 MeV gamma rays. In addition, there is a peak at 6.45 ± 0.05 MeV from a gamma ray which has not previously been observed. This is ascribed to the transition from the 16.11 MeV capture state to the 9.63

MeV state of C^{12}. A small satellite peak appears 0.5 MeV higher in energy than the peak due to the very intense 4.43 MeV gamma ray. This results from incomplete suppression of the one-escape peak.

For a single gamma ray, the three-crystal pair spectrometer essentially give a single peak together with a low energy tail which is nearly flat. The peak-to-tail ratio becomes worse at higher energies with the result that the 6.45 MeV peak sits on top of appreciable tails due to the 11.67 MeV and 16.11 MeV gamma rays. Lines drawn in fig. 1 under the 4.43 MeV and 6.45 MeV peaks indicate estimates as to the size of these tails. The relative intensity of the two

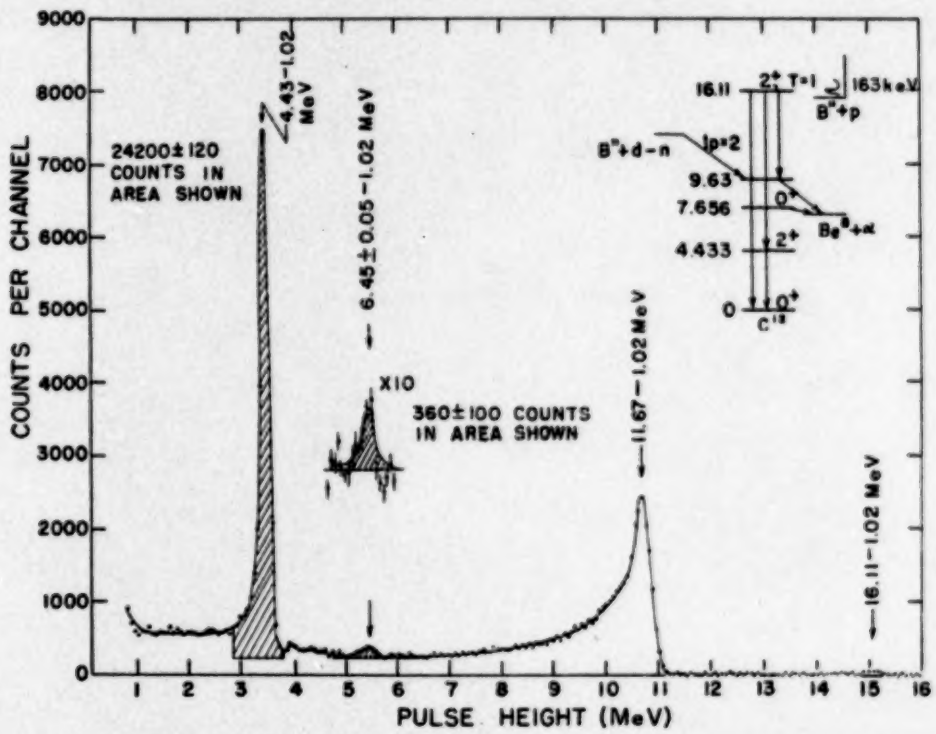

Fig. 1. Pulse-height distribution obtained with a three crystal pair spectrometer from 180 keV proton bombardment of a thick boron target.

radiations was taken to be the ratio of the corresponding areas marked off under the two peaks after correction for the variation in pair production cross-section. The relative intensity is 1 %. Since the 163 keV resonance isformed by p-wave capture and observation was at 55°, the observed relative intensity is the same as the ratio of partial widths for decay by 6.45 MeV and cascade radiation. The latter being 70 eV, the former is 0.7 ± 0.2 eV. The error is primarily due to statistics.

The yield of this 6.45 MeV radiation was measured at one energy below the 163 keV resonance and at two above (154, 172 and 180 keV) with the three-crystal spectrometer. The yield shows resonance the same as the cascade radiation. A more complete yield curve was measured using the more efficient single crystal detector and is described below.

3. Coincidence Spectra

The 9.63 MeV state [5]) of C^{12} has a width of 30 keV, decaying by alpha emission to Be^8. Consequently, the 6.45 MeV gamma radiation should not be accompanied by an appreciable amount of coincident gamma radiation. In order to show that this was the case, large 15 cm long by 12 cm diameter NaI (Tl) single-crystal detectors were used. Fig. 2 shows the pulse-height distribution obtained

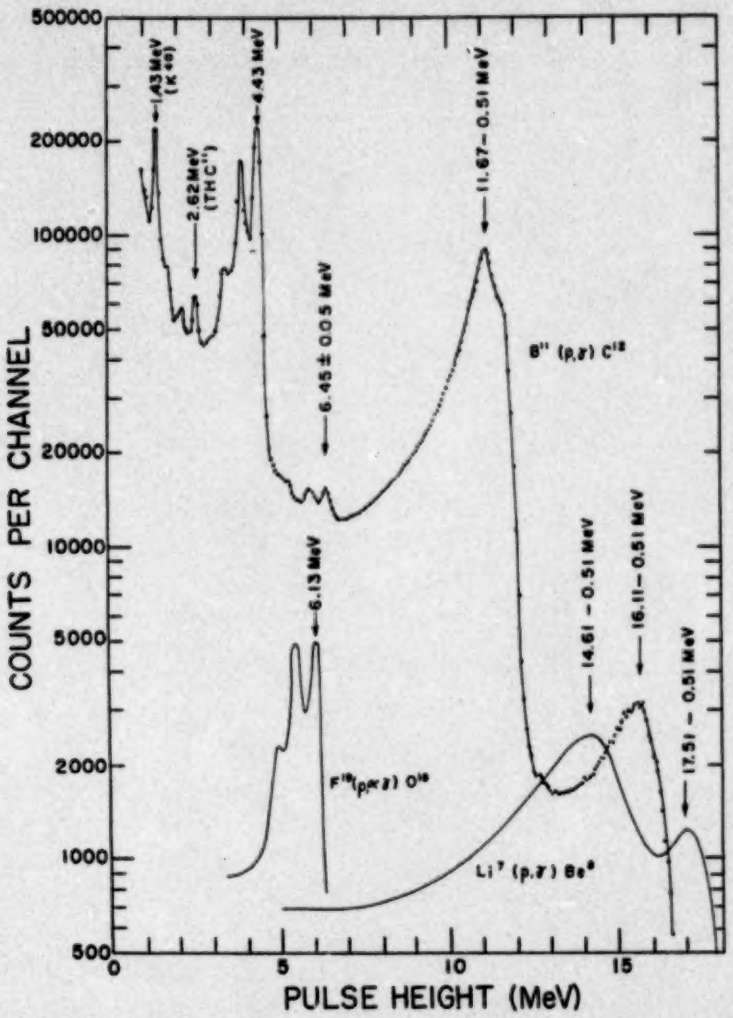

Fig. 2. Pulse-height distribution obtained with a 15 cm long by 12.7 diameter NaI (Tl) crystal from 172 keV proton bombardment of a thick boron target. Detector was at 90° to the beam direction. Smooth lines without data points show pulse-height distributions obtained under the same conditions with a LiH target and 295 keV protons and with a CaF_2 target and 340 keV protons.

with one of these crystals for a proton energy of 172 keV. The other gave the same results. A structure characteristic of 6 MeV gamma radiation in such crystals appears superimposed on the tail of the pulse-height distribution due to the 11.67 MeV and 16.11 MeV gamma rays. The gamma-ray energy giving rise to this structure in fig. 2 is again 6.45 ± 0.05 MeV. Fig. 2 also shows the pulse-height distribution obtained in this crystal from the 6.13 MeV gamma

radiation from $F^{19}(p, \alpha\gamma)O^{16}$ for comparison. This pulse-height distribution is, of course, not superimposed on that due to an appreciable amount of other gamma radiation as is the case with the 6.45 MeV radiation.

Fig. 3, curve a, shows the coincidence pulse-height distribution taken with the two detectors biased at 1.0 MeV. The 16.11 MeV gamma ray is suppressed and

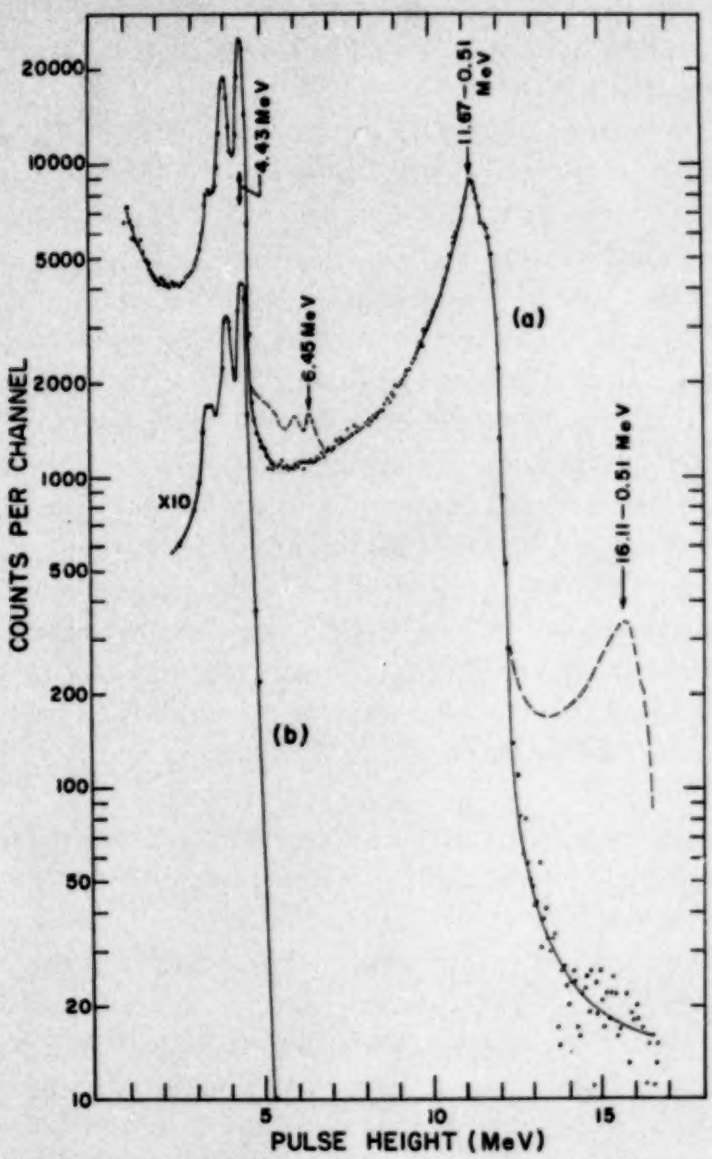

Fig. 3 (a) Pulse-height distribution obtained with the detector as in fig. 2. but with the requirement of coincidence with a second identical detector, where each detector was biased at 1 MeV; for comparison, the dotted lines give the pulse-height distribution from fig. 2, normalized to the peak of the 11.67 MeV radiation. (b) Pulse-height distribution obtained under the same conditions as in (a) but with the bias raised to 5.5 MeV in the second detector.

the structure at 6.45 MeV is eliminated in confirmation of the ascription. The room background due to Th C″ and K^{40} also is eliminated. The dashed lines give the ungated pulse-height distribution from fig. 2, normalized at the peak due to the 11.67 MeV radiation.

The shape of the pulse-height distribution from just above 6.5 MeV to just above 11.7 MeV is exactly the same as the ungated distribution, if the slight effect of the shape of the tail of the 16.11 MeV radiation is taken into account in fig. 2. The shape of this tail in the neighbourhood of the peak due to the 11.67 MeV radiation is indicated by the pulse-height distribution obtained from the 14.6 MeV and 16.51 MeV gamma rays resulting from 295 keV proton bombardment of lithium hydride. This pulse-height distribution is also shown in fig. 2 for comparison.

There is some change in the relative amounts of 11.67 MeV and 4.43 MeV gamma radiation in the coincidence spectra as compared with the ungated spectra because of angular correlation. The counter, whose spectra are shown in figs. 2 and 3, had its front face 18 cm from the target, at 90° to the beam direction. The other counter was 8.8 cm away from the target, also at 90° to the beam. The solid angle of the near counter, especially, would tend to reduce the effect of the angular correlation. The other detector was used at the above distance in order to determine the pulse-height distribution under the same conditions used to measure the angular distribution of the 6.45 MeV gamma ray below.

The pulse-height distribution obtained in the far detector when the bias on the near detector was raised to 5.5 MeV is shown in fig. 3, curve b. It is due to 4.43 MeV gamma radiation alone. This has no appreciable contribution to the distribution in the region of 6.5 MeV so the angular correlation should have no effect on the pulse-height distribution in this region. Consequently, the gated pulse-height distribution gives the shape of the pulse-height distribution upon which the counts due to the 6.45 MeV radiation are superimposed in the ungated distribution.

Anticipating the spin and parity assignments made below for the 9.63 MeV level, it would be expected that any gamma decay branch would occur by cascade decay through the 2^+ first excited state. Taking into account the two associated gamma rays and their expected correlation (very little) with the 6.45 MeV gamma ray, it is estimated that no more than 2.5×10^{-2} of the observed 6.45 MeV gamma rays can be accompanied by coincident gamma radiation. One would expect that there should be far less. On the basis of the single-particle widths [6]), this branching ratio would be 75 eV/30 keV = 2.5×10^{-3} and, if the gamma radiation from the 9.63 MeV state to the 4.43 MeV state has the average width for uninhibited E1 transitions [6]), it would be 2.5 eV/30 keV = 8×10^{-5}, which is considerably less than the upper limit above. The inhibition resulting from the isobaric spin selection rule [7]) for E1 transitions would depress this still further.

4. Angular Distribution

Fig. 4 shows the pulse-height distributions taken at 0° and 90° to the beam direction at a proton energy of 172 keV. Data were taken at the two angles

alternately with the total time broken into eight roughly equal periods. The total pulse-height distributions are plotted as obtained with no corrections applied. No gain shifts were observed. The distributions were taken so that the same number of counts were obtained in the peak due to the 11.67 MeV gamma ray. The shapes are identical from just above 6.5 MeV to just above 11.7 MeV if the different angular distribution of the ground-state gamma ray is taken into account. Furthermore, this only causes a shift in the pulse-height

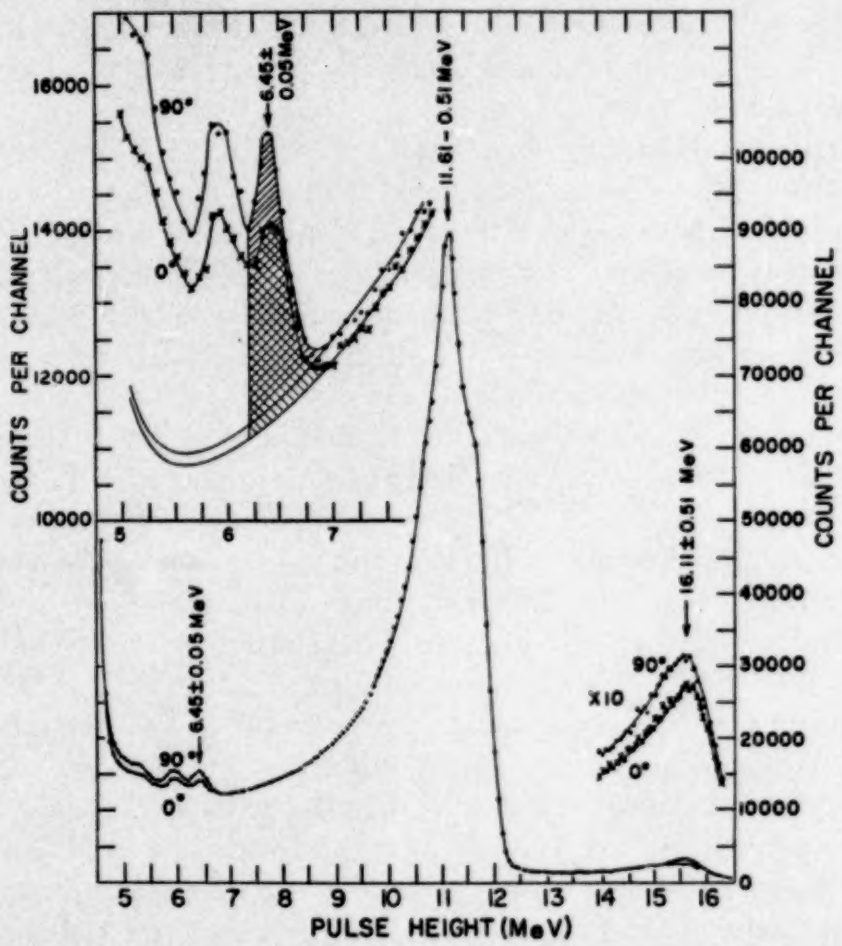

Fig. 4. Pulse-height distributions taken at 0° and 90° to the beam with the detector as in fig. 2. No normalization has been done. Points are plotted as obtained. Places where a single point is plotted actually have a second point which cannot be distinguished. The inset plots the region of interest on an expanded scale. Cross-hatched areas were taken as measures of yield of 6.45 MeV radiation. The ratio of area for 0° curve to that for 90° curve is 0.82 ± 0.05. There were 440 000 μC of bombardment at 0° and 525 000 μC at 90°, all with 25μA of beam.

distribution in the region of 6.5 MeV and no appreciable change in shape between the two angles of observation. This can be seen quite clearly in the expanded plot in fig. 4.

The relative amount of 6.45 MeV radiation at the two angles was obtained by fitting the coincidence pulse-height distribution shown in fig. 3 to the pulse-

height distributions in the region just above the 6.45 MeV peak and extending these shapes down into the region below the 6.45 MeV peak. The number of counts in the photopeak of the 6.45 MeV radiation at the two angles was then taken to be the number of counts in the areas indicated in the expanded plot in fig. 4. The ratio of these areas is 0.82 ± 0.05. The estimate of error is based on extremes of fitting the coincidence distribution for the subtractions involved. It should be noticed that such extremes should deviate in the same direction for the two angles so the error in the relative value should be considerably reduced. Also, only the photopeak was used to obtain the relative intensity in order to reduce the errors arising from subtraction. Statistical errors alone would give ± 0.01.

At 0° and 90° the detector saw the same amount of absorbing material. The target was at 45° to the beam and showed the target backing (0.08 cm copper) to the detector at both angles. The target chamber had symmetry about the axis of rotation for the counter position, except for the beam direction. The chamber wall thickness was 0.08 cm brass and the cold trap, 0.08 cm copper. These would not have an appreciable effect on the relative intensities of the gamma rays under discussion here.

The two angles 0° and 90° were investigated in most detail, but data were also taken at 45°, 60° and 120°. The yield at 45° was taken with the target in the same orientation as at 0° and 90° and the correction for the different effective target backing was determined by measuring the absorption of the backing for the 11.67 MeV radiation. This was done by placing the target at 90° to the beam and measuring the difference in the yield at 60° and 120°. The difference was ascribed to the target and backing absorption since, as is seen below, the yield at these two angles is the same. To put the 45° data on the same absorption basis as that at 0° and 90°, a 2 % correction was necessary.

Data were also taken at 60° and 120°, with the target at 40° to the beam and with the target face to the detector, so that there would be no need for absorption corrections. These data were taken to investigate the possibility of interference from states of opposite parity to the capture state at 16.11 MeV. Within the experimental uncertainty there is no difference in the yields at 60° and 120°. Observations were also made at 90° for this target orientation so that these results could be related to those measured through the backside of the target.

The intensity of the 6.45 MeV radiation relative to that of the 11.67 MeV radiation was converted to an angular distribution by the use of the angular distribution of the 11.67 MeV radiation which was measured in the course of the above work. This was found to be $1+(0.21\pm0.02)\cos^2\theta$, or $1+(0.13\pm0.01)\times P_2(\cos\theta)$, including a small correction for the solid angle of the detector. It is in good agreement with previous measurements [8,9]). Fig. 5 shows the angular distribution points for the 6.45 MeV radiation. These are shown relative to the 90° point because an error arising from subtraction procedure will cause the

same deviation at angle θ as at angle 90° making relative values more meaningful. The data are fitted by $1+(-0.015\pm0.05)\cos^2\theta$, or $1+(-0.01\pm0.03)\times P_2(\cos\theta)$. It should be noted that the near isotropy is consistent with the data in fig. 4 because the bombardments were carried out so that equal numbers of counts were obtained in the peaks due to 11.67 MeV radiation.

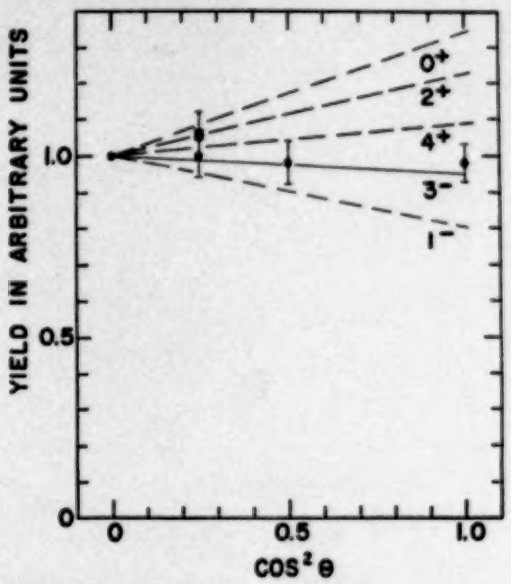

Fig. 5. Angular distribution of 6.45 MeV radiation. Circles give results for 0°—90° to the beam and the square for 120°. Lines are calculated for the indicated spin-parity choices for the 9.63 MeV level.

5. Yield Curve

The large single crystal detector was used to investigate the contribution of higher excited states in C^{12} to the yield of 6.45 MeVradiation by measuring the yield of this radiation as a function of bombarding energy. It is well-known [10]) that the 2^- state in C^{12} which is resonant at 670 keV proton bombardment gives a large yield of 12 MeV radiation but no ground state radiation. The broad 1^- state at 1.4 MeV proton energy gives ground state radiation as well as radiation to the first excited state [10]). The contributions to the yield, of radiation from the low energy tails of these resonances to the 9.63 MeV state, depend on the spin and parity of the 9.63 MeV state. Different choices for these imply different multipolarities for the transitions and, consequently, different intensities relative to the other transitions.

The yields of the ground, first-excited state and third-excited state transitions are shown in fig. 6 as functions of bombarding energy from 146 keV to 352 keV. The yields were obtained from pulse-height distributions, as in fig. 3, taken at each bombarding energy. The first two yields were simply taken by summing the counts in the neighbourhood of the peak channels. In both cases it was noticed that the peak shifted upward in energy by about 2 % as would be expected. The third yield was obtained in the same manner as in the case of

the angular distribution measurements. In this case there was no noticeable ($< 1\,\%$) shift in the position of the total capture peak of the 6.45 MeV line. For this reason, the yield is indicated as due to "6.45 MeV" radiation.

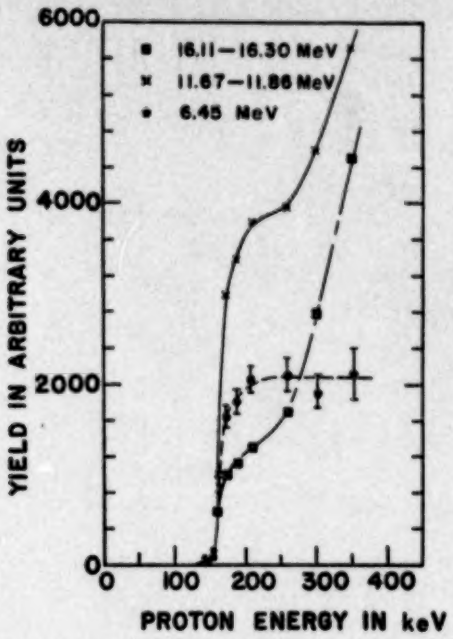

Fig. 6. Yield curve for 6.45 MeV, 12 MeV and 16 MeV radiation.

The yield curve in the case of the 6.45 MeV radiation is characteristic of the thick target yield from a single isolated resonance. In the other two cases the effect of the tails of the higher energy resonances is obvious.

6. Discussion

The identification of the 6.45 MeV line as due to a transition in C^{12} from the excited state at 16.11 MeV to that at 9.63 MeV has been made on the basis of the gamma ray energy measurements, the coincidence measurements, and the resonant yield at 163 keV proton energy. The spin and parity choices for the 9.63 MeV state of C^{12} are limited by the angular distribution measurements and the thick target yield curve of the 6.45 MeV line. These limitations, together with information from other experiments serve to determine the spin and parity of the 9.63 MeV state.

The possible choices are limited to 0^+, 1^-, 2^+, 3^- and 4^+ by the observation that the 9.63 MeV state breaks up by alpha particle emission and has a width of 30 keV. This results from measurements on the $N^{14}(d, \alpha)C^{12*}$ reaction [5]). The maximum spin is set by application of the Wigner limit criterion.

The observed angular distribution of 6.45 MeV radiation is only consistent with the 3^- choice. The angular distributions corresponding to the other choices are indicated as dashed lines in fig. 5 whereas that corresponding to the

3^- choice is shown as a solid line. The angular distributions were calculated [11]) on the assumption of pure p-wave capture so they all have the form

$$W(\theta) = 1+\alpha\frac{1-\chi}{1+\chi}P_2(\cos\theta),$$

where χ is the ratio of intensity of channel spin 2^- to that of channel spin 1^- in the formation of the 2^+ capture state. There is no interference between the two channel spins. The ratio χ was taken from the work on the $B^{11}(p,\alpha)Be^8$ reaction in the neighbourhood of the 163 keV resonance [12]). This gave a value of 0.42 ± 0.02. Table 1 gives the calculated values of the quantity α. With the exception of the 2^+ choice, α is completely determined. For the 2^+ choice, the E2/M1 intensity ratio δ^2 enters as a parameter in the determination of α. An estimate for δ^2 is discussed below. The conclusion about the spin and parity of the 9.63 MeV level is not sensitively dependent on the value of the channel spin parameter χ; for instance, the conclusion would not be changed if χ were taken to be 0.51, as has been proposed [9]).

TABLE 1

Calculated angular distribution for 6.45 MeV radiation

Spin-parity 9.63 MeV level	Transition multipolarity	α	$\alpha\frac{1-\chi}{1+\chi}$ ($\chi = 0.42$)
0^+	E2	$+\frac{1}{2}$	$+0.205$
1^-	E1	$-\frac{7}{20}$	-0.142
2^+	M1+E2	$\frac{\frac{7}{20}-\frac{3\delta^2}{28}+\delta\sqrt{\frac{21}{20}}}{1+\delta^2}$	$+0.176,\ \delta=+\sqrt{0.006}$ $+0.142,\ \delta=0$ $+0110,\ \delta=-\sqrt{0.006}$
3^-	E1	$-\frac{1}{10}$	-0.041
4^+	E2	$+\frac{1}{7}$	$+0.058$
		observed value	-0.01 ± 0.03

An estimate of the E2/M1 ratio was obtained from the single-particle transition probabilities. These gave a value $\delta^2 = 0.006$ which was taken as the maximum value to calculate the expected range of values of α. It might be added here that the estimated E2/M1 ratio for the 11.67 MeV, $2^+ \rightarrow 2^+$ transition is 0.017 whereas the value obtained from the measured angular distribution and the expression in table 1 (which is also applicable to the 11.67 MeV transition) is 0.001. This is considerably less than the estimate. The curve for the 2^+ choice in fig. 5 was drawn for $\delta^2 = 0$ but deviates by only ±5 % for the maximum

value for δ^2 and one would expect a value considerably less than the maximum by comparison with the 11.67 MeV transition.

Additional evidence against the 0^+ and 2^+ choices is contained in the yield curves in fig. 6. Both the ground state and first excited state transitions show the effect of the tails of the higher energy resonances. Since the former is a transition to a 0^+ state and the latter to a 2^+ state there is every reason to expect that the yield curve of the 6.45 MeV radiation would resemble that of the two other radiations if it arose from a transition to a 0^+ or 2^+ state.

The results of measurements on the $B^{11}(d, n)C^{12}$ reaction have been interpreted in terms of stripping theory as showing that an angular momentum transfer of two units occurs in the formation of the 9.63 MeV state [13,14]). This means that the latter has odd parity and is additional evidence ruling out the even parity choices.

In a recent paper [2]), all the experimental evidence relevant to the 9.63 MeV state was analyzed and found to be consistent with either the 1^- or the 3^- choice. The present work indicates that the spin and parity of this state are 3^-. It indicates that the gamma-decay branching ratio of this state is less than 2.5×10^{-2}. It also indicates that the partial width of the state at 16.11 MeV for decay to the 9.63 MeV state is 0.7 ± 0.2 eV. The single-particle estimate for the latter is 155 eV; using an average uninhibited E1 transition strength ($\Delta T = 1$), the estimate is 5 eV. Since a variation about the average of about a factor of seven includes most of the observed E1 transitions [6]), the present case is definitely inside the group of observed E1 widths. The single-particle E2 estimate for this width is 0.036 eV, implying an unreasonably large enhancement if the transition were E2 and giving additional evidence against the 0^+ and 4^+ choices.

The application of a cluster model to nuclei has recently undergone a revival. The experimental evidence for such structure in light nuclei has been reviewed and certain predictions made [15]). In particular, it is expected that the low levels of C^{12} could be interpreted in terms of a $Be^8-\alpha$ cluster with a harmonic oscillator potential. The ground and first excited states arise from the same, even, oscillator excitation. The first odd-parity state comes from the next oscillator excitation which gives rise to excited states with spin 1, 3 and 5 in order of increasing energy. The present measurements are not in agreement with this prediction since they indicate that the lowest-lying odd-parity state in C^{12} has spin 3.

A simplified shell model calculation of the excitation energies of the lowest 1^- and 3^- states of C^{12} leads to the expectation that the two would be in the neighbourhood of 10 MeV with the 3^- slightly lower [2]). This is in agreement with the present results.

References

1) F. Ajzenberg and T. Lauritsen, Nuclear Physics **11** (1959) 1
2) F. C. Barker, E. Bradford and L. J. Tassie, Nuclear Physics **19** (1960) 101
3) A. G. Gregory, Nuclear Physics **23** (1961) 518
4) R. R. Carlson, E. H. Geer and E. B. Nelson, Phys. Rev. **94** (1954) 1311
5) R. A. Douglas, J. W. Broer, R. Chiba, D. F. Herring and E. A. Silverstein, Phys Rev. **104** (1956) 1059
6) D. H. Wilkinson, Phil. Mag. **1** (1956) 127
7) L. A. Radicati, Phys. Rev. **87** (1952) 521
8) T. P. Hubbard, E. B. Nelson and J. A. Jacobs, Phys. Rev. **87** (1952) 378
9) D. S. Craig, W. G. Cross and R. G. Jarvis, Phys. Rev. **103** (1956) 1414
10) G. Dearnaley, G. A. Dissanaike, A. P. French and G. L. Jones, Phys. Rev. **108** (1957) 743
11) W. T. Sharp, J. M. Kennedy, B. J. Sears and M. G. Hoyle, Tables of coefficients for angular distribution analysis, Chalk River (1954) unpublished
12) D. M. Thomson, A. V. Cohen, A. P. French and G. W. Hutchinson, Proc. Phys. Soc. **65** (1952) 745
13) E. E. Maslin, J. M. Calvert and A. A. Jaffe, Proc. Phys. Soc. **69** (1956) 754
14) A. Graue, Phil. Mag. **45** (1954) 1205
15) R. K. Sheline and K. Wildermuth, Nuclear Physics **21** (1960) 196

2.C:2.E *Nuclear Physics* **28** (1961) 456—463; © *North-Holland Publishing Co., Amsterdam*
Not to be reproduced by photoprint or microfilm without written permission from the publisher

LEVELS IN A^{38} OBSERVED THROUGH THE Cl^{37} (p, n) A^{37} REACTION NEAR THRESHOLD

G. S. MANI, A. C. L. BARNARD, T. A. TOMBRELLO
Rice University, Houston, Texas
and
D. A. A. S. N. RAO †
Physics Department, Texas Southern University, Houston, Texas ††

Received 3 June 1961

Abstract: Thin Cl^{37} targets were bombarded with monoenergetic protons, the overall proton energy resolution being about 1.7 keV. A long counter was used to observe neutrons from the Cl^{37}(p, n)A^{37} reaction at energies up to 0.8 MeV above the reaction threshold. The widths and spacings of 91 resonances were measured. A gross structure was discerned, believed to be related to a neutron independent-particle state near the neutron separation energy.

1. Introduction

A large amount of information concerning the level structure of medium-weight nuclei has been accumulated as the result of neutron cross section measurements. Work with thermal and epithermal neutrons gives information about levels very close to the neutron threshold, and this can be extended to higher levels using neutrons obtained from reactions induced by charged particles. In these experiments, the density of levels in the compound nucleus is very high and correspondingly good energy resolution is required to examine individual levels. Since it is difficult to obtain reasonable intensities of neutrons with energy of the order of an MeV and energy spread only about 1 keV, this method is inconvenient for observing the higher levels. In this experiment an alternative method was used; individual levels were examined through the (p, n) reaction.

The particular interest of the experiment was the study of fairly large numbers of levels in the region up to about an MeV above the neutron threshold. It was desirable to have access to many levels decaying through a single neutron channel to simplify analysis. The Cl^{37}(p, n)A^{37} reaction is well suited for such a study. It leads to high excitation in the compound nucleus A^{38}($E_x = 11.8$ MeV at the threshold, $E_p = 1.64$ MeV) and the first excited state in A^{37} is 1.42 MeV above the ground state, so that this channel is closed for $E_p < 3.1$ MeV.

† Present address: The University of Alberta, Canada.
†† Work supported in part by the U.S. Atomic Energy Commission.

Levels in A^{38} have been studied through the $Cl^{37}(p, \alpha)S^{34}$ reaction by Clarke *et al.* [1]) and through the (p, α), (p, n) and (p, γ) reactions by Schoenfeld *et al.* [2]) and Brostrøm Madsen and Madsen [3]). The former group observed about 100 resonances in the (p, n) cross section in the range $1.65 < E_p < 3.0$ MeV and the latter group reported 86 (p, γ) resonances in the range $0.5 < E_p < 2.15$ MeV. An average level spacing of 10—14 keV was obtained by both groups, but the experimental energy resolution permitted the measurement of only a few level widths. The (p, α) cross sections showed many fewer resonances than the other reaction cross sections. Since only levels of natural parity can decay to $S^{34}+\alpha$, the number of alpha resonances would be expected to be about half the number of neutron or gamma resonances.

2. Experimental Arrangement

A beam of protons from the Rice University 5.5 MeV Van de Graaff accelerator was incident on thin sodium chloride targets evaporated on 0.010 cm thick tantalum backings. These targets were placed in aluminium holders. From other experiments with similar slit settings, the energy spread of the beam is estimated as about 1 keV and the results indicate an over-all energy resolution of about 1.7 keV.

The Q-values of the relevant reactions are given in table 1.

TABLE 1

Q-values

Reaction	Q (MeV)
$Na^{23}(p, n)\ Mg^{23}$	−4.84
$Cl^{35}(p, n)\ A^{35}$	−6.76
$Cl^{37}(p, n)A^{37}$	−1.598
$Cl^{37}(p, n)A^{37*}$	−2.99
$Al^{27}(p, n)Si^{27}$	−5.588

A^{37*} represents the first excited state of A^{37}

Thus, for incident proton energies below 3.1 MeV, only neutrons from the third reaction are observed.

These neutrons were detected with a long counter placed close to the target, subtending a solid angle of nearly 2π at it. The thin-target yield curves should therefore be almost undistorted by the effects of changing angular distribution and neutron energy E_n. The worst of these effects occurs at low E_n, as the efficiency of the long counter varies by 10—15 % over the range $0 < E_n < 1$ MeV. The yield curve in the low-energy region should therefore be raised by this amount.

Some deterioration of targets was experienced and to detect this a well-known small part of the yield curve was repeated at intervals. In the absence of

deterioriation, which if it occurred was usually drastic, agreement was within about 10 %. Extensive parts of the yield curve were repeated three times during different phases of the experiment, and good agreement was obtained.

The data for the thin-target curve were mostly taken under circumstances where there was an appreciable background. Since part of this was proportional to the elapsed time of a counting period and part proportional to the number of protons incident on the target during the period, it was difficult to make a good estimate of the combined background effect. The correction was finally made in the following way. First the thin-target data were averaged over energy intervals of 100 keV, correcting roughly for the background. It was found that in general this integrated curve agreed well with data taken with a target of the order of 100 keV thick under low-background conditions [4]). Above $E_p = 2.5$ MeV, however, the integrated curve was appreciably below the thick-target curve, showing overcorrection for background. A final correction was made to force agreement between the two curves above $E_p = 2.5$ MeV.

3. Results

Fig. 1 is the thin-target yield curve, corrected for background, showing about 90 resolved or partially resolved resonances in the energy range $1.7 < E_p < 2.5$ MeV. The narrowest resonance seen with this target had an apparent width little over 1 keV, but allowing for the possibility of an experimental fluctuation decreasing the apparent width of this resonance, the combined effect of target thickness and beam energy spread has been taken as 1.7 keV. In the upper part of fig. 2, the data of fig. 1 are shown integrated over energy intervals of 100 keV. The quantity $\gamma_n = \Gamma_T(E_n)^{-\frac{1}{2}}$ (where Γ_T is the resonance total width and E_n the emergent neutron energy) is represented for each resonance in the lower part of fig. 2. The distribution of resonance spacings D and γ_n appear in figs 3 and 4.

4. Discussion and Analysis of Results

The average apparent width of the resonances which includes the effect of target thickness is 4.3 keV (with a maximum width of about 10 keV), whereas the average spacing between adjacent resonances is 8.1 keV. Thus it is likely that most resonances have been resolved. The level density in A^{38} at an excitation of 12 to 13 MeV is then about 120 levels per MeV.

From fig. 2 it can be seen that the integrated thin-target yield curve shows a broad maximum centred at about $E_p = 2.0$ MeV and about 0.25 MeV wide at half-maximum height. The envelope of this can be seen in fig. 1, and it is believed to correspond to an independent particle (IP) state. Lane, Thomas and Wigner [5]) have explained how an IP state of a nucleon N, which has a

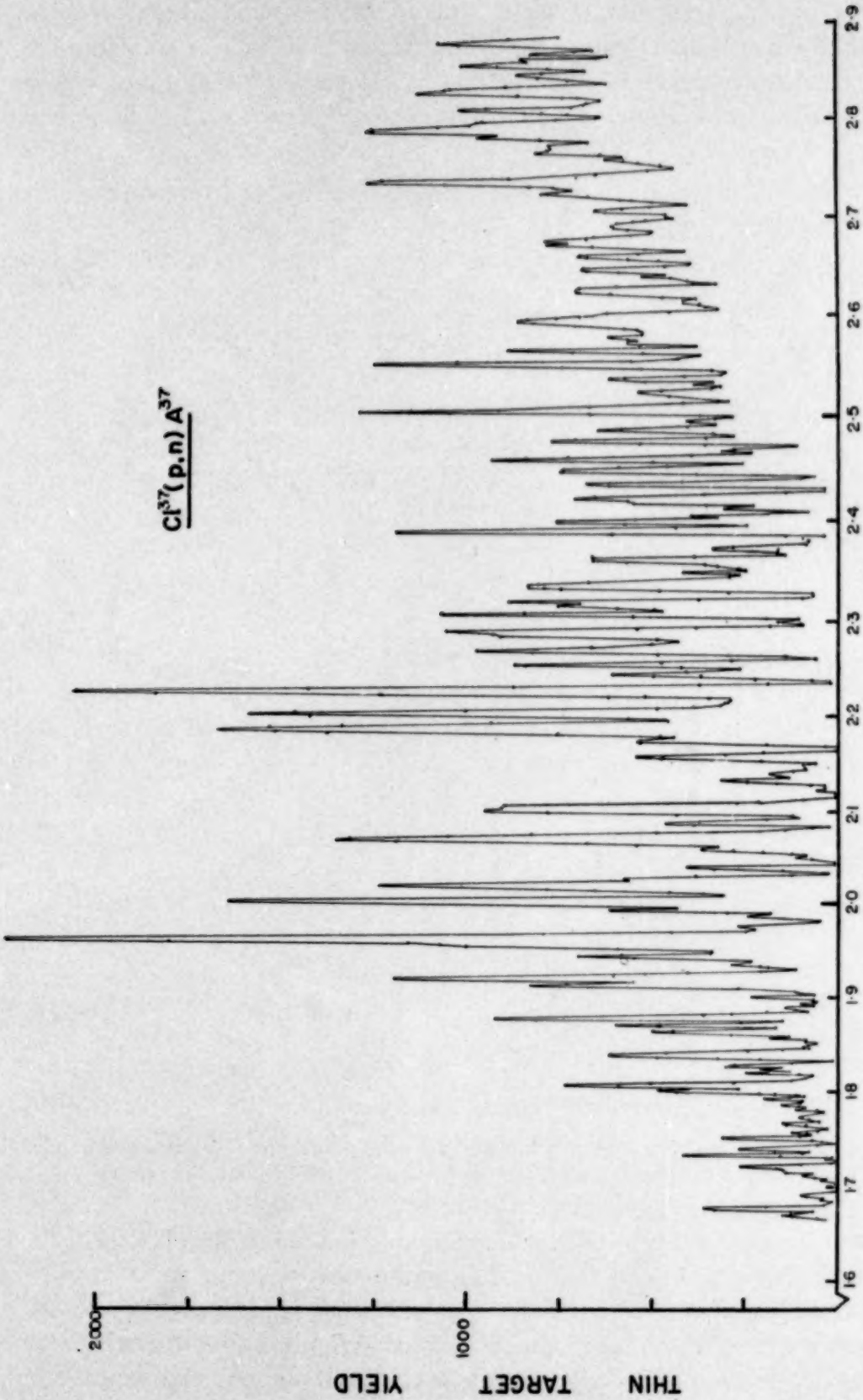

Fig. 1. Yield of neutrons from $Cl^{37}(p, n)A^{37}$ measured with target/beam energy resolution 1.7 keV. There are about 90 resonances in the range $1.7 < E_p < 2.5$ MeV.

reduced width of the order of the Teichmann-Wigner value, may be mixed with neighbouring compound-nucleus states by intermediate coupling. The IP reduced width is distributed among many states, the largest contributions being to the states nearest in energy to the IP state, so that the envelope of a thin-target yield curve has a "giant resonance" structure. It follows that

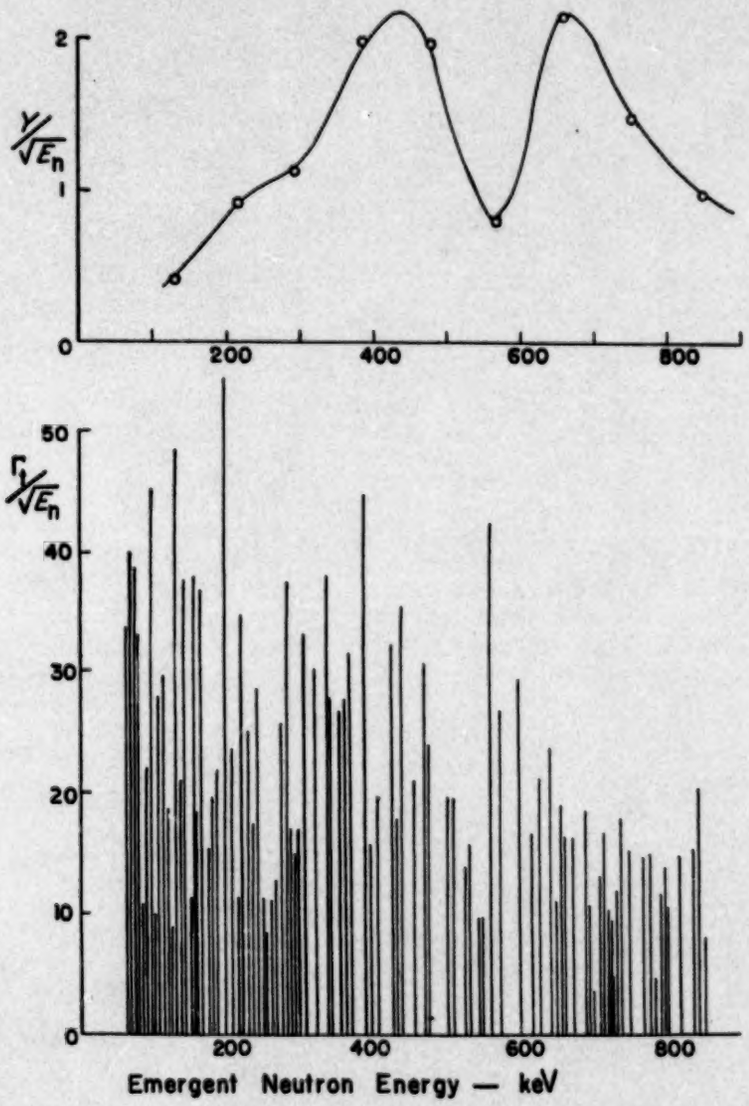

Fig. 2. Upper: the neutron yields of fig. 1. integrated over 100 keV energy interval and divided by $(E_n)^{\frac{1}{2}}$. Lower: the quantity $\Gamma_T(E_n)^{-\frac{1}{2}}$ represented for the individual resonances.

the sum of the reduced partial widths for N-emission for the levels within the broad maximum is of the order of the Teichmann-Wigner value, and that these levels have $\Gamma_N \approx \Gamma_T$.

For a reduced width equal to the Teichmann-Wigner value, the widths of $l = 0$ proton, neutron and alpha particle states at the appropriate energy in A^{38} are respectively 100 keV, 1.3 MeV and 70 keV (all approximate). However,

the sum of the total widths of the 36 resonances within the first broad maximum $1.8 < E_p < 2.1$ MeV is about 170 keV. This suggests that a neutron IP state is responsible. If it is assumed to be an s-wave neutron state, then $\gamma_n = \Gamma_n(E_n)^{-\frac{1}{2}}$

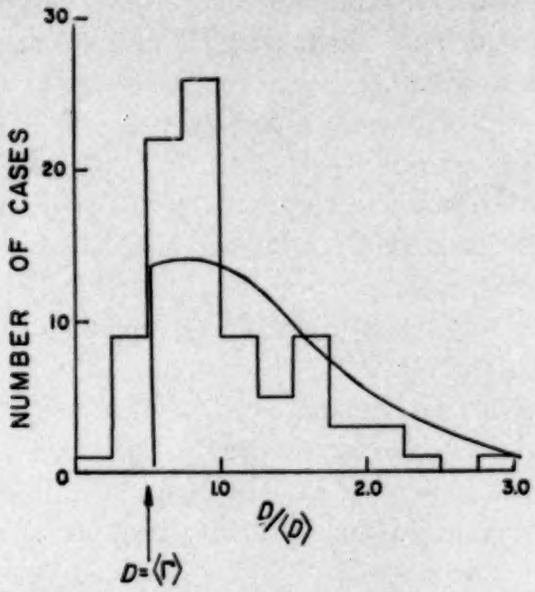

Fig. 3. Distributions of resonance spacings D in units of the average spacing $\langle D \rangle$ for the 90 resonances in the range $1.7 < E_p < 2.5$ MeV. Experimental data are plotted as a histogram and the curve is the extended Wigner distribution.

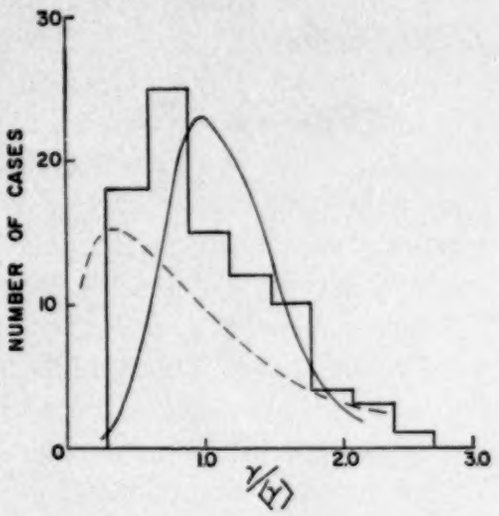

Fig. 4. Distributions of relative neutron reduced widths γ_n in units of the average $\langle \gamma_n \rangle$. Reduced widths obtained on assumptions in text. Experimental data are plotted as a histogram and the curves are Porter-Thomas distributions for 3(dashed) and 16(solid) degrees of freedom.

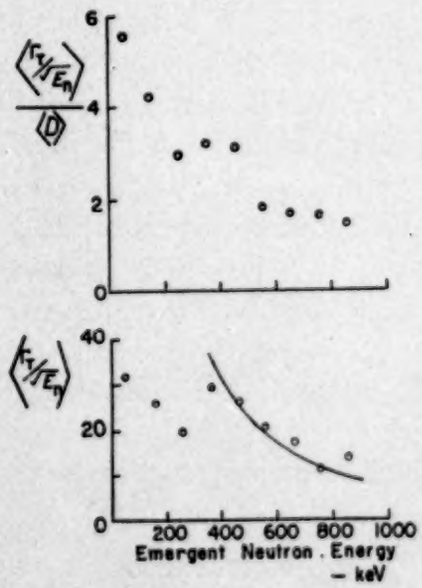

Fig. 5. Upper: the quantity $\gamma_n \langle D \rangle^{-\frac{1}{2}}$ averaged over 100 keV energy intervals. Lower: relative neutron reduced widths (obtained on assumptions in text) averaged over 100 keV energy intervals. Points are experimental data and the curve is the cluster model prediction valid for E_n not small.

is proportional to the reduced width for neutron emission. On the assumption $\Gamma_n \approx \Gamma_T$ the reduced widths are shown in the lower part of fig. 2. It can be seen that there is some, but not perfect correspondence between the two halves of the figure. These reduced widths averaged over 100 keV energy intervals are plotted in the lower part of fig. 5. The "cluster model" calculations of Phillips and Tombrello [6]) suggest that the partial widths for the decay of a nucleus C into the channel (A+a) are approximately inversely proportional to ε, except for small ε. Here ε is the difference between the energy of C and the separation energy (A+a). Since the ordinate in the lower part of fig. 5 is $\Gamma_T(E_n)^{-\frac{1}{2}}$, this prediction corresponds to the curve $(E_n)^{-\frac{1}{2}}$ drawn on the figure. This is seen to reproduce the trend of the data away from threshold. The strength function $\langle\gamma_n\rangle/\langle D\rangle$ (where the quantities are averages over 100 keV energy interval) is plotted in the upper part of fig. 5.

There are signs of a further broad maximum in the envelope of the thin-target yield curve about 300 keV higher than the first. Since the target nucleus has non-zero spin, two neutron IP states with $l_n = 0$ are possible, corresponding to the two possible channel spins. This was mentioned by Lane, Thomas and Wigner but no estimate of the splitting has been made.

Wigner has suggested [7]) a distribution function $P(D') = D' e^{-\frac{1}{2}D'^2}$ where $D' = D_{jj}/\langle D_{jj}\rangle$ for the spacing D_{jj} between levels of the same spin and parity. This suggestion was made without justification, but recently Mehta [8]) has produced an exact solution very similar to it. In the present case two j-values of the compound-nucleus state are possible for each l-value of the incident proton. If it is assumed that only one l-value contributes appreciably, the measured spacing between adjacent resonances may be $D_{j_1j_1}$, $D_{j_1j_2}$, $D_{j_2j_1}$ or $D_{j_2j_2}$. Taking a random distribution for $D_{j_1j_2}$ and $D_{j_2j_1}$, a combined distribution of the form $P(D') \propto D' e^{-\frac{1}{2}D'^2} + e^{-D'}$ suggests itself. It is clear that closely-spaced pairs of resonances cannot be detected, and it is reasonable to cut off this distribution when the level spacing falls to the mean level width. Thus a cut-off was made at $D = \langle\Gamma\rangle$ and the calculated curve was normalized to the experimental data above this. The result, seen in fig. 3, is that the theoretical curve is somewhat deficient at small spacings, but is in fair agreement with experiment.

In fig. 4, the distribution of relative neutron reduced widths is plotted, obtained as before, on the assumption that $\Gamma_n \approx \Gamma_T$. The curves on the figure are chi-squared distributions for 3 and 16 degrees of freedom. A value of 18 was obtained by maximum-likelihood analysis [9]) of the data.

References

1) R. L. Clarke, E. Almquist and E. B. Paul, Nuclear Physics **14** (1959/60) 472
2) W. A. Schoenfeld, R. W. Duborg, W. M. Preston and C. Goodman, Phys. Rev. **85** (1952) 873
3) K. J. Brostrøm, B. S. Madsen and C. D. Madsen, Phys. Rev. **83** (1951) 1265 (L)

4) A. C. L. Barnard, G. S. Mani and P. D. Forsyth, Nuclear Physics **28** (1961) 464
5) A. M. Lane, R. G. Thomas and E. P. Wigner, Phys. Rev. **98** (1955) 693
6) G. C. Phillips and T. A. Tombrello, Nuclear Physics **19** (1960) 555
7) E. P. Wigner, Gatlinberg Conf. Report ORNL 2309 (1957)
8) M. L. Mehta, Proc. Int. Conf. on Nuclear Structure, Kingston, Canada (1960), (North-Holland Publishing Co., Amsterdam, 1960)
9) C. E. Porter and R. G. Thomas, Phys. Rev. **104** (1956) 483

2.C:2E *Nuclear Physics* **28** (1961) 464—470; © *North-Holland Publishing Co., Amsterdam*
Not to be reproduced by photoprint or microfilm without written permission from the publisher

GROSS PROPERTIES OF LEVELS IN A^{38} WITH EXCITATION NEAR NEUTRON SEPARATION ENERGIES

A. C. L. BARNARD, G. S. MANI and P. D. FORSYTH
Rice University, Houston, Texas †

Received 3 June 1961

Abstract: Cl^{37} targets of the order of 100 keV thick to 2 MeV protons were bombarded with monoenergetic protons. Neutron detectors sensitive to neutron energy were used to observe and distinguish between neutrons from the reactions Cl^{37}(p, n)A^{37} and Cl^{37}(p, n)A^{37*}, where A^{37*} refers to the first excited state of A^{37}. Compared to a Hauser-Feshbach statistical calculation, the yield N_0 from the ground-state reaction is anomalous, showing a broad maximum centred about 0.5 MeV above the reaction threshold. A further broad maximum in N_0 is seen about 0.5 MeV above the threshold for the excited state reaction, and in this region there is also a broad maximum in the yield N_1 from the excited state reaction. The yields N_0 and N_1 behave somewhat similarly up to about 1 MeV above the respective thresholds.

1. Introduction

Measurements made with semi-thick targets of medium weight nuclei can be used to reveal gross features of the level structure of the compound nuclei. In this experiment the yields of neutrons from the reactions Cl^{37}(p, n)A^{37} and Cl^{37}(p, n)A^{37*}, where A^{37*} represents the first excited state of A^{37}, were observed from targets of the order of 100 keV thick to 2 MeV protons. Detectors sensitive to neutron energy [1]) were used to observe and distinguish between neutrons from the two reactions.

In this and similar experiments with medium weight nuclei, the density of levels in the compound nucleus is high, and measurements with semi-thick targets are sometimes assumed to be averages over a statistical sample of levels. The interpretation is then insensitive to the unknown properties of the individual levels of the compound nucleus, since calculations can be made on this statistical assumption [2]). The original intention of this experiment was to compare the measured neutron yields with statistical calculations for various assumed values of the spins and parities of the two A^{37} states. The threshold for the ground state reaction has been reported at $E_p = 1.641$ MeV. Excited states in A^{37} have been detected at $E_x = 1.42$, 1.61 and 2.25 MeV with corresponding thresholds at $E_p = 3.08$, 3.29 and 3.94 MeV (ref. [3])).

However, it will be seen that the neutron yields were anomalous, so that the spins and parities could not be determined. The nature of the anomalous behaviour will be discussed.

† Work supported in part by the U.S. Atomic Energy Commission.

2. Experimental Arrangement

A mono-energetic proton beam from the Rice University 5.5 MeV Van de Graaff accelerator was incident upon a semithick sodium chloride target, evaporated onto a 0.10 cm thick tungsten disc. The target was mounted in an aluminium holder. The measurements were made over a "neutron pit" to minimize the background from neutrons scattered from the floor. The detector described by Bramblett, Ewing and Bonner [1]) was used. It consists of a Li^6I (Eu) scintillator over which can be slipped a polyethylene sphere, so that the scintillator is at the centre of the sphere. The efficiency of the detector has been measured as a function of energy and found to be strongly dependent on the size of the sphere. If neutrons of only one energy are emitted, which is the case in the present experiment for $E_p < 3.1$ MeV, measurements with only one sphere give the neutron yield. If two neutron groups are emitted, measurements with two spheres of different size enable the yield of both to be determined. (See sect. 3).

The best data in the present experiment were obtained by using 7.6 cm and 20.3 cm diameter spheres, placed at a distance of 40 cm from the target in the beam direction. Neutron yields were measured for incident proton energies in the range $1.5 < E_p < 4.0$ MeV. In order to minimize possible target, deterioriation and other changes between the 7.6 cm and 20.3 cm measurements, these measurements were made one after another before increasing the beam energy. Since in the range $1.5 < E_p < 3.1$ MeV there is only one neutron group, the 7.6 cm and 20.3 cm data are independent measurements of the yield. A 5.1 cm sphere was also used. Since the counting rate was low at 40 cm, the 5.1 cm measurements were made with the detector 20 cm from the target.

3. Calculation of Neutron Yields

If N_0 and N_1 are the number of neutrons having energies E_0 and E_1, respectively, emitted by a target, the number of counts C_3 obtained by using the 7.6 cm sphere at a distance of 40 cm from the target, is given by

$$C_3 = N_0 \mathscr{E}_3(E_0) + N_1 \mathscr{E}_3(E_1).$$

Here $\mathscr{E}_3(E)$ is the measured efficiency [1]) of the detector with the 7.6 cm sphere at 40 cm for neutrons of energy E. A similar expression can be written for the 20.3 cm sphere. Then N_0 is given by

$$N_0 = \frac{C_3 \mathscr{E}_8(E_1) - C_8 \mathscr{E}_3(E_1)}{\mathscr{E}_3(E_0)\mathscr{E}_8(E_1) - \mathscr{E}_3(E_1)\mathscr{E}_8(E_0)}$$

and N_1 is given by a similar expression.

If only N_0 neutrons of energy E_0 can be emitted, as is the case in the present

experiment for $E_p < 3.1$ MeV, the expressions are simpler:

$$C_3 = N_0 \mathscr{E}_3(E_0), \qquad C_8 = N_0 \mathscr{E}_8(E_0).$$

Since the efficiencies are known, two independent values of N_0 are obtained in this case.

4. Results

The subscript zero now refers to the neutron group to the ground state of A^{37} and subscripts 1, 2, ... to the excited state groups. The neutron yields

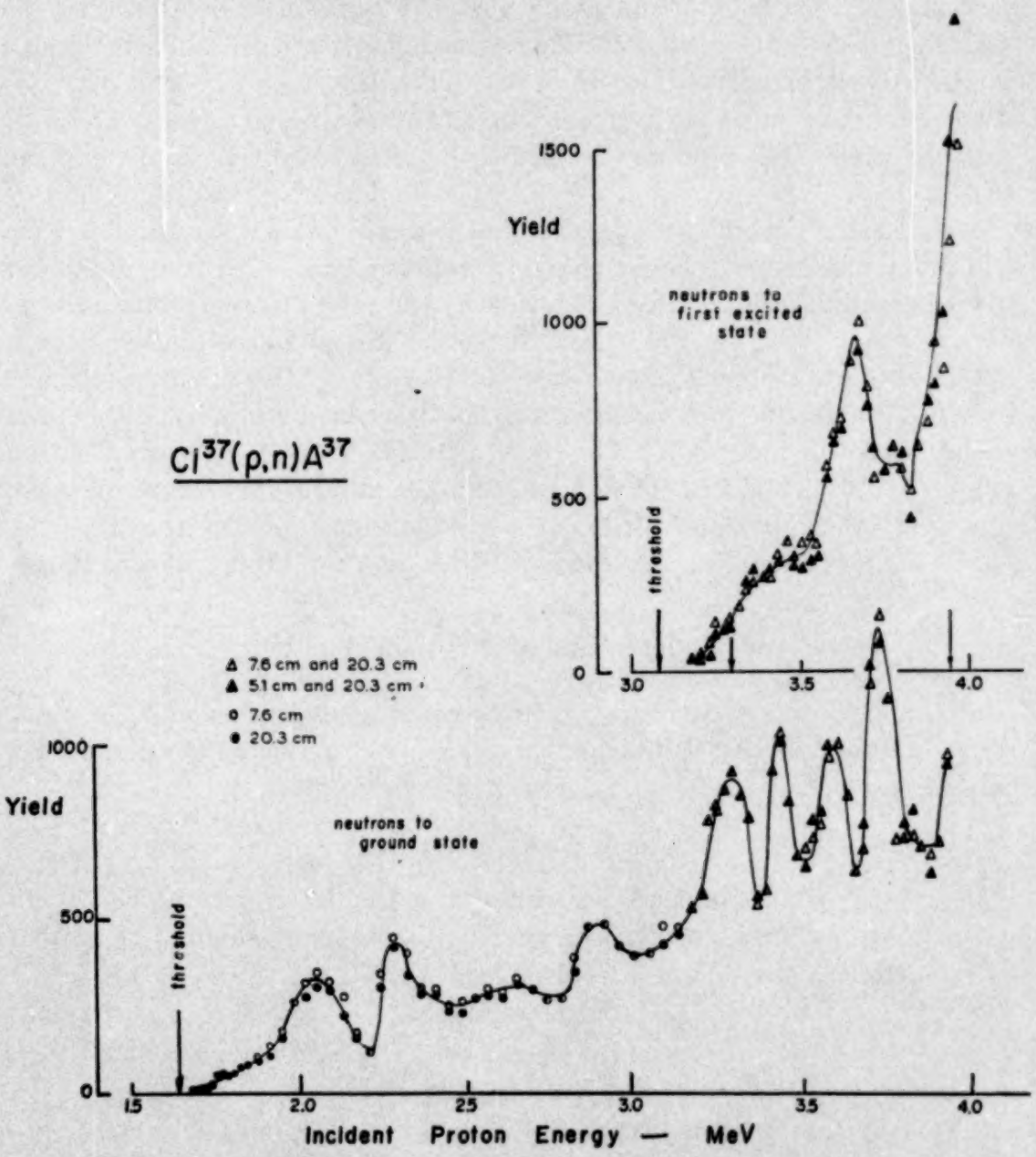

Fig. 1. Neutron yields from $Cl^{37}(p, n)A^{37}$ and $Cl^{37}(p, n)A^{37*}$.

in the beam direction are shown in fig. 1. Below $E_p = 3.1$ MeV, the two values of N_0 are plotted and are seen to agree very well. At higher energies it was assumed that neutron groups to the ground and first excited state only were present. N_0 and N_1 were extracted from the 7.6 cm and 20.3 cm data and also from the 5.1 cm and 20.3 cm data. The values of N_0 and N_1 obtained in the two ways are plotted in fig. 1, where it is seen that the two values of each quantity agree well. Other sets of neutron yield measurements have been made, with different target thicknesses and at different angles of observation. The main features of fig. 1 have been confirmed several times. In a previous

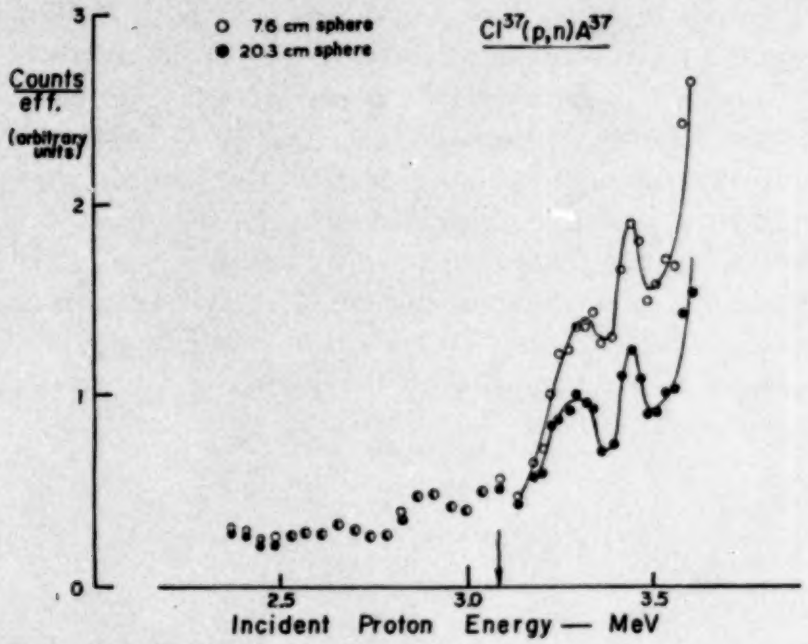

Fig. 2. Use of the sphere detectors to obtain neutron thresholds (see text).

experiment [4]) N_0 was measured for proton energies up to 2.9 MeV with a thin target and long counter. These results, integrated over energy intervals of 100 keV, are in agreement with the present results. As an illustration of the result of making the wrong assumption about the neutron groups incident on the sphere detectors, the yields of neutrons have also been calculated from the 7.6 cm and 20.3 cm data on the assumption that only neutrons from the reaction to the ground state are emitted. The resuits appear in fig. 2 where it is seen that the curves for the two spheres begin to diverge near the threshold for the excited state reaction, where the assumption breaks down. Similarly the two values of N_1 obtained from the 5.1, 7.6 and 20.3 cm data (fig. 1) would diverge if the assumption of two neutron groups were wrong. These two values of N_1 agree within the experimental error of about 10 %. The implications of this were examined at $E_p = 3.37$ and 3.81 MeV and in both cases it was found that $N_2 \lesssim 0.15\, N_1$. Thus it is concluded that the neutron group

to the second excited state of A^{37} is weak. The observation by Ferguson and Paul [3]) of a neutron group with energy $E_n = 258$ keV at a proton energy $E_p = 3.62$ MeV tends to disagree with this result. However, comparisons between the two experiments are somewhat indirect. It should also be remarked that the discussion of sect. 5 would be largely unaffected by an admixture of neutrons to the second excited state.

5. Discussion of Results

The level density in A^{38} at excitation corresponding to the range $1.8 < E_p < 2.5$ MeV in the (p, n) reaction has been shown [4]) to be about 120 levels per MeV. The semi-thick target used here was of the order of 100 keV thick, so that the measured yields are averages over roughly 10 levels.

If the statistical assumption were correct, the neutron yields could be calculated using the Hauser-Feshbach formulation. The cross sections for the reaction from an ingoing channel denoted by unprimed quantities (energy of incident particle E, spin of target nucleus i, orbital angular momentum l, channel spin j) through a compound nucleus of spin J to an outgoing channel denoted by singly primed quantities (with all other open channels denoted by doubly primed quantities) may be written

$$\sigma_{ii'} = \frac{\pi\lambda^2}{2(2i+1)} \sum_{lJ} \frac{(2J+1)A_J}{1+\dfrac{\sum A_{J''}}{\sum A_{J'}}},$$

where $A_J = \varepsilon_{lj}^J T_l(E)$ and $A_{J'}$ and $A_{J''}$ are the same combination of primed quantities. Here ε is a statistical factor and T the penetrability.

Such a calculation has been made for N_0, the yield of neutrons from the ground state reaction up to $E_p = 3.1$ MeV with various assumptions for $j\pi$, the unknown spin and parity of the A^{37} ground state. Simple square-well penetrabilities were used. The calculated curves for N_0 are shown in the upper part of fig. 3. For the case $j = \frac{1}{2}$, the results were found to be insensitive to parity. For the other values of j, only the positive parity cases were calculated. In the lower part of the figure, the experimental yields are shown, integrated over energy intervals of approximately 170 keV, i.e. about 20 levels. The curve for $j = \frac{1}{2}$ is also shown, normalized to the experimental curve. It can be seen that the experimental data have anomalous features, the most prominent being the broad maximum from 0.3 to 0.8 MeV above threshold.

It is possible to continue the calculation of N_0 to higher proton energies and to calculate N_1, the yield from the excited state reaction. However, with $j\pi$ unknown for both the ground state and the first excited state of A^{37}, an unreasonable number of cases would have to be considered. The results would

be various smooth curves and the experimental behaviour of N_0 and N_1 would again be seen to be anomalous. More sophisticated calculations can also be

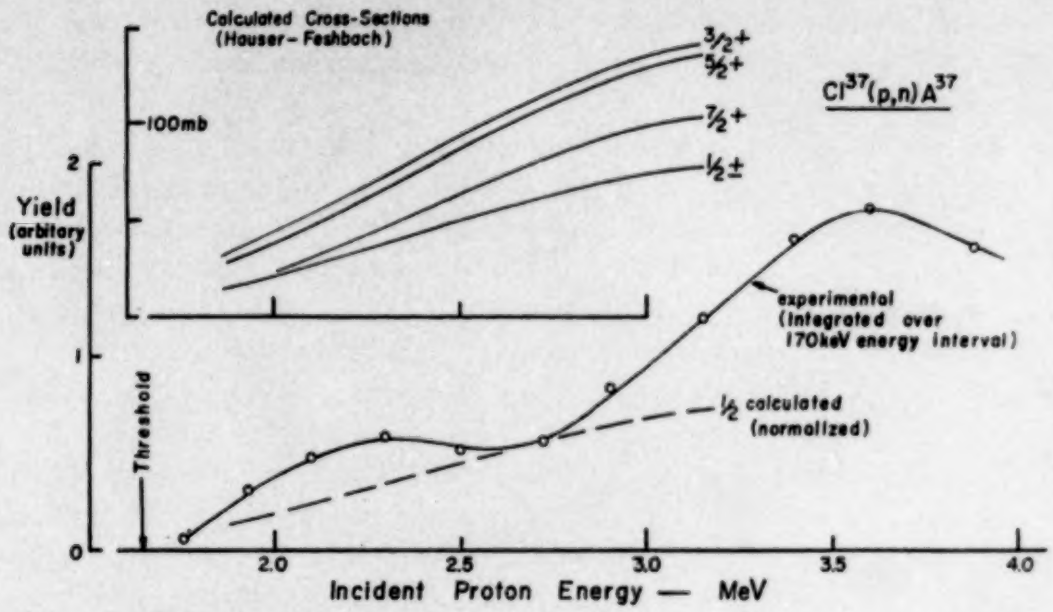

Fig. 3. Upper: Hauser-Feshbach calculations for various A^{37} ground state spin and parity assignments. Lower: comparison with the experimental yield of neutrons to the A^{37} ground state, integrated over 170 keV energy intervals.

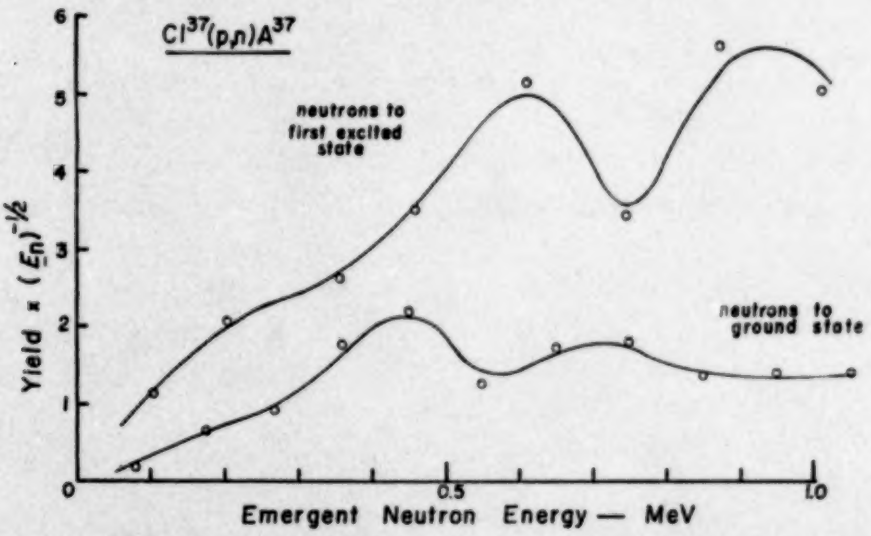

Fig. 4. The quantity $N(E_n)^{-\frac{1}{2}}$ plotted against E_n for both neutron groups. The gross behaviour is seen to be rather similar for the two groups.

made, using optical-model potentials instead of a simple square well. However, such calculations also give smooth curves.

For s-wave neutrons with energy E_n the penetrability is proportional to $(E_n)^{\frac{1}{2}}$. The quantity $N/(E_n)^{\frac{1}{2}}$ is then related to the averaged neutron strength function. This quantity is plotted against E_n for both neutron groups in fig. 4.

It is assumed that s-wave neutrons are involved. There are similarities in the behaviour of the yield of the two neutron groups, in the energy range up to 1 MeV above threshold; both yields show a double broad maximum. This behaviour has been noted before [4]) for the ground state group, and some discussion has been given in terms of the "giant resonance" mechanism of Lane, Thomas and Wigner [5]).

If this is the correct interpretation, the statistical assumption underlying the Hauser-Feshbach calculations is invalid. This is also indicated by the large number of degrees of freedom obtained for the distribution of the reduced widths of the A^{38} levels. A statistical assumption leads to the Porter-Thomas distribution with two degrees of freedom.

The gross structure in the yield curves is in qualitative agreement with other data. With thermal neutrons, the "giant resonance" corresponding to the 3s neutron independent-particle state is observed at $A \approx 50$. There are indications that for targets of lower A it would occur at higher incident neutron energies [6]). The present data on the yield of neutrons to the A^{37} ground state indicate that for an A^{37} target it would occur at a neutron energy of a few hundred keV. The yield of neutrons to the first excited state is qualitatively explained in a similar way; the giant resonance for neutrons incident on an A^{37*} target would occur at neutron energies of a few hundred keV. Slight differences in the optical-model potentials for A^{37} and A^{37*} would account for the shift between the centre of the anomalous broad maxima in the two cases (fig. 4).

The width of the broad maxima observed in this experiment is considerably less than that usually associated with giant resonances. The suggestion [7]) that the imaginary part of the optical potential is anomalously small near closed shells may be relevant here.

The authors thank Dr. T. W. Bonner, Dr. G. C. Phillips, Dr. G. E. Brown, Dr. J. P. Schiffer, Dr. L. C. Biedenharn and Dr. T. A. Tombrello for valuable discussions.

References

1) R. L. Bramblett, R. I. Ewing and T. W. Bonner, Nuclear Instr. and Methods **9** (1960) 673
2) W. Hauser and H. Feshbach, Phys. Rev. **87** (1951) 366
3) A. T. G. Ferguson and E. B. Paul, Nuclear Physics **12** (1959) 426
4) G. S. Mani, A. C. L. Barnard, T. A. Tombrello and D. A.A.S.N. Rao, Nuclear Physics **28** (1961) 456
5) A. M. Lane, R. G. Thomas and E. P. Wigner, Phys. Rev. **98** (1955) 693
6) J. P. Schiffer, Proc. Int. Conf. Nuclear Structure, Kingston, Canada (North-Holland Publishing Co., Amsterdam, 1960) p. 676
7) A. M. Lane, J. E. Lynn, E. Melkonian and E. R. Rae, Phys. Rev. Lett. **2** (1959) 424

3.B *Nuclear Physics* **28** (1961) 471—477; © *North-Holland Publishing Co., Amsterdam*
Not to be reproduced by photoprint or microfilm without written permission from the publisher

MEASUREMENTS OF INTERNAL CONVERSION COEFFICIENTS

SÖLVE HULTBERG †, DANIEL J. HOREN AND JACK M. HOLLANDER
Lawrence Radiation Laboratory, University of California, Berkeley, California

Received 13 July 1961

Abstract: Internal conversion coefficients of M1, M4 and E2 transitions from the Y^{97}, Cs^{137}, Au^{198} and Ir^{193} decays have been studied by using the internal-external conversion (IEC) method. For unhindered transitions of the $2+ \rightarrow 0+$ type we have found $(\alpha_2)_{317} = 0.054 \pm 0.003$ for the 317 keV transition from Ir^{193} and $(\alpha_2)_{412} = 0.028 \pm 0.0015$ for the 412 keV transition from Au^{198}, the theoretical values being 0.054 and 0.030, respectively.

1. Introduction

Recently a considerable effort has been devoted to the experimental study of internal conversion coefficients of E2 transitions, particularly those proceeding from $2+$ to $0+$ states in even-even nuclei. Because these transitions are pure it is possible to make a detailed comparison of the experimental results with the calculations of Rose and of Sliv [1]). The theoretical calculations take into account the influence of finite nuclear size by the application of certain corrections which are much smaller for E2 than for M1 conversion coefficients [1]). However, some evidence has been found for significant deviations between theoretical and experimental E2 conversion coefficients, deviations amounting to some 10 % or more [2]). Most of the experimental values have been obtained by the peak-to-beta-spectrum (or PBS) method or by the internal-external conversion (or IEC) technique. However, the experimental situation is not satisfactory because in some cases the measured values spread fairly much. This is particularly evident in the well-known case of the 412 keV E2 transition which follows the decay of Au^{198}. Here the experimental results range from agreement with theory to figures that are about 20 % low [2, 6]).

It is important to clarify the situation in general and in the 412 keV (Au^{198}) case in particular. Therefore we have re-measured the $(\alpha_2)_{412}$ and other conversion coefficients, using the IEC method.

2. Experimental Technique

The technique for measuring internal conversion coefficients absolutely with the IEC method has been described elsewhere [3, 4]) and need not be repeated here.

† On leave from the Nobel Institute of Physics, Stockholm, Sweden

The instrument used is a flat, double-focussing beta-ray spectrometer of 25 cm mean radius which employs as a detector a flow-type methane proportional counter. To accommodate the activity and the photoelectric converter a

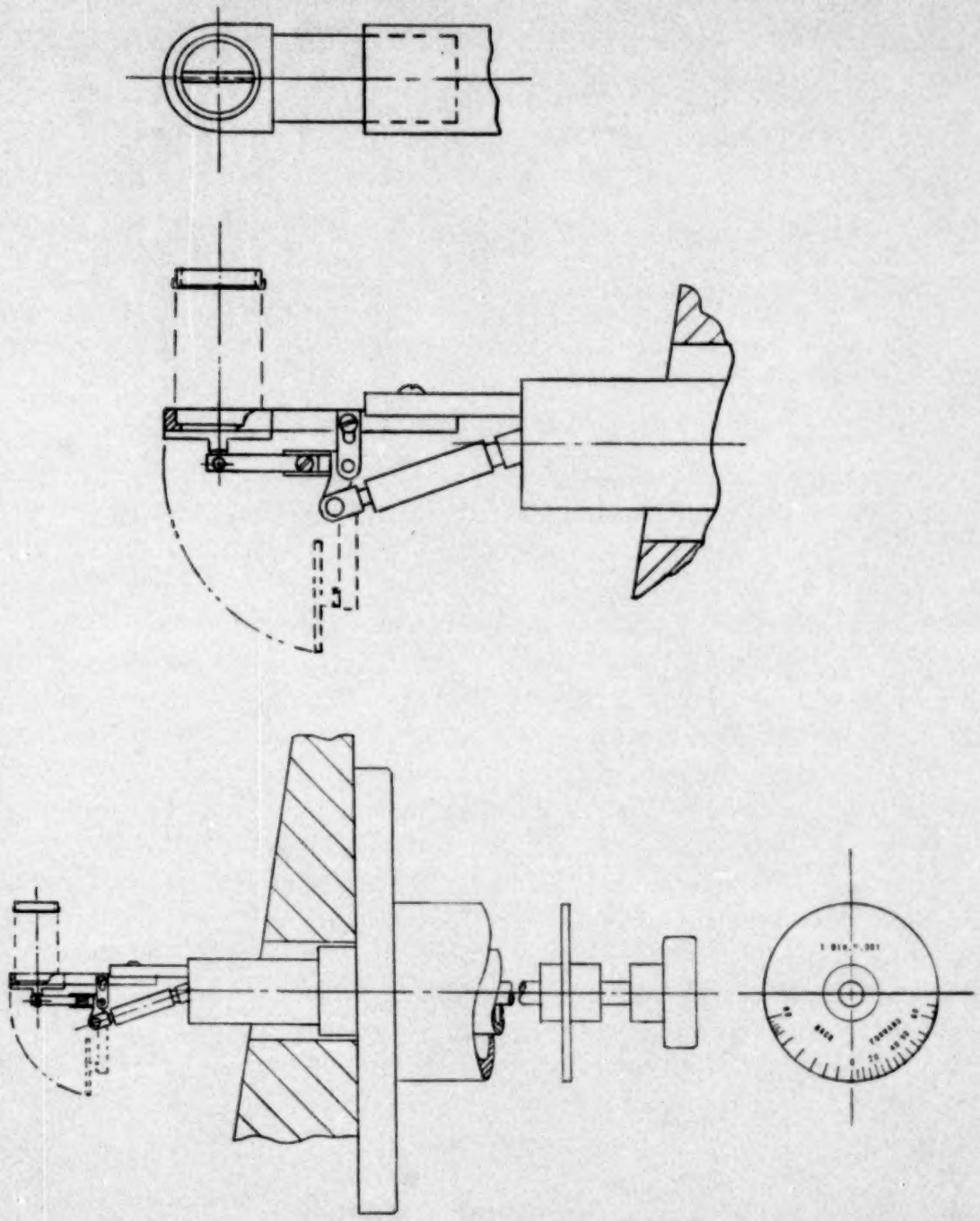

Fig. 1. Source-holder-converter assembly.

special holder has been constructed which permits the location of the converter to be shifted from outside the spectrometer. Thus, by operating a shaft the converter could be placed either in front of the source or in a position where

it did not obstruct the beam of internal conversion electrons emitted from the source. The arrangement is shown in fig. 1.

We used two rectangular uranium converters of dimensions 5.0×9.8 mm² (both) and of surface thicknesses 2.19 ± 0.02 and 0.75 ± 0.02 mg/cm². The following activities were studied:

$$Y^{87}(388, 483);\ Cs^{137}(662);\ Au^{198}(412);\ Ir^{192}(296, 308, 317).$$

Figures inside parentheses give energies in keV of the gamma rays investigated. The yttrium source was liquid deposited, the cesium was vaporized and the gold source was chemically plated. The iridium was painted as inactive material onto an aluminium backing and a rectangular 3×8 mm² piece, was then cut out and sent for activation. This method has the advantage of very easy handling after activation and it worked satisfactorily for the iridium experiments.

3. Results

The results obtained for the measured K internal conversion coefficients ε_K are summarized in table 1.

TABLE 1

Experimental results

Isotope	Energy of transition (keV)	Source size (mm²)	Multi-polarity	Experimental ε_K	Theoretical ε_K
$_{38}Sr^{87}$	388	4×10	M4	$0.18\ \pm0.015$	0.17
	483	4×10	M1	0.0026 ± 0.0002	0.0026
$_{56}Ba^{137}$	662	1×9	M4	$0.095\ \pm0.004$ [a])	0.093
$_{80}Hg^{198}$	412	2×4	E2 [b])	$0.028\ \pm0.0015$ [c])	0.030
$_{78}Pt^{192}$	296	3×8	E2	$0.063\ \pm0.009$	0.062
	308	3×8	E2	$0.058\ \pm0.005$	0.057
	317	3×8	E2 [b])	$0.054\ \pm0.003$	0.054

[a]) Using the BESK value $\tau_K = 20.2$ b per atom
[b]) $2+\rightarrow 0+$ transition
[c]) Using the BESK value $\tau_K = 59.5$ b per atom

The experimental results given in table 1 represent in each case an average over four to five measurements. In the external conversion measurements on the 483 keV transition in Sr^{87} the 483 K line was not resolved from the 388(L+M+N+ . . .) peaks. However, by using measured values for photoelectric absorption ratios of the uranium K-, L- and M+N+ . . .-shells [4]) together with appropriate *f* factors the contributions from the 388 (L+M+N + . . .) lines to the total external conversion peak could be subtracted off.

For the calculation of the internal conversion coefficients we used the expression [3, 4])

$$\varepsilon_K = \frac{A_\beta}{A_\gamma} \tau_K f_K dkb, \tag{1}$$

where A_β and A_γ are the intensities per unit momentum interval of the internal and external conversion lines, respectively, τ_K is the absolute photoelectric cross-section (in b per atom) for the K-shell of the converter and f is a correction factor which depends upon the photoelectric angular distribution and the particular values of the parameters which describe the sizes of the source and the converter and their relative distance. The appropriate f values were obtained by use of the BESK service. The factor k is the ratio of intensities of sources used to measure the external and internal conversion lines. In these experiments we have $k = 1$ because the same source was employed for both measurements. Finally, the factor b is a dimension factor which is a constant for a given converter material.

In the case of a rectangular converter and a radioactive source of no extension (point source) the factor f is given by

$$f = \frac{\frac{2}{\pi}\int_0^{\vartheta_2} J(\vartheta+\Delta)\operatorname{tg}\vartheta[\arcsin(\operatorname{tg}\vartheta_0/\operatorname{tg}\vartheta) - \arccos(\operatorname{tg}\vartheta_1/\operatorname{tg}\vartheta)]e^{-\mu g/\cos\vartheta}\,d\vartheta}{\int_0^{\pi} J(\theta)\sin\theta\,d\theta} \tag{2}$$

where $J(\theta)$ denotes the photoelectric angular function for unpolarized incident photons. Definition of the various symbols is given in ref. [4]). The attenuation of the gamma rays in the absorbing material between source and converter is taken into account by the exponential factor $\exp(-\mu g/\cos\vartheta)$, where μ is the absorption coefficient in cm^{-1} and g is the absorber thickness in cm. Self-absorption in the source material can also be taken into account by putting in appropriate values for μ and g.

According to a method given in ref. [4]) the source dimensions can be taken into account in the calculation of the f factor. The source and converter are assumed to have rectangular shape. Such an assumption simplifies the analysis and introduces no practical limitation since for flat spectrometers the rectangular shape is nearly always desired. Moreover, the source and converter are assumed to be symmetrically positioned with respect to each other (cf. fig. 12, ref. [4]). The source is "decomposed" into a number of parts, each of which is small compared with the converter, so that eq. (2) can be applied to every such part. The resulting f value will then simply be the arithmetic average of all f values computed. This method has been tested experimentally [4]) and is used in the BESK calculations.

4. Discussion

As a check on the experimental set-up we measured the internal conversion coefficient of the 662 keV M4 transition following the decay of Cs^{137} and the result was found to be in good agreement with theory and earlier measurements of both the PBS and IEC type [2d, 3, 5]). It should be observed that in calculating the result we have used the theoretical BESK value $\tau_K = 20.2$ b per atom while in refs. [2d, 3]) a somewhat lower experimental value has been used.

The main reason for re-measuring the 412 keV E2 internal conversion coefficient, in the following denoted $(\alpha_2)_{412}$, was the peculiar disagreement from various experimental methods on the true value of the $(\alpha_2)_{412}$ (cf. sect. 1). Although the IEC method had already been used twice [2d, 2e]) with consistent results it was thought that an additional effort might possibly be of some value since the experimental conditions could still be somewhat modified and it must be satisfactorily proved that such conditions do not influence the result. Thus it may be observed that the IEC results for the $(\alpha_2)_{412}$ have been obtained by using

1) a GM counter and two different sources for internal and external conversion, the latter process taking place in gold (ref. [2d]),

2) a GM counter with one source, taking advantage of the short half-life of Au^{198} (a uranium converter was used, ref. [2e])),

3) a proportional counter with one source, performing all measurements in rapid succession and using a uranium converter (present paper).

These efforts prove for the $(\alpha_2)_{412}$ that the IEC method is independent of changes in the experimental conditions to within estimates errors, as expected. How then do we explain the difference between our present result and the low values of refs. [2d, 2e])?

Let us turn our attention to eq. (1). The quantities A_β, A_γ, d and k require no particular comment as their evaluation is quite straightforward; we shall only observe here that the d values were determined by two independent methods of analysis, the results agreeing to within 1-3 %, and that any error in the k factor may be avoided by using the same source for both internal and external conversion, as was done in the measurements reported here.

It remains to consider the factors τ and f, the determination of which is more complicated. The "integrated" or "total" photoelectric cross-section τ (for a particular shell) forms the basis for the determination of ε from eq. (1). Most often τ_K (K denoting the K-shell) is used and can conveniently be derived from the τ_a values (a denoting the whole atom) of the NBS Circular No. 583. Because of the importance of τ_K for determining ε it is necessary to know τ_K accurately. However, it is not possible to estimate the error in τ_K from the NBS tables since the underlying theoretical and experimental information is scanty and very approximate, except for the six numerical values of Hulme *et al.* Only

very recently has it been possible, through calculations by Hultberg, Nagel and Olsson [8]) on the electronic computer BESK, to compare the NBS values for τ_K with accurate theoretical computations. The numerical work is based on the formalism of Nagel [7]) whose formulae are, theoretically, valid at all energies. In practice, however, the calculations cannot at present be carried much above 800-1000 keV for $Z = 92$ because of limitations in computer capacity and speed. For $Z = 92$ the results from the BESK calculations so far show that, below 500 keV, the NBS tables give τ_K values that are generally good to within 1-3 %. For computing the $(\alpha_2)_{412}$ of table 1 we used the BESK value $\tau_K = 59.5$ b per atom which agrees to within 1 % with the NBS table.

For $Z = 92$, BESK has also computed differential photoelectric cross-sections at $h\nu = 412$ and 662 keV and also at some other energies. These numerical results are correct to any order in αZ and should thus be directly compared with the experimental angular functions $J(\theta)$ of refs. [4]) and [10]). Such a comparison shows that theory and experiment agree much more satisfactorily at 279 and 662 keV than at 412 keV. This is not surprising since in the first two cases careful "extrapolation" experiments were carried out [4, 10]). However, at 412 keV no such extrapolation experiments were done and the "true" shape of the angular function was obtained only approximately by using observable trends at the two higher energies 662 and 1332 keV. Thus theory and experiment can be expected to compare less favourably at 412 than at 279 and 662 keV. At 412 keV significant differences occur at large angles (larger than 40 to 50°) and are such that the experimental angular function is higher.

Though mathematically involved the process of photoelectric conversion of photons is a straightforward physical problem where effects from nuclear finite size and radiative corrections are expected to be unimportant. Moreover, for the K-shell screening effects should be small so that the BESK calculations should be accurate and one should not expect experiment to show deviations of any significance. The differences that are observed between the tabulated 412 keV angular function of ref. [4]) and the BESK calculations are possibly connected with scattering phenomena and have the consequence of correcting the f_{412} factor so that the latter will become larger than before. By introducing such a correction we have arrived at a value for $(\alpha_2)_{412}$ that agrees with theory much better than before (cf. table 1). The IEC results reported in refs. [2d–2f]) should then be subjected to corresponding adjustments of τ_K and f_K, the combined effect of which may be of the order of 5–10 % and will thus be brought into agreement with the results from other investigations. Moreover, it has been suggested [2d]) that the PBS value of De Vries should be adjusted upwards on account of certain scattering effects, bringing his PBS value into better agreement with the results from other PBS investigation. Two very recent PBS measurements [9]) give values in the range 0.027-0.029 and thus there now seems to be little doubt that the

$(\alpha_2)_{412}$ agrees with theory to within some 10 %. Whether the rather persistent tendency (except for ref. [6])) towards values that are somewhat lower than theory is a significant effect remains, however, to be seen.

Correction of the f_{412} factor also leads to agreement of $(\alpha_2)_{317}$ with theory (cf. table 1). This is important since the 317 keV transition in Pt^{192} is of pure E2 character. To within the experimental accuracy it must therefore be concluded for mass numbers around 200 that our experiments do not give clear evidence for a deviation from theory of α_2 for unhindered E2 transitions.

One of us (S. H.) would like to express his sincere gratitude to Professor I. Perlman for the opportunity of spending the summer (1960) with the Chemistry Division of the Radiation Laboratory. We wish also to thank Mr. A. D. Carneiro for his careful design of the source-holder and converter assembly

References

1) L. A. Sliv and I. Band, Tables of internal conversion coefficients (The Academy of Sciences of the USSR, Moscow-Leningrad, 1956);
M. E. Rose, Internal conversion coefficients (North-Holland Publ. Co., Amsterdam, 1958);
L. S. Kisslinger, Phys. Rev. **114** (1959) 292
2) a) A. H. Wapstra, G. Nijgh, N. Salomons-Grobben and L. Ornstein, Nuclear Physics **9** (1958) 538
b) G. Nijgh and A. H. Wapstra, Nuclear Physics **9** (1958) 545
c) F. K. McGowan and P. H. Stelson, Phys. Rev. **107** (1957) 1674
d) C. de Vries, E. J. Bleeker and Mrs. N. Salomons-Grobben, Nuclear Physics **18** (1960) 454
e) J. H. Hamilton, W. F. Frey and S. Hultberg, Bull. Am. Phys. Soc. **5** (1960) 449
f) J. H. Hamilton, W. F. Frey, S. Hultberg and T. Duncan, Bull. Am. Phys. Soc. **6** (1961) 50
3) S. Hultberg and R. Stockendal, Ark. fys. **14** (1959) 565
4) S. Hultberg, Ark. fys. **15** (1959) 307
5) A. H. Wapstra, Ark. fys. **7** (1954) 275
6) B. G. Pettersson, J. Thun and T. R. Gerholm, Nuclear Physics **24** (1961) 243
7) B. Nagel, Ark. fys. **18** (1960) 1;
B. Nagel and P. O. Olsson, Ark. fys. **18** (1960) 29
8) S. Hultberg, B. Nagel and P. O. Olsson, Ark. Fys., in print
9) R. Stockendal and J. H. Hamilton, private communication;
J. H. Hamilton, private communication
10) Z. Sujkowski, Arkiv för fysik **20** (1961) 269

1.E.1:
2.C

Nuclear Physics **28** (1961) 478—493; © *North-Holland Publishing Co., Amsterdam*
Not to be reproduced by photoprint or microfilm without written permission from the publisher

DISINTEGRATION OF K^{39} BY FAST NEUTRONS

R. BASS †, H. P. HÄENNI, T. W. BONNER and F. GABBARD ††
Rice University, Houston, Texas †††

Received 6 June 1961

Abstract: The nuclear reactions $K^{39}(n, p)A^{39}$ and $K^{39}(n, \alpha)Cl^{36}$ have been studied by bombarding a KI(Tl) crystal with mono-energetic fast neutrons and observing scintillations due to emitted protons and α particles. Using good energy resolution (less than 10 keV) a yield curve has been obtained for the p_0-group for neutron energies from 1.46 to 3.05 MeV, which exhibits 60 narrow resonances. Measurements with poorer energy resolution, varying between 70 and 150 keV, have been made in the neutron energy region from 2.3 to 8.7 MeV. From these absolute values of the reaction cross sections for the p_0-group (E_n = 2.3 to 8.7 MeV), the α_0-group (E_n = 2.3 to 3.8 MeV) and the p_1-group (E_n = 2.5 to 3.5 MeV) have been extracted. Fourteen proton groups are seen in the pulse-height spectra, and from an analysis of the associated pulse-heights as a function of neutron energy, ten new excited states of A^{39} have been derived. The measured cross sections are compared with values obtained by other groups and with theoretical predictions.

1. Introduction

The nuclear reactions $K^{39}(n, p)A^{39}$ and $K^{39}(n, \alpha)Cl^{36}$ can be conveniently studied by bombarding a KI(Tl) scintillation crystal with monoenergetic fast neutrons and observing scintillations due to the charged particles produced in these reactions. The Q-value of the (n, p)-reaction is +0.22 MeV, and that of the (n, α)-reaction +1.35 MeV, for reactions going to the ground states of the respective final nuclei. Consequently one would expect appreciable yields from both reactions at neutron energies above about 2 MeV. Fast neutron induced reactions in I^{127}, the other major constituent of the KI(Tl) crystal, should not become noticeable at neutron energies below about 8 MeV because of the higher Coulomb barrier for the outgoing charged particles. Similarly, reactions in K^{41} would be expected to be unimportant because of its comparatively low isobaric abundance (6.8 %) and less favourable Q-values.

Practical interest in the cross sections of the K^{39} reactions and their variation with neutron energy arises in connection with the possible use of KI(Tl) crystals for neutron flux measurements. In other applications neutron induced reactions may produce undesirable background, and again some knowledge of the cross sections involved may be required. From a more fundamental

† On leave from Institut für Kernphysik der Universität Frankfurt, Frankfurt am Main, Germany.
†† Present address: University of Kentucky, Lexington, Kentucky.
††† Work supported in part by the U.S. Atomic Energy Commission.

point of view, information on the cross sections and their variation over wide regions of neutron energy can be used to test the assumptions and predictions of nuclear reaction theories. Finally from the energies of the proton groups emitted in the reaction $K^{39}(n, p)A^{39}$, energy levels in A^{39} can be obtained, which are not easily accessible by other reactions.

Previous studies of the reactions $K^{39}(n, p)A^{39}$ and $K^{39}(n, \alpha)Cl^{36}$ have been made at a few, isolated neutron energies and with comparatively poor neutron energy resolution [1–4]). It was therefore thought worthwhile to investigate these reactions systematically over the neutron energy range from 1.5 to 8.7 MeV and, in particular, to cover part of this range with good energy resolution (< 10 keV) in order to resolve a possible fine structure of the (n, p_0)-excitation curve.

2. Measurements with Neutrons from the Reaction $Li^7(p, n)\ Be^7$

Thin lithium metal targets were prepared by evaporating lithium onto clean 0.05 cm thick tantalum blanks and were bombarded with protons from the Rice University 5.5 MeV electrostatic accelerator, in order to produce neutrons from the reaction $Li^7(p, n)Be^7$. The proton beam was magnetically analyzed; the magnetic field was measured with a NMR magnetometer and calibrated in terms of proton energy at the $Li^7(p, n)$ threshold. The spread in neutron energy due to the finite thickness of the lithium metal targets was obtained from the shape of the neutron yield curve just above threshold and was found to be 5 keV and 9 keV, respectively, for the two targets used in the measurements. Absolute values of the average neutron energy are believed to be known to better than ± 10 keV in the region from 1.46 to 3.05 MeV. Neutrons emerging at 0° with respect to the proton beam were incident on a KI(Tl) crystal of 6 mm thickness and 6 mm diameter, which was placed at a distance of approximately 2 cm from the lithium target. The crystal was mounted on a Dumont 6292 photomultiplier tube, the output pulses of which were fed, after amplification, to a 256-channel pulse-height analyzer. The neutron flux was monitored with a long counter, which was positioned at a distance of 1 m and an angle of 0° with respect to the lithium target and incident proton beam.

Observations using the $Li^7(p, n)$ neutron source were restricted to the ground state proton group (p_0) from the reaction $K^{39}(n, p)A^{39}$; other charged particle groups are comparatively weak in the energy region accessible with this source and were obscured by reactions due to the second group of neutrons from the $Li^7(p, n)$ reaction. In spite of the higher Q-value of the (n, α_0) reaction, the (n, p_0) reaction produces larger pulses in the KI(Tl) crystal at neutron energies above 1 MeV; this is a consequence of the smaller scintillation efficiency of the crystal for α particles compared to that for

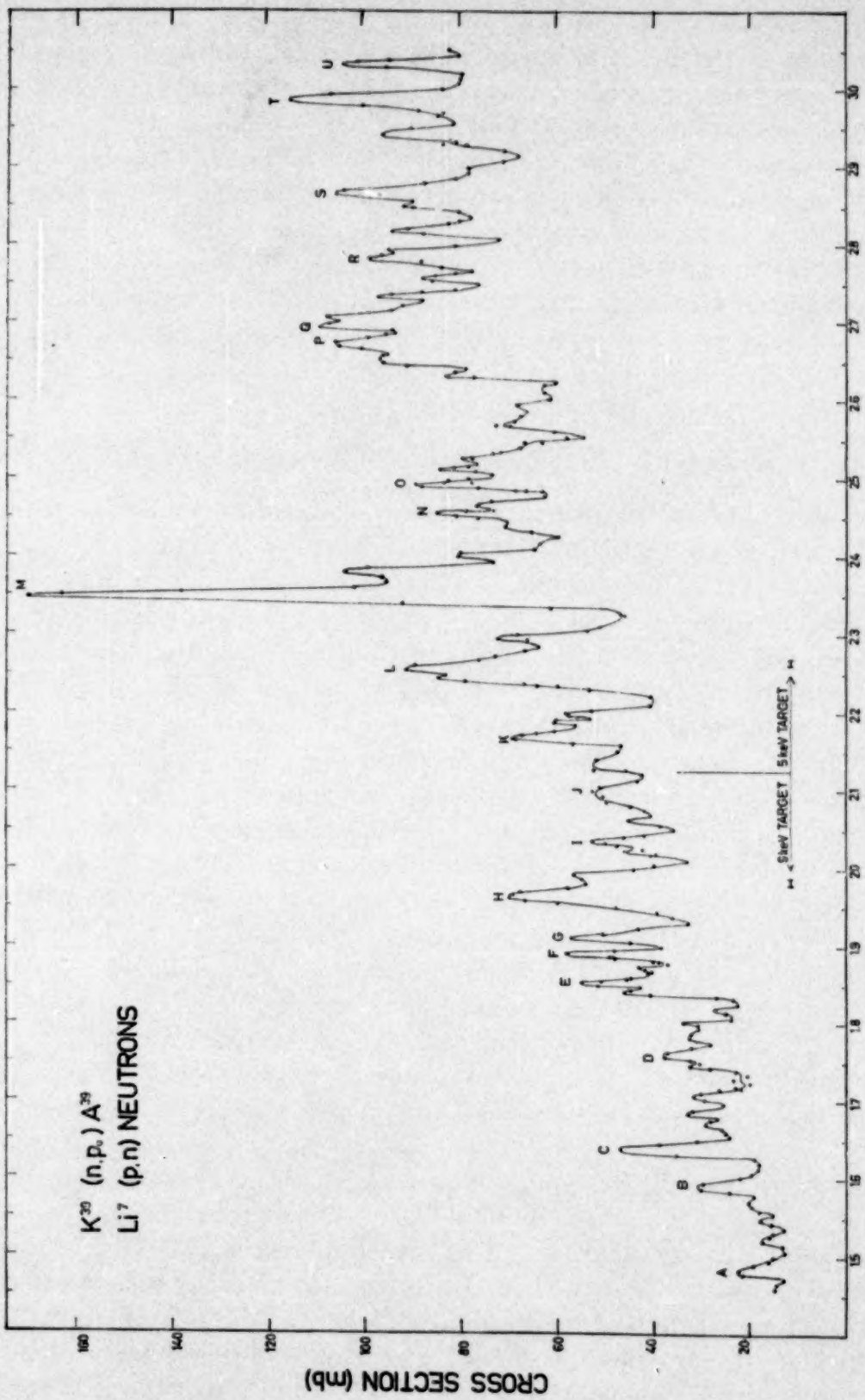

Fig. 1. Excitation curve for the reaction $K^{39}(n, p_0)A^{39}$ obtained with neutrons from the reaction $Li^7(p, n)Be^7$ for neutron energies from 1.46 to 3.05 MeV. The lithium metal targets had thicknesses at threshold of 9 keV and 5 keV, respectively. The observed resonances are listed in table 1.

protons [1,2]). Scattering of neutrons in the crystal, photomultiplier and pre-amplifier assembly, which was located between the lithium target and the long counter, reduced the neutron flux at the long counter by about 40 %. However, no absolute measurement of the neutron flux or reaction cross section was attempted at this stage, and therefore no correction was applied to the long counter readings for neutrons scattering in the equipment, for variation of long counter efficiency with neutron energy or for the contribution of the second neutron group from the Li^7(p, n) reaction. An approximate relative measure of the (n, p_0) cross section was obtained by taking the ratio of the number of counts in the clearly resolved p_0-peak of the pulse-height spectra to the uncorrected long counter readings. The long counter data did not follow the rapid and pronounced fluctuations of the p_0-yield as a function of neutron energy, but behaved smoothly in approximate accordance with the expected neutron yield from the Li^7(p, n) reaction.

The results are shown in fig. 1, where the ratio of the p_0-yield to the uncorrected long counter readings is plotted as a function of neutron energy. The cross section scale, which is shown on the ordinate, has been deduced from a different set of data obtained with neutrons from the reaction T(p, n) He^3. In the latter experiment the neutron energy region from 2.30 to 4.55 MeV was covered with a neutron energy spread of approximately 70 keV. The neutron flux was again measured with the long counter, but the geometry was more favourable for a measurement of the absolute flux, and scattering and background were corrected for as discussed in sect. 3. In order to establish the cross section scale for the p_0-excitation curve obtained with the Li^7(p, n) neutron source (fig. 1), the data were averaged over neutron energy intervals of 70 keV in the region from 2.3 to 3.1 MeV. The resulting excitation curve agreed well in shape with the excitation curve obtained with the T(p, n) neutron source (fig. 4) and could easily be normalized to the latter. The accuracy of the cross section values given in fig. 1 is therefore comparable to that obtained with the T(p, n) neutron source ($\pm$20 %) at neutron energies above 2 MeV. At lower energies the cross section scale of fig. 1 is less reliable and should be accurate to about $\pm$50 % in the neighbourhood of 1.5 MeV.

Fig. 1 combines the results from two runs, covering neutron energy regions of 1.4 to 2.1 and 2.0 to 3.1 MeV, respectively. The lithium targets used for neutron production had thicknesses, at threshold, of 9 keV for the lower energy run and 5 keV for the higher energy run. The two sets of data were normalized to each other at the comparatively broad peak designated by J in fig. 1. During preliminary runs data points were also taken at a number of isolated neutron energies down to less than 1 MeV. These data indicated that near 1 MeV the reaction K^{39}(n, p)A^{39} still has an appreciable cross section, of the order of 30 to 50 % of the cross section at 1.5 MeV.

Fig. 1. shows a very pronounced resonance structure for the p_0-cross section.

A total of 60 resonances are seen in the energy region covered; most of these are incompletely resolved, and in many cases the apparent width seems to be limited by neutron energy resolution. Table 1 gives a list of neutron bombarding

TABLE 1

List of resonances in the reaction $K^{39}(n, p_0)A^{39}$ (see fig. 1)

Number and letter of identification	Neutron bombarding energy (MeV)	Apparent width (a: < 10 keV, b: 10-20 keV, c: > 20 keV)	Number and letter of identification	Neutron bombarding energy (MeV)	Apparent width (a: < 10 keV, b: 10-20 keV, c: > 20 keV)
1 (A)	1.480	b	31 (L)	2.257	b
2	1.522	b	32	2.297	a
3	1.547	b	33 (M)	2.346	b
4	1.567	b	34	2.380	b
5 (B)	1.590	b	35	2.403	b
6 (C)	1.638	b	36	2.440	b
7	1.672	a	37 (N)	2.455	a
8	1.685	a	38	2.466	b
9	1.708	b	39 (O)	2.492	a
10	1.746	a	40	2.512	a
11 (D)	1.760	b	41	2.525	a
12	1.785	b	42	2.546	a
13	1.802	a	43	2.568	a
14	1.818	a	44	2.595	a
15	1.840	a	45	2.616	b
16 (E)	1.854	a	46	2.630	a
17	1.874	a	47	2.652	b
18 (F)	1.892	a	48 (P)	2.673	b
19 (G)	1.912	a	49 (Q)	2.694	a
20 (H)	1.964	c	50	2.707	a
21	1.993	b	51	2.773	a
22	2.023	a	52	2.757	b
23 (I)	2.035	a	53 (R)	2.781	b
24	2.062	a	54	2.818	b
25 (J)	2.097	c	55	2.850	a
26	2.133	c	56 (S)	2.866	b
27 (K)	2.167	b	57	2.898	b
28	2.188	a	58	2.942	b
29	2.199	a	59 (T)	2.986	b
30	2.245	a	60 (U)	3.032	b

energies for the observed resonances, which are numbered in order of increasing energy. In order to facilitate identification, some of the more pronounced resonances are designated by letters in fig. 1 and in the first column of table 1. In the third column of table 1 the resonances are coarsely classified in three groups according to their apparent width (not corrected for energy resolution): (a) indicates a width of less than 10 keV, (b) a width of between 10 and 20 keV and (c) a width of more than 20 keV. For resonances of group (a) the apparent

width could be essentially due to experimental energy spread. There are roughly equal numbers of resonances in groups (a) and (b), but only very few in group (c). It is evident from a closer inspection of fig. 1, that this classification is necessarily rather inaccurate, and also that there are additional unresolved resonances apart from those listed in table 1.

3. Measurements with Neutrons from the Reaction T(p, n)He^3

Mono-energetic neutrons in the energy region from 2.30 to 4.54 MeV were produced by bombarding a tritium gas target with protons of energies between 3.2 and 5.5 MeV. The gas was contained in a thin-walled steel chamber of 2.7 cm length, which was internally lined with tantalum and separated from the accelerator vacuum system by means of a 0.00025 cm nickel foil. The KI(Tl) crystal was mounted at 0° with respect to the proton beam, with its centre at a distance of 2.9 cm from the tip of the gas target chamber. The neutrons from the T (p, n) reaction incident on the crystal had an energy spread of approximately 70 keV due to the thickness of the gas target and the finite solid angle subtended by the crystal. The symmetry axis of the crystal and photomultiplier was arranged perpendicular to the direction of motion of the incident neutrons in order to minimize interference with the neutron flux measurement. The neutron flux was measured with a long counter, which was placed at 0° and at a distance of 1 m from the gas target.

The absolute efficiency of the long counter was obtained by calibration with a Pu-α-Be neutron source of known strength and the variation of this efficiency with neutron energy was taken into account according to published data [5]). The contribution of background neutrons from sources other than the gas target was measured by running with the gas target chamber evacuated. The resulting correction to the long counter readings varied between 1 % and 8 %, depending on beam energy. A further correction had to be applied for scattering of neutrons out of the long counter by the crystal and photomultiplier tube; this was found to be 8 %, practically independent of neutron energy.

Neutron scattering in the KI crystal also modifies the neutron flux inside the crystal itself. The magnitude of this effect has been estimated on the basis of the following argument: Elastic scattering by an approximately spherical assembly of heavy nuclei will, to a first, crude approximation, not alter the internal flux of neutrons having the full source energy. In other words, the distance travelled by a neutron inside the crystal is, on the average, not altered appreciably by an elastic collision; since the energy change is also very small, the probability that the neutron will produce a nuclear reaction is essentially unaffected by the elastic collision. However, near the boundaries of the crystal outscattering may outweigh inscattering and the neutron flux may be somewhat reduced. Further inelastic processes will reduce the flux

of primary neutrons inside the crystal. Making rough estimates of the cross sections involved, a neutron flux reduction of approximately 2% was obtained for the 6 mm KI cylinder. Therefore, a scattering correction of +6 % rather than the +8 % mentioned above, was applied to the long counter readings for calculations of the reaction cross sections. The corrected absolute values for the neutron flux inside the crystal are believed to be accurate within ±15 %.

The pulse-height spectra from the KI(Tl) crystal were analyzed with a 256 channel pulse-height analyzer and a number of peaks due to protons and

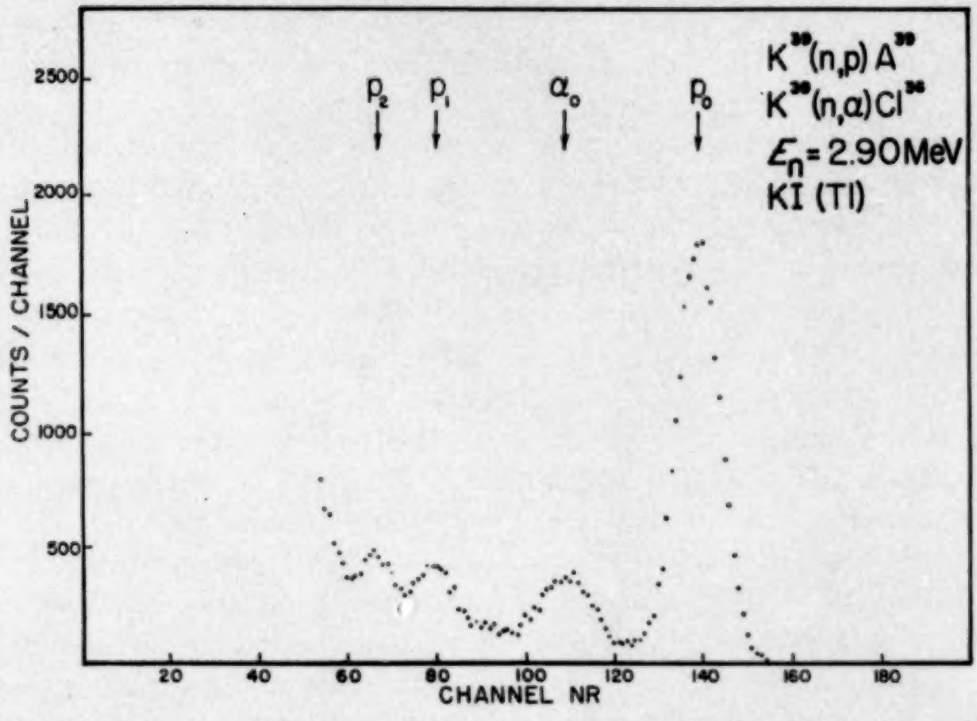

Fig. 2. Pulse-height spectrum of the KI(Tl) crystal at a neutron bombarding energy of 2.90 MeV.

α particles emitted in the reactions $K^{39}(n, p)A^{39}$ and $K^{39}(n, \alpha)Cl^{36}$ were observed. A typical pulse-height spectrum, obtained at an incident neutron energy of 2.90 MeV, is shown in fig. 2. The prominent peak in channel 139 represents the proton group of highest energy, p_0. Other resolved peaks belong to the α particle group α_0 (channel 109) and the proton groups p_1 (channel 80) and p_2 (channel 67). The latter two proton groups leave the A^{39} nucleus in excited states at 1.27 and 1.52 MeV, respectively [6]). The sharp rise of the spectrum with decreasing channel number below channel 60 is largely due to γ radiation.

The identification of the peaks observed in any one spectrum would be possible in principle, provided the relative response of the KI(Tl) crystal to protons and α particles and the level schemes of the final nuclei A^{39} and Cl^{36} were known from independent measurements. While complete information on the level scheme of Cl^{36} is available, only three excited states of A^{39} at 1.27,

1.52 and 2.5 MeV, respectively, have been previously observed [6]). The scintillation response of KI(Tl) for protons and α particles has been studied by various groups [1, 2, 4]); the results agree qualitatively, but slight discrepancies remain which may in part be due to true variations from crystal to crystal. In order to identify the particle groups unambiguously in the present experiment, use was made of the fact that a large number of spectra was obtained, covering continuously the energy region from 1.5 to 8.5 MeV. A plot was made of peak pulse-heights, in relative units *versus* neutron energy (fig. 3). Each point

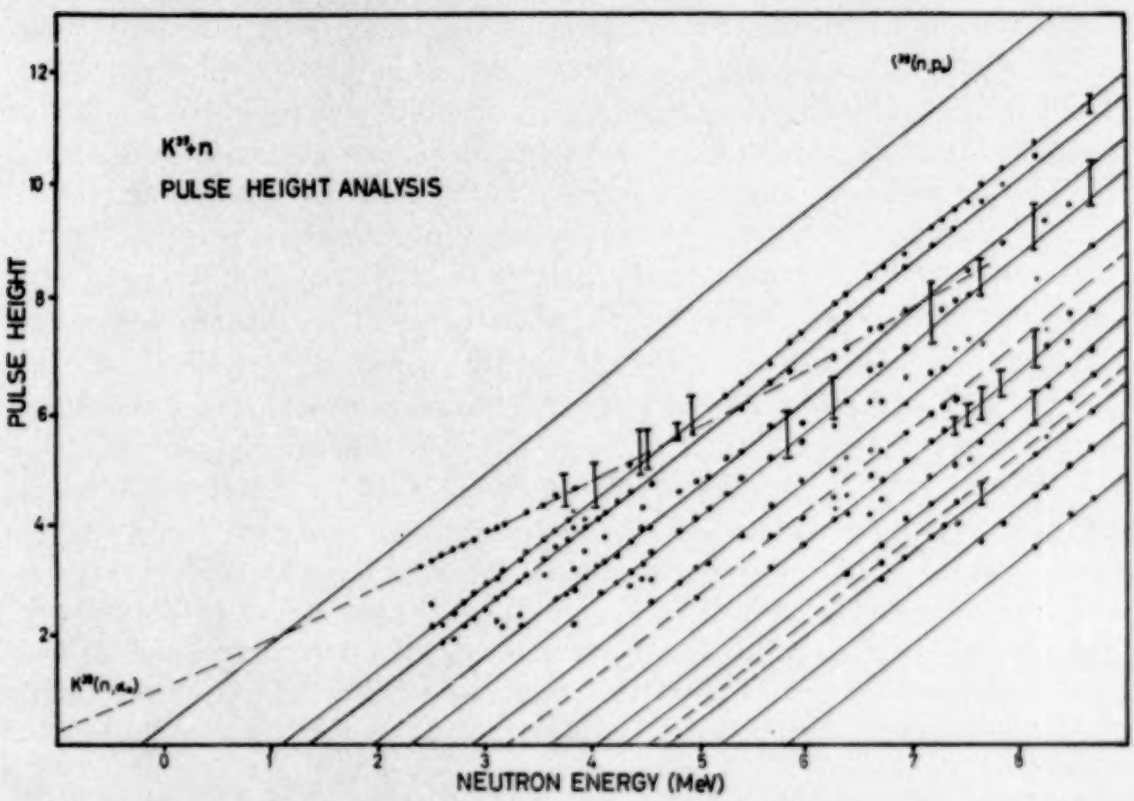

Fig. 3. Pulse-height analysis of charged particle groups produced in the fast neutron bombardment of KI(Tl) crystal. The points mark single peaks and the vertical bars unresolved double or triple peaks observed in the pulse-height spectra at the corresponding neutron energies.

in the diagram shown in fig. 3 represents a peak which was observed at the corresponding neutron energy; approximately straight lines result as loci for all points belonging to the same group of particles. Since protons produce larger pulses than α particles of the same energy, the lines belonging to proton groups have a steeper slope than those belonging to α particles; consequently the nature of each group can be found from the slope of the corresponding line, and its associated Q-value from the intersection of this line with the neutron energy axis. In order to correct for changes in time of the over-all electronic gain, in drawing fig. 3 it was assumed that all points for the p_0-group fall on a straight line with the proper intersection. At each neutron energy the pulse-heights of

all other observed peaks were normalized to the p_0 pulse-height as given by this straight line. The linear dependence of the p_0 pulse-height on neutron energy was checked independently over a large energy region by comparison with γ ray spectra and found to hold within experimental accuracy. The response of the KI(Tl) crystal to α particles, however, deviates somewhat from linearity (fig. 3)

In the spectrum of fig. 2 it is interesting to note the difference in width between the peaks. The full width at half maximum is 8.3 % for the p_0-peak 13.8 % for the α_0-peak and about 11 % for the p_1- and p_2-peaks. Obviously a width of about 9-10 % would have been expected for a proton peak of the same pulse-height as the α_0-peak. The abnormally large width of the α_0-peak is clearly exhibited by all pulse-height spectra in which this peak is resolved. The possibility that the α_0-peak might in fact be an unresolved doublet seems to be ruled out by evidence from other reactions leading to Cl^{36} as the final nucleus[5, 7]). A more likely explanation is the following: if one assumes, that the scintillation efficiency is strongly reduced for the heavy recoiling nuclei A^{39} and Cl^{36}, the width of the observed peaks should in part be due to the angular variation of the laboratory energy of the protons and alpha particles. In the case of fig. 2, the protons of the p_0-group emitted at 0° and 180° with respect to the incident neutrons differ in energy by 10 % while the corresponding difference for the α particles of the α_0-group is 17 %. Assuming isotropic emission of protons and α particles in the centre-of-mass system, it can be shown that the laboratory energies of these particles should follow rectangular distributions, e.g. particles of all energies between the upper (0°) and lower (180°) limit should be emitted with equal intensity. Consequently the p_0- and α_0-peaks in fig. 2. should have widths of at least 10 % and 17 %, respectively, if the contributions of the heavy recoils to the pulse-heights were negligible. If, on the other hand, light and heavy particles would produce scintillations with equal efficiency, the pulse-height would not depend on the angle of emission and the widths of the p_0-and α_0-peaks would be entirely due to instrumental resolution and neutron energy spread. It is evident that the actual behaviour of the crystal is intermediate between the two extreme limits indicated above.

By integrating the areas under the p_0-, α_0- and p_1-peaks, cross sections have been extracted from the data for these three groups in appropriate energy regions; the results are shown in fig. 4. Each group has been analyzed over that range of neutron energies where it is clearly resolved; for the p_0-group this is the case at all energies. The cross section for the latter group has been corrected for the loss of pulses due to protons leaving the crystal before expending their full energy. The magnitude of this 'wall-loss' correction varies between 1.1 and 3.4 % over the energy region covered with the T(p, n) neutron source. The absolute values of the cross sections are believed to be

accurate within ± 20 % for the p_0- and α_0-groups and within ± 40 % for the p_1-group. The cross section ratios are known with considerably better accuracy, since a great part of the quoted errors (± 15 %) is due to the neutron flux determination. It may be noted that peaks in the cross sections as functions of neutron energy are still evident (fig. 4), although much of the pronounced resonance structure apparent in the data obtained with the Li^7(p, n) neutron source (fig. 1) has been lost as a result of the poorer energy resolution.

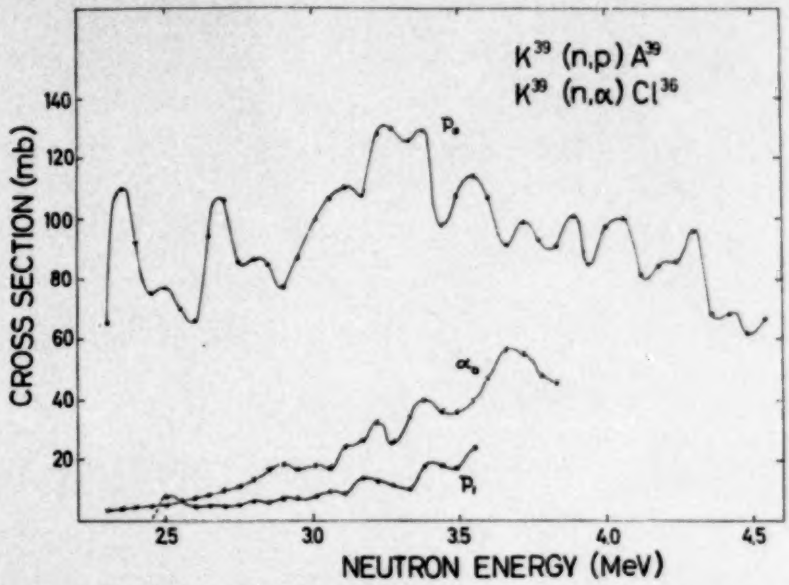

Fig. 4. Cross sections for the reactions K^{39}(n, p_0)A^{39}, K^{39}(n, α_0)Cl^{36} and K^{39}(n, p_1)A^{39} as a function of neutron energy. The neutrons were obtained from the reaction T(p, n)He^3 and had an energy spread of approximately 70 keV.

4. Measurements with Neutrons from the Reaction D(d, n) He^3

A deuterium gas target was bombarded with deuterons in order to produce mono-energetic neutrons in the energy region from 3.8 to 8.7 MeV. The gas was contained in a thin-walled platinum chamber of 4.2 cm length; nickel foils of thicknesses between 0.8 μm and 2.5 μm were used as entrance windows for the deuteron beam. A system of tantalum diaphragms, which were arranged in the beam tube close to the gas target and held at suitable potentials, served to define the beam and to repel secondary electrons; thereby proper measurement of the deuteron beam entering the gas target was insured. The KI(Tl) crystal was placed at a distance of 3 cm from the tip of the gas target chamber and at an angle of 0° with respect to the deuteron beam. The spread in neutron energy at the crystal due to gas target thickness and geometry varied between 100 and 150 keV.

The neutron flux incident on the KI(Tl) crystal was calculated from the integrated beam charge and the amount of deuterium present in the gas target

chamber, using published [8]) values of the cross section for the reaction D(d, n) He^3. This method to determine the neutron flux is estimated to be accurate to ± 10 %. A number of separate tests were made, in which the neutron flux was measured with either a plastic scintillator or a long counter. In all cases the calculated and measured values of the neutron flux agreed within the expected limits of error.

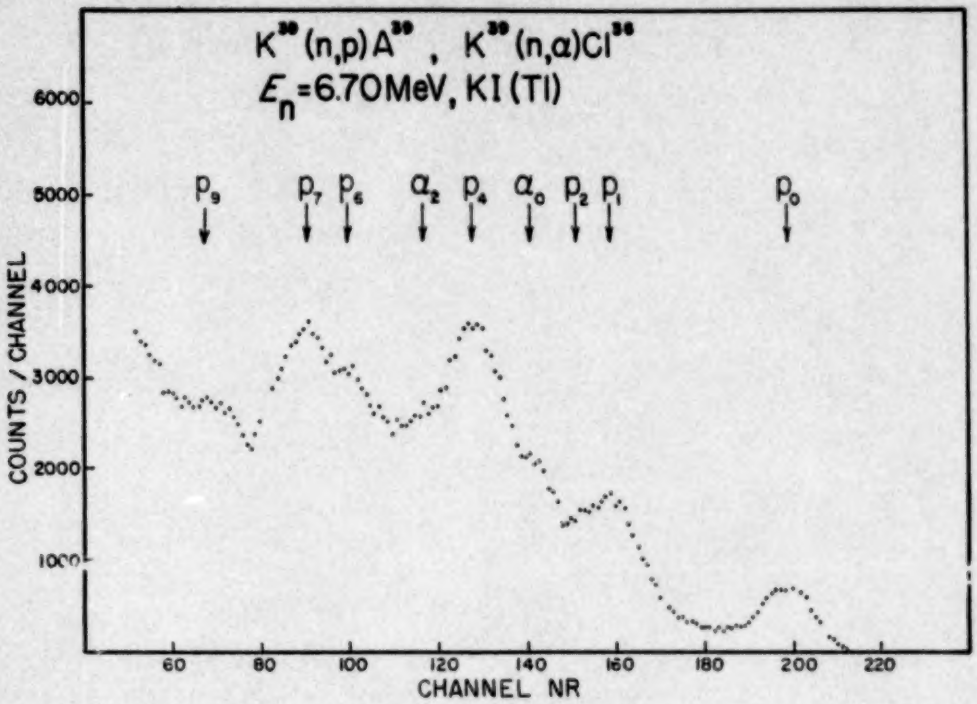

Fig. 5. Pulse-height spectrum of the KI(Tl) crystal at a neutron bombarding energy of 6.70 MeV.

Fig. 5 shows a typical pulse-height spectrum, which was obtained at a neutron energy of 6.70 MeV and again recorded with a 256-channel pulse-height analyzer. The spectrum is evidently quite complex and consists of a considerable number of mostly unresolved peaks. The particle groups corresponding to the various peaks are indicated in fig. 5, as far as they can be assigned on the basis of fig. 3. By combining the pulse-height information obtained at all energies, a total of 14 proton groups can be identified, including the ground state group p_0. All of these give rise to straight lines in fig. 3, which are parallel to the line marked $K^{39}(n, p_0)$; in two cases dotted lines have been drawn to indicate that the evidence seems insufficient to establish the existence of the corresponding proton groups with certainty. The excitation energies in A^{39} associated with the proton groups are listed in table 2; also included are qualitative indications of the relative intensities of the groups and references to earlier observations. Of the thirteen excited states of A^{39} found, only three were known previously [6]).

It is a curious coincidence that practically all but the three proton groups of lowest energy could, on the basis of their Q-values alone, be attributed to the reaction K^{41}(n, p)A^{41}; the measured Q-values agree, within experimental accuracy, with expected Q-values for reactions leaving A^{41} in known excited states [6]). However, any proton group from the reaction K^{41}(n, p)A^{41} would need roughly a fifteen times larger yield, compared to a proton group of similar energy from the reaction K^{39}(n, p)A^{39}, in order to be seen in the present data.

TABLE 2

Energy levels in A^{39} from K^{39}(n, p)A^{39} pulse-height analysis

Excitation energy in A^{39} (MeV) (present results)	Relative intensity of protons group (s: strong w: weak)	Previous observations [6])
0.00	s	Cl^{39} β-decay, K^{39}(n, p)
1.32±0.05	s	Cl^{39} β-decay (1.27 MeV) K^{39}(n, p) (1.24 MeV)
1.57±0.05	w	Cl^{39} β-decay (1.52 MeV)
2.17±0.05	w	none
2.52±0.05	s	K^{39}(n, p) (2.46 MeV)
3.10±0.1	w	none
(3.45±0.1)	w	none
3.82±0.05	s	none
4.25±0.1	w	none
4.52±0.1	w	none
(4.75±0.1)	w	none
4.94±0.1	w	none
5.40±0.1	s	none
6.00±0.1	w	none

Fig. 3 seems to show little direct evidence for the production of α particle groups other than the α_0-group. This is presumably a consequence of the larger widths of the α particle peaks in the pulse-height spectra, which has been discussed in sect. 3. Moreover, the α particle groups are probably, on the average, of smaller intensity than the proton groups. That some of the observed peaks do, in fact, correspond to ((n, α) reactions, can be shown by drawing in fig. 3 the loci for the expected α particle groups on the basis of their known Q-values. These loci have been omitted, however, for greater clarity.

The cross section for formation of the p_0-group has been calculated and is shown in fig. 6. The absolute values of the cross section are believed to be accurate to ±20 %. The data agree well with those obtained with the T(p, n) neutron source (fig. 4) in the region of overlap. In addition, two measurements were made at neutron energies of 5.75 and 7.86 MeV of the combined (n, p)- and (n, α)-cross section, including transitions to all possible states of the final nuclei. For this purpose all pulses in the spectra were added corresponding to

proton energies above 1.5 MeV or α particle energies above 2.8 MeV. The background components due to instantaneous γ rays and delayed activities were determined in separate experiments and subtracted. The following results were obtained: at $E_n = 5.85$ MeV, $\sigma(n, p+n, \alpha) = 400$ mb; at $E_n = 7.86$ MeV, $\sigma(n, p+n, \alpha) = 450$ mb. The estimated accuracy of these values is ± 20 %; the spread in neutron energy was approximately 200 keV.

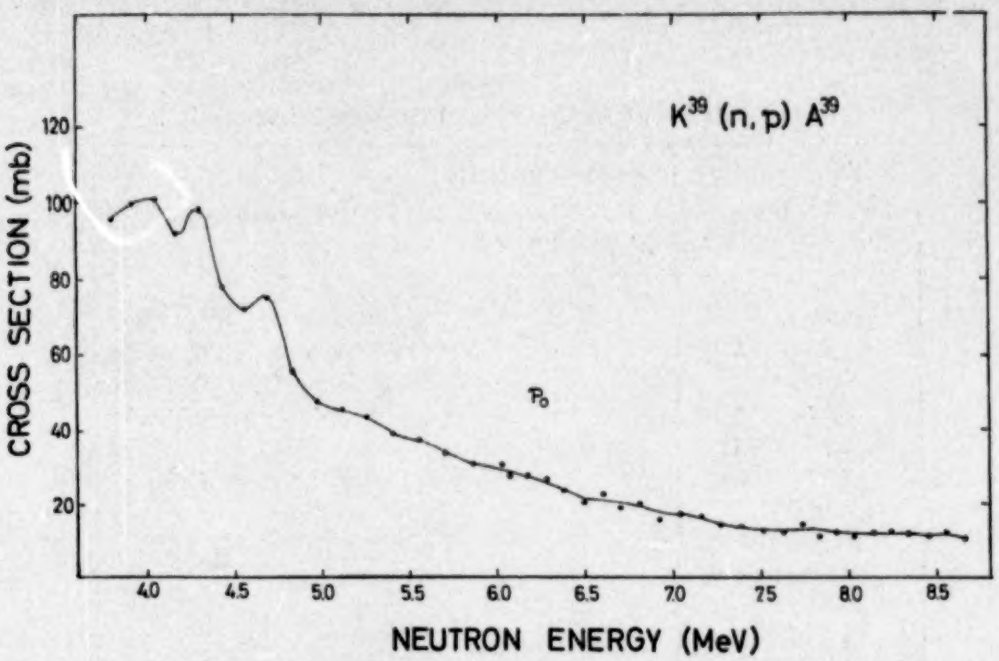

Fig. 6. The cross section for the reaction $K^{39}(n, p_0)A^{39}$ as a function of neutron energy. The neutrons were obtained from the reaction $D(d, n)He^3$ and had an energy spread of 100—150 keV.

5. Discussion

The present results may be compared with two other measurements of the absolute cross sections for the reactions $K^{39}(n, p)A^{39}$ and $K^{39}(n, \alpha)Cl^{36}$ at neutron energies near 2.5 MeV .The values and references are listed in table 3. The sum of the (n, p_0)- and (n, α_0)-cross sections has also been included in table 3, since

TABLE 3

Comparison of the absolute cross sections for the reactions $K^{39}(n, p_0)A^{39}$ and $K^{39}(n, \alpha_0)Cl^{36}$, measured by different laboratories at neutron energies near 2.5 MeV

	Neutron energy and energy spread (MeV)	$\sigma(n, p_0)$ (mb)	$\sigma(n, \alpha_0)$ (mb)	$\sigma(n, p_0)+\sigma(n, \alpha_0)$ (mb)
Lindström and Neuert [2])	2.59±0.05	45±5	36 ±4	81±9
Dixon and Aitken [4])	2.46±0.10	96±6	6	102±8
Present results	2.60±0.10	74±15	7.4±1.5	81±16
	2.60±0.10	80±16	7.5±1.5	87±17
	2.45±0.05	80±16	4.8±1.0	85±17
	2.45±0.10	84±17	5.0±1.0	89±18

in the pulse-height spectra of Lindström and Neuert [2]) and of Dixon and Aitken [4]) the peaks due to these two reactions are not clearly separated; this suggests, that the sum of the cross sections might have been determined more accurately in these cases than the individual cross sections. Further it seems possible that the value of 100 keV quoted for the neutron energy spread in refs. [2, 4]) is somewhat low in both cases; the present results have therefore been averaged over neutron energy intervals of both 100 and 200 keV for comparison. It might be added that the errors assigned to the present data have been estimated generously and are considered as maximum errors rather than standard errors.

Comparison of the present results with those of Lindström and Neuert [2]) shows good agreement with respect to the sum of the (n, p_0) and (n, α_0) cross sections, but clear disagreement with respect to the individual cross sections. This is presumed to be due to incorrect interpretation of the unresolved double peak in the pulse-height spectrum observed by Lindström and Neuert. The cross sections measured by Dixon and Aitken [4]) are somewhat larger than the present values but agree with them within the assigned limits of experimental error. The ratio of the (n, α_0)-cross section to the (n, p_0)-cross section has been given by Dixon and Aitken at 0.06 at $E_n = 2.46$ MeV and as 0.14 at $E_n = 2.85$ MeV. The present results for this ratio are 0.06 and 0.19 at the same two neutron energies. The agreement is as good as can be expected on the basis of Dixon and Aitkens' pulse-height spectra; the present figures should be considerably more accurate, because the p_0- and α_0-peaks have been clearly resolved. (See fig. 2).

The first excited state of K^{39} has an excitation energy of 2.53 MeV (ref. [6])) and inelastic excitation of this state becomes possible at neutron energies above about 2.6 MeV. Below this energy neutron emission in the entrance channel is the only decay mode of the compound nucleus seriously competing with the emission of protons or α particles. In this region the gross shape of the excitation curves for the p_0-and α_0-groups should therefore be determined by barrier penetrabilities only. Assuming a nuclear radius of 5.0 fm for the final nuclei, the Coulomb barrier heights for outgoing protons and α particles are approximately 5 and 8 MeV, respectively. Numerical calculations using simple continuum theory [9]) reproduce approximately the trend and magnitude of the p_0-cross section between 1.5 and 2.5 MeV and of the α_0-cross section between 2.3 and 3.0 MeV. Measurements of the p_0-yield at neutron energies in the region 1.5 to 1.0 MeV seem to indicate that the cross section decreases less strongly with decreasing neutron energy than expected on the basis of barrier penetrability; the accuracy of the data taken in this region is not sufficient, however, to allow quantitative conclusions. Again at higher neutron energies, near 3 MeV and above, the measured cross section increases less rapidly with energy than the barrier penetrabilities. This is attributed to the onset of inelastic neutron

scattering and the competition of the p_1 and p_2 groups of protons. This competition is presumably the reason why the p_0-and α_0-yield curves bend over and reach maxima at neutron energies, where the emitted charged particles still have energies well below the respective Coulomb barrier heights.

Relative values for the $K^{39}(n, p_0)$ cross section have been obtained by Scott and Segel [1]) at ten different neutron energies in the region 2.0 to 5.5 MeV. Their yield curve is similar in shape to the present one, but the maximum seems to be displaced in their data to a somewhat lower neutron energy.

In table 4 values of the $K^{39}(n, p)$ cross section, the $K^{39}(n, \alpha)$ cross section and the sum of both are listed for various neutron energies. In each case transitions to all possible states of the final nuclei are included. The values quoted for a neutron energy of 14 MeV have been taken from the work of

TABLE 4

(n, p) and (n, α) cross sections for K^{39} at various neutron energies

Neutron energy (MeV)	σ(n, p) (mb)	σ(n, α) (mb)	σ(n, p)+σ(n, α) (mb)
2.6	90	7	97
3.6	150	60	210
5.9			400
7.9			450
14 (ref. [3]))	350	110	460

Bormann *et al.* [3]). The (n, np)-cross section is not included in the (n, p)-cross section quoted for 14 MeV, but the (n, α)-cross section may include a small contribution from the (n, nα)-reaction. Furthermore, all the (n, p)-cross sections given in table 4 include contributions from the reaction $K^{41}(n, p)A^{41}$, but these are estimated to be less than 2 % in each case. It appears that the combined (n, p)- and (n, α)-cross section of K^{39} remains fairly constant in the energy range from 6 to 14 MeV; the yield of α particles seems to be one-third to one-half, on the average, of the proton yield. It is interesting to note that at $E_n = 7.9$ MeV the combined cross section for emission of charged particles amounts to approximately $\frac{1}{3}(R+\lambda\!\!\!^{-})^2$, where R is the nuclear radius and $\lambda\!\!\!^{-}$ the wavelength of the incoming neutron divided by 2π. This indicates that charged particles and neutrons are emitted from the compound nucleus in comparable numbers. The relatively high cross sections for charged particle emission seem to be largely due to favourable Q-values in connection with a comparative scarcity of low-lying excited states in K^{39}, which results in a reduction in the number of competing neutron channels. A similar situation exists in the disintegration of Ca^{40} by fast neutrons, where even higher (n, p)- and (n, α)-cross sections are observed than in the K^{39} case [10]).

No detailed analysis can be made of individual resonances in the p_0-yield

curve in the neutron energy region from 1.46 to 3.05 MeV. The observed resonances have an average width of the order of 10 keV and an average spacing of about 25 keV. Similar widths and spacings have been reported for resonances in the total neutron cross section at somewhat lower neutron energies for nuclei in the same mass region[11]). On the other hand, predictions based on the Fermi gas model [12, 13]) seem to indicate an average level spacing of the order of 1 keV for K^{40} near 10 MeV excitation. Apparently either the statistical calculations are not applicable in this case or the observed maxima in the p_0-yield curve represent in part gross structure effects, which may be composed of a number of overlapping or unresolved resonances. Probably both arguments apply, and the true level spacing falls somewhere in the range from 1 keV to 25 keV.

In cases where individual states in K^{40} are observed, one would expect from simple resonance theory [9]), that the ratio of the maximum to the average cross section be approximately equal to the ratio of the reduced width for proton emission to the ground state of A^{39} to that for neutron emission in the entrance channel. The data suggest that this ratio never deviates drastically from unity; this is presumably just what one would expect if the excitation energy of the compound system is well shared among the nucleons.

Since the proton-and α-particle-widths will, in general, vary differently from resonance to resonance, the fluctuations of the p_0- and α_0-excitation curves measured with poor energy resolution (fig. 4) show little correlation. Strong correlation in the positions of peaks and valleys (but not in the associated amplitudes) would be expected, if individual resonant states in K^{40} were resolved. Unfortunately, this criterion cannot be applied to the data obtained with the Li^7(p, n) neutron source, because there the α_0-group is too weak and obscured by background effects.

We are indebted to Dr. E. A. Davis and Dr. Theo Retz-Schmidt for assistance during the early part of these experiments.

References

1) M. J. Scott and R. E. Segel, Phys. Rev. **102** (1956) 1557
2) G. Lindström and H. Neuert, Z. Naturf. **13a** (1958) 826
3) M. Bormann, H. Jeremie, G. Andersson-Lindström, H. Neuert and H. Pollehn, Z. Naturf. **15a** (1960) 200
4) W. R. Dixon and J. H. Aitken, Nuclear Physics **24** (1961) 456
5) W. D. Allen, Fast neutron physics, ed. by J. B. Marion and J. L. Fowler (Interscience Publishers, Inc., New York, 1960)
6) P. M. Endt and C. M. Braams, Rev. Mod. Phys. **29** (1957) 683
7) E. A. Davis, R. Bass, T. W. Bonner and D. M. Worley, Jr., Bull. Am. Phys. Soc. **5** (1960) 110
8) J. E. Brolley, Jr. and J. L. Fowler, in ref. [5])
9) J. M. Blatt and V. W. Weisskopf, Theoretical nuclear physics (John Wiley and Sons, Inc., New York, 1952)
10) R. Bass, T. W. Bonner, and H. P. Hänni, Bull. Am. Phys. Soc. **5** (1960) 248
11) D. J. Hughes and R. B. Schwartz, Brookhaven National Laboratory Report BNL-325 (1958)
12) J. M. B. Lang and K. J. LeCouteur, Proc. Phys. Soc. **67** (1954) 586
13) T. D. Newton, Can, J. Phys. **34** (1956) 804

2.A.1

Nuclear Physics **28** (1961) 494—502; © *North-Holland Publishing Co., Amsterdam*

Not to be reproduced by photoprint or microfilm without written permission from the publisher

NEUTRON THRESHOLD MEASUREMENTS IN THE REACTIONS $^{9}Be(p, n)^{9}B$, $^{10}B(p, n)^{10}C$, $^{11}B(p, n)^{11}C$

S. TAKAYANAGI †, N. H. GALE, J. B. GARG and J. M. CALVERT

The Physical Laboratories, The University, Manchester

Received 16 June 1961

Abstract: Neutron thresholds resulting from proton bombardment of ^{9}Be, ^{10}B and ^{11}B have been investigated by the use of the counter ratio method, in the range of proton energies from 3 to 5.5 MeV. The ground state threshold energy for the $^{10}B(p, n)^{10}C$ reaction was found to be (4.835 ± 0.025) MeV, corresponding to a mass excess for ^{10}C of (18.620 ± 0.025) MeV. An expected low lying excited state threshold for the $^{9}Be(p, n)^{9}$ reaction at about 3.8 MeV was not found, and the first excited state threshold for the $^{11}B(p, n)^{11}C$ reaction was not found up to 5.2 MeV bombarding energy.

1. Experimental Procedure

The method used in these experiments was that of the counter ratio technique introduced by Bonner and Cook [1]). The experimental arrangement adopted

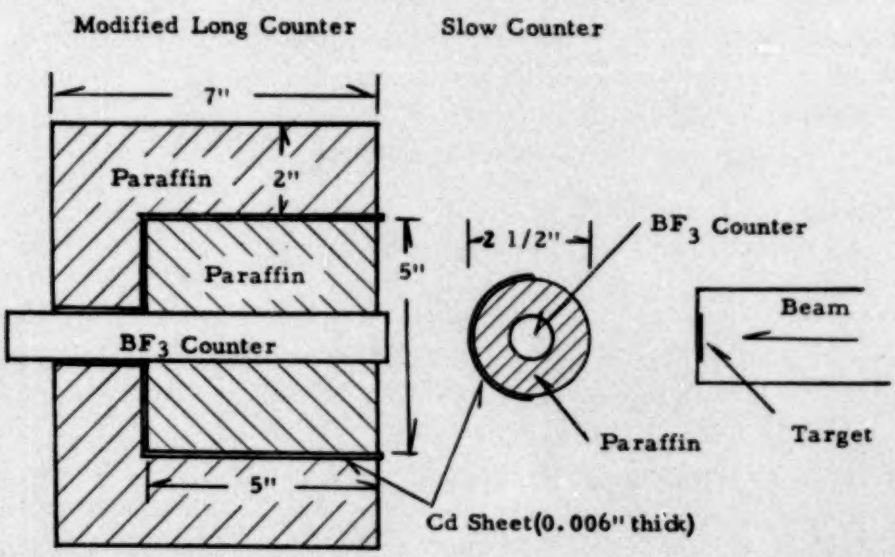

Fig. 1. Arrangement of the counters used in the neutron threshold measurements.

was similar to that described by Brugger *et al.* [2]), and the geometry of the neutron counters is shown in fig. 1. The effect of the background arising from

† On leave of absence from the Tsurumi Research Laboratory, Tokyo Shibaura Electric Co. Ltd., Yokohama, Japan

scattered neutrons was reduced by covering the modified long counter by cadmium sheet 0.015 cm thick at back and sides, and using a 5 cm thick paraffin shield outside this to thermalize the scattered neutrons. The back of the slow neutron counter was also covered by cadmium sheet so as to absorb slow neutrons reflected from the long counter. The counters were spaced so as to subtend approximately the same solid angle at the target; the half-angle of the cone subtended was 20°.

Boron trifluoride proportional counters † filled to a pressure of 400 mm Hg were used in both fast and slow neutron detectors; the pulse-height distribution shown in fig. 2 is typical of those obtained in the course of this work.

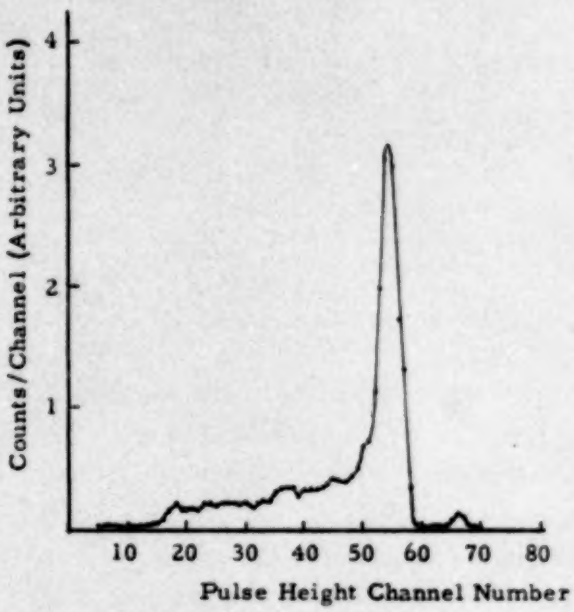

Fig. 2. Typical pulse height distribution from the 12EB40 boron trifluoride counters.

The proton beam from the 6 MV Van de Graaff accelerator of the University of Manchester was analysed by a 90° magnet and refocussed by a pair of magnetic quadrupole lenses. The energy spread of the incident beam was restricted to $\pm\frac{1}{1000}$ by a defining diaphragm placed in front of the target.

The bombarding energy was determined by the use of the generating voltmeter, which was calibrated by using a number of well-known (p, n) thresholds; Li^7(p, n)Be^7 1.8813 MeV; Li^7 (HH^+, n)Be^7 3.763 MeV, F^{19}(p, n)Ne^{19} 4.240 MeV. The bombarding energy could be set to an accuracy of $\pm$ 5 keV.

2. Results and Discussion

2.1. THE Be^9(p, n)B^9 REACTION

Although the level structure of the ^{9}B nucleus has been investigated by the study of a number of nuclear reactions, yet little is known about this nucleus

† Type 12 EB 40, manufactured by 20th Century Electronics Ltd.

compared with the available data for the level structure of its mirror nucleus ^{9}Be. The first, second and third excited states in the ^{9}Be nucleus are known to be 1.75 MeV ($\frac{1}{2}+$), 2.43 MeV ($\frac{5}{2}-$) and 3.04 MeV ($\leq \frac{3}{2}$), respectively, whilst the known low-lying excited levels in ^{9}B are at 2.37 MeV ($> \frac{1}{2}-$) and 2.83 MeV (ref. [3]). These level schemes are illustrated in fig. 3. The level at $E_x = 2.37$

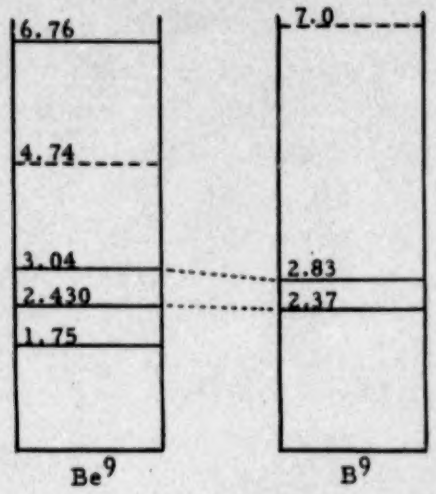

Fig. 3. Energy levels of Be^9 and B^9 as reported by Ajzenberg-Selove and Lauritsen [3]).

MeV in ^{9}B is believed to correspond with the level at $E_x = 2.43$ MeV in ^{9}Be, and the level at $E_x = 2.83$ MeV in ^{9}B is similarly believed to correspond with the level at $E_x = 3.04$ MeV in ^{9}Be. It may therefore be concluded that the level corresponding to the level at $E_x = 1.75$ MeV in ^{9}Be has not so far been found in ^{9}B, and that it may be expected near $E_x \approx 1.6$ MeV. The ^{9}Be(p, n)^{9}B reaction has already been investigated by Marion *et al.* [4]) using the counter ratio technique. They observed a broad rise in the counter ratio centred on a bombarding energy of $\approx$ 3.6 MeV. An unambiguous interpretation of the broad rise has not so far been possible [3–7]). It has usually been attributed to one of three possible causes:

(i) a variation in counter sensitivity with neutron energy,
(ii) a three-body break up in the process ^{9}Be (p, pn)^{8}Be,
(iii) a broad level in ^{9}B.

Since it appeared not improbable that an additional small sharp rise in the counter ratio superimposed on the broad maximum (and corresponding to the missing excited state) might have been overlooked, it was decided to investigate the ^{9}Be(p, n) ^{9}B reaction again, using the counter ratio technique.

A Bradner foil of Be^9 metal, which was about 60 keV thick at a proton energy of 2 MeV, was used in the experiment. The counter ratio and the forward yield of neutrons were measured from threshold to a bombarding energy of 4.6 MeV; in particular, the counter ratio was investigated closely from a bombarding energy of 3.15 MeV to 4.55 MeV. The results are presented in

figs. 4 and 5. The ground state threshold was found to be 2.055 ± 0.010 MeV, which was in good agreement with the previous more accurate values of

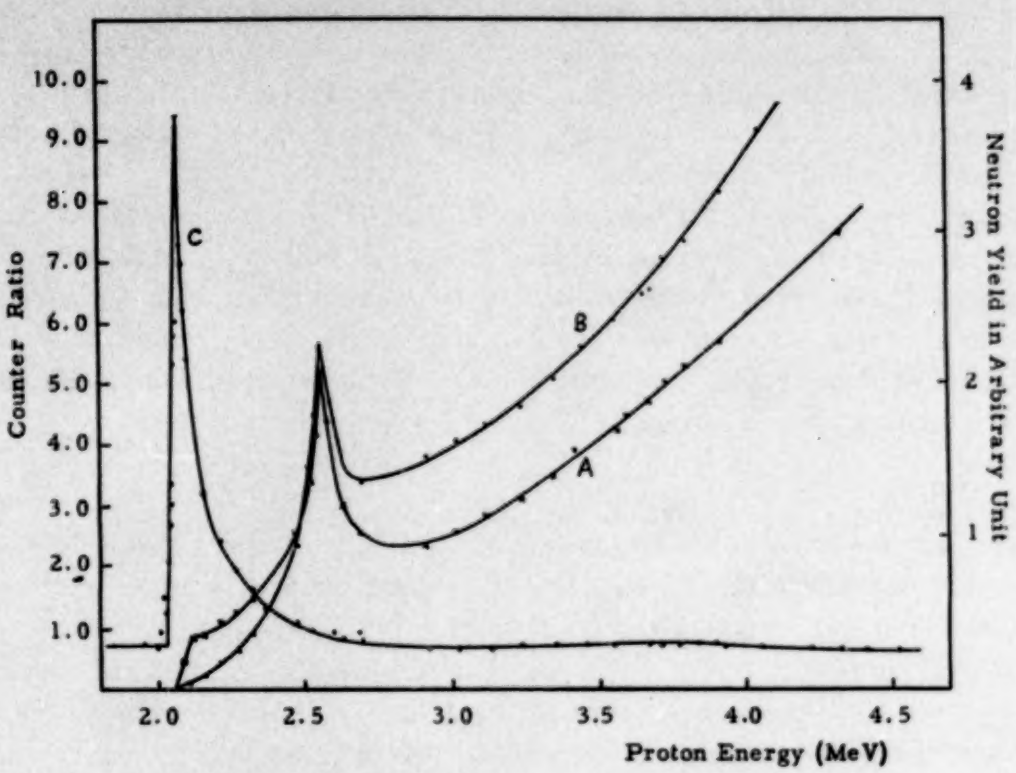

Fig. 4. $Be^9(p, n)B^9$. Counter ratio and yield of neutrons in the forward direction as a function of bombarding energy. Curve A is the neutron yield measured by the slow neutron counter; curve B is the yield measured by the modified long counter; curve C is the counter ratio. This convention is preserved in all subsequent figures.

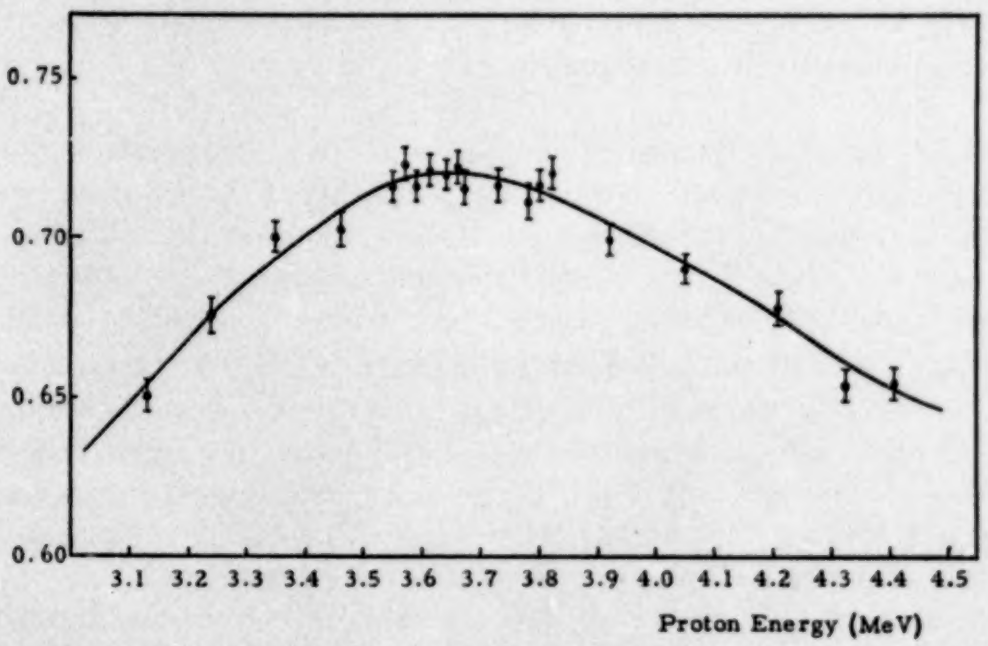

Fig. 5. $Be^9(p, n)B^9$. Counter ratio as a function of bombarding energy in the region of the expected first excited state threshold of B^9.

(2.059±0.002) MeV obtained by Richards *et al.* [9]) and of (2.060±0.003) MeV found by Marion *et al.* [4]). The yield curve of fig. 4 shows a well-known resonance at a bombarding energy of 2.56±0.02 MeV, which was in good agreement with previous values obtained by Marion [10]) (2.562±0.006 MeV) and by others [11–13]). The expected threshold was not observed from the counter ratio curve shown in fig. 5. There is no evidence of a sharp rise in the ratio apart from that due to the ground state threshold.

A broad maximum at a bombarding energy of about 3.65 MeV was found which had also been observed by Marion *et al.* [4]) and was discussed in detail by them. However, as thresholds with quite small intensities could have been detected, it was not clear why the expected excited state should be so weak as to be lost in the background; unless in fact the broad maximum is due to the level being very broad indeed.

2.2 THE $B^{10}(p, n)C^{10}$ REACTION

The reaction $^{10}B(p, n)^{10}C$ has been investigated previously, using the photographic plate technique [8]) and using the single neutron counter method [14]) It was found by the use of the photographic plate technique that the ground state Q value for the $^{10}B(p, n)^{10}C$ reaction was −4.35±0.2 MeV. The attempt to measure the slow neutron threshold by using a conventional long counter did not succeed; preliminary data up to proton energies of 6 MeV showed that no ^{10}B threshold could be observed through the $^{11}B(p, n)^{11}C$ background due to the 2% ^{11}B content in the ^{10}B targets [14]). The mass difference $^{10}C-^{10}B$ is given as 3.84±0.1 MeV from β-end-point measurements [15]), and as 3.57±0.2 MeV from the $^{10}B(p, n)^{10}C$ Q-value obtained by the photographic plate technique [8]). In neither case is the accuracy very high, and it appeared to be of interest to investigate the ground state threshold of the $^{10}B(p, n)^{10}C$ reaction more closely.

A thick, enriched ^{10}B target (> 99 % B^{10} and < 1 % B^{11}) prepared by means of electromagnetic separation on a tungsten backing 0.012 cm thick, was obtained from the Atomic Energy Research Establishment, Harwell. The target thickness was about 1 mg/cm², corresponding to about 70 keV proton energy loss at 5 MeV. The counter ratio and the forward yield of neutrons were measured closely from the bombarding energy of 4.5 MeV to that of 5.2 MeV. The results are shown in fig. 6. A definite ratio rise in the counter ratio curve was found at a bombarding energy of 4.835±0.025 MeV, corresponding to the ground state threshold of C^{10}. The ground state threshold obtained was in agreement with that determined by Ajzenberg and Franzen [8]), who found a value of 4.75±0.2 MeV, but was determined more accurately.

The shape of the ratio rise was rather peculiar for a ground state threshold. Unambiguous interpretation of the data is not possible, but it is believed that one of the reasons for this peculiarity was due to the fact that there was a large

number of background neutrons coming from the impurity of $\lesssim 1\,\%$ B^{11} in the target. Another reason for the peculiar behaviour of the counter ratio is that the outgoing neutrons in this case carry off angular momentum corresponding to $l_n > 0$ (ref. [16]). It was at first suspected that the ratio rise might have originated from the first excited state of C^{11} or from the resonance neutrons of the $B^{11}(p, n)C^{11}$ reaction. It will be shown in the following subsection that the counter ratios measured for the $B^{11}(p, n)C^{11}$ reaction using an

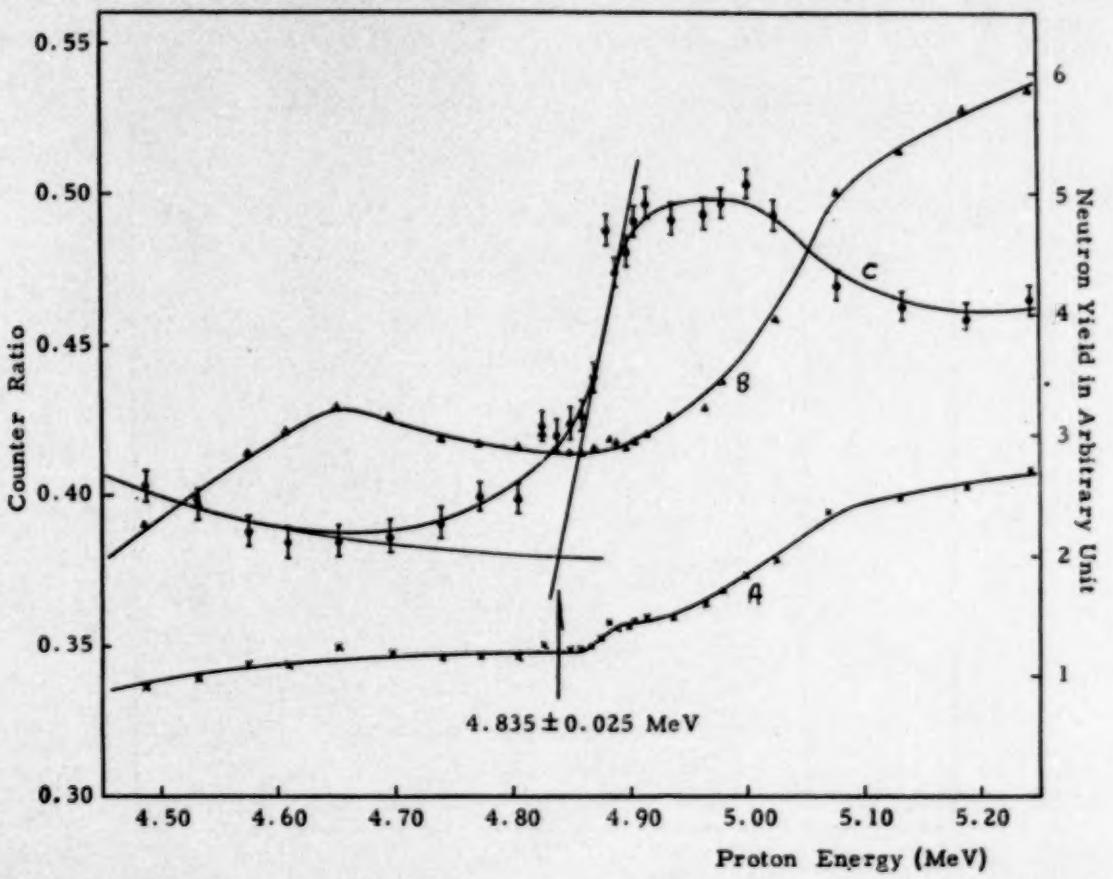

Fig. 6. $B^{10}(p, n)C^{10}$. Counter ratio and yield of neutrons in the forward direction as a function of bombarding energy in the region of the ground state threshold of C^{10}.

enriched ^{11}B target indicated no definite ratio rise between the bombarding energy of 3.1 MeV and that of 4.4 MeV; consequently it is established that the rise in the ratio from the ^{10}B target is due to the ground state threshold for ^{10}C.

2.3 THE B^{11} (p, n)C^{11} REACTION

The reaction $^{11}B(p, n)^{11}C$ has been investigated by Richards *et al.* [9]), who established the ground state threshold as (3.015 ± 0.003) MeV, by Ajzenberg *et al.* using the photographic plate technique [17]) and by Marion *et al.* using the counter ratio technique [4]). The photographic plate measurements indicated the existence of the first excited state of ^{11}C at an energy of (2.01 ± 0.06) MeV and gave

the ratio of the intensities of the neutron groups leading to the ground state and first excited state of ^{11}C as 2.5 at a proton bombarding energy of 7.03 MeV. On the other hand, the expected first excited state threshold was not observed by Marion *et al.* [4]), as it was lost in the background. If, as is suggested by the data from the photographic plate work, the first excited state neutron group is not much less intense than the ground state neutron group, it is not entirely clear why the first excited state threshold as measured by the counter ratio method should have been masked by the background. It therefore appeared to be of interest to make a further search for this level. Apart from its intrinsic

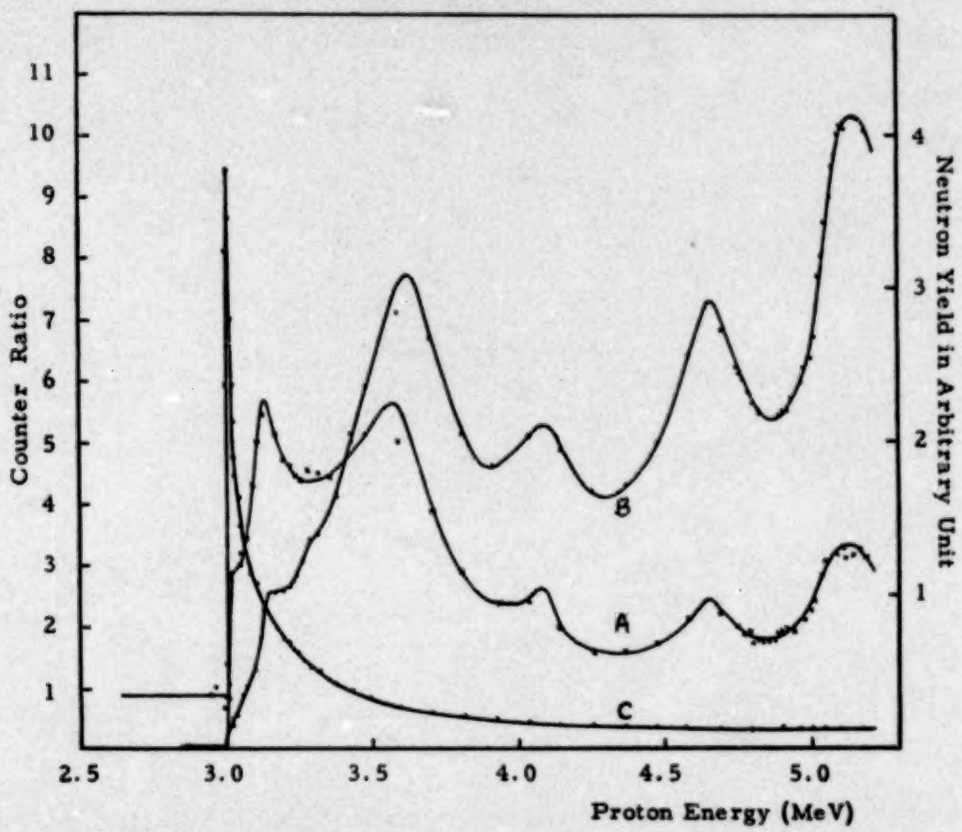

Fig. 7. $B^{11}(p, n)C^{11}$. Counter ratio and yield of neutrons in the forward direction as a function of bombarding energy.

interest, it was estimated that the first excited state threshold energy for ^{11}B (p, n)^{11}C might not be very far away from the ground state threshold for the ^{10}B(p, n)^{10}C reaction. Since it was estimated that there might be up to 1 % ^{11}B in our enriched ^{10}B targets, it was essential to investigate the ^{11}B(p, n) ^{11}C reaction so as to exclude all possibility of confusion between the ground state threshold of ^{10}B(p, n)^{10}C and the first excited state threshold of ^{11}B(p, n)^{11}C.

A thick, enriched B^{11} target (> 99 % B^{11} and < 1 % B^{10}) was also obtained from the Atomic Energy Research Establishment, Harwell. The target was prepared on a 0.012 cm thick gold backing by electromagnetic separation.

The target thickness was about 175 $\mu g/cm^2$, corresponding to about 18 keV proton energy loss at 3 MeV. The counter ratio and the forward yield of neutrons were measured from the threshold to a bombarding energy of approximately 5.2 MeV. The counter ratio was measured closely from the bombarding energy of 4.7 MeV to 5.2 MeV. The results are presented in figs. 7 and 8. The ground state threshold was found to be 3.008 ± 0.013 MeV, which was in good agreement with the value of 3.015 ± 0.003 MeV obtained by Richards *et al.* [9]) previously. The threshold obtained is in slight disagreement with Ajzenberg *et al's* data [17]) of $3.09\ ^{+0.06}_{-0.05}$ MeV. The forward yield of neutrons showed resonances at

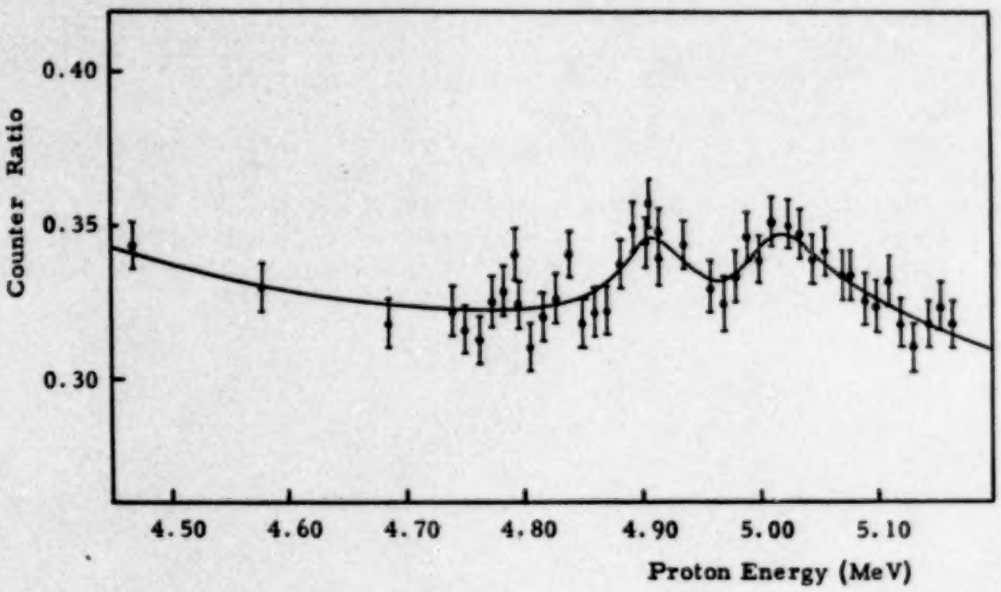

Fig. 8. $B^{11}(p, n)C^{11}$. Counter ratio as a function of bombarding energy in the region of the expected thresholds corresponding to the first excited state of C^{11}.

bombarding energies of 3.15, 3.62, 4.08, 4.65 and 5.15 MeV, in good agreement with previous data [13, 14, 18]). The counter ratio data presented in fig. 8 shows no sharp rise in the expected region of bombarding energy centred at about 4.85 MeV, although there is a very small rise of about 6 % at 4.86 MeV. The expected first excited threshold of C^{11} was not found up to the bombarding energy of 5.15 MeV, if the small rise at 4.86 MeV is ignored. Since this work was completed it has been brought to our notice that the ground state threshold for the reaction has been remeasured by Bromley *et al.* [19]), who found the value 3.019 ± 0.004 MeV.

One of us (S.T.) is greatly indebted to Professor S. Devons for having provided the opportunity of working in his laboratory, and is also grateful to the International Atomic Energy for the grant of a fellowship.

References

1) T. W. Bonner and C. F. Cooke, Phys. Rev. **96** (1954) 122
2) R. M. Brugger, T. W. Bonner and J. B. Marion, Phys. Rev. **100** (1955) 84
3) F. Ajzenberg-Selove and T. Lauritsen, Nuclear Physics **11** (1959) 1
4) J. B. Marion, T. W. Bonner and C. F. Cook, Phys. Rev. **100** (1955) 91
5) B. Jennins, K. H. Sun and H. A. Leiter, Phys. Rev. **80** (1950) 109
6) F. Ajzenberg and W. W. Buechner, Phys. Rev. **91** (1953) 674
7) J. B. Marion and J. S. Levin, Phys. Rev. **115** (1959) 144
8) F. Ajzenberg and W. Franzen, Phys. Rev. **95** (1954) 1531
9) H. T. Richards, R. V. Smith and C. P. Browne, Phys. Rev. **80** (1950) 524
10) J. B. Marion, Phys. Rev. **103** (1956) 713
11) T. M. Hahn, C. W. Snyder, H. B. Willard, J. K. Bair, E. D. Klema, J. D. Kingston and F. P. Green, Phys. Rev. **85** (1952) 934
12) J. B. Marion and J. S. Levin, Phys. Rev. **115** (1959) 144
13) J. H. Gibbons and R. L. Macklin, Phys. Rev. **114** (1959) 571
14) J. K. Bair, J. H. Kington and H. B. Willard, Phys. Rev. **100** (1955) 21
15) R. Sherr and J. B. Gerhart, Phys. Rev. **91** (1953) 909
16) J. B. Marion and T. W. Bonner, Fast neutron physics (Interscience Publishers, New York) Chapt. 5 part II
17) F. Ajzenberg-Selove, G. D. Johnson, A. Rubin and M. Mazari, Phys. Rev. **100** (1955) 84
18) J. B. Blaser, F. Boehm, P. Marmier and P. Sherrer, Helv. Phys. Acta **24** (1951) 465
19) D. A. Bromley, A. J. Ferguson, H. E. Gove, J. A. Kuehner, A. E. Litherland, E. Almquist and R. Batchelor, Can. J. Phys. **37** (1959) 1514

1.D.2:
1.E.1:
3.A

Nuclear Physics **28** (1961) 503—511; © *North-Holland Publishing Co., Amsterdam*
Not to be reproduced by photoprint or microfilm without written permission from the publisher

ON THE LEVELS AND TRANSITIONS IN Gd^{155}

B. N. SUBBA RAO
Tata Institute of Fundamental Research, Bombay-5, India

Received 12 June 1961

Abstract: Gamma-gamma coincidences of transitions in Gd^{155} have been studied. The (45 keV gamma)—(60 keV gamma) angular correlation was measured and could be represented by $W(\theta) = 1+(0.155\pm0.016)\ P_2(\cos\theta)+(0.028\pm0.025)\ P_4(\cos\theta)$, which requires, together with the other properties of the 60 keV transition, $\frac{3}{2}^+$ assignment to the 105 keV level. This is identified with the $\frac{3}{2}^+$ [651] orbital in the Mottelson-Nilsson classification. The mixing ratio of the 45 keV transition is found to be $\delta_1^2 = \text{M2/E1} = 0.0074$ ($\delta_1 = +0.086$) with the mixing ratio of the 60 keV transition of $\delta_2^2 = \text{E2/M1} = 0.04$ ($\delta_2 = -0.20\pm0.03$). A level scheme based on these studies is presented and the properties of levels and transitions are discussed.

1. Introduction

From measurements [1]) of the conversion coefficients of the 86.5 keV and 105 keV transitions in Gd^{155}, they were inferred to be El in multipole nature. Discounting the $\frac{1}{2}^+$ assignment to the excited states at these energies on the basis of the log ft values of β-transitions from Eu^{155}, these excited states were left with an assignment of the spin of $\frac{3}{2}$ or $\frac{5}{2}$. In order to determine the spin of the 105 keV state, 45 keV gamma → 60 keV gamma angular correlation has been measured. To obtain further information on the decay scheme, gamma-gamma coincidences have been studied in this work. With the help of the measured [2]) intensities of gamma-rays following the decay of Eu^{155} and Tb^{155}, the properties of the levels and transitions are discussed in order to examine further the extent of validity of the unified model.

2. Coincidence Measurements with Eu^{155}

A fast-slow coincidence set up consisting of a 3.8× 3.8 cm and 3.8 cm×0.64 cm NaI(Tl) crystals optically coupled to RCA 6810A photomultipliers with an overall resolution time of 26 ns was used. The details of the set up have been given elsewhere [3]). To study coincidences of gamma transitions, the two counters were kept at 90° with respect to each other with a graded shield between them in order to suppress radiations scattered from one crystal to another. The spectra of Eu^{155} in coincidence with radiations in channel settings A, B, C and D in the singles spectrum are shown in fig. 1. From these coincidence spectra

which have been corrected for chance coincidences, it is found that (i) the 105 keV transition is in coincidence with only a 40 keV radiation, (ii) the 87 keV transition is in coincidence with 18 keV, 30 keV and 58 keV radiations, (iii) the 60 keV transition is in coincidence with the 45 keV and 27 keV transi-

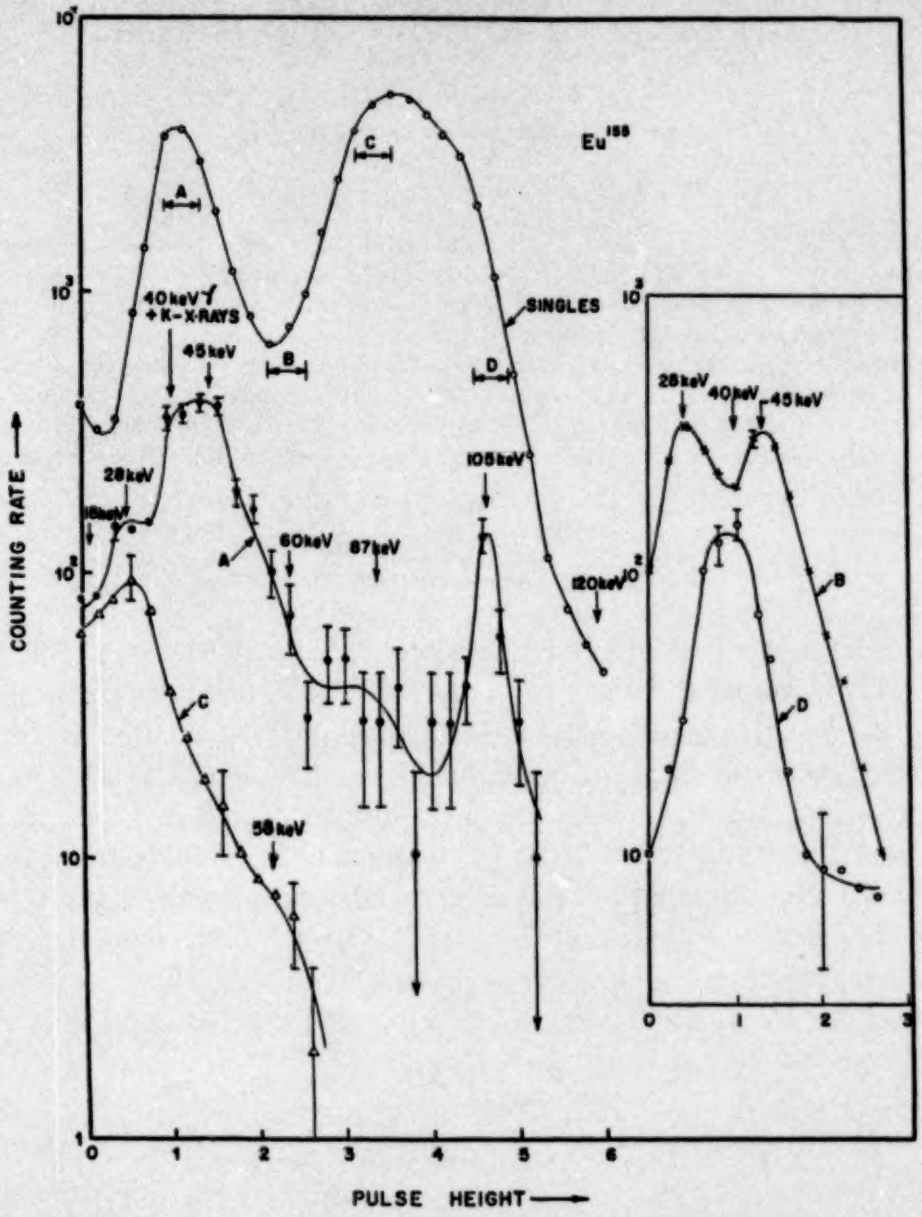

Fig. 1. Gamma-spectra A, B, C, D, refer to the spectra in coincidence with the gamma channels A, B, C, D shown in the singles spectrum.

tions, and (iv) the 45 keV radiations consisting of internal conversion X-rays, 41 keV and 45 keV gamma-rays are in coincidence with almost all the radiations and very prominently with the 40—45 keV radiations and 105 keV transitions.

The source of Eu^{155} employed in these experiments was obtained by neutron irradiation of samarium oxide enriched in Sm^{154} to 99.1 %. The isotope Gd^{152}

could have been present to not more than 0.01 % in it according to isotopic and spectrographic analyses †. Irradiation of this sample for only one week and allowing the sample to decay for nearly 650 days should leave a negligible amount of Gd^{153} in the source at the time of study. Shorter lived Sm^{153}, Eu^{156} ($Sm^{154} \xrightarrow{(n,\gamma)} Sm^{155} \xrightarrow{\beta^-} Eu^{155} \xrightarrow{(n,\gamma)} Eu^{156}$) had totally disappeared. Thus the observed coincidences are concluded to be genuine since the chance coincidences have been deducted from each point and care has been taken to suppress radiations scattered from one crystal to another.

3. The 45 keV Gamma → 60 keV Gamma Angular Correlation

The angular correlation set up and the details of the method of measurement have been described earlier [3]). With one channel set to accept the 60 keV gamma-ray and the other the 45 keV gamma-ray (fig. 1) coincidences were measured in steps of 45° from 90° to 270°. About 5000 counts were collected at each angular position, deducting the chance coincidences from each observation. True to chance ratio was mostly about 38. The true coincidence rate was divided by the singles counting rate of the movable counter seeing the 60 keV gamma-ray. After correcting for finite solid angle attenuation effects, the angular correlation function could be represented by

$$W(\theta) = 1 + (0.155 \pm 0.016) P_2(\cos\theta) + (0.028 \pm 0.025) P_4(\cos\theta).$$

In the coincidence measurements with the 60 keV transition (fig. 1), the 45 keV and 27 keV transitions are seen to be very pronounced and the presence of any feeble 41 keV transition, internal conversion X-ray of transitions from the 146 keV level, being in coincidence with the 60 keV transition through the 27 keV or 45 keV transitions appears to be negligible since the 146 keV level is only feebly (< 1 %) populated in the decay of Eu^{155} and since this level de-excites through many transitions. The 45 keV channel setting was of 6 keV width in the central region of the 45 keV peak in the coincidence spectrum (fig. 1B).. Therefore these contributions have been neglected.

From the reduced transition probability for de-excitation $B(E2) = 2.7\ e^2 \times 10^{-48}\ cm^4$ obtained from Coulomb excitation experiments [5]), the mean life of the 60 keV transition is deduced to be about 2×10^{-10} sec. With this short life time, attenuation of the angular correlation anisotropy due to the coupling between the nuclear spin and internal fields at the nucleus are considered to be negligible. Since the 60 keV state is well-known to be the rotational state corresponding to the ground state as the intrinsic state, the spin and parity of the ground and 60 keV states will be adopted to be $\frac{3}{2}^-$ and $\frac{5}{2}^-$, respectively. The 105 keV state could have $\frac{5}{2}$ or $\frac{3}{2}$ spin, as already pointed out. Measurements [5, 6]) of L-subshell ratio for the 60 keV transition require a E2/M1 mixing ratio

† Isotope supplied by the ORNL.

of 0.04 ± 0.01. It was noted that the $\frac{5}{2}\xrightarrow{1}\frac{5}{2}\xrightarrow{2}\frac{3}{2}$ spin sequence requires a very large M2/E1 ratio for the 45 keV transition of $\delta_1 = -0.65$ with $\delta_2 = -0.20$. The alternative of $\delta_2 = +0.20$ does not satisfy the observed value of the coefficient A_2 for any allowed value of δ_1 (fig. 2). The single-particle estimate of the transition probability for M2 and E1 transitions of 45 keV together with a possible hindrance factor of 10^5 for the E1 component leads to M2/E1 $\approx 5\times10^{-4}$. Thus, the mixing ratio required by this spin sequence is very large. Also, the coefficient A_4 of the P_4 (cos θ) term being positive does not permit this spin sequence. The $\frac{3}{2}\xrightarrow{1}\frac{5}{2}\xrightarrow{2}\frac{3}{2}$ spin sequence satisfies both the sign of A_4 and the approximate order of magnitude of M2/E1. It leads to $\delta_1 = +0.086\pm0.006$ with $\delta_2 = -0.20\pm0.03$. The positive value

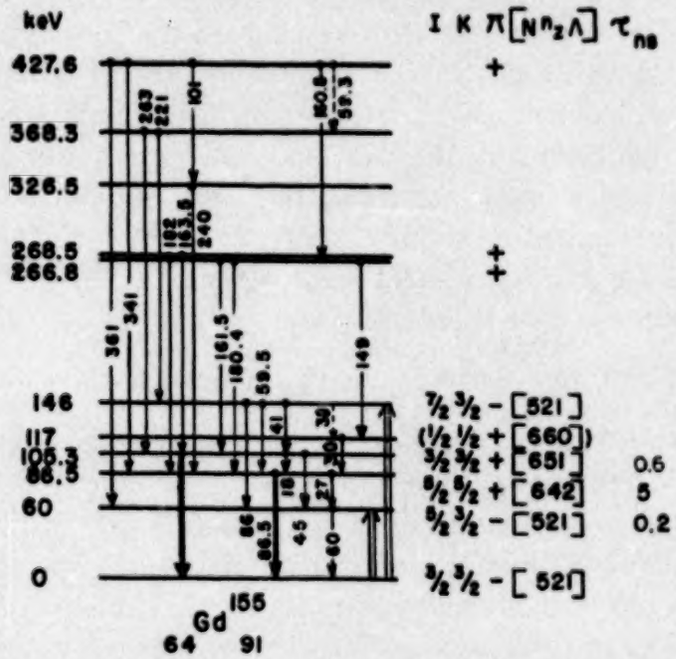

Fig. 2. Level scheme in $_{64}Gd^{155}_{91}$. On the left hand side are shown level energies in keV and on the right are indicated the quantum numbers $IK\,\pi[Nn_z\Lambda]$ needed for the full description of nucleonic states in deformed nuclei. τ_{ns} is the mean life of the state in ns.

of δ_2 cannot be brought into agreement with the observed coefficient A_2 for any allowed value of δ_1. Thus, the spin of the 105 keV state is concluded to be $\frac{3}{2}$, the mixing ratio of the 45 keV transition being $\delta_1^2 = \text{M2/E1} = 0.0074\pm 0.0011$ and the mixing ratio of the 60 keV being $\delta_2^2 = \text{E2/M1} = 0.04\pm0.01$ with $\delta_2 = -0.20\pm0.03$.

4. Level Scheme

From the angular correlation measurements, the spin of the 105 keV state is required to be $\frac{3}{2}$ which may be identified with the $\frac{3}{2}^+$ [651] orbital in the

Mottelson-Nilsson classification [8]). The E1 nature of the 105 keV transition has been inferred [1, 2]) from the measured K-conversion coefficient $\alpha^K = 0.22 \pm 0.05$. With this orbital assignment to the 105 keV state, as pointed out earlier, the 86.5 keV state may now be assigned $\frac{5}{2}^+$ [642].

The 40 keV transition observed in the present work to be in coincidence

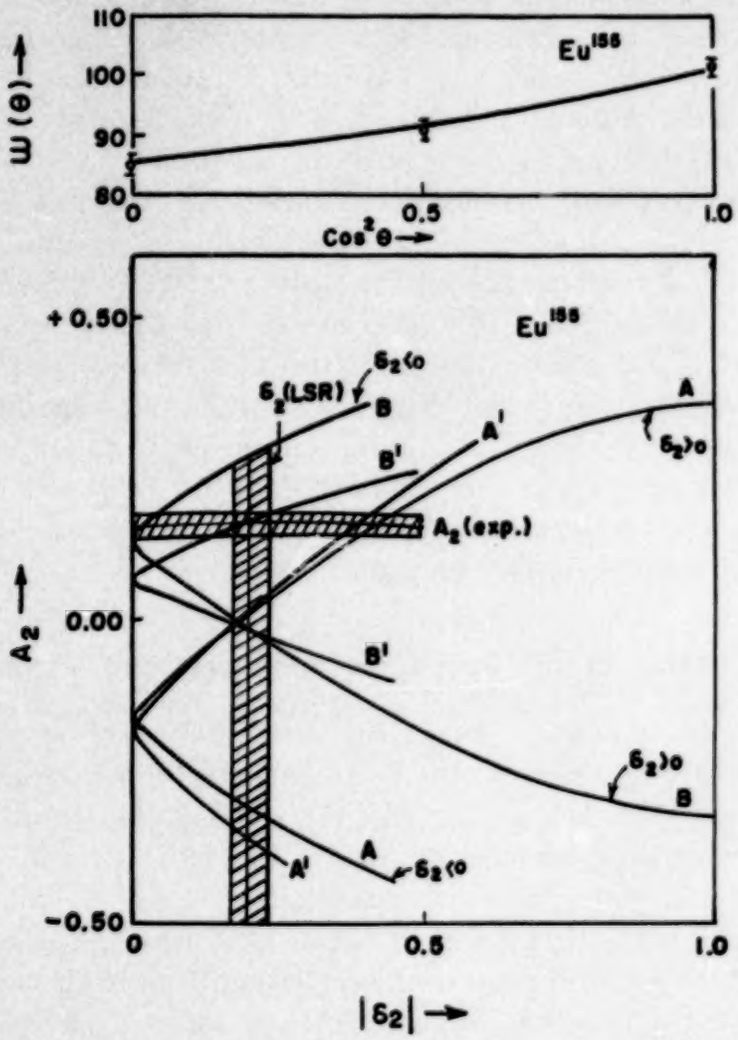

Fig. 3. Upper part shows the observed points of 45 keV → 60 keV γ-γ angular correlation fitted to the expression given in the text. Lower part shows the plot of he coefficient A_2 of the P_2 (cos θ) term against the mixing amplitude of the 60 keV transition for spin sequences (A) $\frac{5}{2} \to \frac{5}{2} \to \frac{3}{2}$ (A is for $\delta_1 = 0$, A^1 is for $\delta_1 = +0.0086$) and (B) $\frac{3}{2} \to \frac{5}{2} \to \frac{3}{2}$ (B is for $\delta_1 = 0$, B^1 for $\delta_1 = +0.086$). The parts corresponding to the two different phases of mixing amplitude δ_2 are indicated for both sets of curves. δ_2 (LSR) is the mixing amplitude based on L-subshell ratios. A_2(exp) is the experimentally measured value of the coefficient of the P_2 (cos θ) term.

with the 105 keV transition, together with the 58 keV transition in coincidence with the 86.5 keV transition, require a level at about 145 keV. A level at about this energy has been observed in Coulomb excitation of Gd^{155}. The K-conversion line of a 85.9 keV transition noted by Juliano [4]) also supports such a level

with that transition leading to the 60 keV state. While in the present work a not very weak 45 keV transition is observed in coincidence with the 60 keV transition apart from the 40 keV transition in coincidence with the 105 keV transition, Juliano [4]) has noted the presence of only the 41.6 keV transition which he excluded from the decay scheme, owing to some inconsistencies in the observed data. However, crystal diffraction spectrometer observations [6]) do indicate the presence of a not very weak 45.3 keV transition corresponding to the difference between the 105.3 keV and 60 keV levels. Thus both the 41 keV and 45.3 keV transitions should exist in Gd^{155} though the absence of the 45 keV transition in the observations of Juliano [4]) cannot be explained.

Gamma-rays of about 30 keV in coincidence with the 86.5 keV transition support the existence of a level at about 117 keV. This transition is different from the 27 keV transition in coincidence with the 60 keV transition.

The relative intensities of gamma-rays following the decay of Tb^{155} have been measured [2]). The source being a mixture of Tb^{155} and Tb^{156}, there was no possibility of obtaining any coincidence information. With the aid of transition energies measured with high resolution spectrometers [7]), the level scheme that explains most of the observed data from the study of Eu^{155} and Tb^{155} is shown in fig. 3. The parity assignments to levels above the 145.8 keV level are based on the multipolarities [6]) of gamma-rays.

5. Discussion of the Properties of Levels and Transitions

The 60 keV and 145.8 keV levels, observed in Coulomb excitation and in the decay of Eu^{155}, correspond to the two members of the rotational band based on the ground state $\frac{3}{2}^-$ [521] as the intrinsic configuration. Adopting the crystal diffraction spectrometer value [7]) of 60.00 ± 0.02 keV for the energy of the first excited state, the inertial parameter $\hbar^2/2\mathcal{I}$ in the formula for the rotational spectrum is obtained to be 12.00 keV. However, the ratio of the energy E_2 of the second member of the rotational band to that E_1 of the first member is $E_2/E_1 = 2.43 \pm 0.01$ compared with the value of 2.40 expected by the theory of rotational excitation of an axially symmetric nucleus under strictly adiabatic conditions of the intrinsic nucleonic motion with respect to the finite frequency of rotation of the orientation of the nuclear field. The difference, though small, is definitely positive and indicates that the partial break down of the adiabatic approximation is not due to rotation-vibration interaction, which would depress this energy ratio. This could be due to the coupling of the ground state rotational band and the rotational band based on the $\frac{5}{2}^+$ [642] state at 86.5 keV. The first rotational level of this second band falls at about 146 keV, if the inertial parameter is assumed to be the same as for the ground state rotational band. The assignment of $\frac{5}{2}^+$ [642] to the 86.5 keV state is based on the E1 nature [1]) of the 86.5 keV transition, angular correlation work present-

ed in this paper, together with the Mottelson-Nilsson calculations [8]) of the orbitals. From measurements of lifetime of this level [9]), the E1 transition is found to be retarded by a factor of about 2.8×10^4 with respect to the single particle estimate. This retardation is related to collective motion of nucleons represented in terms of the violation of selection rules, in this case for the asymptotic number n_z. Similarly, the 105 keV E1 transition has a measured transition probability [9, 10]) retarded with respect to the single-particle estimate by a factor of about 10^4. The Mottelson-Nilsson orbital $\frac{3}{2}^+$ [651] for the 105 keV level, relates this retardation to the violation of selection rules for the asymptotic quantum number n_z. Existence of members of rotational band based on these two intrinsic states cannot be inferred at present. The 117 keV level appears to be only feebly populated both in the decay of Eu^{155} $\{\frac{5}{2}^+$ [413]$\}$ and Tb^{155} $\{\frac{3}{2}^+$ [411]$\}$ so that it could have the $\frac{1}{2}^+$ [660] orbital, in which case transitions from both sides are forbidden or highly hindered.

The transition probability for the E2 component in the 60 keV transition has been obtained from Coulomb excitation measurements to be $B(\mathrm{E2})_d = 2.7\ e^2\times10^{-48}$ cm^4. With the E2/M1 ratio of 0.04, the reduced transition probability for the M1 component $B(\mathrm{M1})_d$ is deduced to be 0.093 $(e\hbar/2Mc)^2$. The gyromagnetic factors g_K and g_R corresponding respectively to the intrinsic and rotational motion of the nucleus are related to the reduced M1 transition probability through

$$B(\mathrm{M1})_d = \frac{3}{4\pi}(g_K-g_R)^2K^2|\langle I_i 1K0|I_i 1I_{ff}K\rangle|^2 \qquad (2)$$

for a transition from a state with angular momentum I_i to another state with angular momentum I_{ff} both belonging to the same rotational band characterised by $K(\neq\frac{1}{2})$. Further the magnetic moment μ_0 of the ground (intrinsic) state is related to these gyromagnetic factors and the ground state spin I_0 by

$$\mu_0 = \{I_0^2/(I_0+1)\}(g_K-g_R)+I_0g_R. \qquad (3)$$

From these relations, with the measured magnetic moment [12]) $\mu_0 = -0.30$ n.m., the gyromagnetic factors are obtained with the sign undetermined. The relative phase of the E2/M1 amplitude δ_2 is the same as the sign of the ratio of g_K-g_R and the intrinsic quadrupole moment Q_0. The intrinsic quadrupole moment Q_0 is deduced with its sign from the measured [12]) hyperfine structure value of $Q = +1.1$ b and from the formula

$$Q_0 = Q\Big/\left[\frac{I_0(2I_0-1)}{(I_0+1)(2I_0+3)}\right]$$

to be +5.5 b. Since from the present angular correlation measurement δ_2 has been determined to be -0.2, the difference g_K-g_R must be negative, so that

the gyromagnetic factors are $g_K = -0.52$ and $g_R = +0.28$. These values derived from the properties of the 60 keV transition are to be compared with $g_K = -0.54 \pm 0.05$ and $g_R = +0.34 \pm 0.07$ derived from the properties of the 86 keV cascade from the 146 keV level in Coulomb excitation experiments [13]). The value $|g_R| = Z/A = 0.41$ corresponding to the rotational motion of uniformly charged nuclear matter is much larger than the observed value, as in the case of many other nuclei [13]).

From the simple geometrical relations anticipated [14]) by the unified model for the ratio of the reduced probabilities of transitions from an intrinsic state to members of a rotational band, the relative intensities [2]) of gamma-rays from 87 keV and 105 keV intrinsic states to the 60 keV and ground state may be utilised for a further check of the predictions of the model. Thus, we have

$$\gamma_{27}/\gamma_{87} = \frac{T(\mathrm{E1}; \frac{5}{2}\,\frac{5}{2}^{+} \to \frac{5}{2}\,\frac{3}{2}^{-})}{T(\mathrm{E1}; \frac{5}{2}\,\frac{5}{2}^{+} \to \frac{3}{2}\,\frac{3}{2}^{-})}$$

$$= 00{,}3\,\frac{\langle \frac{5}{2}\,1\,\frac{5}{2}\,1|\frac{5}{2}\,1\,\frac{5}{2}\,\frac{3}{2}\rangle^2}{\langle \frac{5}{2}\,1\,\frac{5}{2}\,1|\frac{5}{2}\,1\,\frac{3}{2}\,\frac{3}{2}\rangle^2} = 0.013, \qquad (4)$$

which is to be compared with the experimental value[2]) of 0.005 ± 0.001. Similarly, the value

$$\gamma_{45}/\gamma_{105} = \frac{T(\mathrm{E1}; \frac{3}{2}\,\frac{3}{2}^{+} \to \frac{5}{2}\,\frac{3}{2}^{-})}{T(\mathrm{E1}; \frac{3}{2}\,\frac{3}{2}^{+} \to \frac{3}{2}\,\frac{3}{2}^{-})} = 0.060$$

is to be compared with the experimental value of 0.036 ± 0.006 based on the value of Boehm and others [7]). In both cases the experimental values are lower than theoretical expectations much beyond experimental errors. This further implies particle-rotation couplings [15]) which lead to a partial breakdown of the adiabatic approximation and which appear to be the cause of the enhancement of the energy ratio E_2/E_1 of the members of the ground state rotational band.

Thus, the relative intensities of gamma-rays, coincidences and angular correlation measurements of the present work have brought out a few features of the nuclear properties more clearly.

I am very thankful to Professor B. V. Thosar for some discussions and continued interest.

References

1) B. N. Subba Rao, Nuovo Cim. **16** (1960) 283
2) B. N. Subba Rao, to be published
3) B. N. Subba Rao, Nuclear Physics, submitted
4) J. Juliano, UCRL 3733

5) E. M. Bernstein and H. W. Lewis, Phys. Rev. **105** (1957) 1524;
J. H. Bjerrgaard and V. Meyer-Berkhout, Z. Naturforsch. **11** (1956) 273;
J. De Boer, M. Martin and P. Marmier, Helv. Phys. Acta. **32** (1959) 377
6) H. Harmatz *et al.*, Phys. Rev. **114** (1959) 1082
7) F. Boehm *et al.*, Bull. Amer. Phys. Soc. **2** (1957) 231
8) B. R. Mottelson and S. G. Nillsson, Mat. Fys. Skr. Dan. Vid. Selsk. **1**, No. 8 (1958)
9) M. Vergnes, Compt. Rendus **248** (1959) 1158
10) B. I. Deutch, F. R. Metzger and F. J. Wilhelm, Nuclear Physics **16** (1960) 81
11) K. Alder *et al.*, Rev. Mod. Phys. **28** (1956) 432
12) D. Strominger *et al.*, Rev. Mod. Phys. **30** (1958) 735
13) E. M. Bernstein and J. De Boer, Nuclear Physics **18** (1960) 740
14) G. Alaga *et al.*, Mat. Fys. Medd. Dan. Vid. Selsk. **29**, No. 9 (1955)
15) A. Kerman, Mat. Fys. Medd. Dan. Vid. Selsk. **30**, No. 15 (1955)

9.B

Nuclear Physics **28** (1961) 512—518; © *North-Holland Publishing Co., Amsterdam*

Not to be reproduced by photoprint or microfilm without written permission from the publisher

MULTIPLE COULOMB SCATTERING FROM FINITE NUCLEI

M. A. MEYER

Department of Physics, Potchefstroom University for C.H.E., Potchefstroom, South Africa

Received 2 June 1961

Abstract: A general expression is derived for the multiple Coulomb scattering of charged particles by finite nuclei. This expression is valid for any charge distribution in the nucleus. The general expression is integrated by assuming Olbert's form factor and more realistic ones.

1. Introduction

The existing theories of multiple Coulomb scattering by Olbert [1]), Cooper and Rainwater [2]) and Ter-Mikaelyan [3]), which take into account the effect of screening of the Coulomb field of the nucleus by the atomic electrons and the effect of the finite size of the nucleus, are restricted to the calculation of the distribution of the projected angle of scattering. The distribution of spatial angles is potentially more interesting because of the absence of blurring which is introduced when projected angles are measured. It is the purpose of this paper to obtain a general scattering distribution in terms of the spatial angle of scattering also including the effect of screening and nuclear extension and restricting the calculations to situations where the small angle approximation $\sin x = x$ is valid as in the theories mentioned above.

It will be assumed that the single scattering law is of the Rutherford type for a wide middle region, but modified at small angles by electron screening and at large angles by the finite dimensions of the nucleus. The Molière [4]) single scattering probability for a screened point nucleus will be assumed and modified to include the effect of the finite dimensions of the nucleus. Molière's derivation of the single scattering probability is based on the Fermi-Thomas charge distribution of the atomic electrons and does not involve restrictions resulting from the use of the first Born-approximation. In terms of Molière's theory, one may write the probability $f(\chi)\chi\mathrm{d}\chi$, that a particle will suffer a deflection through a spatial angle between χ and $\chi+\mathrm{d}\chi$ as a result of a single deflection occurring in a thickness of t g/cm^2 of scattering material as

$$f(\chi)\chi\mathrm{d}\chi = 2\chi_c^2\chi\mathrm{d}\chi/(\chi^2+\chi_a^2)^2, \tag{1.1}$$

where

$$\chi_c = \frac{Zze^2}{pc\beta}\sqrt{\frac{4\pi N_0 t}{A}}, \tag{1.2}$$

$$\chi_a^2 = \chi_0^2(1.13+3.76\alpha^2), \qquad \chi_0 = \lambda\!\!\!^{-}/a, \qquad \alpha = Zze^2/\hbar v. \tag{1.3}$$

Here, N_0 is Avogadro's number, A the atomic weight of the scatterer, Ze the nuclear charge of the scattering atom, ze the charge of the scattered particle of momentum p and velocity $v = \beta c$; further $2\pi\lambda\!\!\!^{-}$ is the de Broglie wavelength of the scattered particle and a the Fermi-Thomas radius of the atom. The numbers 1.13 and 3.76 in the expression for χ_a arise from an empirical fit to a Thomas-Fermi single-scattering calculation. It is seen that $f(\chi)\chi\,d\chi$ is essentially the Rutherford formula when $\chi \gg \chi_a$ and changes more or less rapidly when $\chi \approx \chi_a$.

The effect of the nuclear dimensions may be taken into account by multiplying (1.1) by a nuclear form factor $q(\chi/\chi_n)$ where $\chi_n \approx \lambda\!\!\!^{-}/r_n$, the quantity r_n being of the order of the nuclear radius. The function $q(\chi/\chi_n)$ must have the following properties:

$$q = 1 \quad \text{when} \quad \chi/\chi_n \ll 1, \qquad q \ll 1 \quad \text{when} \quad \chi/\chi_n \gg 1,$$

with a rapid change occurring at $2\chi_n$.

2. General Expression for Multiple Scattering Distribution

The multiple scattering from finite nuclei will be treated as a correction to the Molière theory [5]) of multiple scattering. Following Molière, we introduce a quantity $\Omega(\eta)$ by means of the Bessel function J_0, such that

$$\Omega(\eta) = \int_0^\infty J_0(\eta\chi)q(\chi/\chi_n)f(\chi)\chi\,d\chi. \tag{2.1}$$

Setting $q = 1+(q-1)$ and substituting (1.1) for $f(\chi)\chi\,d\chi$, one obtains

$$\Omega(\eta) = 2\chi_c^2\left[\int_0^\infty \frac{J_0(\eta\chi)\chi\,d\chi}{(\chi^2+\chi_a^2)^2} + \int_0^\infty \frac{J_0(\eta\chi)\chi\,d\chi}{(\chi^2+\chi_a^2)^2}(q-1)\right],$$

and hence

$$\Omega(\eta)-\Omega(0) = 2\chi_c^2\left[\int_0^\infty \frac{J_0(\eta\chi)-1}{(\chi^2+\chi_a^2)^2}\chi\,d\chi + \int_0^\infty \frac{J_0(\eta\chi)-1}{(\chi^2+\chi_a^2)^2}(q-1)\chi\,d\chi\right]. \tag{2.2}$$

The first integral is the appropriate integral for a screened point nucleus which was treated by Molière [5]) and Bethe [6]); they have shown that to sufficient accuracy, it may be written as

$$2\chi_c^2\int_0^\infty \frac{J_0(\eta\chi)-1}{(\chi^2+\chi_a^2)^2}\chi\,d\chi = \tfrac{1}{4}\chi_c^2\eta^2 \ln\left[\frac{\chi_a^2\gamma^2}{e}\cdot\tfrac{1}{4}\eta^2\right],$$

where $\ln\gamma$ is Euler's constant and $\ln e = 1$. The second integral in (2.2) represents a correction to the Molière theory as a result of the finite size of the nucleus. Substituting the above value for the first integral in (2.2), one obtains

$$\Omega(\eta)-\Omega(0) = \chi_c^2\left[\tfrac{1}{4}\eta^2 \ln\left(\frac{\chi_a^2\gamma^2}{e}\cdot\tfrac{1}{4}\eta^2\right) + 2\int_0^\infty \frac{J_0(\eta\chi)-1}{(\chi^2+\chi_a^2)^2}(q-1)\chi\,d\chi\right]. \tag{2.3}$$

The multiple scattering distribution $F(\varphi, t)$, defined in such a manner that $F(\varphi, t)\,\varphi\,\mathrm{d}\varphi$ represents the number of particles in the angular interval $\mathrm{d}\varphi$ at an angle φ after traversing a thickness t, is given by

$$F(\varphi, t)\varphi\,\mathrm{d}\varphi = \varphi\,\mathrm{d}\varphi\int_0^\infty \eta\,\mathrm{d}\eta J_0(\eta\varphi)\mathrm{e}^{\Omega(\eta)-\Omega(0)}. \tag{2.4}$$

This equation, which was first obtained by Bothe[7]) and later by Molière[5]) and Bethe[6]), holds when the deflections are small and is valid for any single scattering probability.

Introducing with Molière a new dimensionless parameter B defined by the transcendental equation

$$B = -\ln\left[\frac{\chi_a^2\gamma^2}{\mathrm{e}}\,\frac{1}{B\chi_c^2}\right] \tag{2.5}$$

and transforming simultaneously the variables χ, φ and η into the new variables

$$x = \chi/\chi_c\sqrt{B}, \qquad \theta = \varphi/\chi_c\sqrt{B}, \qquad y = \eta\chi_c\sqrt{B}, \tag{2.6}$$

eq. (2.4) may be written as

$$F(\varphi, t)\varphi\,\mathrm{d}\varphi = \theta\,\mathrm{d}\theta\int_0^\infty y\,\mathrm{d}y J_0(\theta y)\mathrm{e}^{s(y)}, \tag{2.7}$$

where

$$s(y) = \Omega\left(\frac{y}{\chi_c\sqrt{B}}\right) - \Omega(0) = -\tfrac{1}{4}y^2 + \frac{1}{B}\left[\tfrac{1}{4}y^2\ln\left(\tfrac{1}{4}y^2\right) + I(y)\right], \tag{2.8}$$

$$I(y) = 2\int_0^\infty \frac{J_0(xy)-1}{(x^2+x_a^2)^2}(q-1)x\,\mathrm{d}x, \tag{2.9}$$

and $x_a = \chi_a/\chi_c\sqrt{B}$. Since B is appreciably larger than unity, we can expand the exponential in (2.7) in powers of $1/B$ and neglect terms containing higher orders than the first. This yields

$$F(\varphi, t)\varphi\,\mathrm{d}\varphi = \theta\,\mathrm{d}\theta\left[f^{(0)}(\theta) + \frac{1}{B}\{f^{(1)}(\theta) - K(\theta, x_n)\}\right] \tag{2.10}$$

for the multiple scattering distribution. In this expression $x_n = \chi_n/\chi_c\sqrt{B}$ and

$$f^{(0)}(\theta) = \int_0^\infty y\,\mathrm{d}y J_0(\theta y)\mathrm{e}^{-\frac{1}{4}y^2} = 2\mathrm{e}^{-\theta^2},$$

$$f^{(1)}(\theta) = \int_0^\infty y\,\mathrm{d}y J_0(\theta y)\mathrm{e}^{-\frac{1}{4}y^2}\left(\tfrac{1}{4}y^2\ln\left(\tfrac{1}{4}y^2\right)\right),$$

$$K(\theta, x_n) = 2\int_0^\infty y\,\mathrm{d}y J_0(\theta y)\mathrm{e}^{-\frac{1}{4}y^2}\int_0^\infty \frac{J_0(xy)-1}{(x^2+x_a^2)^2}\{1-q(x/x_n)\}x\,\mathrm{d}x.$$

It is easily seen that the expression (2.10) for the function $F(\varphi, t)$ is normalized in such a way that $\int_0^\infty F(\varphi, t)\varphi\,\mathrm{d}\varphi = 1$. The first term in (2.10) is the well-known Gaussian which arises from a great number of small deflections, the second term represents

the effect of single scattering and the third term describes the effect of the nuclear extension. For a point nucleus one has $q(x/x_n) = 1$ and hence $K(\theta, x_n) = 0$. Consequently, we have

$$F(\varphi, t)\varphi \mathrm{d}\varphi = \theta \mathrm{d}\theta \left[2\mathrm{e}^{-\theta^2} + \frac{1}{B} f^{(1)}(\theta) \right], \tag{2.11}$$

which is Molière's function without the second order term. Molière and Bethe have tabulated values of the function $f^{(1)}(\theta)$.

We now return to the correction function $K(\theta, x_n)$ which may be written as

$$K(\theta, x_n) = 2\int_0^\infty \frac{1-q(x/x_n)}{(x^2+x_a^2)^2} \left[\int_0^\infty y \mathrm{d}y J_0(\theta y) J_0(xy) \mathrm{e}^{-\frac{1}{4}y^2} - \int_0^\infty y \mathrm{d}y J_0(\theta y) \mathrm{e}^{-\frac{1}{4}y^2} \right]$$

$$= 4\mathrm{e}^{-\theta^2} \int_0^\infty \frac{1-q(x/x_n)}{(x^2+x_a^2)^2} [\mathrm{e}^{-x^2} I_0(2\theta x) - 1] x \mathrm{d}x,$$

where I_0 is the modified Bessel function of the first kind. Since q starts to differ from unity when $x \gg x_a$ and since

$$I_0(2\theta x) = 1 + \frac{(\theta x)^2}{(1!)^2} + \frac{(\theta x)^4}{(2!)^2} + \ldots,$$

one obtains for $K(\theta, x_n)$ the following result:

$$K(\theta, x_n) = 4\mathrm{e}^{-\theta^2} \sum a_{2\nu} \theta^{2\nu}, \tag{2.12}$$

where

$$a_0 = \int_0^\infty (1-q) x^{-3} (\mathrm{e}^{-x^2} - 1) \mathrm{d}x,$$

$$a_{2\nu} = \frac{1}{(\nu!)^2} \int_0^\infty (1-q) x^{2\nu-3} \mathrm{e}^{-x^2} \mathrm{d}x, \qquad \nu = 1, 2, \ldots.$$

The expression (2.10) becomes inaccurate for large θ since the difference between two almost equal numbers is then used to find a small number. This can be avoided by expanding Molière's expression for $f^{(1)}(\theta)$,

$$f^{(1)}(\theta) = 2\mathrm{e}^{-\theta^2} \{(\theta^2 - 1)[\bar{\mathrm{E}}\mathrm{i}(\theta^2) - \ln \theta^2] + 2 - \mathrm{e}^{-\theta^2}\}$$

$$= 2\mathrm{e}^{-\theta^2} \left(b_0 + b_2 \theta^2 + \sum_{\nu=2}^{\infty} b_{2\nu} \theta^{2\nu} \right), \tag{2.13}$$

where

$$b_0 = 0.423, \qquad b_2 = -1.423, \qquad b_{2\nu} = \frac{(\nu-2)!}{(\nu!)^2}, \qquad \nu \geqq 2.$$

Finally, combining (2.12) and (2.13) with (2.10) one obtains for the multiple scattering distribution, including the effect of the finite size of the nucleus,

$$F(\varphi, t)\varphi \mathrm{d}\varphi = 2\mathrm{e}^{-\theta^2} \theta \mathrm{d}\theta \left[1 + \frac{1}{B} \left(c_0 + c_2 \theta^2 + \sum_{\nu=2}^{\infty} c_{2\nu} \theta^{2\nu} \right) \right], \tag{2.14}$$

where

$$c_0 = 0.423+2\int_0^\infty (1-q)(1-e^{-x^2})x^{-3}dx, \tag{2.15}$$

$$c_2 = -1.423-2\int_0^\infty (1-q)e^{-x^2}x^{-1}dx, \tag{2.16}$$

$$c_{2\nu} = \frac{(\nu-2)!}{(\nu!)^2} - \frac{2}{(\nu!)^2}\int_0^\infty (1-q)x^{2\nu-3}e^{-x^2}dx$$

$$= \frac{2}{(\nu!)^2}\int_0^\infty qx^{2\nu-3}e^{-x^2}dx, \qquad \nu \geqq 2. \tag{2.17}$$

The eq. (2.14) is valid for any nuclear form factor. The constants c_0, c_2 and $c_{2\nu}$ depend on the assumed form factor.

3. Olbert's Form Factor

Olbert assumed a step-function for q such that

$$q(\chi/\chi_n) = \begin{cases} 1 & \text{for } \chi/\chi_n \leqq 1, \\ 0 & \text{for } \chi/\chi_n > 1, \end{cases} \tag{3.1}$$

where $\chi_n = (\lambda\!\!\!^{-}/r_n)[1.13+3.76\alpha^2]^{\frac{1}{2}}$. This assumption leads to a gross underestimate of the scattering. However, Olbert's distribution has in the past been used as a lower limit in muon scattering experiments, and furthermore, some experiments on muon scattering in the momentum range 200—600 MeV/c appear to agree with this distribution [8, 9]). In view of this, Olbert's assumption is of some interest.

The constants (2.16) and (2.17), using Olbert's form factor, are given by

$$c_0 = 0.423+\frac{(1-e^{-x_n^2})}{x_n^2} - \mathrm{Ei}(-x_n^2), \qquad c_2 = -1.423+\mathrm{Ei}(-x_n^2), \tag{3.2}$$

$$c_{2\nu} = \frac{(\nu-2)!}{(\nu!)^2} I(x_n^2, \nu-2),$$

where $-\mathrm{Ei}(-u) = \int_u^\infty e^{-t}dt/t$ is the exponential integral and

$$p!I(u, p) = \int_0^u t^p e^{-t}dt$$

is the incomplete gamma-function [10]).

4. Realistic Form Factors

The effect of nuclear extension can be taken into account in a more realistic way by writing the nuclear form factor in the usual form

$$q(\chi/\chi_n) = q_e(\chi/\chi_n)+Z^{-1}[1-q_e(\chi/\chi_n)].$$

The first term represents elastic coherent scattering by the nucleus as a whole while the second term represents the inelastic scattering by individual protons. Various estimates for q_c are available. Using the Born-approximation, Williams [11]) showed that

$$q_c(\chi/\chi_n) = \left[1+\left(\frac{\chi}{2\chi_n}\right)^2\right]^{-2} \tag{4.2}$$

for a potential of the form $(Ze^2/r)\{1-\exp(-2r/r_n)\}$, for which the charge density is rather strongly peaked about $r = 0$. Rose [12]) has evaluated in the Born-approximation the form factor for a nucleus of uniform charge density and found

$$q_c(\chi/\chi_n) = \frac{9}{(\chi/\chi_n)^4}\left[\frac{\sin(\chi/\chi_n)}{\chi/\chi_n} - \cos(\chi/\chi_n)\right]^2. \tag{4.3}$$

Cooper and Rainwater noted that in exact calculations the diffraction minima of this expression are greatly reduced in magnitude and assumed for q_c the values 1.00, 0.82, 0.50 and 0.15 when $\chi/\chi_n = 0, 1, 2$, and 3, to approximate the form (4.3). A smooth curve through these points is joined smoothly to $q_c = 12/(\chi/\chi_n)^4$ for $\chi/\chi_n \geqq 4$. These values were chosen by Cooper and Rainwater in such a way as not to underestimate the multiple scattering of muons. A few values for q_c are shown in table 1 from which it follows that $\exp[-0.2(\chi/\chi_n)^2]$ is a very reasonable approximation for Cooper and Rainwater's values for q_c in view of the uncertainty concerning the exact form for the true q_c. This approximation is adequate for not too large χ/χ_n.

TABLE 1

Values for the function q_c

χ/χ_n	0	1	2	3	4	5	6
Williams	1.00	0.64	0.25	0.09	0.04	0.02	0.01
Cooper *et al.*	1.00	0.82	0.50	0.15	0.05	0.02	0.01
$\exp[-0.2(\chi/\chi_n)^2]$	1.00	0.82	0.45	0.16	0.04	0.01	0.00

In general, if q_c can be approximated by $\exp[-a(x/x_n)^2]$, we have

$$\begin{aligned} c_0 &= 0.423 - \left(1-\frac{1}{Z}\right)\left[\frac{a}{x_n^2}\ln\frac{a}{x_n^2} - \left(1+\frac{a}{x_n^2}\right)\ln\left(1+\frac{a}{x_n^2}\right)\right], \\ c_2 &= -1.423 - \left(1-\frac{1}{Z}\right)\ln\left(1+\frac{a}{x_n^2}\right), \\ c_{2\nu} &= \frac{(\nu-2)!}{(\nu!)^2}\left[\frac{1}{Z} + \left(1-\frac{1}{Z}\right)\left(1+\frac{a}{x_n^2}\right)^{1-\nu}\right], \qquad \nu = 2, 3.\ldots. \end{aligned} \tag{4.5}$$

The above formulae present a simple method for determining the constant a from experiment. Cooper and Rainwater's distribution is obtained when $a = 0.2$.

This work forms part of a project for which financial assistance was obtained from the South African Council for Scientific and Industrial Research.

References

1) S. Olbert, Phys. Rev. **87** (1952) 319
2) L. N. Cooper and J. Rainwater, Phys. Rev. **97** (1955) 492
3) M. L. Ter-Mikaelyan, JETP (Soviet Physics) **9** (1959) 177
4) G. Molière, Z. f. Natur. **2a** (1947) 133
5) G. Molière, Z. f. Natur. **3a** (1948) 78
6) H. A. Bethe, Phys. Rev. **89** (1953) 1256
7) W. Bothe, Handbuch der Physik, vol. **22** (Springer Verlag, Berlin, 1933) p. 1
8) G. N. Fowler and A. W. Wolfendale, Progress in cosmic ray physics vol. **III** (1958) 107.
9) W. F. Nash and A. J. Poynton, Nuovo Cim. **9** (1958) 412
10) K. Pearson, Tables of the incomplete gamma-function (Cambridge University Press, 1946)
11) E. J. Williams, Proc. Roy. Soc. **169** (1939) 531
12) M. E. Rose, Phys. Rev. **73** (1948) 279

8.B

Nuclear Physics **28** (1961) 519—523; © *North-Holland Publishing Co., Amsterdam*

Not to be reproduced by photoprint or microfilm without written permission from the publisher

ON THE ANALYSIS OF THE REACTION $\pi^- + p \to \Lambda^0 + K^0$

R. J. N. PHILLIPS

A.E.R.E., Harwell, England

Received 20 May 1961

Abstract: A modified partial wave method is suggested, in which K′ and Σ pole terms describe the higher waves. It appears that the s- and p- wave amplitudes must still be found empirically, even fairly close to threshold.

1. Introduction

It has been suggested [1, 2]) that the $\pi^- + p \to \Lambda^0 + K^0$ differential cross section can be largely explained by a pole in the amplitude, due to a virtual K′ process (when this K—π resonant state [3]) is treated as a particle). There should also be another pole [4]), due to a virtual Σ, though there is no evidence yet that it is important.

Now such pole terms alone give no Λ^0 polarization (as already remarked by Gell-Mann [5]), but large values are observed, so that there must be other important contributions to the amplitude. Since the latter are presumably associated with more distant singularities, however, we may still expect the poles to dominate the higher partial waves.

This suggests that a sound way to exploit the poles is a modified partial wave analysis, in which higher partial amplitudes are predicted (or at least described compactly) by the poles, in terms of one or two coupling constants. The lower partial amplitudes are to be found empirically. This is analogous to the modified phase-shift analysis of N—N scattering, due to Moravcsik [6]).

The present note is to propose such a modified partial wave method, and to discuss its application and possible advantages. It appears that even for fairly low energies in the final state, both s- and p-wave amplitudes must still be found empirically. However, the poles should be useful in giving the higher partial amplitudes, which are detectable even at lower energies [7]). They should also serve to resolve some ambiguities in the ordinary analysis and to fix the overall phase of the amplitude.

A similar approach may be useful for other two-body production channels, such as $\Sigma + K$.

2. The Production Amplitude

The present evidence [8]) suggests that the ΛK parity is odd. Then the produc-

tion amplitude M, a 2×2 matrix in spin space, has the form

$$M = G+iH\sin\theta\,\boldsymbol{\sigma}\cdot\mathbf{n}, \tag{1}$$

and the cross section $\sigma_\Lambda(\theta)$ and Λ^0 polarization $P_\Lambda(\theta)$ are

$$\begin{aligned}\sigma_\Lambda(\theta) &= |G|^2+|H|^2\sin^2\theta,\\ P_\Lambda(\theta) &= 2\,\mathrm{Im}\,(GH^*)\sin\theta/\sigma_\Lambda(\theta).\end{aligned} \tag{2}$$

Here, θ is the c.m. angle of Λ relative to π, G and H are functions of energy and $\cos\theta$, the quantity $\boldsymbol{\sigma}$ denotes the Pauli spin matrices and the polarization is in the direction of $\mathbf{n} = \mathbf{p}_\pi\times\mathbf{p}_\Lambda/|\mathbf{p}_\pi\times\mathbf{p}_\Lambda|$, where $\mathbf{p}_\pi$ and $\mathbf{p}_\Lambda$ are the c.m. momenta of π and Λ.

In general $\sigma_\Lambda(\theta)$ and $P_\Lambda(\theta)$ do not determine M. However, if only s and p waves are assumed, they are enough to fix M within certain ambiguities [5, 9]) and an overall phase. For this case, $G = a+b\cos\theta$ and $H = c$, where a, $-\frac{1}{3}(b-2c)$ and $-\frac{1}{3}(b+c)$ are the $s_{\frac12}$, $p_{\frac12}$ and $p_{\frac32}$ amplitudes, within a trivial factor.

3. The Pole Contributions

The K′ spin is not yet certain; there are arguments [1, 2, 8, 10]) both for spin 0 and for spin 1; therefore we consider both possibilities. The isobaric spin appears [3]) to be $\frac12$.

For scalar K′, suppose the Lagrangian density contains the couplings [1])

$$2m_K f_1\bar{\mathrm{K}}\boldsymbol{\tau}\cdot\boldsymbol{\pi}\mathrm{K}'+f_2\bar{\mathrm{K}}'\bar{\Lambda}\mathrm{N}+\mathrm{h.c.}, \tag{3a}$$

in an obvious symbolic notation, where f_1 and f_2 are dimensionless coupling constants and we use units $\hbar = c = 1$.

Alternatively, for vector K′, suppose the couplings are [2])

$$if_3\left(\frac{\partial\bar{\mathrm{K}}}{\partial x_\mu}\boldsymbol{\tau}\cdot\boldsymbol{\pi}-\bar{\mathrm{K}}\boldsymbol{\tau}\cdot\frac{\partial\boldsymbol{\pi}}{\partial x_\mu}\right)\mathrm{K}'_\mu+if_4\bar{\mathrm{K}}'_\mu\bar{\Lambda}\gamma_\mu\mathrm{N}+\mathrm{h.c.} \tag{3b}$$

Suppose also that Σ has couplings

$$f_5\bar{\Lambda}\Gamma\boldsymbol{\Sigma}\cdot\boldsymbol{\pi}+f_6\bar{\boldsymbol{\Sigma}}\Gamma\bar{\mathrm{K}}\boldsymbol{\tau}\mathrm{N}+\mathrm{h.c.}. \tag{3c}$$

where we take Σ to have spin $\frac12$ and Γ stands for 1 or $i\gamma_5$ according as the $\Lambda\Sigma$ parity is odd or even.

In Born approximation, the corresponding pole terms in M are

$$\frac{f_1f_2}{4\pi}\frac{2Cm_K}{\Delta+m_{K'}^2}\{r_\Lambda r_p+p_\pi p_\Lambda(\cos\theta-i\sin\theta\,\boldsymbol{\sigma}\cdot\mathbf{n})\}, \tag{4a}$$

$$\frac{f_3 f_4}{4\pi}\frac{C}{\Delta+m_{K'}^2}\{r_\Lambda r_p(m_\Lambda+m_p-2E)+p_\pi p_\Lambda(m_\Lambda+m_p+2E)(\cos\theta-i\sin\theta\,\boldsymbol{\sigma}\cdot\mathbf{n})$$
$$-m_K^{-2}(m_K^2-m_\pi^2)(m_\Lambda-m_p)[r_\Lambda r_p+p_\pi p_\Lambda(\cos\theta-i\sin\theta\,\boldsymbol{\sigma}\cdot\mathbf{n}]\}, \quad (4b)$$

$$\frac{f_5 f_6}{4\pi}\frac{C}{\Delta'+m_\Sigma^2}\{r_\Lambda r_p(m_\Lambda+m_p\pm m_\Sigma-E)$$
$$+p_\pi p_\Lambda(m_\Lambda+m_p\pm m_\Sigma+E)(\cos\theta-i\sin\theta\,\boldsymbol{\sigma}\cdot\mathbf{n})\}, \quad (4c)$$

taking the upper (lower) sign in (4c) for $\Lambda\Sigma$ parity odd (even). In the above formulae, m_i, p_i, E_i denote the mass, c.m. momentum and total c.m. energy of particle i, and $r_i = E_i + m_i$, while $E = E_\pi + E_p = E_\Lambda + E_K$. Further, Δ and Δ' are the invariant squares of momentum transfer and C is a kinematical constant:

$$\Delta = 2E_\pi E_K - m_\pi^2 - m_K^2 + 2p_\pi p_\Lambda \cos\theta, \quad (5)$$

$$\Delta' = 2E_\pi E_\Lambda - m_\pi^2 - m_\Lambda^2 - 2p_\pi p_\Lambda \cos\theta, \quad (6)$$

$$C = \sqrt{p_\Lambda / 2E^2 p_\pi r_p r_\Lambda}. \quad (7)$$

Assuming the theory can be renormalized, higher-order corrections to the K′ and Σ-exchange processes replace the bare coupling constants f_i by renormalized constants. This applies strictly only to the residues at the poles themselves; additional unknown polynomials in Δ or Δ' also result (multiplied by suitable spinor matrix elements). Simply to take the Born approximation (4) with renormalized constants implies an assumption about these polynomials. Different forms of bare coupling † give Born approximations which differ essentially by polynomials like these, and lead naturally to different assumptions about the renormalized pole term.

For later discussion, we now record the form of the pole terms (4) for pion lab. momentum 1.12 GeV/c. Within various trivial constants, they are

$$[1+0.04(\cos\theta-i\sin\theta\,\boldsymbol{\sigma}\cdot\mathbf{n})]/(3.4+\cos\theta), \quad (8a)$$

$$[1-0.15(\cos\theta-i\sin\theta\,\boldsymbol{\sigma}\cdot\mathbf{n})]/(3.4+\cos\theta), \quad (8.b)$$

$$[1\ {}^{+0.13}_{-0.12}(\cos\theta-i\sin\theta\,\boldsymbol{\sigma}\cdot\mathbf{n})]/(4.4-\cos\theta). \quad (8c)$$

4. Discussion

At energies not far above threshold, an s and p-wave analysis suggests itself; such analyses have been reported [5]) by the Berkeley and Columbia groups, at or near pion momentum 1.12 GeV/c. However, there is now evidence [7]) of higher waves in this region. We may hope that pole terms will describe them

† E.g. Chan [3]) suggests various gradient $KK'\pi$ couplings, for scalar K′.

adequately, which would certainly be helpful, but there are not enough data available to allow a decision.

The poles would be even more helpful if they also described the p-waves, leaving only the s-wave free. This we now discuss.

For convenience, let us denote the pole terms by $M_P = G_P + iH_P \sin\theta\, \boldsymbol{\sigma}\cdot\mathbf{n}$. If the s-wave is arbitrary, the amplitude also contains an arbitrary constant $A_R + iA_I$ (see sect. 2). The quantities G_P, H_P, A_R and A_I are real. Then we have

$$\sigma_A(\theta)P_A(\theta) = 2A_I H_P \sin\theta, \qquad \sigma_A(\theta) = (A_R+G_P)^2 + A_I^2 + H_P^2 \sin^2\theta. \quad (9)$$

For P_A to be very large at a given angle, both A_I and $H_P \sin\theta$ must be of the same order of magnitude and $A_R + G_P$ must be rather smaller. Clearly we can arrange for P_A to be very large at any particular angle, by judicious choice of A_R and A_I. However, since G_P and H_P both vary with angle, P_A cannot remain large over wide ranges of angle if H_P is much smaller than G_P. Furthermore, since we have to rely on G_P to produce the large observed ratio of $\sigma_A(180°)/\sigma_A(0°)$, it is clear that this term must not be dwarfed by A_R and A_I.

Now the data in refs. [5, 8]) for this energy region show that P_A is large (≈ 0.5 or more) over wide ranges of angle and that the ratio $\sigma_A(180°)/\sigma_A(0°)$ is 5 or more. Without going into more detail, we can already see that any possible combination of the pole terms (8) plus an arbitrary S-wave amplitude are inadequate. The most favourable case, (8b) alone, cannot give P_A much above 0.3, over a small range of angles, without violating the $\sigma_A(180°)/\sigma_A(0°)$ ratio.

The crucial point here is the small value of H_P compared to G_P. For the scalar K′ case, this is a property of the Λ-p spinor matrix element, which multiplies any unknown polynomial arising from renormalization. Our conclusions therefore hold also for the other scalar K′ interactions suggested by Chan [2]).

A briefer and more general argument can be made — though it is also less conclusive. Since the poles in (8) are some way from the physical range of $\cos\theta$, an expansion of M in partial waves should converge quite fast †, and the s+p wave analyses should not be very misleading. Now both published analyses [5]) agree in assigning a big phase difference to $p_{\frac{1}{2}}$ and $p_{\frac{3}{2}}$ amplitudes, whereas pole contributions would have the same phase. It therefore seems unlikely that any pole terms can adequately represent the p-wave amplitudes.

Beside giving higher partial amplitudes, the poles should help to resolve some ambiguities [5, 9]) in the ordinary s and p wave analysis. For if enough higher-wave effects were detectable in σ_A and P_A, the "s plus p plus pole" analysis would be overdetermined. Of course, this may not be easy in practice. For instance, if G_1 and H_1 fit σ_A and P_A, so do $G_2 = G_1^*$ and $H_2 = -H_1^*$; it would

† E.g. in (eq. 8a), s and p waves account for G_P within 6 % and H_P within 30 %.

be hard to resolve this "phase ambiguity" if H_p were rather small, as in the scalar K′ case.

By providing terms of known phase, the poles should also fix the overall phase of M, at least within π. Incidentally, the phase relations suggested by Amati and Vitale [11, 9]) could then be more closely tested.

Finally, this modified partial wave method should give information about the renormalized coupling constants concerned, and could in principle help to determine the K′ spin and $\Lambda\Sigma$ parity.

References

1) J. Tiomno, A. L. L. Videira and N. Zagury, Phys. Rev. Lett. **6** (1961) 120
2) C.-H. Chan, Phys. Rev. Lett. **6** (1961) 383
3) M. Alston, L. W. Alvarez, P. Eberhard, M. L. Good, W. Graziano, H. K. Ticho and S. G. Wojcicki, Phys. Rev. Lett. **6** (1961) 300
4) J. G. Taylor, Nuclear Physics **9** (1959) 357
5) Proc. Conf. High Energy Physics, CERN, 1958
6) P. Cziffra, M. H. MacGregor, M. J. Moravcsik and H. P. Stapp, Phys. Rev. **114** (1959) 880
7) M. Schwartz, Proc. Conf. Strong Interactions, Berkeley, 1960 (published in Rev. Mod. Phys. **33** (1961) 436)
8) Proc. Conf. High Energy Physics, Rochester, 1960
9) R. J. N. Phillips, Nuclear Physics **23** (1961) 345
10) M. A. B. Bég and P. C. De Celles, Phys. Rev. Lett. **6** (1961) 145, 428
11) D. Amati and B. Vitale, Nuovo Cim. **9** (1958) 340

2.I: 3.A

Nuclear Physics **28** (1961) 524—528; © *North-Holland Publishing Co., Amsterdam*

Not to be reproduced by photoprint or microfilm without written permission from the publisher

TWO-PHOTON DECAY AND THE LIFETIME OF GIANT RESONANCE STATES

B. MARGOLIS †

Physics Department, The Ohio State University, Columbus, Ohio ††

Received 6 June 1961

Abstract: The relative probability for two-photon decay in a low energy 0^+–0^+ transition is shown to be related to the lifetime of the 1^- states of these nuclei in the giant resonance region. Estimates of this lifetime are made using nuclear reaction theory. Comparison of the resulting two-photon decay probability is made with experiment.

Recently [1, 2]) Ericson has pointed out the connection between the lifetime of excited states of a nucleus and fluctuations in reaction cross sections in the continuum region of the compound nucleus. If one knows the lifetimes, one can infer the fluctuations and conversely.

The object of this note is to point out an independent method of getting information about the lifetimes of states in the continuum region. Moreover, the method to be described relates to the lifetimes of states of a particular spin and parity, namely, the 1^- states in the region of the giant resonance observed in photonuclear processes.

We consider a low energy 0^+–0^+ transition to the ground state of a nucleus (e.g. Zr^{90}). A small fraction of these transitions will proceed by two-photon decay. This is a second order process and will proceed predominantly by electric dipole transitions through the 1^- intermediate nuclear states.

Since electric dipole matrix elements are very weak to low lying levels and very strong to states in the giant dipole region ($\approx$ 20 MeV excitation), we find that the process proceeds predominantly through the giant dipole states despite the larger energy denominators involved.

The process of two-photon decay has been considered previously by several authors [3–6]). We can write this probability as

$$T_{if}\,\mathrm{d}\omega\,\mathrm{d}\Omega\mathrm{d}\Omega' = \frac{\mathrm{d}\varepsilon\mathrm{d}\Omega'\mathrm{d}\Omega}{8\pi^3}\left(\frac{e^2}{\hbar c}\right)^2 \varepsilon^3(\varepsilon')^3\,\frac{c}{(\hbar/Mc)^5}\,M^2c^4$$
$$\times \sum_{p,p'}\left|\sum_n\left[\frac{(\mathbf{e}'\cdot\mathbf{r})_{fn}(\mathbf{e}\cdot\mathbf{r})_{n1}}{\hbar(\omega_1-\omega_n-\omega)}+\frac{(\mathbf{e}\cdot\mathbf{r})_{fn}(\mathbf{e}'\cdot\mathbf{r})_{n1}}{\hbar(\omega_1-\omega_n-\omega')}\right]\right|^2. \quad (1)$$

† Now at McGill University, Montreal, Canada

†† Work supported in part by the U.S. Atomic Energy Commission.

In the above the photons have energies, momenta and polarizations $\hbar\omega$, $\mathbf{k}$, $\mathbf{e}_p(\mathbf{k})$ and $\hbar\omega'$, $\mathbf{k}'$, $\mathbf{e}_{p'}(\mathbf{k}')$. The matrix elements are

$$e(\mathbf{r})_{fn} \equiv \langle f|\sum_s e_s \mathbf{r}_s|n\rangle,$$

where e is the proton charge and e_s and $\mathbf{r}_s$ are the effective charge and position vector of the s^{th} nucleon. In eq. (1), $\varepsilon = \hbar\omega/Mc^2$, where M is the nucleon mass.

The electric dipole matrix elements are very weak for low energy transitions and very strong for transitions between the ground state and states in the giant resonance region. One also expects large matrix elements for transitions from the giant resonance region to low lying excited states when the excitation of these states is considerably less than the width of the giant resonance. This is certainly the case for the first excited 0^+ states of Zr^{90} and Ge^{72}. For the other two cases where the first excited state has spin and parity 0^+, Ca^{40} and O^{16}, the excitations are of the order of the giant resonance width or larger.

Since we get the strong contributions to the sum in (1) from the terms corresponding to $\omega_n - \omega_1 \gg \omega$ we drop ω and ω' in these sums. Summing over polarizations of the photon and integrating over photon energies and angles, we get the transition probability for two-photon decay

$$W_{\gamma\gamma} = \frac{2}{105\pi}\frac{1}{(\hbar c)^4}\left(\frac{e^2}{\hbar c}\right)^2 (E_1 - E_f)^7 \left|\sum_n \frac{(z)_{fn}(z)_{n1}}{\hbar(\omega_n - \omega_1)}\right|^2. \tag{2}$$

We are then led to consider sums of the form

$$S = \sum_n \frac{(z)_{fn}(z)_{n1}}{\hbar(\omega_n - \omega_1)}. \tag{3}$$

We now compare this sum with the (-2)-moment of the photonuclear absorption cross section [7]). This quantity is given by

$$\sigma_{-2} \equiv \int \frac{\sigma}{W^2}\,dW \approx 4\pi^2 \frac{e^2}{\hbar c}\sum_n \frac{(z)_{fn}(z)_{nf}}{\hbar(\omega_n - \omega_f)}, \tag{4}$$

where σ is the total photon absorption cross section for photon energy W. We now write

$$|S| = f\sum_n \frac{(z)_{fn}(z)_{nf}}{\hbar(\omega_n - \omega_f)}. \tag{5}$$

We have then

$$W_{\gamma\gamma} = \frac{1}{840\pi} f^2 \left(\frac{E_1 - E_f}{Mc^2}\right)^7 \frac{M^2c^4(\sigma_{-2})^2}{\left(\pi\dfrac{\hbar}{Mc}\right)^4}\frac{c}{\hbar/Mc}. \tag{6}$$

It is to be noted that any convenient mass can be used in formula (6).

TABLE 1

Theoretical and experimental two photon decay probabilities and related quantities

Nucleus	$E_i - E_f$ (MeV)	B (MeV)	U (MeV)	Γ (MeV)	$W_{\gamma\gamma}/f^2$ ($\sec^{-1}$)	W (exp) ($\sec^{-1}$)	τ_e (sec)	$W_{\gamma\gamma}$ (theor) ($\sec^{-1}$)	$\frac{W_{\gamma\gamma}(\text{theor})}{W(\text{exp})}$	$\frac{W_{\gamma\gamma}(\text{exp})}{W(\text{exp})}$
O^{16}	6.07	15.6	21.7	3.4	6.7×10^{9}	1.4×10^{10}	2×10^{-21}	$<6.4\times10^{8}$	$<5\times10^{-2}$	
Ca^{40}	3.35	15.8	19.3	4.2	5.1×10^{8}	2.9×10^{8}	1×10^{-20}	$<7.9\times10^{6}$	$<3\times10^{-2}$	$<6\times10^{-3}$
Ge^{72}	0.69	≈10	≈20	≈7	5.7×10^{4}	3.4×10^{6}	4×10^{-20}	1.3×10^{2}	4×10^{-5}	
Zr^{90}	1.73	12.0	15.8	4.3	7.3×10^{7}	1.1×10^{7}	1.5×10^{-19}	7×10^{4}	6×10^{-3}	1.1×10^{-3}

Table 1 gives two-photon decay probabilities divided by f^2, calculated by eq. (6). The values for σ_{-2} have been taken from the paper of Levinger [7]; $\sigma_{-2} \approx 7A^{\frac{1}{3}}$ μb/MeV for O^{16} and $\sigma_{-2} \approx 3.5\ A^{\frac{1}{3}}$ μb/MeV for the other nuclei. The total measured decay probabilities $W(\text{exp})$ are also tabulated [8]). The predominant mode of decay is by monopole transitions. In order to have a theoretical number for $W_{\gamma\gamma}$ we must know f. For cases when $E_1 - E_f$ is considerably less than the giant resonance width, we expect that for the states E_n within the giant resonance $|(z)_{fn}| \approx |(z)_{n1}|$.

These matrix elements are expected to change sign randomly at energy intervals $\hbar/\tau_c$, where τ_c is the lifetime of a state in this region. We have then $f^2 \approx \hbar/(\tau_c \Gamma)$, where τ_c is the lifetime of a state in the giant resonance region and Γ is the width of the giant resonance. We see then that for a nucleus like Zr^{90} a measurement of $W_{\gamma\gamma}$ will yield an estimate of τ_c. Conversely, we may use the estimate of Ericson [1]) for τ_c based on neutron reaction theory, to estimate the probability of two-photon decay:

$$\tau_c \approx \frac{\rho_c(U)}{\rho_n(U-B)} \frac{2\pi^2}{\frac{2M}{\hbar^2} T\bar{\sigma}_c} \frac{\hbar}{T}. \tag{7}$$

In the above $\bar{\sigma}_c$ is the average cross section for formation of a compound nucleus with neutrons of energy a few MeV; B is the binding energy of the last neutron; U is the giant resonance excitation energy; $\rho_c(E)$ and $\rho_n(E)$ are the level densities for the compound and residual nuclei at excitation E. We take $\rho_n(E) = \rho_c(E+\delta)$ to compensate for the odd-even effect in nuclear densities, with $\delta = 34/A^{\frac{1}{2}}$ MeV (the nuclear pairing energy). We use the form $\rho_c(E) = C\exp(\sqrt{aE})$ with $a = 7, 10, 4, 1$ MeV^{-1} for Zr^{90}, Ge^{72}, Ga^{40} and O^{16}, respectively [9]).

The nuclear temperature of the residual nucleus is given by $T = [(U-\overline{B-\delta})/a]^{\frac{1}{2}}$.

The values of τ_c obtained from (7) are given in table 1 along with the value of $W_{\gamma\gamma}$ calculated using these values of τ_c. Values of $W_{\gamma\gamma}/W(\text{exp})$ are also tabulated. For Ca^{40} and especially for O^{16} it is expected that the calculations of $W_{\gamma\gamma}$ based on the above considerations will be overestimates since the spacing between the two 0^+ states is not considerably less than the giant resonance width. We indicate this in table 1 by affecting our estimates with $<$ signs.

The upper limit or value of $W_{\gamma\gamma}(\text{exp})/W(\text{exp})$ is also listed in table 1 in the cases in which experiments have been performed [8, 10]). Reide, Thieberger and Alvager [10]) have recently reported detecting two-photon decay in Zr^{90}, giving a value of $W_{\gamma\gamma}/W \approx 1.1 \times 10^{-3}$. This leads to $\tau_c \approx 9 \times 10^{-19}$ sec, in good agreement with our theoretical value which is expected to be of the right order of magnitude.

The author wishes to thank Dr. A. Schwarzschild for discussions concerning the experimental data. He also wishes to thank Dr. M. K. Ramaswamy for drawing his attention to this problem.

References

1) T. Ericson, Advances in Physics **9** (1960) 425
2) T. Ericson, Phys. Rev. Lett. **5** (1960) 439
3) M. Goeppert-Mayer, Ann. Physik **9** (1931) 273
4) R. G. Sachs, Phys. Rev. **57** (1940) 194
5) J. Eichler and G. Jacob, Zeits. f. Phys. **157** (1959) 286
6) D. P. Grechukhin, JETP **5** (1957) 846
7) J. S. Levinger, Phys. Rev. **107** (1957) 554
8) M. Nessin, Report CU(PNPL)—201 (available from the Office of Technical Services, Department of Commerce, Washington 25, D.C.)
9) K. L. Le Couteur and D. W. Lang, Nuclear Physics **13** (1959) 32
10) Reide, Thieberger and Alvager, Phys. Rev. Lett. **6** (1961) 475

NORTH-HOLLAND BOOKS

Elements of Hamiltonian Mechanics

by D. TER HAAR

University Reader in Theoretical Physics and Fellow of Magdalen College, Oxford

CONTENTS:

1. Newtonian mechanics
2. The Lagrangian equations of motion
3. Small vibrations
4. Dynamics of rigid bodies
5. The canonical equations of motion
6. Hamilton-Jacobi theory
7. Perturbation theory
8. Continuous systems

Bibliography - Problems

This book is based upon a course of lectures given to final year undergraduates and first year graduate students at Oxford University. The emphasis and the selection of subject matter differs in a number of points from those in existing modern text-books. The main differences are in the way constraints are introduced by freezing in of degrees of freedom, and in the discussion of classical perturbation theory.

6 x 9" 196 pp. Gld. 20.— (40s.)

NORTH-HOLLAND PUBLISHING COMPANY

P. O. BOX 103 - AMSTERDAM

Distributor for U.S.A.: Interscience Publishers, Inc. — New York

NORTH-HOLLAND BOOKS

QUANTUM MECHANICS

VOL. I

by ALBERT MESSIAH (Centre d'Etudes Nucléaires de Saclay)

translated from the French by G. M. Temmer (Florida State University, Tallahassee)

6×9" 520 pp. Gld. 50.- (100s.)

CONTENTS VOL. I. *The formalism and its interpretation.* Origins of the Quantum Theory. Matter waves and the Schrödinger equation. One dimensional quantum systems. Statistical interpretation of the wave-corpuscle duality and uncertainty relations. The development of the formalism of Wave Mechanics and its interpretation. Classical approximation and WKB method. The general formalism of Quantum Theory: A) Mathematical framework. B) Description of physical phenomena. — *Simple systems.* Solution of the Schrödinger equation by separation of variables. Central force field. Scattering problems. Central force field and the method of phase shifts. Coulomb interaction. Harmonic oscillator. — *Appendices:* «δ function» and distributions. Special functions and related formulae.

". . . . the reviewer would like to recommend the book to students taking a beginner's course in quantum mechanics, to teachers for broadening the scope of such courses, and also to research workers in understanding the principles and methods of quantum mechanics and for acquiring the necessary knowledge for an understanding of the advanced parts of the field."

(PHYSICS TODAY on the original French Edition)

VOLUME II
in preparation

Ask your bookseller or

NORTH-HOLLAND PUBLISHING COMPANY

P.O. BOX 103—AMSTERDAM

Distributor for U.S.A.: Interscience Publishers, Inc. — New York